NUREG/CR-1729
BMI-2066
Vol. 1

Evaluating Strength and Ductility of Irradiated Zircaloy Task 5

Experimental Data Final Report

Prepared by L. M. Lowry, A. J. Markworth, J. S. Perrin, M. P. Landow

Battelle Columbus Laboratories

Prepared for U.S. Nuclear Regulatory Commission

Available from

GPO Sales Program
Division of Technical Information and Document Control
U. S. Nuclear Regulatory Commission
Washington, D. C. 20555

Printed copy price: $9.50

and

National Technical Information Service
Springfield, Virginia 22161

NUREG/CR-1729
BMI-2066
Vol. 1
R3

Evaluating Strength and Ductility of Irradiated Zircaloy Task 5

Experimental Data
Final Report

Manuscript Completed: November 1980
Date Published: May 1981

Prepared by
L. M. Lowry, A. J. Markworth, J. S. Perrin, M. P. Landow

Battelle Columbus Laboratories
505 King Avenue
Columbus, OH 43201

Prepared for
Division of Reactor Safety Research
Office of Nuclear Regulatory Research
U.S. Nuclear Regulatory Commission
Washington, D.C. 20555
NRC FIN A4068

ABSTRACT

The objective of this program was to provide a mechanical-property data base that could be used to predict the performance of Zircaloy cladding under various off-normal, transient and accident conditions in a power reactor. The mechanical properties of both unirradiated and irradiated Zircaloy were determined under uniaxial and biaxial stress conditions for the purpose of simulating the loading and stress conditions encountered by cladding under these postulated conditions. Claddings for the tests were obtained from spent commercial fuel rods irradiated to various burnup levels. Tensile tests were performed principally to provide a comparison with the results of other uniaxial test data. Burst tests were performed to simulate fuel-rod pressure loading due to internal gases and to evaluate strain capabilities of the cladding under uniform pressure loading. Loads imposed on the cladding from fuel-cladding interaction and from restraint by spacer grids were simulated by expanding mandrel and bend tests. Tests were conducted using specimens in either the as-irradiated condition or the annealed condition.

Comparison of the tensile-test results at the four test temperatures within the 300 to 400 C range revealed substantial changes in the mechanical properties of both the unirradiated and irradiated cladding materials. These changes were attributed to dynamic strain aging. Stresses for all lots of material exhibited some peaking at annealing temperatures below 600 C and lagged the strain above 600 C. This suggested that defect arrays serve as crack nuclei to initiate premature failure during plastic straining. Irradiation changed the response of mechanical properties to transient and isothermal annealing as compared with those of unirradiated cladding materials subjected to identical annealing and testing conditions. Irradiation also appeared to produce a more isotropic acting material and annealing appeared to produce a return to the anisotropic behavior characteristic of unirradiated cladding. It was concluded from the test results of irradiated and annealed Zircaloy-4 fuel-rod cladding that the tube-burst (biaxial) and tensile (uniaxial) data curves exhibit the same general trends. Transient-heating burst tests were conducted to determine the behavior of the cladding when subjected to a loss-of-coolant accident (LOCA) reactor conditions.

SUMMARY

Analytical and empirical correlations have been or are being developed that are combined into mathematical codes to describe the thermal and mechanical response of fuel rods subjected to postulated off-normal, transient, and accident conditions. A major requirement for use of these codes is a reliable data base. This requirement includes a variety of thermal, physical, chemical, and mechanical properties that influence the Zircaloy cladding behavior under the postulated reactor conditions.

The objective of this program was to provide a mechanical-property data base that could be used to predict the performance of Zircaloy cladding under various power reactor conditions. The data were developed both for low-temperature off-normal and transient conditions, where the source of cladding loads includes thermal stresses, internal fuel-rod gas pressure, fuel-cladding interaction, and spacer restraint, and for high-temperature accident conditions, where the principal load is produced by the internal gas pressure. Data were sought for strain-to-failure correlations when burnup is high and a failure is probably due to mechanical interaction at relatively low temperature.

The mechanical properties of both unirradiated and irradiated Zircaloy were determined under uniaxial and biaxial stress conditions for the purpose of simulating the loading and stress conditions encountered by cladding under postulated reactor accident conditions. Claddings of various textures were obtained for the tests from spent commercial fuel rods irradiated to various burnup levels.

Unirradiated material for this program was acquired from Oak Ridge National Laboratory and was part of the tubing supplied for their multirod burst tests. Also, a limited amount of unirradiated material was acquired from Babcock and Wilcox from their archive stock for the Oconee I commercial power reactor.

The irradiated Zircaloy-4 fuel-rod cladding was supplied by three commercial power reactors. Irradiated fuel-rod cladding material for scoping and preliminary mechanical tests was supplied by one spent fuel rod from Westinghouse Point Beach reactor. The irradiated fuel-rod cladding material designated Lot 1 was obtained from 27 spent fuel rods from the Westinghouse H.B. Robinson reactor. The remainder of the irradiated fuel-rod cladding material (designated Lot 2 for one cycle of irradiation, Lot 3 for two cycles of irradiation, and Lot 4 for three cycles of irradiation) was supplied by 26 spent fuel rods from the Oconee I reactor.

The nondestructive characterization of the fuel-rod cladding involved visual examination, gamma scanning, spiral profilometry, and eddy-current testing. The characterization provided the means to assess the general condition of the as-received, irradiated fuel rods and provided evidence of mechanical and chemical interactions to which the rods may have been subjected. This assessment was used to determine the suitability of all or part of the rod cladding for mechanical properties testing and to assess possible differences between various fuel rods and sections of these rods.

The destructive characterization of the fuel-rod cladding involved plenum punch and gas collection, burnup analysis, fluence determination, microhardness testing, metallographic examination, and annealing of cladding. This characterization was used along with the nondestructive characterization results to guide the choice of test specimens. Specimens were then sectioned, the fuel was removed, and cladding sections were prepared for tensile, tube-burst, bend, expanding mandrel, and transient-heating burst tests.

Tensile tests were performed principally to provide a standard of comparison with the results of other uniaxial test data. Burst tests were performed to simulate fuel-rod pressure loading due to internal gases and to evaluate strain capability of the cladding under uniform pressure loading. Loads imposed on the cladding due to fuel-cladding interaction and to restraint by spacer grids were simulated by expanding mandrel and bend tests.

Tests were conducted on specimens in either the as-irradiated condition or the annealed condition. As-irradiated specimens were tested at room temperature to 427 C and at strain rates of 0.001/min to about 2/min. The mechanical properties were then determined as a function of test temperature and of strain rate.

A comparison of mechanical properties for irradiated specimens of both H.B. Robinson and Oconee I fuel-rod cladding showed that irradiation increased the stress values and decreased the strain values at a particular test temperature or strain rate. However, the trends for both the unirradiated and irradiated curves were the same and the rapid increase in the total strains observed between 300 and 400 C was attributed to recovery, relaxation of residual and irradiation-induced stresses, and defect motion and agglomeration. One possible explanation for the rapid changes observed in the mechanical properties of Zircaloy-4 was dynamic strain aging. Strain aging occurred in zirconium and many of the zirconium alloys. A variety of mechanisms have been proposed to account for the strain aging, including the formation of tin-rich precipitates, segregation of hydrogen, and Cottrell locking of dislocation-interstitial interaction as with oxygen.

The unirradiated specimens tested in tensile, tube-burst, and expanding mandrel tests exhibited similar trends, including a rather smooth decrease in strength (engineering stress) with either an increase in test temperature or a decrease in strain rate. The important facts noted here were that, for the unirradiated cladding material, yield and ultimate stresses decreased rather smoothly as the test temperature was increased, the total strains began to increase above 400 C, and the uniform strains were essentially unaffected by either test temperature or strain rate.

Bend tests were conducted using irradiated H.B. Robinson and one-cycle Oconee I material (Lots 1 and 2) and unirradiated Oconee I archive material. Strength values obtained in these tests were similar to those obtained in tube-burst and expanding mandrel tests when the test temperature was increased. However, little information concerning cladding ductility was produced from the bend tests except for the significant observation that the cladding was highly ductile in bending. Specimens were routinely bent to a 10-cm radius of curvature, and smaller, without producing failure.

To determine the fuel-rod cladding mechanical properties after annealing, each irradiated specimen was either transient annealed or isothermally annealed. The H.B. Robinson and Oconee I fuel-rod cladding specimens were then tested in tensile, tube-burst, or expanding mandrel tests at 371 C and at the appropriate nominal strain rate. A limited study to determine the mechanical properties caused by annealing was conducted using unirradiated Sandvik and Oconee I archive fuel-rod tubing. The unirradiated tubing was also tested in tensile, tube-burst, and expanding mandrel tests. Several important facts emerged from this transient annealing and testing data:

(1) The stress values peaked at transient annealing temperatures between 350 and 600 C if the heating rate was greater than or equal to 14 C/sec. This peaking of stress suggested a thermal aging process possibly involving interactions between impurity atoms and irradiation-induced defects. Overaging also appeared to occur rapidly as recovery processes associated with defect agglomeration proceeded at transient annealing temperatures below 600 C.

(2) Perhaps of greatest significance was the fact that the recovery of ductility (increase in strain) lagged the decrease in strength (stress) in the irradiated fuel-rod cladding, but the recovery of stress and strain appeared to begin at the same transient annealing temperature for unirradiated fuel-rod cladding that was transient annealed. Only after recovery, as measured by stress decreases, was

essentially completed did the total strain values recover to those characteristic of the as-irradiated specimens. This lag suggested that the defect arrays produced during the irradiation and possibly defect agglomeration during annealing at temperatures between 400 and 600 C served as crack nuclei to initiate premature failure during plastic straining. Whether this was the mechanism for decreased ductility was uncertain, but such an explanation would be consistent with the fact that ductility recovery significantly lags the recovery in strength properties.

(3) Another significant observation was the fact that, at least for the transient annealing temperature range chosen for these tensile tests, once recovery occurred, the ultimate and yield stresses dropped below those of the unirradiated tubing at the same transient annealing temperature and the uniform and total strains increased above those of the unirradiated tubing. This suggested that because of increased nucleation sites at irradiation-induced-defects, the grain structure of the irradiated and annealed material was finer and, therefore, the material had somewhat lower strength and higher ductility after annealing as compared with unirradiated material.

(4) The data from tensile and tube-burst tests of annealed specimens from Lots 2, 3, and 4 material, irradiated for one, two, and three cycles in the Oconee I reactor, indicated that the strengths peaked or saturated at between 20,000 and 30,000 MWD/MTU.

(5) For Lot 1 fuel-rod cladding annealed and tensile tested, an apparent change in anisotropy accompanied annealing. The tube-wall- and tube-diameter-reduction measurements indicated that the wall reduction exceeded the diametral reduction in the as-irradiated fuel-rod cladding and was reversed after annealing. Thus, irradiation appeared to produce a more isotropic acting material, and annealing caused a return to the anisotropic behavior characteristic of unirradiated cladding.

(6) The effects of isothermal annealing on the mechanical properties in tensile, tube-burst, and expanding mandrel tests were similar and the mechanical property versus annealing time curves exhibited similar trends for these types of tests. The changes in properties were caused primarily by recovery, recrystallization, and grain growth. However, the exact manner in which the material properties change was related to a complicated interaction of residual stresses, number of defects, defect structure, microstructure, temperature, and time.

(7) The final fact became apparent when the mechanical properties results from the tensile, tube-burst, and expanding mandrel tests were

compared. All the test results exhibited the same trends after specimens were transient or isothermally annealed and tested at 371 C and at nominal strain rates. Because of this, annealing of tensile and expanding-mandrel specimens was dropped and emphasis was placed primarily on the tube-burst annealing test data.

Transient-heating burst tests were conducted at temperatures to 1250 C to evaluate cladding behavior under simulated LOCA conditions. Sections of a fuel rod were internally pressurized and then heated using an internal heater at rates up to 100 C/sec. The interdependence of heating rate, internal pressure, temperature at failure, and failure strain was examined.

The burst hoop stresses for a particular burst temperature were consistently lower for Battelle's Columbus Laboratories (BCL) irradiated transient-heating burst tests than for the Oak Ridge National Laboratory (ORNL) unirradiated transient-heating burst tests. Therefore, the ORNL curve of burst hoop strain versus burst temperature appeared to be an upper bound for the BCL test data. It was believed that the strength was lower for irradiated cladding than for unirradiated cladding in the range 700 to 1000 C. This was confirmed by the lower tensile stresses exhibited by irradiated specimens transient annealed in this temperature range as compared with those of unirradiated specimens transient annealed and tested under identical conditions. Little difference in results could be found between H.B. Robinson and Oconee I test results, although it appeared, as expected, that the lower heating rates generally resulted in lower burst temperatures at a specific burst hoop stress level.

Also, the data generated for Lots 2, 3, and 4 (Oconee I one-, two-, and three-cycle) material indicated that there was little effect on the transient-heating burst hoop stress caused by increasing the neutron exposure from 10,000 to 30,000 MWD/MTU. This was in agreement with results from tensile, tube-burst, and expanding-mandrel tests using annealed specimens which indicate that removal of irradiation damage was essentially complete above annealing temperatures of approximately 700 C. All the results for irradiated cladding fell below the curve generated from data for the unirradiated cladding obtained in burst tests performed at ORNL. Several factors were explored in an attempt to explain this fact. However, it was concluded that although residual stresses and many of the point defects were annealed out at temperatures about 700 C, enough dislocations would be present and available (if the strain rate was high enough) to be nucleation sites for recrystallization and subsequent grain growth at a lower temperature in the irradiated cladding specimens when compared with unirradiated cladding specimens. Therefore, at any given pressure, an irradiated cladding specimen with advanced grain growth would be expected to fail at a

lower temperature than an unirradiated cladding specimen with a comparatively retarded grain growth.

The data base produced during this program can and is being used to evaluate mathematical codes which attempt to describe the thermal and mechanical response of fuel rods subjected to postulated reactor off-normal, transient, and accident conditions. However, because the data generated are generally in terms of engineering stresses or strains, these parameters cannot be used directly in the codes. One attempt to quantify the data into true stress-true strain values and thereby describe the responses empirically and to derive constitutive equations characterizing the measured mechanical behavior is presented in Volume II.

TABLE OF CONTENTS

TABLE OF CONTENTS

TABLE OF CONTENTS

TABLE OF CONTENTS

TABLE OF CONTENTS

TABLE OF CONTENTS

TABLE OF CONTENTS

TABLE OF CONTENTS

LIST OF FIGURES

LIST OF FIGURES

LIST OF FIGURES

LIST OF FIGURES

LIST OF FIGURES

LIST OF FIGURES

APPENDIX A

APPENDIX B

APPENDIX C

APPENDIX D

LIST OF TABLES

LIST OF TABLES

LIST OF TABLES

LIST OF TABLES

LIST OF TABLES

LIST OF TABLES

FOREWORD

This work is part of the Division of Reactor Safety Research/Fuel Behavior Branch's program being performed at a number of sites throughout the country on Zircaloy fuel cladding performance during various postulated reactor transients and accidents. The data available on the mechanical properties of irradiated Zircaloy cladding as functions of irradiation level, texture, temperature, and condition of loading are not sufficient to permit predictions of cladding performance to the level of accuracy desired. They do not permit prediction of the onset of plastic instability, definition of strain to failure at relatively low temperatures, or estimates of the response to multiaxial stresses during temperature transients. In addition, the data available on irradiated Zircaloy show considerably greater scatter than that available on unirradiated material. A body of data must be obtained under carefully designed experimental conditions if a statistically valid data base is to be made available for code development.

ACKNOWLEDGMENTS

The authors acknowledge support of this research by the U.S. Nuclear Regulatory Commission under Contract No. AT (49-24)-0293. They are particularly grateful for the direction offered by Dr. M. L. Picklesimer of the USNRC. In addition, the authors wish to acknowledge A. A. Bauer for his contribution in the management of this program from 1975 to 1978. The authors are also grateful to the staff at the H. B. Robinson reactor, Babcock & Wilcox, and the Oconne I reactor for providing unirradiated material, irradiated fuel rods and pertinent information needed to complete this program.

STRENGTH AND DUCTILITY OF IRRADIATED ZIRCALOY

INTRODUCTION

Analytical and empirical correlations have been or are being developed that are combined into mathematical codes to describe the thermal and mechanical response of fuel rods subjected to postulated off-normal, transient, and accident conditions. A major requirement for use of these codes is a reliable data base. This requirement includes a variety of thermal, physical, chemical, and mechanical properties that influence the Zircaloy cladding behavior under the postulated reactor conditions.

In the area of mechanical properties, the data base for irradiated Zircaloy cladding is particularly weak. Therefore, in 1974, Battelle's Columbus Laboratories (BCL) proposed to determine and evaluate the strength and ductility of irradiated Zircaloy fuel-rod cladding. The present program was designed to rectify this weakness by providing mechanical-property data and information concerning the response and deformation behavior of Zircaloy to the types of loads encountered under off-normal operation and accident conditions in a reactor core. It was undertaken as part of a major effort involving a variety of programs designed to provide the information for predicting the behavior of Zircaloy under these conditions.

PROGRAM OBJECTIVE

The objective of the proposed program was to provide a mechanical-property data base that could be used to predict the performance of Zircaloy cladding under various off-normal, transient, and accident conditions in a power reactor. The data were developed for both low-temperature off-normal and transient conditions, where the source of cladding loads includes thermal stresses, internal fuel-rod gas pressure, fuel-cladding interaction, and spacer restraint, and for high-temperature accident conditions, where the principal load is produced by the internal gas pressure. Data were sought for strain-to-failure correlations when burnup is high and a failure is probably due to mechanical interaction at relatively low temperature.

PROGRAM PHILOSOPHY

An operating reactor is potentially subject to power transients, reactivity insertions, and power cooling mismatches that can produce

rapid changes in fuel and cladding temperatures. These, in turn, can produce cladding stresses as a result of fuel-cladding interaction, cladding interaction with the grid spacers, and increased internal gas pressures. The stresses under these conditions are imposed at relatively low cladding temperatures (near normal operation temperatures or slightly above). However, in the case of a postulated loss-of-coolant accident (LOCA), much higher temperatures may be encountered; while the cladding is subject to stresses from the same sources as mentioned above, the source of major concern is the internal gas pressure, which can produce ballooning and bursting of the cladding.

Regardless of the origin of reactor instability, the result is a transient increase in temperature and stress, with the stress state generally being multiaxial in nature. To predict the response of Zircaloy cladding under such conditions, a reliable data base for Zircaloy including its strength, uniform strain limit, and strain to failure when subjected to uniaxial and multiaxial stresses is needed. Furthermore, a precise determination of the effect of irradiation must be provided.

Aside from limited tensile and burst test data, which indicate a general increase in strength and decrease in ductility, the effects of irradiation on the mechanical properties of Zircaloy are incompletely known. Furthermore, there are several complicating factors in predicting the response of irradiated Zircaloy cladding. The first concerns the effect of increased neutron exposure on property changes and is not well defined. Then there is the question of annealing of irradiation damage. While recovery of a considerable portion of the irradiation damage can be expected as the temperature is increased, the time-temperature relationship of annealing can profoundly influence response behavior under transient heating conditions. Furthermore, a fuel rod is subject to a unique stress-strain, corrosion, and temperature history over its life that can influence its end-of-life properties, and data illustrating the importance of typical irradiated fuel rod variables are needed. A further source of differences in properties and response of irradiated Zircaloy cladding is the differences in fabrication processes used by the various cladding vendors.

As discussed in the previous section, a number of complicating factors exist that must be considered in interpreting the mechanical properties of irradiated Zircaloy. These include the irradiation exposure level, annealing response, and in-pile and fabrication history. Consequently, material variables evaluated included mechanical-properties differences, as introduced by various cladding fabricators and fuel-rod burnup or neutron exposure. The annealing response as a function of time and temperature during isothermal annealing, and as a function of heating rate and temperature during

transient heating, was also defined. In addition, individual fuel rods used for test purposes were well characterized as to dimensions, corrosion attack, and possible in-pile distortion or deformation. The purpose of this effort was to establish a basis for choosing a series of test specimens from particular fuel rods or fuel-rod sections and to permit interpretation of scatter in the mechanical-property data generated.

Mechanical-property tests were generally intended to simulate the loading and stress conditions encountered by the cladding under postulated off-normal transient and accident conditions. A variety of tests were performed at temperatures up to 700 C. In addition, hardness, tensile, burst, bend, and expanding-mandrel tests were conducted to evaluate the annealing of irradiation damage in Zircaloy. Specimens were annealed under both isothermal and transient heating conditions and tested to determine the time-temperature characteristics of annealing under both types of conditions. Changes in failure strain and in failure pattern and behavior were examined as annealing proceeded. Limited studies were also performed to characterize the annealing behavior of unirradiated Zircaloy cladding.

Tensile tests were performed principally to provide a standard of comparison with the results of other uniaxial test data. Burst tests were performed to simulate fuel-rod pressure loading due to internal gases and to evaluate strain capability of the cladding under uniform pressure loading. Loads imposed on the cladding due to fuel-cladding interaction and to restraint by spacer grids were simulated by expanding mandrel and bend tests.

In the tensile tests, strain rate was a test variable. Strength, uniform strain, and total strain data were generated where possible. Fracture and deformation areas were examined metallographically and information concerning deformation patterns was sought for correlation with the behavior of unirradiated Zircaloy.

Transient burst tests were conducted at temperatures to 1250 C to evaluate cladding behavior under simulated LOCA conditions. Sections of a fuel rod were internally pressurized and then heated using an internal heater at rates up to 28 C/sec. The interdependence of heating rate, internal pressure, temperature at failure, and failure strain was examined.

PROGRAM APPROACH

The mechanical properties of irradiated Zircaloy were determined under uniaxial and biaxial stress conditions for the purpose of simulating the loading and stress conditions encountered by cladding under postulated off-normal, transient, and accident conditions. Claddings of various textures were obtained for the tests from spent commercial fuel rods irradiated to various burnup levels.

The cladding was subjected to detailed examination in order to establish pretest characteristics. As-irradiated strength and ductility characteristics from room temperature to 480 C and at strain rates in the range 0.001 to 2/min were evaluated by tests that included tensile, burst, and expanding mandrel. The annealing of irradiation damage was evaluated under both transient and isothermal heating conditions to temperatures of 800 C. Transient-heating burst tests were conducted at temperatures to 1250 C to evaluate cladding behavior under simulated LOCA conditions.

The objective of this program was to provide data concerning the mechanical properties and annealing and burst behavior of irradiated Zircaloy fuel-rod cladding for use in the development of codes that will model fuel-rod performance under LOCA conditions and during off-normal and transient reactor operation. Cladding from three reactors and fabricated by two vendors was evaluated in the program. The program was then divided into tasks. The first involved material selection and nondestructive testing (NDT) for material characterization. The next was the performance of mechanical-properties tests to characterize the as-irradiated properties of the Zircaloy fuel-rod cladding when tested at room temperature to over 400 C and at strain rates of 0.001 to 2/min (test temperature of 371 C). The third task involved annealing studies to evaluate the effect of transient and isothermal anneals on the strength and ductility of irradiated Zircaloy fuel-rod cladding. The fourth task involved conducting transient-heating burst tests of irradiated cladding to 1250 C to determine the cladding response under simulated LOCA conditions. Limited studies using unirradiated cladding material were also conducted (as material permitted) to evaluate the mechanical properties under conditions listed in all four tasks described above. Also, evaluation of the generated data to develop correlations between experimental variables and the strength and ductility properties was a continuous effort during the course of the program.

TASK I

Material Selection

Material selection fell into three categories: unirradiated Zircaloy-4 fuel-rod cladding material, pressurized-water-reactor (PWR)-irradiated Zircaloy-4 fuel-rod cladding, and boiling-water-reactor (BWR)-irradiated Zircaloy-4 fuel-rod cladding. The unirradiated material was fabricated by Sandvik. However, the unirradiated material acquired early in the program (1976) was sent to Battelle from Oak Ridge National Laboratory (ORNL) and was part of the material supplied to ORNL by Sandvik for the multirod burst tests.[1] A limited amount of unirradiated material acquired later in the program (1978) was supplied by Babcock and Wilcox (B&W) from their archive stock for the Oconee I commercial power reactor. This archive material was also fabricated by Sandvik. To differentiate between the two unirradiated Zircaloy-4 fuel-rod cladding materials, the material acquired in 1976 was designated Sandvik while that acquired in 1978 was designated Archive.

The PWR-irradiated Zircaloy-4 fuel-rod cladding was supplied by three commercial power reactors but was somewhat dependent upon availability and heavily dependent upon the reactor vendor's willingness and ability to supply the material for this NRC program. Irradiated fuel-rod cladding material for scoping and preliminary mechanical tests was obtained from one spent fuel rod from the Westinghouse Point Beach reactor. The irradiated fuel-rod cladding material designated Lot 1 was obtained from 27 spent fuel rods from the Westinghouse H. B. Robinson reactor. The remainder of the irradiated fuel-rod cladding material (designated Lot 2 for one cycle of irradiation, Lot 3 for two cycles of irradiation, and Lot 4 for three cycles of irradiation) was obtained from 26 spent fuel rods from the Oconee I reactor.

Point Beach Fuel Rod

One fuel rod, Westinghouse Rod A25-06, from the Westinghouse Point Beach reactor, was being stored at BCL and was obtained for preliminary Zircaloy-cladding studies.

Several lengths of unirradiated Sandvik Zircaloy fuel-rod cladding were procured from Oak Ridge National Laboratory to be used to establish some representative baseline mechanical properties.

H. B. Robinson Fuel Rods

The fuel assembly from the H. B. Robinson reactor, containing 204 fuel rods, was received at the Aerojet Nuclear Idaho Facility on June 1, 1975. Aerojet was responsible for unloading the assembly from the shipping cask and removing 15 predesignated rods from the assembly and packaging them in a shipping basket for shipment to Battelle Columbus Laboratories (BCL). The Aerojet unloading took place in the TAN Hot Shop/canal complex. A representative of BCL's Hot Cell Laboratory was on site to observe the individual rods during removal from the assembly and their packaging for shipment.

The shipping cask was received at Aerojet and, after the cask was placed in the cell, a dry transfer of the assembly from cask to canal (storage pool) was made. Upon removal from the cask, the overall assembly was visually inspected. No bowing of the rods could be detected. During the dry transfer, the assembly was not cooled for a period of approximately 2 hours. Subsequently, upon lowering into the pool, generous amounts of steam were generated at the water surface. This led, several minutes later, to alarming of the constant air monitors in adjoining support rooms of the area. Activity release was apparently related to release of crud from the cladding surface.

Approximately 24 hours later, the assembly was taken from the pool and the nozzle head was removed by cutting with a metal bandsaw. The assembly was then returned to the pool for rod removal. During the nozzle-cutting operation, the assembly was out of the pool and uncooled for a period of approximately 6 hours. Upon its return to the pool, however, the amount of steam generated was almost negligible and no airborne activity was detected.

Rod removal proceeded smoothly. The lifting force required for removal of each rod was recorded. At no time did the force exceed 10 to 15 pounds except for the initial lift of Rod A-1 which recorded a pulse of approximately 75 pounds. Each rod was visually inspected during the transfer from assembly to shipping basket. Each rod was thoroughly identified and documented as it was placed in the shipping basket. The 15 rods were received at the BCL Hot Cell Laboratory on June 9, 1975, and were transferred underwater from the shipping cask to the hot cells for fuel-rod characterization.

Considerable uncertainty existed as to the temperatures that may have been reached within the fuel assembly when it was held in air in the Aerojet hot cell. There was concern that temperatures sufficient to cause annealing of irradiation damage in the rods had been produced by gamma heating. Consequently, Aerojet was requested to bring the remainder of the assembly back into the cell and let it rest in air

while rod temperatures were monitored with thermocouples. This was done and the measurements indicated that cladding temperatures did not exceed 90 to 150 C after a period of about 7 hours. Tests of a second set of rods from the H. B. Robinson reactor showed no apparent harm due to the mild heatup.

The second set of 12 fuel rods from the H. B. Robinson reactor was shipped to BCL by EG&G and was received April 18, 1977. Of the 12 rods, 7 were used in the current experimental work and the remaining 5 were stored for future use. All 27 fuel rods from the H. B. Robinson reactor were designated Lot 1 material.

Oconee I Fuel Rods

Twelve fuel rods were received at the BCL Hot Cell Laboratory in December 1976. These were received from B&W and had come from the Oconee I reactor. Fuel burnup of the rods averaged about 10,000 MWD/MTU with a peak burnup in the 15,000 MWD/MTU range. The corresponding peak fast-neutron-fluence exposure (< 1 MeV) of the cladding was 2.3×10^{21} n/cm^2. The twelve fuel rods had been irradiated for one cycle and supplied the Zircaloy fuel-rod cladding for the experimental program. These rods had been removed from the Oconee I reactor as part of a fuel-surveillance program being conducted by B&W. They had previously been examined at the B&W hot cells, with visual examinations, gamma scanning, profilometry, eddy-current inspection, and fission-gas puncturing having been performed. The twelve one-cycle-burnup rods were designated Lot 2 material.

A third lot of spent fuel (10 rods) was received at BCL to provide Zircaloy cladding for use in the program. This lot, provided by B&W and irradiated in the Oconee I reactor, was received March 21, 1978. The cladding was from the same lot as the earlier Oconee cladding but had been irradiated for two cycles instead of one cycle. Estimated fuel burnup for this lot of spent fuel was about 20,000 MWD/MTU.

The 10 fuel rods had been subjected to visual examination, gamma scanning, profilometry, eddy-current testing, and fission-gas recovery at the B&W hot cell. These rods were designated Lot 3 material.

The Lot 4 (Oconee I, three cycle) spent fuel rods were received at the Battelle hot cell on June 21, 1979, to provide Zircaloy cladding for use in this program. This lot, consisting of four rods, was provided by B&W and was irradiated in the Oconee I reactor for three cycles. The fuel burnup for these rods was estimated to be 26,000 MWD/MTU.

The fuel rods were previously subjected to visual examination, gamma scanning, profilometry, eddy-current testing, and fission-gas recovery at the B&W hot cells. Also, because of the licensing problems with the large shipping casks, these rods were sectioned into approximately four equal lengths (38 inches) by B&W and shipped to the BCL Hot Cell Laboratory in shipping cask BCL-4. These four rods were designated Lot 4 material. B&W also provided several lengths of Oconee I unirradiated archive cladding to be used for establishment of baseline mechanical properties.

The BWR irradiated Zircaloy-4 fuel-rod cladding (Lot 5) had not been received at the time of this writing.

Material Characterization (NDT Testing)

The characterization of the fuel rod cladding involved visual examination, gamma scanning, spiral profilometry, and eddy-current testing. The characterization provided the means to assess the general condition of the as-received, irradiated fuel rods and provided evidence of mechanical and chemical interactions to which the rods may have been subjected. This assessment was used to determine the suitability of all or part of the rod cladding for mechanical-properties testing and to assess possible differences between various fuel rods and sections of these rods. A full description of the equipment and procedures for gamma scanning, spiral profilometry, and eddy-current testing is included in Appendix A.

Visual Examination

The visual examination of the fuel rods was performed at a magnification of 3.2X using the in-cell Lenox Model 8700/A stereoviewer and a positioning support stage. The support stage is movable in the x, y, and z planes. A scale attached to the fuel rod supports indicates the axial location of rod features relative to the bottom of the rod. The fuel rod can also be indexed from 0 to 360 degrees about its longitudinal axis.

Each rod was placed on the traversing stage, set under the objective lens which was then focused. Unless otherwise specified, an arbitrary zerowas chosen and the entire length of the rod examined. The rod was rotated and examined at four 90-degree orientations and 3.2X photographs were taken of areas of interest. Higher magnifications were available for closer examinations of features.

Point Beach Fuel Rod. A fuel rod, Westinghouse Rod A25-06 from the Westinghouse Point Beach Reactor, was obtained for preliminary tensile tests, microhardness tests, annealing studies, and metallography studies on irradiated Zircaloy cladding. One 51-cm section of cladding was selected for a single transient-heating burst test.

The visual examination was performed and the rod appeared to be sound, with a thin, dark, and tenacious oxide present over the entire rod. No abnormalities were observed.

H. B. Robinson Fuel Rods. The primary objective of the visual examination was to assess the general surface conditon of the H.B. Robinson fuel rods as related to their suitability for mechanical testing.

In general, the rods appeared to be in very good condition. Slight fretting wear was observed at grid locations on several rods. This observation suggested that grid locations should generally be avoided in selecting rod sections for mechanical-property studies. Crud deposits on the rods were sparse except at the top regions of the rods. Most of the rods had heavy deposits of a dark flaky crud starting at about 335 cm from the rod bottom. The crud persisted from that area to the tops of the rods, but in decreasing quantities on approaching the rod tops. Crud deposits in other regions of the rods were patchy. As far as could be determined from the visual examination, the crud had no adverse effects on the cladding. Water marks, indicative of water level at some point in the rod transfers, were observed between 292 and 297 cm from the bottom of the rods.

Oconee I Fuel Rods. The primary objective of the visual examination was to assess the general surface condition of the Oconee fuel rods and to use the results to determine the suitability of the rods or rod sections for use in mechanical-properties evaluation tests.

Upon removal of the 22 rods from the shipping basket, it was noted that they had been previously punched for fission-gas removal at B&W and the holes welded shut. Rods 47125, 47118, 32013 and 31956 appeared to have water leaking from the welds, indicating that these rods were not successfully sealed by welding. Rod 31785 showed no evidence of the punch hole being welded shut. All other rods appeared to be sealed satisfactorily.

The fuel-rod identifying numbers were stamped on the bottom end caps. However, during the visual examination, no number was found on the bottom end cap of Rod 47118, but the number was found on the top end cap. It was later confirmed by B&W personnel that Rod 47118 had been inverted and subsequently punched in the opposite, or bottom, end plenum area. The four Lot 4 rods were sectioned prior to shipment but all rods appeared satisfactory.

Detailed examinations were performed using a Lenox Model 8700/A stereo-viewer equipped with a Polaroid camera and a magnification of 3.2X. During the examination, each fuel rod was placed on a traversing stage set under the viewer objective lens. A ruled scale attached to the stage indicated the axial location of rod features relative to the rod bottom.

In general, the rods exhibit the typical variation in oxide coloring and normal longitudinal marks induced during removal from the fuel assembly. Slight fretting wear was observed at grid locations on several rods and these areas were not used in the gage sections of the mechanical test specimens. Several large pitted or splatter pit areas were observed and these appeared to be caused by an electrical arc between the cladding and the welding ground clamp when the punch holes for fission-gas removal were welded shut. However, the pitted areas occur at the upper rod ends, above the sections from which mechanical properties test specimens were selected.

Gamma Scanning

The primary objective of gamma scanning was to measure gross gamma activity (> 0.5 MeV) along the length of a fuel rod and to determine fuel column length. The level of activity was to be related to the cladding thermal-neutron exposure and to fuel burnup and used to provide comparative burnup data. Secondarily, fuel-column gaps or areas of unusual gamma activity can be distinguished. See Appendix A for a full description of equipment and procedures.

Point Beach Fuel Rod. The Point Beach Rod A25-06 was gamma scanned to identify the length of cladding over which fuel burnup and neutron fluence were relatively uniform. This rod exhibited no abnormal indications. Average fuel burnup and rod fluence (>1 MeV) were 15,500 MWD/MTU and 2.9×10^{21} n/cm^2, respectively. The gamma profile for the rod was relatively flat (± 5 percent, from 66 to 305 cm as measured from the bottom of the fuel column) and this was the length selected

for sectioning to provide test specimens. The gamma intensity also was about 10 percent lower in the grid regions as compared with that in adjacent regions. The grids were located at 69, 132, 198, and 264 cm.

H. B. Robinson Fuel Rods. The 15 H. B. Robinson fuel rods were gamma scanned to measure the gross gamma activity (> 0.5 MeV) along the length of the rods and thereby provide a relative measure of fuel burnup along the rods. The gamma scans were used to guide sectioning of samples for subsequent hardness, mechanical-property, and transient-burst tests.

The gamma scans were also used to indicate the condition of the fuel pellets and to select fuel samples for burnup determinations. Rod C-8 contained a pellet at 91.1 to 92.4 cm, as measured from the bottom of the fuel stack, with a gamma intensity about 10 percent greater than average. This probably reflects an above-average enrichment for that pellet.

The maximum and minimum relative gamma intensities for 15 rods, from 50 to 290 cm as measured from the bottom of the rod, are given in Table 1. The values do not include the depressed gamma activity levels in the region of the fuel assembly grid spacers or the lower values associated with pellet interfaces. The values show a uniformity of activity over the 50 to 290 cm length. This was the fuel-rod length used for mechanical-property studies.

A reproduction of a typical gamma scan over regions of Rod D-4 is shown in Appendix A, Figure A-1. This shows the upper length of the fuel rod, in the plenum region, and an intermediate portion of the rod. Numerous cracked pellets are evident at the top of the rod. A depressed burnup region in the vicinity of a grid spacer as well as fuel pellet gaps in the fuel column can be seen in the intermediate region of the rod. The fuel stack height, number of fuel pellet gaps, and general comments are given in Table 1. It should be noted that the pellet cracking and gaps were probably not present during irradiation but were produced during fuel transport and handling.

Oconee I Fuel Rods. The Oconee I fuel rods had previously been gamma scanned at the B&W hot cells and the scans provided to BCL as a data package. Therefore, these rods were not gamma scanned at BCL.

TABLE 1. SUMMARY OF GAMMA SCAN OBSERVATIONS FOR H. B. ROBINSON FUEL RODS

Rod	Fuel Stack Height[a], cm	Relative Flat γ Intensity, counts/min Max	Min	No. of Gaps[b] > 0.8 mm	Comments
A-1	364.82	53	52	8	Several large gaps at top end of rod (cracked pellet fragments)
A-8	364.34	55	52	8	--
C-8	364.97	57	55	6	Several large gaps at top end of rod (cracked pellet fragments)
D-4	365.91	55	54	8	
D-9	363.07	58	57	5	--
F-8	365.61	54	53	7	Several large gaps at top end of rod (cracked pellet fragments)
G-8	364.64	56	55	3	--
H-6	364.97	54	53	9	Several large gaps at top end of rod (cracked pellet fragments)
H-10	364.49	54	52	3	--
H-13	362.43	59	56	4	--
K-8	363.55	55	54	2	One large (∿ 5.1 mm) gap at ∿91 cm from bottom of rod
M-12	365.13	56	55	11	--
O-14	363.37	55	54	8	--
P-4	363.22	54	53	8	--
P-8	366.09	55	55	4	Several large gaps at top end of rod (cracked pellet fragments)

(a) Fuel stack height including all gaps.
(b) Interpellet low-activity regions are not considered gaps.

Spiral Profilometry

Spiral profilometry is performed for fuel-rod diametral measurements and for detection and characterization of local cladding anomalies such as blisters, depressions, and ovality. Just prior to loading into the profilometer, each rod is wiped with an acetone-soaked Shurwipe towel to remove loose material. Each rod is scanned in an upward direction from the bottom to the top of the rod at about 2 in./min axial travel of the sensing heads. The nominal chart speed is 3 in./min. See Appendix A for a full description of equipment and procedures.

The major profilometry observations concern ovality of the tubing and cladding creep down, as evidenced by a reduction in average cladding diameter. Typical measurements at preselected positions along the fuel-rod length as well as measurements at the position of maximum cladding ovality are presented in Table 2. Maximum ovality occurred for all rods in the upper 105 to 140 in. of the fuel-rod length and ranged from 10.9 to 19.0 mils. As compared with a nominal preirradiation diameter of 0.4220 in., the average diameter of the irradiated fuel-rod cladding over the central fuel region was about 0.4180 in. Cladding-diameter extremes of 0.4283 and 0.4086 in., representing major and minor axes of cladding ovality, were measured. Both values were measured on Rod H-6. It is noted in a later section of this report that the internal pressure of this rod was less than half that of the remaining rods. A typical portion of an extremely oval section of Rod A-8 is shown in Appendix A, Figure A-2.

Rod A-8 was also profiled without rod rotation, at 0 and 90 degrees with respect to the rod axis, to obtain linear rather than spiral traces. Portions of both the spiral and linear scans are shown in Appendix A, Figure A-3. Several observations were made by comparing the spiral and linear traces. One is that changes in orientation of the major axis of ovality occur by two means, either by simple rotation around the axis of the rod or by going through a minimum in ovality. The other observation is of a fairly regular pulsating ovality, less than 1 mil in size, that overlays the major ovality variations. The significance of this ovality form is unknown.

Maximum ovality occurred in the upper 105 to 140 in. of Rods D-4 and C-8, with maximum ovalities of 18.1 and 14.6 mils, respectively, being recorded. With one exception, maximum ovality for all rods occurred in this region which is also a region of considerable crud deposition. Rod K-8 exhibited relatively uniform ovality and was the only fuel rod in which the maximum ovality (11.0 mils) occurred outside the upper 105 to 140-inch region. The maximum ovality

TABLE 2. SUMMARY OF PROFILOMETRY MEASUREMENTS FOR IRRADIATED H. B. ROBINSON ZIRCALOY FUEL RODS

Rod	Rod Position From Bottom of Fuel Rod, in.	Total Ovality, mils	Rod Diameter, in.		
			Max	Avg	Min
A-1	2	3.1	0.4221	0.4205	0.4190
	36	3.9	0.4194	0.4175	0.4155
	71	4.7	0.4199	0.4176	0.4152
	106	2.7	0.4191	0.4178	0.4164
	134[a]	10.9	0.4255	0.4201	0.4146
	146	0.7	0.4222	0.4219	0.4215
A-8	2	2.5	0.4223	0.4211	0.4198
	36	1.5	0.4181	0.4174	0.4166
	71	4.0	0.4192	0.4172	0.4152
	106	7.8	0.4218	0.4179	0.4140
	125.5[a]	19.0	0.4280	0.4185	0.4090
	146	0.2	0.4220	0.4219	0.4218
D-9	2	0.8	0.4214	0.4210	0.4206
	36	7.3	0.4217	0.4181	0.4144
	71	2.4	0.4188	0.4176	0.4164
	106	8.6	0.4216	0.4173	0.4130
	107.5[a]	16.6	0.4259	0.4176	0.4093
	146	0.8	0.4225	0.4221	0.4217
F-8	2	0.8	0.4204	0.4200	0.4196
	36	2.1	0.4182	0.4172	0.4161
	71	1.7	0.4183	0.4175	0.4166
	106	3.7	0.4192	0.4174	0.4155
	133.6[a]	12.8	0.4269	0.4205	0.4141
	146	1.3	0.4219	0.4213	0.4206
G-8	2	2.5	0.4220	0.4208	0.4195
	36	1.8	0.4191	0.4182	0.4173
	71	1.7	0.4190	0.4182	0.4173
	106	1.2	0.4189	0.4183	0.4177
	124.8[a]	11.6	0.4250	0.4192	0.4134
	137.3[a]	11.6	0.4264	0.4206	0.4148
	146	0.8	0.4226	0.4222	0.4218
H-6	2	4.2	0.4223	0.4202	0.4181
	36	7.9	0.4214	0.4175	0.4135
	71	8.2	0.4217	0.4176	0.4135
	106	13.5	0.4244	0.4177	0.4109
	125.4[a]	18.7	0.4283	0.4180	0.4086
	146	0.6	0.4222	0.4219	0.4216

TABLE 2. (Continued)

Rod	Rod Position From Bottom of Fuel Rod, in.	Total Ovality, mils	Rod Diameter, in.		
			Max	Avg	Min
H-10	2	0.8	0.4219	0.4215	0.4211
	36	7.4	0.4215	0.4178	0.4141
	71	1.8	0.4185	0.4176	0.4167
	106	7.3	0.4209	0.4173	0.4136
	133[a]	12.8	0.4267	0.4203	0.4139
	146	4.7	0.4251	0.4228	0.4204
H-13	2	1.6	0.4204	0.4196	0.4188
	36	4.7	0.4190	0.4167	0.4143
	71	2.2	0.4179	0.4168	0.4157
	106	6.9	0.4205	0.4171	0.4136
	123.3[a]	15.3	0.4253	0.4177	0.4100
	146	0.8	0.4216	0.4212	0.4208
M-12	2	2.7	0.4217	0.4204	0.4190
	36	5.2	0.4200	0.4174	0.4148
	71	3.6	0.4192	0.4174	0.4156
	106	8.9	0.4222	0.4178	0.4133
	127.1[a]	18.8	0.4283	0.4189	0.4095
	146	0.2	0.4217	0.4216	0.4215
O-14	2	2.4	0.4222	0.4210	0.4198
	36	5.5	0.4216	0.4189	0.4161
	71	4.1	0.4201	0.4188	0.4160
	106	5.2	0.4212	0.4186	0.4160
	126*	11.0	0.4248	0.4193	0.4138
	146	0.8	0.4229	0.4225	0.4221
P-4	2	0.6	0.4199	0.4196	0.4193
	36	2.7	0.4181	0.4168	0.4154
	71	1.5	0.4177	0.4170	0.4162
	106	5.6	0.4205	0.4177	0.4149
	137.3[a]	12.7	0.4254	0.4191	0.4127
	146	1.7	0.4214	0.4206	0.4197
P-8	2	2.9	0.4216	0.4202	0.4187
	36	3.8	0.4191	0.4172	0.4153
	71	1.0	0.4178	0.4173	0.4168
	106	8.4	0.4211	0.4169	0.4127
	132.3[a]	11.8	0.4258	0.4199	0.4140
	146	0.8	0.4218	0.4214	0.4210

TABLE 2. (Continued)

Rod	Rod Position From Bottom of Fuel Rod, in.	Total Ovality, mils	Rod Diameter, in.		
			Max	Avg	Min
D-4	2	4.2	0.4210	0.4189	0.4168
	36	4.2	0.4189	0.4168	0.4147
	71	6.4	0.4199	0.4167	0.4135
	106	5.6	0.4200	0.4192	0.4144
	113.0[(a)]	18.1	0.4263	0.4173	0.4082
	146	1.2	0.4217	0.4211	0.4205
C-8	2	4.1	0.4230	0.4211	0.4190
	36	1.1	0.4188	0.4183	0.4177
	71	3.1	0.4200	0.4185	0.4169
	106	7.5	0.4225	0.4188	0.4150
	135.8[(a)]	14.6	0.4270	0.4197	0.4124
	146	2.8	0.4226	0.4212	0.4198
K-8	2[(a)]	3.2	0.4232	0.4216	0.4200
	13	11.0	0.4250	0.4185	0.4130
	36	5.2	0.4197	0.4185	0.4173
	71	5.3	0.4215	0.4189	0.4163
	106	5.3	0.4215	0.4189	0.4162
	146	2.3	0.4240	0.4229	0.4217

(a) Maximum ovality.

for this rod occurred at about 13 in. from the rod bottom. The maximum ovality occurred for K-10, N-8, and O-4 rods at the upper end of the rod from 133 to 135 in. and ranged from 9.3 to 12.6 mils. As compared with a nominal preirradiation diameter of 0.4220 in., the average diameter of the irradiated fuel-rod cladding over the central fuel region was about 0.4180 in. Cladding-diameter extremes of 0.4272 in., representing the major axis of cladding ovality in Rod O-4, and of 0.4175 in., representing the minor axis of cladding ovality in Rod K-10, were measured. A small ridge indication (1 mil) on Rod O-4 at 70.85 in. was verified as being a ridge by visual examination.

A transition area of rapidly changing diameter and ovality was observed on Rod K-10 and, to a lesser extent, on Rod N-8. This area, from about 132 to 134 in. of the rod length, coincides with the change in oxide or crud appearance from a thin oxide with light color to a heavy oxide with dark color. Thus, the profilometry changes, at about 132 to 134 in., appear to reflect a change in diameter caused by a combination of cladding creep down and heavy crud buildup. It might be noted that this upper portion of the fuel-rod cladding is not used for mechanical-properties tests since the fluence is relatively low (< 90 percent of maximum) in this region.

The presence of extreme ovality in many portions of the rods precluded use of these sections in tests such as the expanding mandrel and transient-heating burst where a relatively symmetric test section is desired.

Oconee I Fuel Rods. Spiral profilometer traces were obtained for ten of the Oconee fuel rods for diametral measurements and for detection and characterization of local cladding anomalies such as blisters, depressions, and ovality, if present.

The major profilometry observations concern ovality of the tubing and cladding creep down, as evidenced by a reduction in average cladding diameter. Typical measurements at preselected positions along the fuel-rod length, as well as measurements at the position of maximum cladding ovality, are presented in Table 3. Maximum ovality for the ten rods ranged from 6.3 to 10.7 mils. The average diameter of the irradiated fuel-rod cladding over the central fuel region was about 0.427 in., as compared with a nominal preirradiation diameter of 0.430 in. Cladding-diameter extremes of 0.4339 and 0.4140 in.,

TABLE 3. SUMMARY OF PROFILOMETER MEASUREMENTS FOR IRRADIATED OCONEE 1 (ONE CYCLE) FUEL RODS

Rod	Rod Position From Bottom of Fuel Rod, in.	Total Ovality, mils	Rod Diameter, in.		
			Max	Avg	Min
47010	2	0.7	0.4290	0.4287	0.4283
	22	4.8	0.4290	0.4266	0.4242
	42	5.6	0.4297	0.4269	0.4241
	62	2.9	0.4281	0.4267	0.4252
	82	1.0	0.4275	0.4270	0.4265
	102	2.3	0.4282	0.4271	0.4259
	110*	8.0	0.4312	0.4272	0.4232
	122	0.3	0.4276	0.4275	0.4273
	142	1.4	0.4289	0.4282	0.4275
47015	2	0.9	0.4278	0.4274	0.4269
	22	4.4	0.4289	0.4267	0.4245
	29.5[a]	10.5	0.4323	0.4271	0.4218
	42	6.6	0.4304	0.4271	0.4238
	62	2.2	0.4283	0.4272	0.4261
	82	3.1	0.4292	0.4277	0.4261
	102	3.6	0.4289	0.4271	0.4253
	122	5.0	0.4303	0.4278	0.4253
	142	0.6	0.4287	0.4284	0.4281
47021	3	1.2	0.4292	0.4286	0.4280
	22	5.5	0.4291	0.4264	0.4236
	42	9.1	0.4312	0.4267	0.4221
	62	6.0	0.4294	0.4264	0.4234
	65.5[a]	10.4	0.4318	0.4266	0.4214
	82	4.9	0.4291	0.4267	0.4242
	102	1.3	0.4274	0.4268	0.4261
	122	1.1	0.4275	0.4270	0.4264
	142	2.2	0.4288	0.4277	0.4266
47101	2	1.4	0.4310	0.4303	0.4296
	22	.07	0.4280	0.4277	0.4273
	42	5.1	0.4301	0.4276	0.4250
	62	6.7	0.4309	0.4276	0.4242
	82	4.0	0.4296	0.4276	0.4256
	102	2.0	0.4289	0.4279	0.4269
	122	2.1	0.4291	0.4281	0.4270
	127.5[a]	10.7	0.4339	0.4286	0.4232
	142	4.2	0.4310	0.4289	0.4268

TABLE 3. (Continued)

Rod	Rod Position From Bottom of Fuel Rod, in.	Total Ovality, mils	Rod Diameter, in.		
			Max	Avg	Min
47103	3	1.1	0.4295	0.4290	0.4284
	22	4.4	0.4270	0.4258	0.4246
	39.6[a]	9.8	0.4319	0.4270	0.4221
	42	7.6	0.4307	0.4269	0.4231
	62	5.7	0.4296	0.4268	0.4239
	82	3.4	0.4289	0.4272	0.4255
	102	2.9	0.4286	0.4272	0.4257
	122	6.5	0.4308	0.4276	0.4243
	142	0.7	0.4286	0.4283	0.4279
47104	2	1.4	0.4306	0.4299	0.4292
	22	5.5	0.4302	0.4275	0.4247
	42	8.1	0.4314	0.4274	0.4233
	42.6[a]	9.7	0.4324	0.4276	0.4227
	62	5.6	0.4302	0.4274	0.4246
	82	4.1	0.4297	0.4277	0.4256
	102	6.2	0.4305	0.4274	0.4243
	122	3.1	0.4295	0.4280	0.4264
	142	0.6	0.4292	0.4289	0.4286
47110	2	0.6	0.4297	0.4294	0.4291
	22	5.0	0.4298	0.4273	0.4248
	39.5[a]	6.3	0.4306	0.4275	0.4243
	42	1.3	0.4280	0.4274	0.4267
	62	5.0	0.4299	0.4274	0.4249
	82	2.4	0.4285	0.4273	0.4261
	102	1.2	0.4280	0.4274	0.4268
	122	1.7	0.4286	0.4278	0.4269
	130.2[a]	6.4	0.4311	0.4279	0.4247
	142	1.2	0.4289	0.4283	0.4277
47111	2	0.8	0.4303	0.4299	.4295
	22	1.1	0.4282	0.4277	.4271
	42	3.0	0.4295	0.4280	.4265
	60.5[a]	7.1	0.4322	0.4287	.4251
	62	5.6	0.4309	0.4281	.4253
	82	3.4	0.4300	0.4283	.4266
	102	2.0	0.4294	0.4284	.4274
	122	3.3	0.4303	0.4287	.4270
	142	1.6	0.4299	0.4291	.4283

TABLE 3. (Continued)

Rod	Rod Position From Bottom of Fuel Rod, in.	Total Ovality mils	Rod Diameter, in.		
			Max	Avg	Min
47118	13.2	5.0	0.4288	0.4273	0.4258
	22	4.2	0.4294	0.4273	0.4252
	42	2.4	0.4286	0.4274	0.4262
	62	5.2	0.4300	0.4274	0.4248
	66.1[(a)]	9.8	0.4320	0.4271	0.4222
	82	4.7	0.4295	0.4272	0.4248
	102	1.6	0.4280	0.4272	0.4264
	122	2.0	0.4286	0.4276	0.4266
	142	1.0	0.4290	0.4285	0.4280
47125	2	0.9	0.4297	0.4293	0.4288
	22	2.3	0.4278	0.4267	0.4255
	42	3.0	0.4281	0.4266	0.4251
	62	2.2	0.4278	0.4267	0.4256
	82	3.7	0.4285	0.4267	0.4248
	102	3.0	0.4286	0.4271	0.4256
	122	5.0	0.4296	0.4271	0.4246
	130[(a)]	10.3	0.4320	0.4269	0.4217
	142	1.5	0.4289	0.4282	0.4274

(a) Maximum ovality for a given rod.

representing major and minor axes of cladding ovality, were measured. The extreme major axis occurred on Rod 47101 and the extreme minor axis on Rod 47021.

Rods 47015 and 47103 were also profiled without rod rotation, at 0, 60, and 120-degree orientation with respect to the rod axis, to obtain linear rather than spiral traces.

Eddy-Current Testing

Rods are inspected in eddy-current systems designed to detect a wide variety of defects and anomalies that can occur in fuel rods during service. Two types of systems can be used: a single frequency, encircling coil system and a two-frequency probe coil system.

The encircling-coil system uses both in-phase and quadrature phase-sensitive detectors. The signal outputs or readouts indicate relatively gradual variations in electrical properties over the length of the fuel rod as well as the abrupt changes in signals caused by certain defects. The system employs a electronic-signal differentiation to accentuate the signals caused by defects such as small holes, short cracks, and pitted areas. These three readouts used in combination help identify defects and provide interpretation of the signal indications.

The probe coil system is employed for the detailed examination of potential defect areas identified by the encircling-coil system. This system, through the use of a two-frequency electronic system, has the potential for reducing unwanted "noise" signals and, because it interrogates a smaller cladding-material volume, offers improved sensitivity in the detection and location of small defects. The system instrumentation separates and records the voltage output from each of two exciting frequencies (100 and 700 kHz). A third recorded output is a summation of the output signals from the two output-signal detectors. This signal combination enhances the defect signals while minimizing signals caused by unwanted variables (e.g., probe wobble, ridging, etc.). A fourth channel provides a differential signal of the third-channel output and is used as an indicator of abrupt signal changes associated with defects such as pits and cracks.

See Appendix A for a full description of equipment and procedures.

H.B. Robinson Fuel Rods. All the H.B. Robinson fuel rods were inspected using the encircling coil eddy-current system.

Only one fuel rod (P-4) provided an eddy-current signal response that could be considered to be caused by a defect. The eddy-current scan on this rod indicated a relatively long anomaly located in the fuel cladding about 213 cm from the bottom of the rod. The anomaly appeared to cover about 7.6 cm along the length of the rod in this area. This relatively gradual signal indication was not observed on fuel rods very frequently and was much different from the abrupt indication caused by pits, holes, and internal hydride cracking in the cladding between the fuel pellets. However, the relatively strong signal voltage in the horizontal output suggested that the defect was on the ID of the cladding. This section of cladding was not used as a test section specimen.

Rod K-10 exhibited an eddy-current indication at 80 cm from the rod bottom which correlated well with a gap in the fuel column, as indicated by the gamma scan. Rod N-3 exhibited eddy-current indications at 61 and 79 cm which also corresponded to fuel-column gaps detected in the gamma scan. Rod O-4 exhibited an eddy-current indication at 79 cm, although no correlation with gamma scan or profilometry data was possible. This may indicate a defect region.

All three rods showed eddy-current indications in the region of 335 to 340 cm. These indications are believed to be caused by the increase in rod diameter and oxide or crud deposits in this region.

The eddy-current results, in conjunction with the other characterization data, were used to determine the suitability of fuel rods or rod sections for mechanical-properties evaluation tests. Sections of cladding that have eddy-current indications were not used as test-section specimens.

Oconee I Fuel Rods. All ten rods of Lot 2 (Oconee I, one cycle) were inspected using the encircling coil and probe coil eddy-current systems described above.

Only three fuel rods provided encircling-coil eddy-current signal responses that could potentially be considered to be caused by defects. The indications occurred at 120, 122, and 125.5 cm from the bottom of Rod 47105; at 100.7, 124.7, 139.4, and 163.1 cm from the bottom of Rod 47104; and at 110.8, 112.1, and 125.4 cm from the bottom of Rod 47118.

Subsequent probe coil eddy-current examinations were made at 45-degree intervals around these three rods. Initial evaluation suggested that the indications were caused by a fission-product buildup on the internal circumference. Therefore, eddy-current testing of Lots 3 and 4 cladding material was eliminated because very little definitive information was produced by the scans.

Material Characterization (DT Testing)

The destructive (DT) characterization of the fuel-rod cladding involves plenum punch and gas collection, burnup analysis, fluence determination, microhardness testing, metallographic examination, and annealing of cladding. A full description of the equipment and procedures for all the destructive characterizations is included in Appendix B.

Plenum Punch and Gas Collection

The purpose of plenum punch and gas collection is to determine the fuel-rod void volume and to collect the rod internal gases for isotopic analysis. See Appendix B for a full description of equipment and procedures.

H. B. Robinson Fuel Rods. Plenum-gas collection procedures are described in Appendix B. Briefly, the rod is sealed in a leaktight punch system, evacuated, and punched, and the gas is allowed to expand into a calibrated volume. The pressure in this volume is measured with a

sensitive Wallace-Tiernan pressure gage, and the gas quantity is calculated from the ideal gas law. The gas is then expanded a second time into a calibrated volume for a second measurement. The rod gas is collected in two vials; one is sent for analysis using a mass spectrometer and the other is stored as a reserve if additional analysis is required. The quantity of gas at STP and the rod internal pressure at 0 C are given in Table 4. Also shown are the void volumes determined by expanding a known volume of gas into the evacuated rod. Helium at 0.55 MPa is utilized to assure complete filling of the rod internal volume. Ten measurements are made to establish a highly accurate value for the void volume. Table 5 shows the mass-spectrometer analytical results for the gas constituents and Table 6 gives the krypton and xenon isotopic analysis results for Rods K-10, N-8, and O-4. The oxygen, nitrogen, and argon detected in Rod N-8 are assumed to have been introduced by air leakage into the vial during collection.

The internal gas pressures ranged from about 1.38 to 1.53 MPa, as calculated at 0 C, except for Rod H-6 where the pressure was less than half that for the other rods. The reason for this low pressure is unknown. Pressures in the rods at operating temperature are estimated to have been on the order of 3.45 MPa.

Oconee I Fuel Rods. All the Oconee I fuel Rods used in this program were plenum punched and the gases collected at the B&W hot cells. Therefore, no additional work was performed at BCL.

Burnup Analysis

Burnup analysis was performed by the mass-spectrometric neodymium-148 method[2] to determine the total fission of heavy-element atoms.

The results of the burnup analysis for Rod P-8 are given in Table 7. See Appendix B for a full description of equipment and procedures.

Fluence Determination

Cladding samples in the form of rings were sectioned from the irradiated fuel rods for analysis and for determination of fast-neutron flux and fluence. Prior to analysis, the cladding samples were mechanically

defueled and then cleaned in nitric acid to remove any adhering fuel. They werefurther cleaned in boiling hydrochloric acid for corrosion-product removal. The samples were chemically analyzed for iron content and radiochemically analyzed for Mn-54 activity. The fast-neutron flux wasthen calculated from the Fe-54 (n,p) Mn-54 reaction[3]. See Appendix B for a full description of equipment and procedures.

TABLE 4. H. B. ROBINSON FUEL ROD PLENUM-GAS RESULTS

Rod	Gas Quantity, cm^3 (STP) 1st Expansion	2nd Expansion	Rod Void Volume, cm^3	Internal Gas Pressure at 0 C, MPa
P-8	387.9	387.4	24.52 ± 0.13	1.54
H-10	355.2	355.0	24.67 ± 0.21	1.41
F-8	355.7	355.4	22.73 ± 0.15	1.53
P-4	378.4	377.8	24.17 ± 0.20	1.53
H-13	361.2	360.6	25.04 ± 0.21	1.41
M-12	377.8	376.9	25.30 ± 0.17	1.46
O-14	374.0	373.2	24.56 ± 0.20	1.49
H-6	160.8	160.8	26.34 ± 0.17	0.60
D-9	354.6	353.7	24.98 ± 0.16	1.39
G-8	372.9	372.1	23.52 ± 0.22	1.55
A-8	359.4	358.2	24.98 ± 0.12	1.40
A-1	386.4	385.1	26.14 ± 0.14	1.44
K-10	360.45	359.86	25.35 ± 0.20	1.44
N-8	363.13	362.10	24.34 ± 0.18	1.51
O-4	369.67	367.94	24.50 ± 0.14	1.53
K-8	387.6	377.9	25.23 ± 0.18	1.52
C-8	384.6	374.5	24.11 ± 0.16	1.57
D-4	369.9	369.9	27.16 ± 0.21	1.38

TABLE 5. H. B. ROBINSON FUEL ROD PLENUM-GAS ANALYSIS, PERCENT

Rod	H_2	He	CH_4	H_2O	O_2	N_2	Ar	CO_2	Kr	Xe	Xe/Kr
K-10	<0.01	98.1	<0.01	<0.1	<0.01	0.09	0.72	<0.01	0.12	0.97	8.08
N-8	<0.01	96.5	<0.01	<0.1	0.18	0.74	1.39	<0.01	0.13	1.09	8.38
0-4	<0.01	90.6	<0.01	<0.1	<0.01	0.09	0.33	<0.01	0.10	0.81	8.10

TABLE 6. H. B. ROBINSON FUEL ROD PLENUM-GAS KRYPTON AND XENON ISOTOPIC ANALYSIS, PERCENT

Rod	Krypton				Xenon			
	83	84	85	86	131	132	134	136
K-10	13.1	31.9	5.11	49.9	8.73	20.4	29.7	41.2
N-8	12.4	31.9	5.78	49.9	8.63	20.9	28.4	42.1
0-4	13.1	30.2	6.61	50.1	8.74	20.8	28.5	42.0

TABLE 7. BURNUP RESULTS FOR IRRADIATED H. B. ROBINSON FUEL ROD P-8

Specimen	Burnup		Relative Gamma Scan Intensity(GSI)	MWD/GSI
	F_T, atom percent	MWD/MTU		
1	2.559	24,570	43.5	565
2	3.221	30,920	54.5	567
3	2.877	27,620	48.5	569
			Avg	567

H. B. Robinson Fuel Rods. Three Zircaloy cladding rings were used for fast-neutron dosimetry analysis of H. B. Robinson Rod P-8. The cladding rings enclosed the fuel submitted for fuel-burnup analysis. The burnup results are reported in Table 7.

The samples were taken from three regions of interest along the rod. Sample 1 was taken from the bottom of the rod in a low-flux region, Sample 2 from the center of the rod in a region of unperturbed flux, and Sample 3 from a grid spacer region. The fluence was 3.8×10^{21} n/cm^2 for Sample 1, 4.4×10^{21} n/cm^2 for Sample 2, and 4.3×10^{21} n/cm^2 for Sample 3. As expected, burnup was depressed in the region of grids as well as at the bottom of the fuel rod. The fast fluence, on the other hand, showed a negligible influence of the grid and a lesser reduction at the bottom of the rod.

Oconee I Fuel Rods. Similar samples of Zircaloy cladding rings were used for fast-neutron dosimetry analysis of Oconee I one-cycle, two-cycle, and three-cycle fuel rods. For the Oconee I, one-cycle rods, the fluence was 1.8×10^{21} n/cm^2 for Sample 1, 1.6×10^{21} n/cm^2 for Sample 2, and 1.6×10^{21} n/cm^2 for Sample 3. For the Oconee I two-cycle rods, the fluence was 3.8×10^{21} n/cm^2 for Sample 1, 4.1×10^{21} n/cm^2 for Sample 2, and 4.0×10^{21} n/cm^2 for Sample 3. For the Oconee I three-cycle rods, the fluence was 4.5×10^{21} n/cm^2 for Sample 1, 5.0×10^{21} n/cm^2 for Sample 2, and 3.9×10^{21} n/cm^2 for Sample 3.

Microhardness Tests

The purpose of microhardness measurements is to determine average hardness or hardness gradients of irradiated materials. See Appendix B for a full description of equipment and procedures.

Point Beach Rod. Irradiated samples for microhardness tests were sectioned from the rod using a water-cooled abrasive cutoff wheel. The section of rod from 104 to 160 cm, as measured from the bottom of the rod, was cut into four sections, each approximately 15 cm in length. The fuel was removed from the four sections by tapping the ends of each specimen and then pressing the fuel out using an aluminum mandrel. The sections were then cut into 43 approximately 1.3-cm-long rings.

Rings 4, 10, 22, 28, 34, and 40 were split longitudinally using a jewelers saw. One-half of each ring (except for Ring 22, which was

cut to obtain two quarters) was then mounted as a transverse specimen, ground and polished, and then tested using a Tukon microhardness tester with a diamond indenter and a 1-kg load. Tests were made with the indenter axis oriented both parallel and perpendicular to the tube radius and five indents were made at each orientation (see Figure 1). The results are tabulated in Table 8. The second, third, and fourth Knoop Hardness Numbers were averaged to reduce the effect of readings taken near the inner and outer edges (Readings 1 and 5). The remaining half rings of specimens 4, 10, 16, 28, 34, and 40 were retained for annealing and subsequent microhardness tests.

The half ring of Specimen 22 was mounted as a longitudinal specimen. Five microhardness indents were made both parallel and perpendicular to the longitudinal axis and the results are given in Table 8.

The specimens were annealed isothermally, removed, and mounted in a Bakelite metallographic mount, ground and polished, and then tested as described above. The results for these specimens are given in Table 9. In general, the five hardness impressions mentioned above were made in such a manner as to traverse the cladding width, as shown in Figure 1. The outer readings were observed to show edge effects. Consequently, only the three inner readings have been used to obtain the average values given in Table 9. The range of hardness values is also indicated.

Within the limits of reproducibility, no change in hardness was produced by annealing for up to 1 hr at 371 C and only a slight change was reproduced at 454 C. However, at 538 and 621 C, noticeable step decreases in hardness occurred. A further temperature increase to 704 C caused no additional decrease in hardness. Thus, annealing of irradiation damage appeared to be limited to a temperature range between 454 and 621 C.

Surprisingly, no influence of time at temperature on annealing of hardness was evident. This may be indicative of defects of varying stability that are annihilated by diffusion over relatively short diffusion paths.

Knoop hardness data for both isothermally and transient annealed specimens from Point Beach Rod A25-06 are given in Tables 10 and 11. These data were obtained by making the hardness indents both parallel and perpendicular to the tubing radius. While the hardness values appear to show some differences, depending upon the

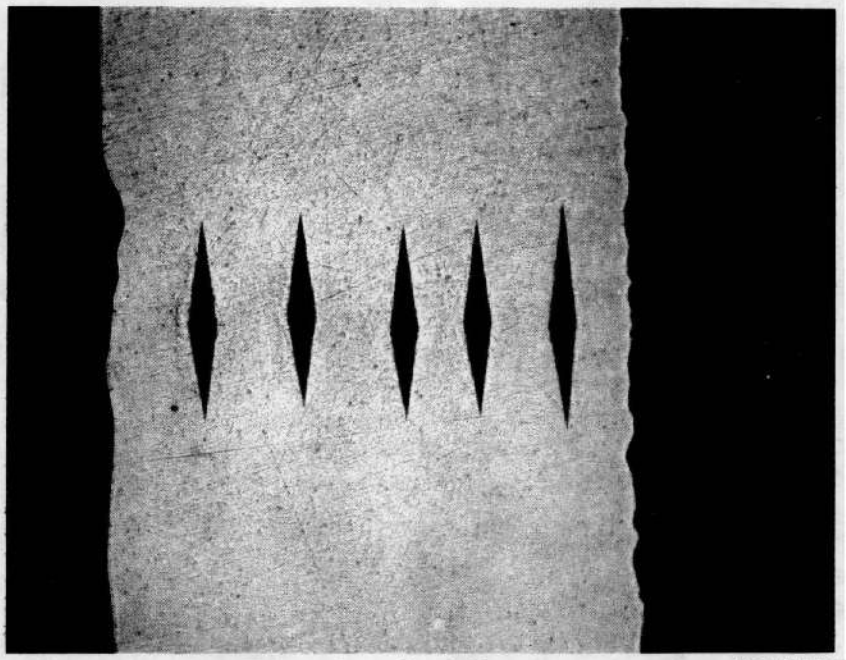

X353 Sample 23A HC41540

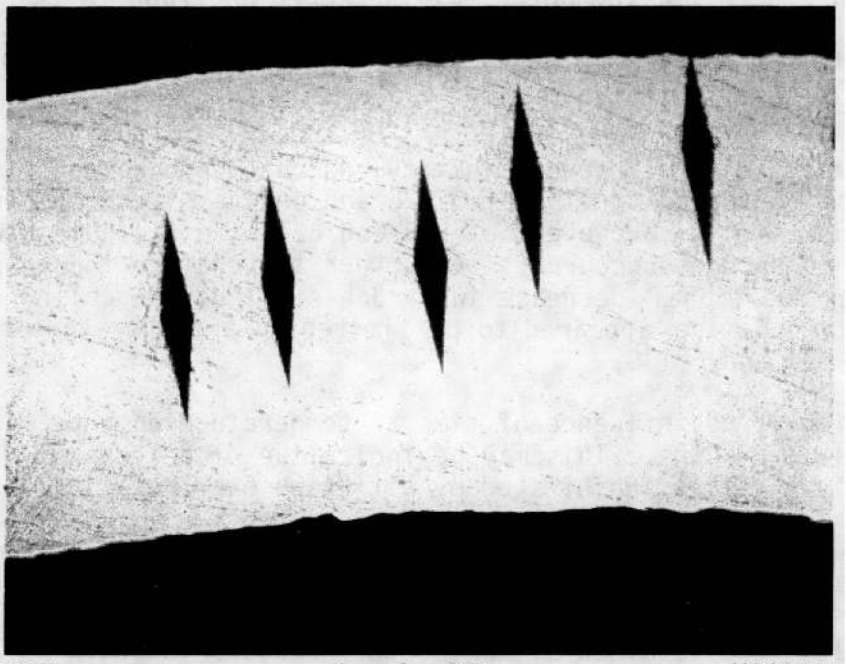

X352 Sample 23B HC41544

FIGURE 1. KNOOP MICROHARDNESS INDENTS (100 X) FOR IRRADIATED POINT BEACH FUEL ROD A25-06

TABLE 8. HARDNESS OF IRRADIATED POINT BEACH FUEL ROD A25-06, 1-KG LOAD

Specimen	Knoop Hardness Number					
	Indent Parallel to Radius	Indent Perpendicular to Radius	Indent Parallel to Axis		Indent Perpendicular to Axis	
A25-06 4	263.7	235.5				
4	231.3	251.6				
4	227.5	264.4				
4	235.5	258.8				
4	228.6	210.0				
10	232.3	213.5				
10	239.4	264.9				
10	223.2	260.3				
10	233.2	267.2				
10	230.4	192.6				
16	267.9	242.6				
16	266.2	267.8				
16	261.0	262.6				
16	262.1	261.0				
16	248.1	216.8				
22	218.5	264.4	157.8	264.4	254.4	243.4
22	270.1	262.4	296.2	284.1	255.9	253.7
22	281.6	261.7	305.0	290.8	261.0	246.0
22	270.8	263.9	290.0	284.1	243.0	242.0
22	245.0	263.9	272.5	261.7	250.1	252.3
28	253.7	227.7				
28	255.5	269.0				
28	265.5	254.4				
28	263.2	256.6				
28	269.0	207.3				
34	252.3	169.4				
34	243.4	254.4				
34	253.3	271.8				
34	253.3	264.9				
34	244.0	244.0				
40	253.3	225.0				
40	249.1	270.2				
40	250.8	271.8				
40	268.5	278.1				
40	257.7	219.1				

TABLE 9. HARDNESS OF IRRADIATED POINT BEACH ROD A25-06, 1-KG LOAD

Specimen	Annealing		Knoop Hardness Number	
	Temperature, C	Time, min	Indent Parallel to Radius	Indent Perpendicular to Radius
27	371	2	270 $^{+4}_{-4}$	257 $^{+3}_{-3}$
13	371	10	251 $^{+5}_{-6}$	258 $^{+2}_{-1}$
33	371	30	234 $^{+10}_{-7}$	257 $^{+7}_{-9}$
29	371	60	255 $^{+4}_{-7}$	249 $^{+5}_{-0}$
12	454	2	250 $^{+7}_{-8}$	223 $^{+4}_{-3}$
20	454	10	249 $^{+9}_{-8}$	237 $^{+3}_{-3}$
31	454	30	243 $^{+6}_{-7}$	217 $^{+4}_{-3}$
41	454	60	243 $^{+9}_{-6}$	224 $^{+4}_{-8}$
4	538	1/2	208 $^{+3}_{-3}$	205 $^{+3}_{-3}$
6	538	1	210 $^{+1}_{-1}$	215 $^{+1}_{-1}$
21	538	2	206 $^{+4}_{-5}$	207 $^{+3}_{-3}$
25	538	10	206 $^{+4}_{-5}$	215 $^{+1}_{-1}$
26	538	30	205 $^{+5}_{-3}$	205 $^{+4}_{-4}$
10	621	1/4	168 $^{+0}_{-0}$	178 $^{+0}_{-0}$

TABLE 9. (Continued)

Specimen	Annealing Temperature, C	Annealing Time, min	Knoop Hardness Number Indent Parallel to Radius	Knoop Hardness Number Indent Perpendicular to Radius
16	621	1/2	174 $^{+1}_{-1}$	184 $^{+1}_{-2}$
36	621	1	168 $^{+4}_{-4}$	179 $^{+5}_{-6}$
38	621	10	171 $^{+3}_{-2}$	181 $^{+4}_{-4}$
28	704	1/4	166 $^{+6}_{-2}$	179 $^{+1}_{-2}$
35B	704	1/2	171 $^{+6}_{-5}$	186 $^{+3}_{-2}$
5	704	1	174 $^{+6}_{-4}$	178 $^{+4}_{-6}$
19	704	10	172 $^{+3}_{-1}$	178 $^{+4}_{-4}$
23B	704	30	177 $^{+2}_{-3}$	181 $^{+5}_{-4}$

TABLE 10. HARDNESS OF IRRADIATED AND ISOTHERMALLY ANNEALED ZIRCALOY CLADDING (POINT BEACH ROD A25-06) 1-KG LOAD

Specimen	Annealing Temperature, C	Annealing Time, min	Knoop Hardness Number Indent Parallel to Radius	Knoop Hardness Number Indent Perpendicular to Radius
4A	As irradiated		230 $^{+5}_{-3}$	258 $^{+6}_{-7}$
10A	As irradiated		232 $^{+7}_{-9}$	264 $^{+3}_{-4}$
16A	As irradiated		264 $^{+4}_{-3}$	264 $^{+4}_{-3}$
22	As irradiated		274 $^{+7}_{-4}$	263 $^{+1}_{-2}$
28	As irradiated		261 $^{+8}_{-8}$	260 $^{+9}_{-6}$
34	As irradiated		249 $^{+4}_{-6}$	264 $^{+8}_{-10}$
40	As irradiated		256 $^{+12}_{-7}$	273 $^{+5}_{-3}$
27	371	2	270 $^{+4}_{-4}$	257 $^{+3}_{-3}$
13	371	10	251 $^{+5}_{-6}$	258 $^{+2}_{-1}$
33	371	30	234 $^{+10}_{-7}$	257 $^{+7}_{-9}$
29	371	60	255 $^{+4}_{-7}$	249 $^{+5}_{-0}$
12	454	2	250 $^{+7}_{-8}$	231 $^{+4}_{-4}$
20	454	10	249 $^{+9}_{-8}$	237 $^{+3}_{-3}$
31	454	30	243 $^{+6}_{-7}$	221 $^{+3}_{-2}$
41	454	60	243 $^{+9}_{-6}$	224 $^{+4}_{-8}$
34A	482	1/2	221 $^{+4}_{-5}$	230 $^{+3}_{-2}$
36A	482	5	222 $^{+3}_{-3}$	233 $^{+4}_{-5}$
40A	482	30	204 $^{+3}_{-3}$	216 $^{+2}_{-2}$

TABLE 10. (Continued)

Specimen	Annealing		Knoop Hardness Number	
	Temperature, C	Time, min	Indent Parallel to Radius	Indent Perpendicular to Radius
38A	510	1/2	216^{+3}_{-4}	228^{+0}_{-0}
25A	510	5	221^{+4}_{-7}	226^{+5}_{-6}
26A	510	30	208^{+1}_{-1}	216^{+1}_{-1}
4	538	1/2	208^{+3}_{-3}	205^{+3}_{-3}
6	538	1	210^{+1}_{-1}	215^{+1}_{-1}
21	538	2	206^{+4}_{-5}	207^{+3}_{-3}
25	538	10	206^{+4}_{-5}	215^{+1}_{-1}
26	538	30	205^{+5}_{-3}	205^{+4}_{-4}
10	621	1/4	168^{+0}_{-0}	178^{+0}_{-0}
16	621	1/2	174^{+1}_{-1}	184^{+1}_{-2}
36	621	1	168^{+4}_{-4}	179^{+5}_{-6}
38	621	10	171^{+3}_{-2}	181^{+4}_{-4}
28	704	1/4	166^{+6}_{-2}	179^{+1}_{-2}
35B	704	1/2	171^{+6}_{-5}	186^{+3}_{-2}
5	704	1	174^{+6}_{-4}	178^{+4}_{-6}
19	704	10	172^{+3}_{-1}	178^{+4}_{-4}
23B	704	30	177^{+2}_{-3}	181^{+5}_{-4}

TABLE 11. HARDNESS OF IRRADIATED AND TRANSIENT ANNEALED ZIRCALOY CLADDING (POINT BEACH ROD A25-06) 1-KG LOAD

Specimen	Heating Rate, C/sec	Maximum Temperature	Knoop Hardness Number	
			Indent Parallel to Radius	Indent Perpendicular to Radius
33A	14	538	245^{+6}_{-4}	242^{+4}_{-4}
1	5.6	538	228^{+3}_{-2}	241^{+2}_{-1}
20A	5.6	510	246^{+3}_{-3}	243^{+2}_{-1}
29A	0.56	538	218^{+3}_{-3}	221^{+2}_{-1}
21A	0.56	510	222^{+0}_{-1}	224^{+2}_{-2}
27A	0.56	482	230^{+4}_{-2}	236^{+4}_{-3}
31A	0.11	510	230^{+3}_{-3}	233^{+4}_{-3}
41A	0.11	482	$233^{+2}_{=2}$	229^{+4}_{-2}

orientation of the hardness indent, the qualitative results and conclusions are independent of orientation.

Annealing of hardness began at a temperature between 371 and 454 C and was complete at 621 C; no further change occurred when the annealing temperature was increased to 704 C. Metallography examination described later, showed that the Zircaloy had recrystallized at 621 and 704 C, but not at 538 C.

The transient annealing data showed a fairly pronounced dependence on heating rate as well as the maximum temperature reached during the transient anneal. The greatest changes in hardness appeared to occur at a heating rate between 5.6 and 0.56 C/sec.

H. B. Robinson Fuel Rods. In the course of transport of the H. B. Robinson reactor subassembly to INEL and its subsequent transfer from the shipping cask to hot cells for disassembly to recover the fuel rods, heating of the fuel rods is known to have occurred. The shipping cask was only half filled with water during shipment and the assembly was subsequently held in the vertical position for a number of hours, a position that provides poor convective cooling, prior to being placed in the cooling pond at INEL. This history raised concern that sufficient heating may have occurred to cause annealing of irradiation damage in the Zircaloy cladding. The possible temperature rise to as high as 465 C was estimated at INEL, based on gamma heat generation in the fuel and convective cooling of the assembly by air.

To determine whether annealing had occurred, hardness and tensile test measurements were performed to provide evidence for or against such annealing. The hardness measurements were made on rods from the extremities of the envelope within the subassembly from which the rods at BCL had been selected as well as from specimens within this envelope. This was done because the rods were shipped in a horizontal position and the side or corner of the assembly could have been out of water during shipment. To investigate possible annealing along the length of the rod, specimens were taken from various axial positions for hardness measurements. In addition, specimens were taken from Rod P-8 in the lower and upper half and at the rod midplane for tensile tests.

The hardness results are given in Table 12. No significant variation either between rods or with position along the length of the rods is evident.

TABLE 12. HARDNESS OF AS-RECEIVED, AS-IRRADIATED ZIRCALOY CLADDING (H. B. ROBINSON RODS) 1-KG LOAD

Rod	Location, cm	Mount	Knoop Hardness Number: Indent Parallel to Radius		Knoop Hardness Number: Indent Perpendicular to Radius	
A-1	41	X401	253 $^{+4}_{-4}$		243 $^{+6}_{-2}$	
	89	X398	250 $^{+1}_{-1}$		249 $^{+2}_{-2}$	
	178	X399	240 $^{+1}_{-1}$		240 $^{+1}_{-1}$	
	267	X396	250 $^{+1}_{-1}$		258 $^{+2}_{-1}$	
	320	X397	249 $^{+3}_{-2}$	Avg 248	246 $^{+5}_{-5}$	Avg 247
A-8	41	X403	240 $^{+5}_{-5}$		248 $^{+3}_{-3}$	
	89	X394	242 $^{+1}_{-1}$		263 $^{+1}_{-1}$	
	178	X408	253 $^{+0}_{-0}$		253 $^{+0}_{-1}$	
	267	X409	239 $^{+0}_{-0}$		252 $^{+1}_{-1}$	
	320	X395	246 $^{+1}_{-1}$	Avg 244	256 $^{+8}_{-5}$	Avg 254
O-14	41	X400	259 $^{+1}_{-1}$		264 $^{+0}_{-2}$	
	89	X390	245 $^{+2}_{-2}$		250 $^{+3}_{-3}$	
	178	X392	244 $^{+1}_{-1}$		239 $^{+0}_{-0}$	
	267	X391	240 $^{+3}_{-3}$		247 $^{+2}_{-2}$	
	320	X393	246 $^{+1}_{-1}$	Avg 247	253 $^{+2}_{-4}$	Avg 251

TABLE 12. (Continued)

Rod	Location, cm	Mount	Knoop Hardness Number: Indent Parallel to Radius	Knoop Hardness Number: Indent Perpendicular to Radius
P-4	41	X402	251 $^{+2}_{-2}$	264 $^{+3}_{-2}$
	89	X404	237 $^{+2}_{-2}$	240 $^{+3}_{-3}$
	178	X406	236 $^{+3}_{-3}$	244 $^{+1}_{-1}$
	267	X407	240 $^{+5}_{-5}$	245 $^{+4}_{-4}$
	320	X405	244 $^{+0}_{-1}$ Avg 242	242 $^{+1}_{-1}$ Avg 247
P-8	41	X380	243 $^{+2}_{-2}$	261 $^{+3}_{-1}$
	93	X381	261 $^{+1}_{-1}$	268 $^{+1}_{-2}$
	178	X382	272 $^{+2}_{-2}$	262 $^{+1}_{-1}$
	236	X383	242 $^{+2}_{-1}$	260 $^{-1}_{-0}$
	267	X384	253 $^{+2}_{-2}$ Avg 254	261 $^{+3}_{-2}$ Avg 262
H-10	41	X385	270 $^{+3}_{-1}$	256 $^{+0}_{-1}$
	89	X386	253 $^{+0}_{-2}$	250 $^{+3}_{-3}$
	178	X387	253 $^{+1}_{-2}$	252 $^{+1}_{-1}$
	267	X388	241 $^{+2}_{-2}$	250 $^{+1}_{-1}$
	320	X389	250 $^{+2}_{-2}$ Avg 253	238 $^{+1}_{-1}$ Avg 249

Previous hardness data indicated that the Knoop hardness decreased significantly during the first 30 seconds of an isothermal at or above 482 C. Consequently, a series of anneals were carried out in which specimens for hardness measurement were heated to the isothermal annealing temperature at a rate of 5.6 C/sec and then were held at that temperature for times of 0 (a transient only), 5 seconds 15 seconds and 30 seconds.

The average as-irradiated Knoop hardness for Zircaloy tubing from Rod P-8 was 254, as measured on a cross section with the indent parallel to the radius, and 262 for the indent perpendicular to the radius. Samples 30, 31, 32A, and 33 were taken from Rod P-8 and annealed as described above. The results are given in Table 13. While the data from indents made perpendicular to the tube radius showed a slight decrease in hardness with increase in time at 538 C, the indents made parallel to the tube radius suggested that the hardness change had equilibrated as soon as the 538 C temperature was attained. The hardness change, therefore, is independent of time at temperature, at least under the heating conditions employed for these specimens.

TABLE 13. KNOOP HARDNESS OF SPECIMENS FROM ROD P-8 ANNEALED AT 538 C AFTER A 5.6 C/SEC TRANSIENT TO 538 C

Specimen	Time at 538 C, sec	Knoop Hardness Number, 1-kg Load	
		Indent Parallel to Radius	Indent Perpendicular to Radius
--	As irradiated	254	262
30	0	216 ± 4	237 ± 6
31	5	220 ± 5	228 ± 0
32A	15	209 ± 1	230 ± 1
33	30	218 ± 1	221 ± 1

Hardness data obtained by heating to the annealing temperature at 5.6 C/sec are given in Table 14. Only at 482 C is a time dependence for recovery evident but a possible time dependence is noted at 704 C. However, at the higher temperature,annealing is occurring in the recrystallization range so that hardness changes are not simply related to annealing of irradiation damage.

The effect of heating in a transient to maximum temperatures between 482 and 704 C at various heating rates is shown in Figure 2. It is

difficult to identify any effect of heating rate on hardness and, furthermore, hardness in a transient did not change consistently with temperature for a given heating rate. Nevertheless, there was a general trend in the data that was independent of heating rate, consisting notably, of an increase in hardness at 482 C followed by a gradual decrease in hardness as the temperature was increased further. The characteristics were typical of an aging process. The fact that heating rate did not influence the results was consistent with the previous observation of the general time independence of annealing of irradiation damage.

TABLE 14. HARNDESS CHANGE[(a)] WITH ANNEALING FOR IRRADIATED H.B. ROBINSON ZIRCALOY CLADDING (Heating Rate, 5.6 C/sec)

Annealing Temperature, C	Knoop Hardness Number After Indicated Time at Temperature, sec				
	0	5	15	30	300
482	266	249	239	220	211
538	232	234	247	--	--
593	220	221	202	--	202
621	235	226	226	--	--
704	205	179	180	--	--

(a) Initial hardness ~250 KHN.

Oconee I Fuel Rods. Because the microhardness yielded no conclusive data about the Zircaloy texture and little comparison data were obtained, the microhardness tests were deleted from this program. Therefore, no microhardness data were obtained for the Oconee I fuel rods.

Metallography Examination

The purpose of metallographic examination is to characterize the optically resolvable microstructural features of fuel and cladding.

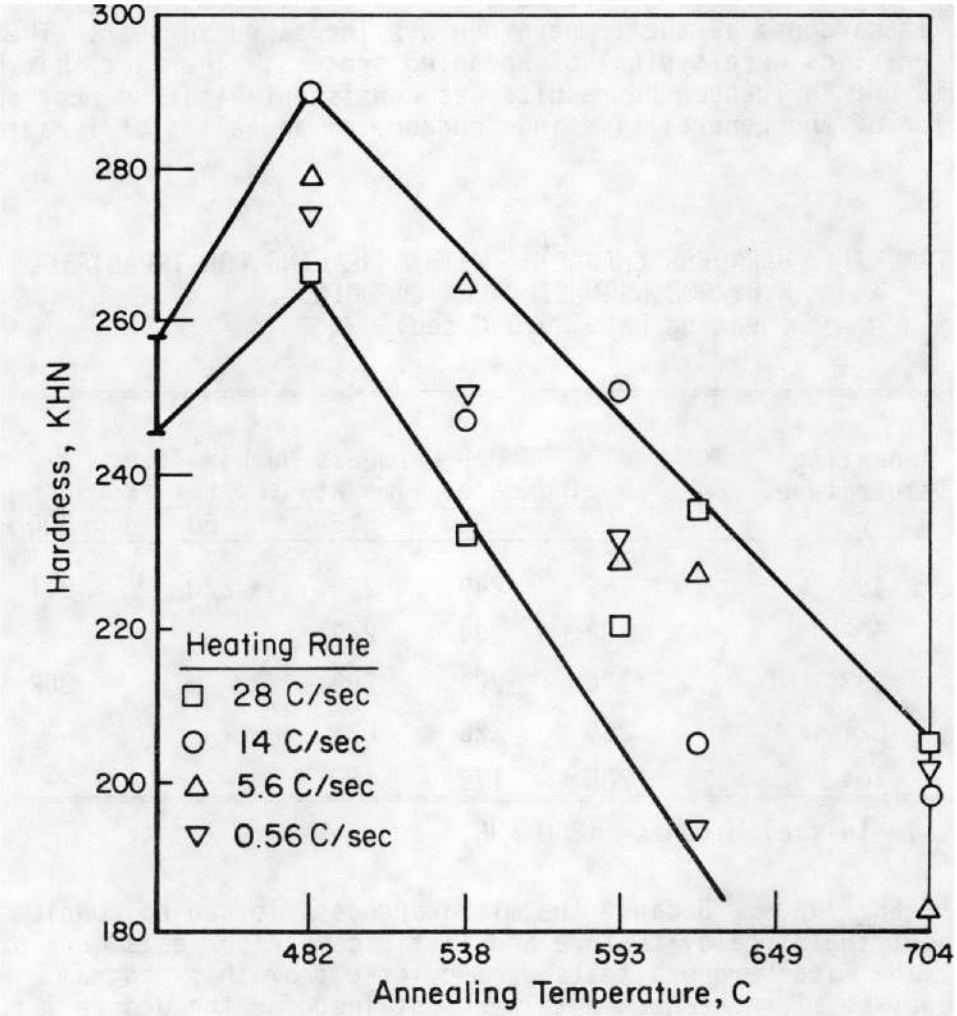

FIGURE 2. EFFECT ON HARDNESS OF TRANSIENT HEATING (ZERO HOLD TIME AT TEMPERATURE) TO THE MAXIMUM ANNEALING TEMPERATURE INDICATED FOR IRRADIATED H.B. ROBINSON FUEL ROD P-8

This includes, but is not limited to:

- Clad corrosion products
- Crud deposits
- Clad hydride formation and orientation
- Fuel-cladding interaction
- Fuel grain size
- Fuel porosity size and distribution.

See Appendix B for a full description of equipment and procedures.

Point Beach Fuel Rod. Cladding samples from Rod A25-06 were sectioned for metallographic examination. Speciman A was sectioned at a position 161.3 to 163.2 cm from the bottom of the rod and mounted as a transverse metallographic sample. Specimen B was sectioned from the rod at a position 164.5 to 165.1 cm from the bottom and mounted as a longitudinal metallographic sample. Also, photomicrographs were taken of typical cladding cross-sectional areas in the etched condition under bright field and polarized light (see Figures 3 and 4).

The grains were elongated in the longitudinal direction and nonequiaxed but uniform in size in the transverse direction. No crud was observed on these samples but a uniform oxide of approximately 2.5 microns was noted on the clad outside diameter. The oxide on the inside diameter varied from essentially zero near the pellet ends, increasing to a maximum of 7 microns near the middle of the fuel pellet. The hydrides, which were seen in both the bright field and polarized light photomicrographs of the etched samples, are relatively random in the transverse sample and uniformly stringered in the longitudinal sample. The hydrides are believed to have been present in the cladding prior to irradiation.

The as-irradiated Zircaloy microstructure was characterized by the original typical cold-worked structure. Annealing at temperatures up to 538 C for times as long as 30 minutes did not appreciably alter the cold-worked microstructure (Figure 5a). However, recrystallization had occurred after annealing at 621 C for 10 min, as evidenced by the fine-grained equiaxed structure seen in Figure 5b. Increasing the annealing temperature to 704 C produced a structure with well-defined equiaxed grains (Figure 5c) that exhibited some growth as compared with those developed after the 621 C anneal.

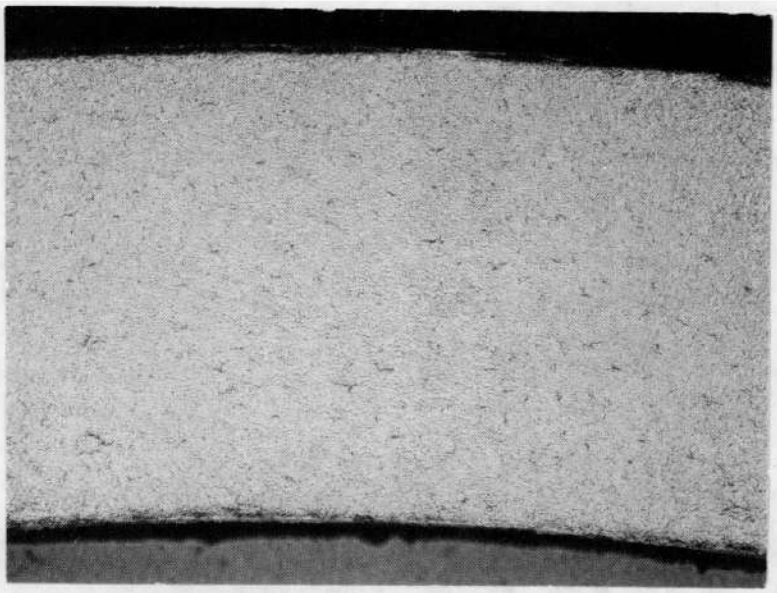

100X HC40832

FIGURE 3. TYPICAL CROSS SECTION OF ROD A25-06 CLADDING
Etched Transverse Sample A

100X HC40837

FIGURE 4. TYPICAL CROSS SECTION OF ROD A25-06 CLADDING
Etched Longitudinal Sample B

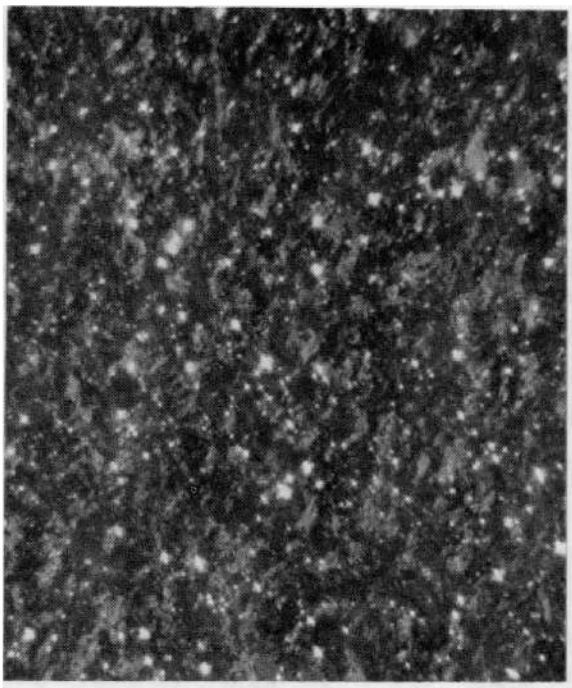

a. Annealed 538 C, 30 Minutes

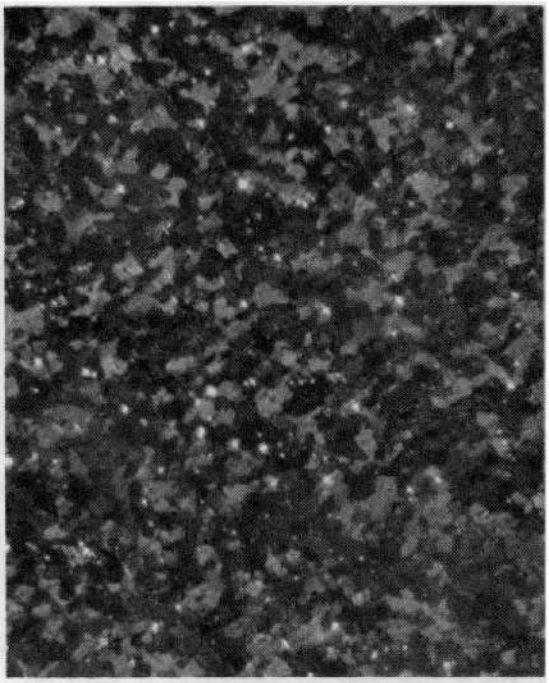

b. Annealed 621 C, 10 Minutes

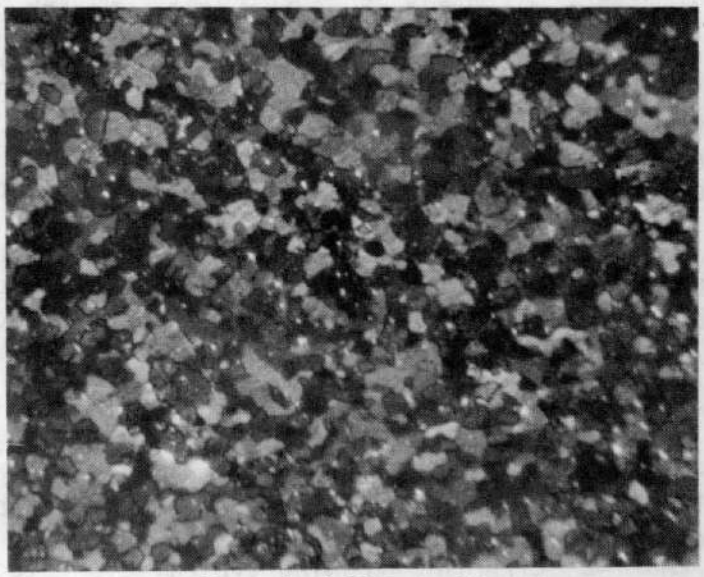

c. Annealed 704 C, 10 Minutes

FIGURE 5. MICROSTRUCTURE OF ISOTHERMALLY ANNEALED IRRADIATED ZIRCALOY FUEL ROD CLADDING FOR ROD A25-06

Polarized Light, 500 X

H. B. Robinson Fuel Rods. Metallographic specimens were prepared from the fracture region of several of the tensile-tested H. B. Robinson fuel-rod cladding samples. Two each were mounted transversely and longitudinally to the tubing axis to examine the manner in which the cross-sectional area of the cladding was reduced during testing. The specimens were 2 cm long as measured from the point of fracture. The longitudinally mounted samples were sectioned and polished to the approximate midplane of the tube axis. The transverse specimens were mounted with the fracture surface up and were ground through eight levels from 0 to about 1.5 cm from the fracture surface. Typical cross sections are shown in Figure 6; the transverse sections are shown at three different levels below the fracture surface.

The longitudinal samples could not be used for quantitative measurements but are useful in showing the general deformation characteristics. Necking was evidenced by the reduction in tube diameter but wall thinning was much less pronounced, which is an indication of material anisotropy.

A qualitative measure of tube ductility was provided by the relative tube-diameter reductions that can be seen in the photographs. For the transverse sections, the first section shown was very close to the fracture region and therefore described, quite closely, the minimum necked-down diameter. As might be expected, the degree of necking increased with the time and temperature of annealing.

On the basis of an initial nominal wall thickness of 0.62 mm, the tube wall appeared to thin uniformly by less than 0.03 mm in either specimen examined. There was a gradual thinning to the point of fracture, with the annealed specimen showing a relatively rapid decrease in wall thickness, as compared with the as-irradiated specimen, in the immediate region of the fracture. Nevertheless, the wall-thickness reduction was relatively small. Reduction in load-bearing area occurred principally by tube-diameter necking rather than wall necking.

Photomicrographs showing the microstructure at various annealing stages and the fracture appearance of specimens tensile tested in these various conditions are presented in Figures 7 through 10. At initial stages of annealing, little recovery of irradiation damage had occurred and the still highly strained grains are defined poorly by polarized light (Figure 7). Recovery of microstrains as annealing proceeded yielded a well-defined structure showing typical elongated cold-worked grains (Figure 8). Recovery was followed by recrystallization (Figure 9) and eventually by grain growth (Figure 10). At the same time, while increased ductility was evident in terms of increased necking and wall thinning, the fracture appearance remained largely unchanged. In all cases, the fracture showed a characteristic ductile

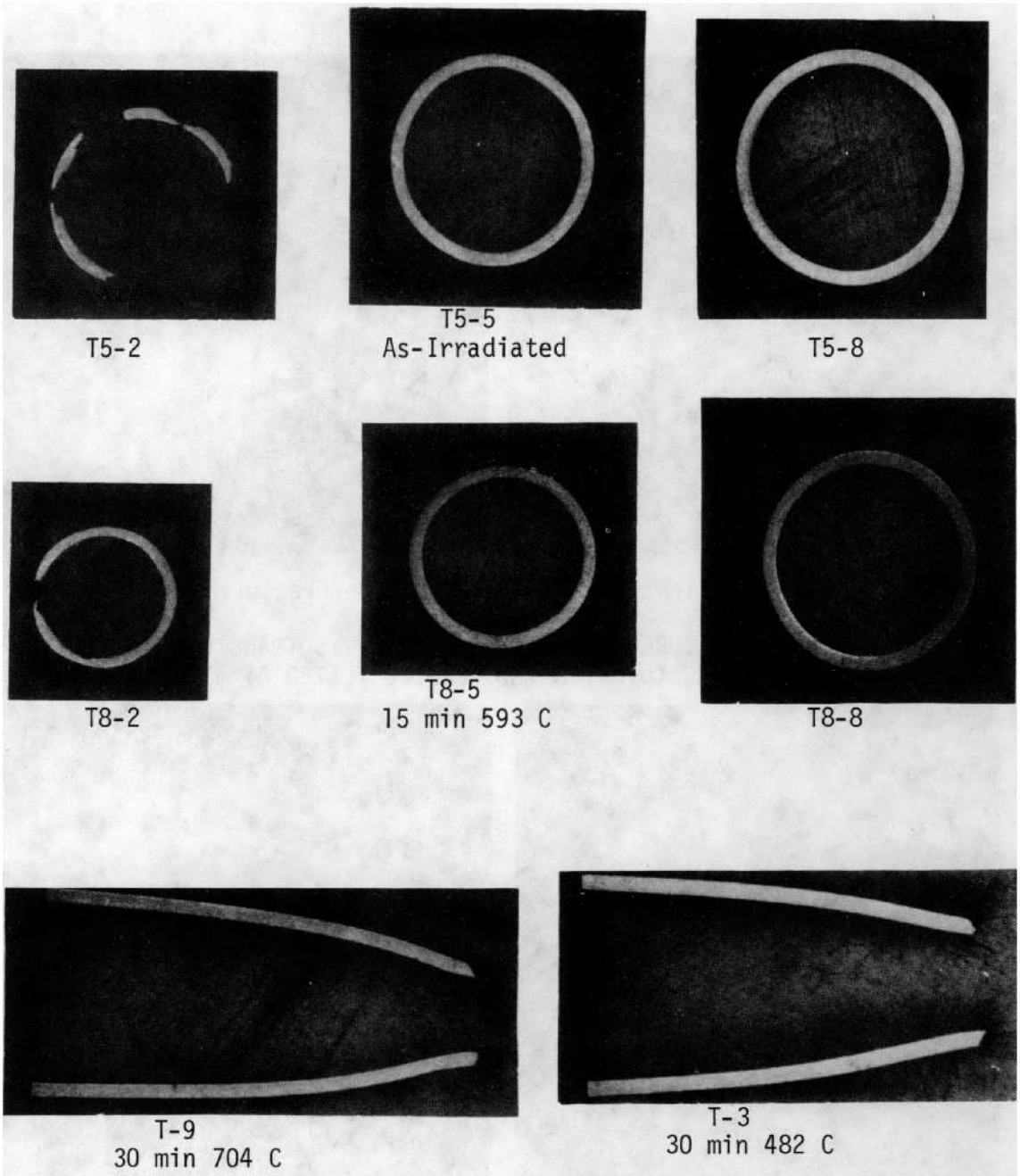

FIGURE 6. H. B. ROBINSON TENSILE SPECIMEN METALLOGRAPHY

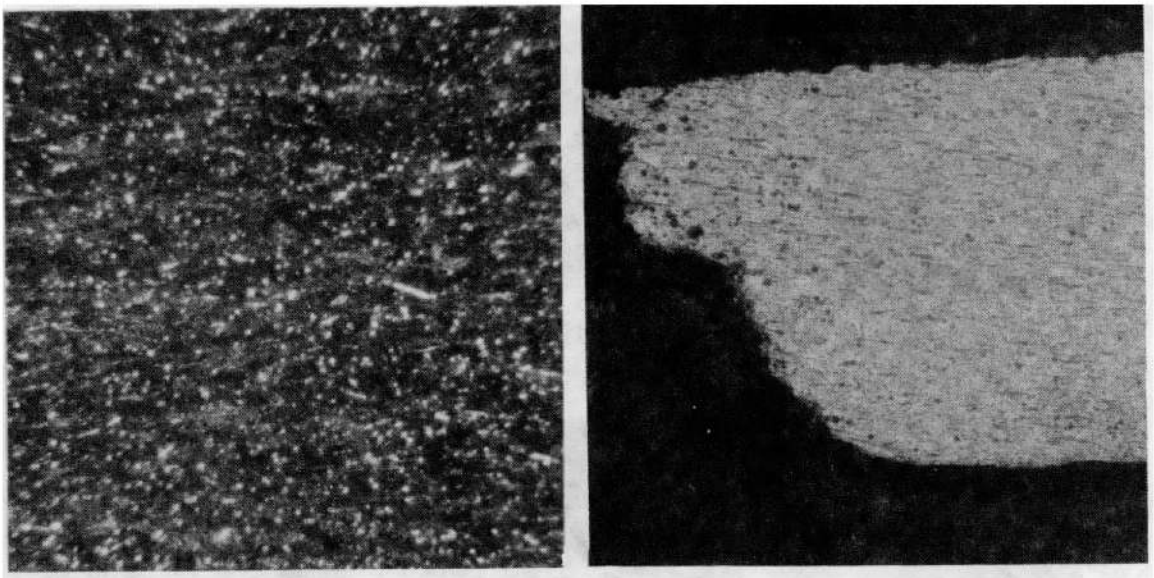

HC43341 Polarized Light 250X HC43342 Fracture Area 100X

FIGURE 7. MICROSTRUCTURE OF SPECIMEN A8-110-115 TRANSIENT ANNEALED AT 28 C/SEC to 621 C AND TENSILE TESTED AT 371 C

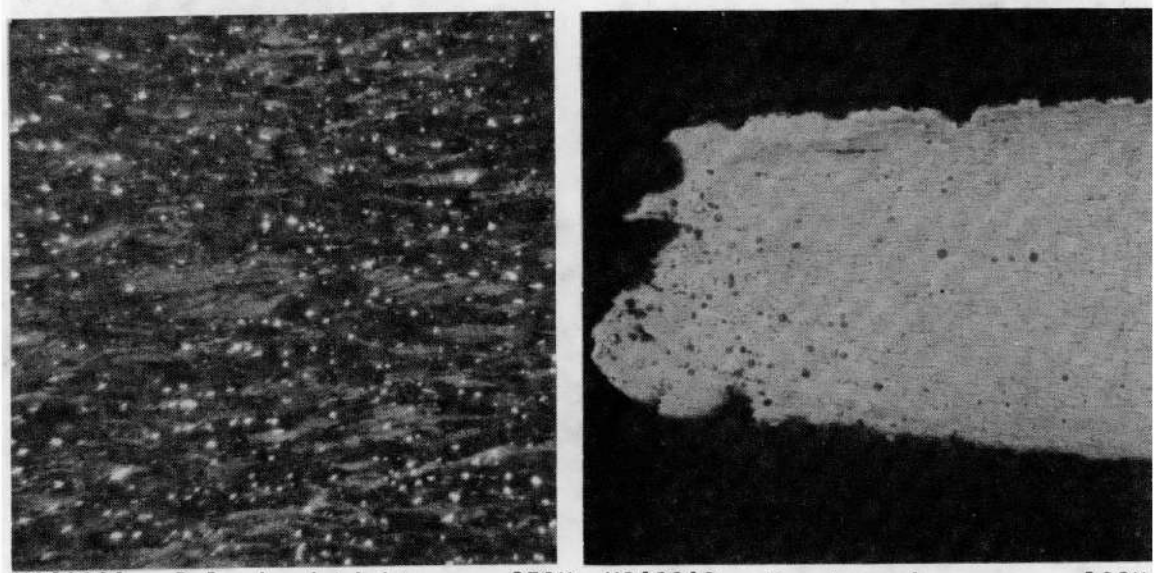

HC43344 Polarized Light 250X HC43343 Fracture Area 100X

FIGURE 8. MICROSTRUCTURE OF SPECIMEN P4-21-26 TRANSIENT ANNEALED AT 14 C/SEC TO 621 C AND TENSILE TESTED AT 371 C

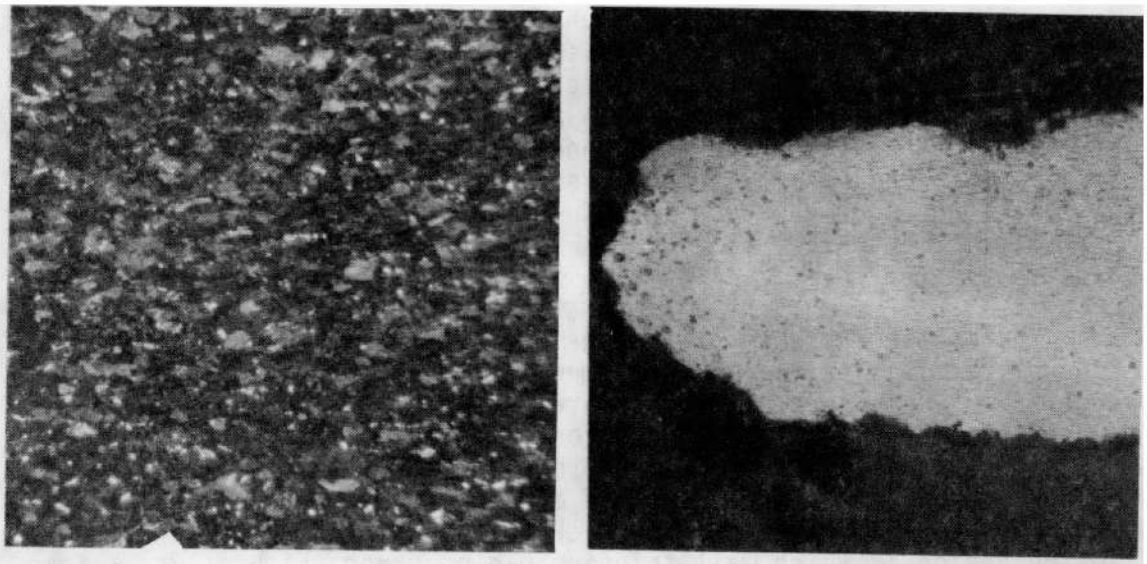

HC43340 Polarized Light 250X HC43339 Fracture Area 100X

FIGURE 9. MICROSTRUCTURES OF SPECIMEN AT A1-110-115 ANNEALED 1 MINUTE AT 621 C

Tensile Tested at 371 C

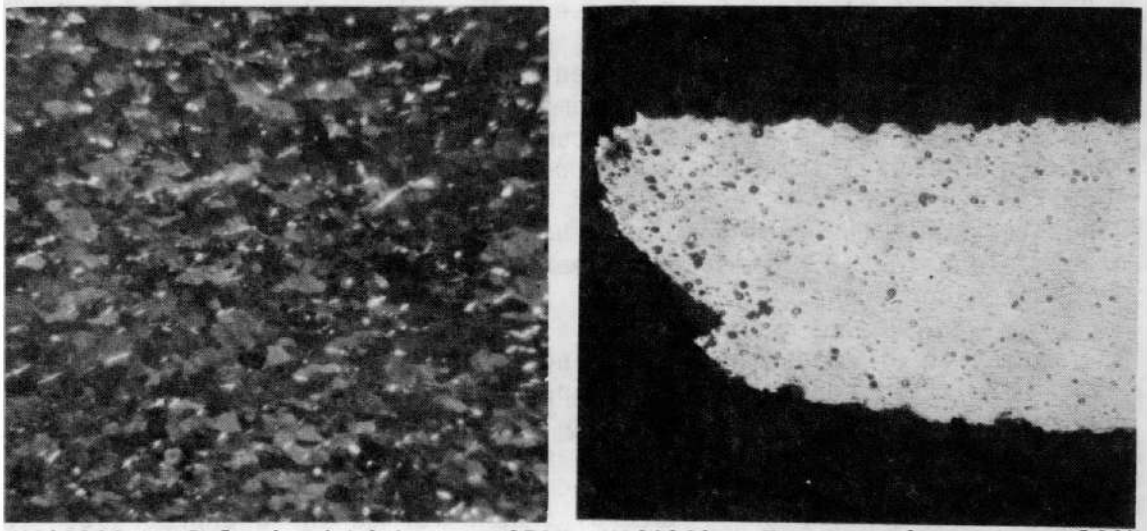

HC43363 Polarized Light 250X HC43364 Fracture Area 100X

FIGURE 10. MICROSTRUCTURE OF SPECIMEN P4-99-104 TRANSIENT ANNEALED AT 1 F/SEC TO 704 C

Tensile Tested at 371 C

shear-type failure.

The tube walls of all specimens, whether tested in the as-irradiated or annealed conditions, contained small cracks that tended to enlarge and blunt as the total strain increased. The tube walls become extremely irregular and roughened in appearance near the fracture area in specimens of high ductility. As one proceeded away from the fracture area, the cracks became finer, as shown in Figure 11. Cracking was most pronounced on the tube ID. The evidence suggested a high-oxygen brittle surface that cracks at low strains, with the cracks blunting in the more ductile interior.

Features of the ruptured expanding-mandrel Specimen O-14 are shown in Figure 12. This particular specimen exhibited two fractures at 180 degrees to each other. The fracture in each case occurred at or near the point where the mandrel edge contacted the specimen ID. The start of a third incipient fracture is shown in Figure 12. Wall thinning had occurred between the points of contact and a neck had formed in the fracture area. Many small cracks were observed on the specimen ID in the region in which wall thinning had occurred (Figure 12c). Some evidence of hydride reorientation to line up perpendicular to the tensile stresses at the tubing ID also was observed, as seen under polarized light in Figure 12d.

Metallographic photographs of expanding-mandrel specimens from the H.B. Robinson fuel rod C-8 are presented in Figure 13. Metallographic examination of test-specimen cross sections did indicate that, while thinning of the tube wall was concentrated for the most part in the region between mandrel sections, some slight reduction might occur completely around the specimen circumference. However, it appeared that the tube-wall thinning in the region between mandrel sections occurred principally as a result of circumferential deformation concentrated at the tubing ID and this in turn led to the formation of cracks along the ID. This concentration of deformation led to straightening of the tubing OD.

The formation of cracks at the tubing ID and their decrease in number with increase in strain rate also appeared to provide an explanation for the decrease in failure stress with increase in strain rate. At the slower strain rate, stress concentrations ahead of the cracks relaxed and the crack blunted as the material strain hardened. At high strain rates, however, only several cracks formed and one propagated to failure before significant strain hardening occurred. Typical cracks, a number of which show evidence of branching, are shown in Figure 14. The number of cracks in the specimens tested at the higher strain rates was severely reduced compared with the number seen in specimens tested at the slower strain rate.

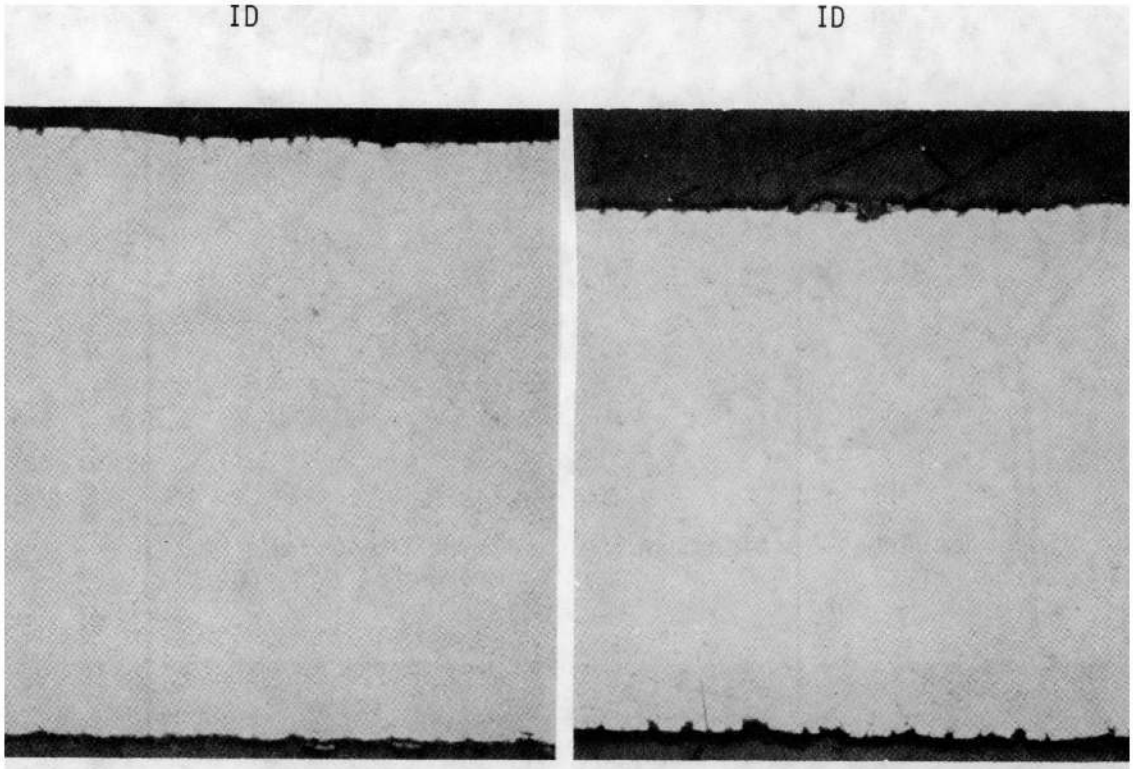

FIGURE 11. PHOTOMICROGRAPHS SHOWING TYPICAL SMALL CRACKS IN TUBING ID AND OD AFTER TENSILE TESTS AT 371 C

Specimen P4-75-80, as Polished

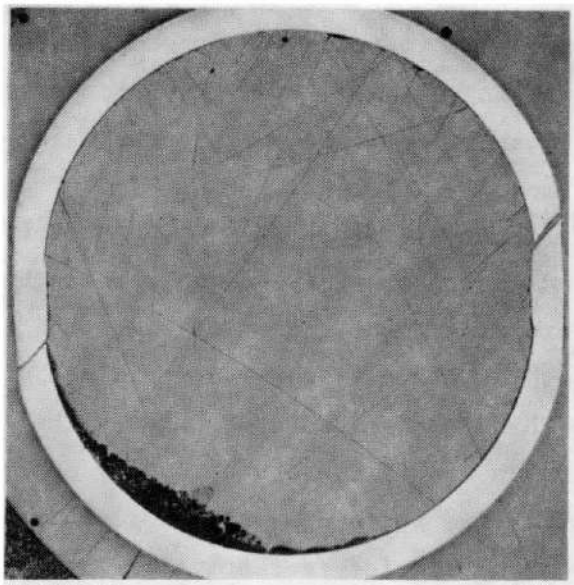

HC44323 7X

(a) Specimen Cross Section Showing Double Fracture

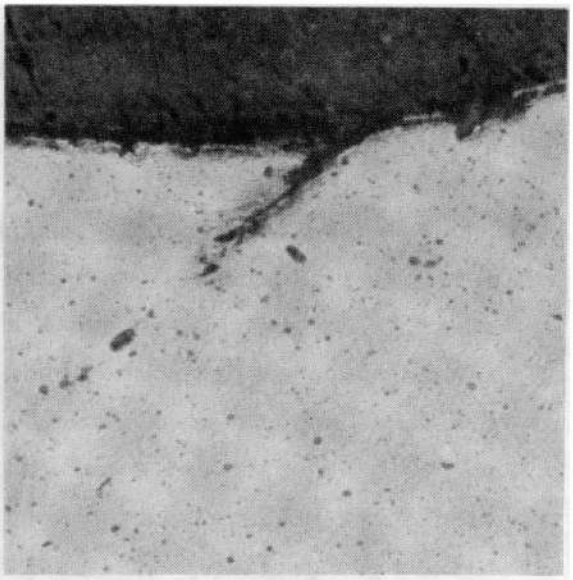

HC44358 250X

(b) Incipient Tube Fracture Near Mandrel Edge (Etched)

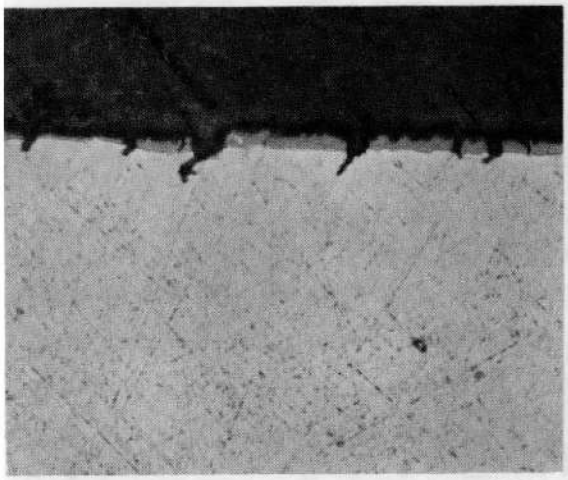

HC44327 250X

(c) Cracks at tubing ID (As Polished)

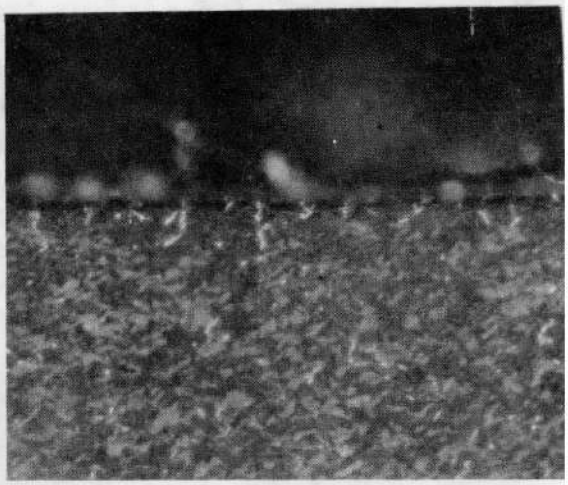

HC44360 250X

(d) Oriented Hydride Near Tubing ID (Polarized Light)

FIGURE 12. FRACTURE AND MICROSTRUCTURAL FEATURES OF H.B. ROBINSON IRRADIATED EXPANDING-MANDREL TEST SPECIMEN

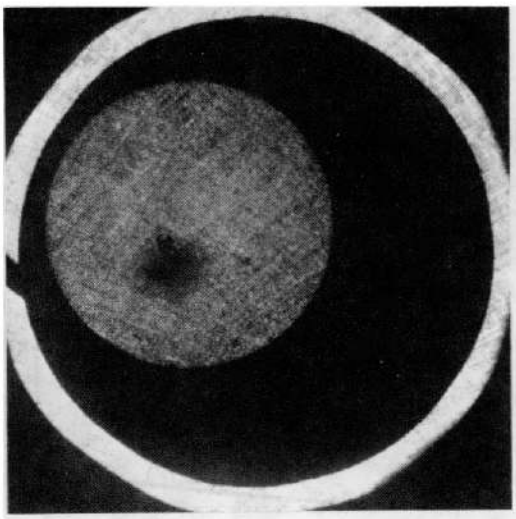

Specimen C8-8 As Irradiated;
S.R. 0.0034/Min

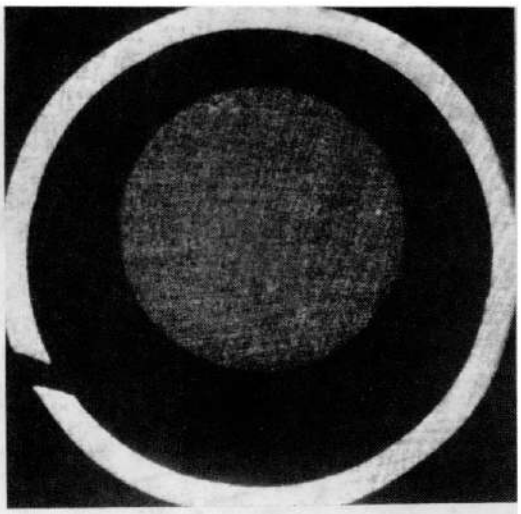

Specimen C8-18 Transient
Annealed, 5.6 C/Sec to 539 C;
S.R. 0.0034/Min

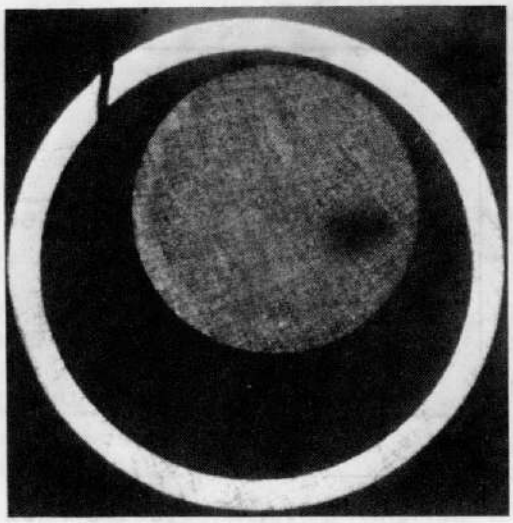

Specimen C8-11 As Irradiated,
S.R. 0.034/Min

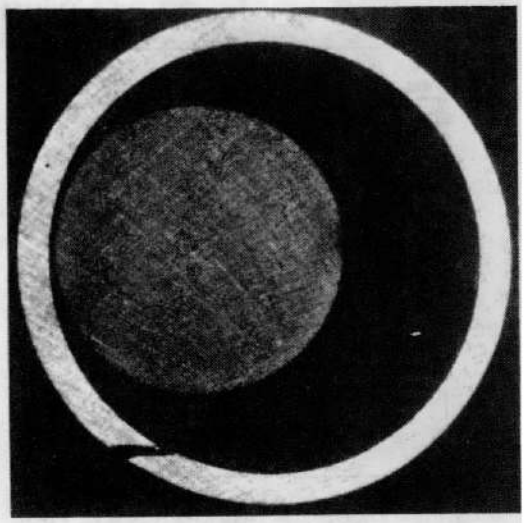

Specimen C8-12 As Irradiated;
S.R. 0.34/Min

FIGURE 13. CROSS SECTIONS OF EXPANDING-MANDREL TEST SPECIMENS (H.B. ROBINSON) TESTED AT 371 C (MAGNIFICATION 7X)

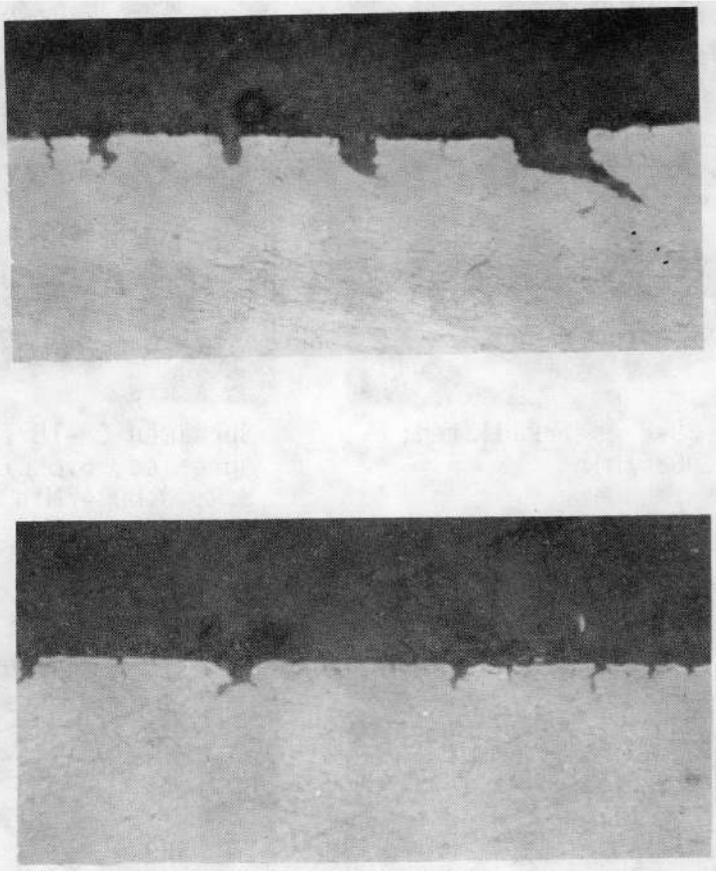

FIGURE 14. MICROCRACKS AT TUBE ID OF EXPANDING-MANDREL TEST SPECIMENS FOR IRRADIATED H. B. ROBINSON FUEL ROD C-8

Metallographic examinations were performed on failed H. B. Robinson transient-heating burst specimens. Cross sections were examined at the burst locations.

Specimens that burst at an axial location that coincided with the location of a thermocouple, and for which the burst temperatures were therefore fairly accurately known, were examined to identify structures presumably characteristic of the highest temperatures achieved in the transient. Results are presented in Table 15 for specimens that serve to delineate the temperature boundaries for the alpha, alpha-plus-beta, and beta phase regions. The temperature corrections employed in obtaining the corrected temperatures listed in Table 15 are based on the analysis of H. B. Robinson burst-temperature data which indicated a circumferential temperature gradient of 20 to 25 centigrade at the burst location. Structures typical of the three phase regions are shown in Figure 15. Specimens that did not exceed alpha phase temperatures exhibited hydrides that were randomly distributed as compared with the circumferentially elongated hydrides observed in the as-irradiated material. In the specimens exhibiting a transformed beta phase structure, a very thin stabilized alpha layer was observed at the specimen surfaces.

A feature of all the specimens was occurrence of the same structure completely around the specimen circumference. It was concluded that temperatures were fairly uniform around the specimen circumference, if not at the time of burst then shortly thereafter. Possibly some degree of temperature equilibration occurs in the cladding following burst failure.

The specimens also were examined to determine relative ID and OD oxide thicknesses. No significant differences were noted. This is probably indicative of the fact that the specimen is exposed to steam at elevated temperature for more time following the burst than it is during heating to the burst temperature so that most of the oxidation occurs immediately following the burst and during subsequent cooling.

Oconee I Fuel Rods. On the basis of eddy-current results obtained with both encircling and probe coils, metallographic examinations were performed on specimens exhibiting the largest potential defect indications to determine the cause of the signals. Metallographic specimens were prepared from Rod 47103 at 119.7 cm, Rod 47104 at 100.7 cm, and Rod 47118 at 111.1 cm, as measured from the rod bottom. Specimens from Rods 47103 and 47118 were mounted transversely and ground to the plane of interest; the specimen from Rod 47104 was mounted longitudinally to reveal the rod length from about 99 to 102 cm and was ground

TABLE 15. RELATIONSHIP BETWEEN BURST TEMPERATURE AND PHASES PRESENT IN BURST REGION AS DETERMINED BY POSTTEST METALLOGRAPHIC EXAMINATION OF IRRADIATED H. B. ROBINSON TRANSIENT-HEATING BURST TEST

Specimen	Phases Present	Burst Temperature	
		Measured	Corrected[a]
K8/35-55	α	825	825
F8/35-55	$\alpha + \beta$	814	854
G8/70-89	$\alpha + \beta$	925	965
N8/112-132	β	978	1018

(a) Corrected for angular location of thermocouple.

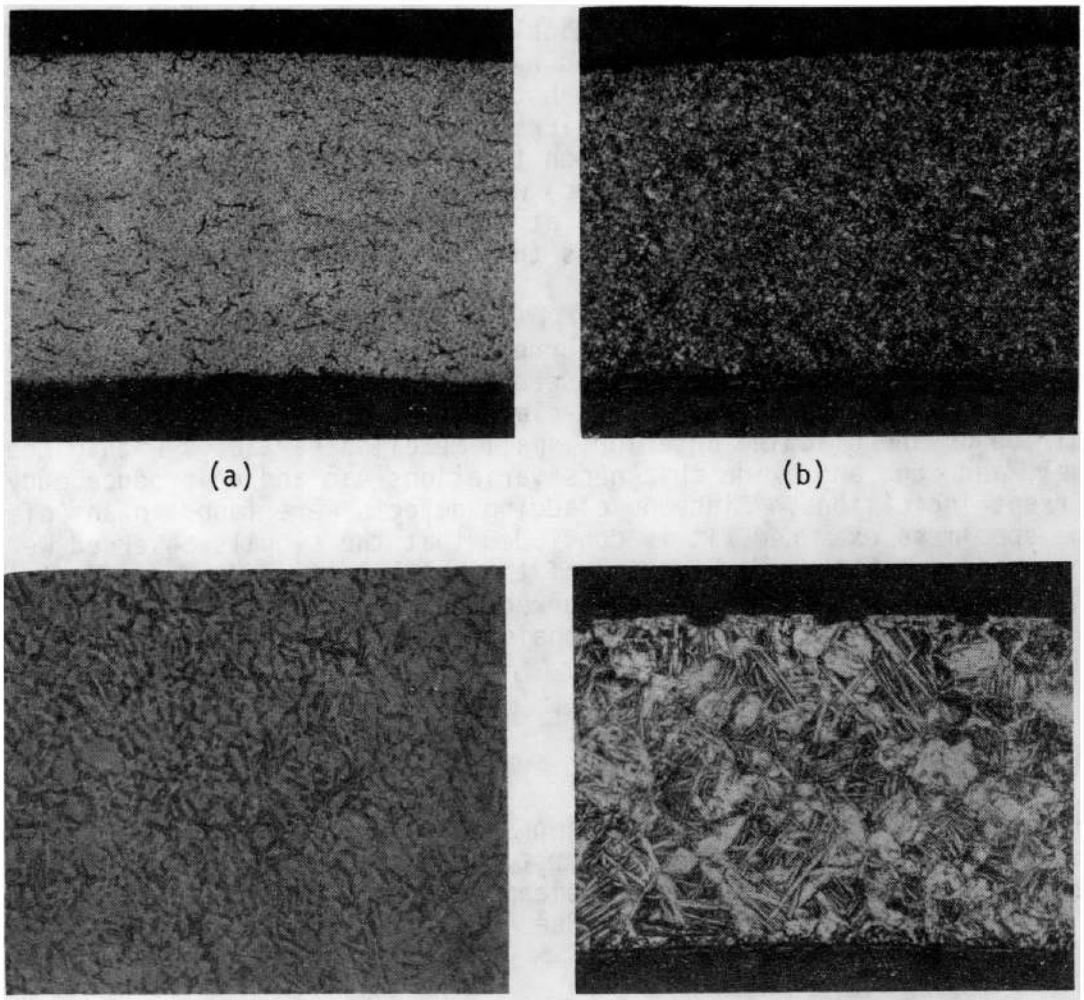

FIGURE 15. MICROSTRUCTURES OF IRRADIATED H. B. ROBINSON TRANSIENT-HEATING BURST-TEST SPECIMENS EXHIBITING STRUCTURES CHARACTERISTIC OF MAXIMUM TRANSIENT-HEATING TEMPERATURE

(a) Alpha phase, note hydrides, 100X; (b) alpha-plus-beta phase, 100X; (c) alpha-plus-beta phase, 500 X; (d) transformed beta phase, 100X

to the midplane. The eddy-current results are given in a previous section of this report, and it appears that the defect signals were caused by fission-product buildup on the cladding interior since the eddy-current probe coil produced a signal around the entire rod circumference.

No obvious causes of the eddy-current indications were found in either the transverse or longitudinal metallographic sections examined. During the examinations, coalesced hydrides were observed (Figures 16a and 16b); these were relatively few but large and long compared with the size and number of hydrides in unirradiated archive cladding. However, the hydrides in a specimen taken from an area which produced no eddy-current signal (Figure 16c) were found to be as large if not larger than the hydrides observed at the points of eddy-current defect signals. Consequently, it appears that hydrides do not significantly affect the eddy-current signals.

Experience with evaluating eddy-current signals has led to the conclusion that defect signals are produced by a number of phenomena. Slight cladding ridging caused by pellet-cladding interaction, fission-product buildup on the cladding interior, small metallic particles within the fuel, and crud and oxide thickness variations can and do produce eddy-current indications. Since no cladding defects were found in any of the specimens examined, it is concluded that the signals observed were produced by one or a combination of the above-mentioned sources. In any event, areas producing eddy-current defect signals will continue to be excluded for the purpose of choosing mechanical-properties test specimens.

Annealing of Cladding

Unirradiated and irradiated cladding specimens were annealed and subsequently tested in tensile, tube-burst, or expanding-mandrel tests to determine the effect of both transient and isothermal annealing on the cladding mechanical properties. See Appendix B for a full description of equipment and procedures.

TASK II

Description of Mechanical Properties Tests (As Irradiated Specimens)

To determine the as-irradiated, fuel-rod-cladding mechanical properties, the rods are cut into sections and defueled; specimens are then prepared and tested in tensile, tube-burst, expanding mandrel, and bend

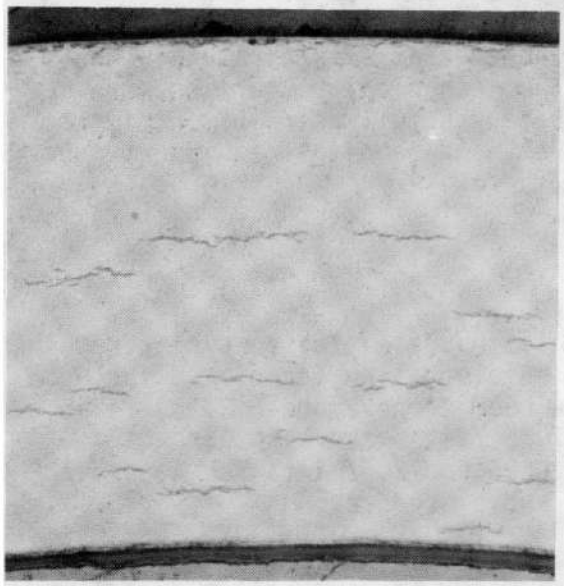

HC45634 1000X

a. Specimen 47118/43.75

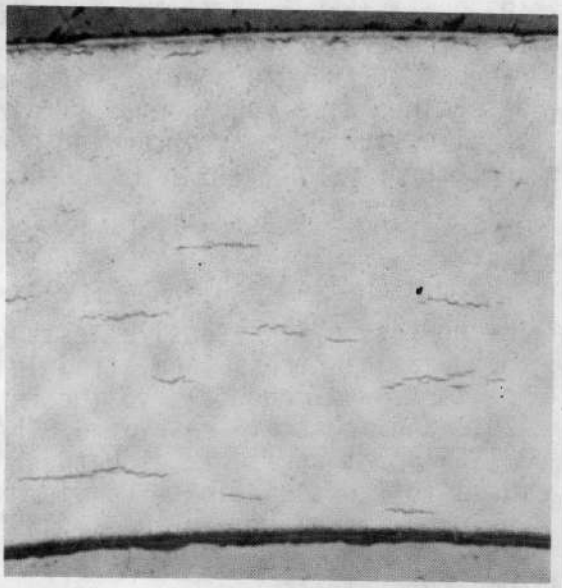

HC45633 1000X

b. Specimen 47103/47.13

Hydrides in Areas Providing Potential Eddy-Current Defect Signal

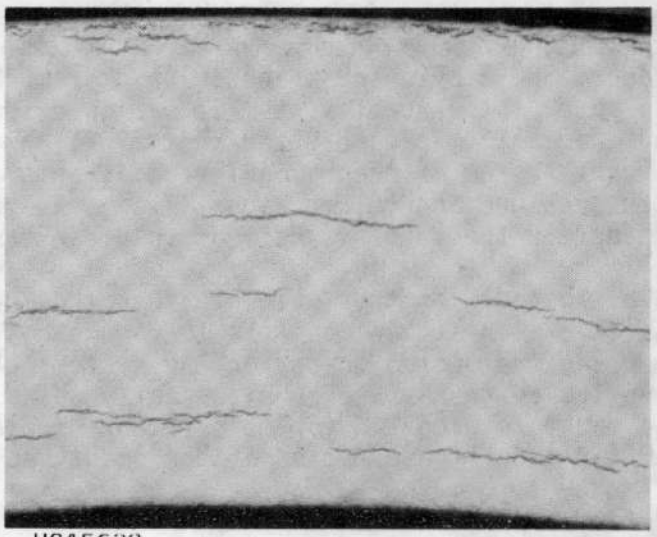

HC45632 100X

c. Specimen 47021/73
Hydrides in Area Providing No Eddy-Current Signal

FIGURE 16. HYDRIDES OBSERVED IN OCONEE FUEL-ROD CLADDING

tests. Tests were conducted in the range from room temperature to 427 C and the mechanical properties are determined as a function of test temperature. Tests are also conducted at strain rates in the range 0.001/min to about 2/min and the mechanical properties were determined as a function of strain rate. A full description of the tensile, tube-burst, expanding mandrel, and bend-test equipment and procedures is presented in Appendix C.

Tensile Tests

The purpose of the tensile tests was to induce a stress which resembles the uniaxial stress (and strain) in an elongating irradiated fuel rod. The tests were conducted in the range room temperature (∿27 C) to about 425 C and at strain rate of 0.025/min. Tests were also conducted at 371 C and at strain rates between 0.0025 and 2.5/min. See Appendix C for a full description of equipment and procedures.

Tube-Burst Tests

The objective of cladding burst tests was to determine the mechanical properties of cladding materials under biaxial stress conditions.

Burst tests were performed at 27 C to 425 C under internally pressuring with a silicon oil. For these tests the maximum temperature can be increased to about 550 C by using a special high-temperature oil. The pressurization rate of the burst system is variable from 0.15 to 140 $kg/mm^2/min$ and the maximum pressure the system will produce is 14 kg/mm^2. The burst system is programmable and is automatically controlled through pressure and volume signal feedback circuits. The control parameter for the tests is rate of volume expansion.

Specimens can be tested with the fuel intact or the fuel can be removed and the tube filled with alumina pellets to reduce both the oil volume in the specimen and the stored energy in the system. After a specimen has been either tested to rupture or plastically deformed, a transverse metallographic mount is prepared for measurement of plastic strain. See Appendix C for a full description of equipment and procedures.

Expanding Mandrel Tests

The expanding mandrel test was intended to simulate the interaction of a longitudinally cracked fuel pellet with the restraining Zircaloy cladding. The mechanical properties were then determined in the range 28 C to 425 C and at strain rates from 0.0062 to 6.2/min. See

Appendix C for a full description of equipment and procedures.

Bend Tests

The purpose of the bend tests was to simulate the bending of a fuel rod due to thermal and mechanical stresses. The bend test was designed to evaluate the bending behavior of a fuel rod under the restraint of in-reactor grid supports. The mechanical properties were then determined as a function of temperature and strain rate. However, after testing the as-irradiated Lot 1 and Lot 2 material, the bend-test strength measurements showed similar trends with temperature when compared with tube-burst-test and expanding mandrel-test strength measurements. A greater degree of irradiation strengthening for the cladding from the higher burnup H. B. Robinson rods as compared with Oconee spent fuel rods was evident from the bend-test results. However, little information concerning cladding ductility was available from the tests, except for the significant observation that the cladding is highly ductile in bending. Specimens were routinely bent to a 10.8-cm radius of curvature, and smaller, without producing failure. Therefore, bend tests were not conducted on Lot 3 or Lot 4 material. See Appendix C for a full description of equipment and procedures.

TASK III

Description of Mechanical-Properties Tests (Annealed Specimens)

To determine the fuel-rod cladding mechanical properties after transient and isothermal annealing, the rods are cut into sections and defueled; specimens are then prepared for tensile, tube-burst, or expanding mandrel testing. Each specimen was either transient annealed or isothermally annealed. The specimens were then tested in tensile, tube-burst, or expanding mandrel tests at 371 C and at the appropriate nominal strain rate. For a full description of the annealing apparatus, see Appendix B. For a full description of equipment and procedures for testing, see the preceding section on Task II and Appendix C.

TASK IV

Description of Transient-Heating Burst Tests

The purpose of the transient-heating burst tests of irradiated Zircaloy fuel-rod cladding was to simulate conditions encountered in a

fuel rod during a postulated loss-of-coolant accident (LOCA). To simulate the environment, internal heat generation, heat transfer, and specimen deformation as closely as possible, the specimen length was chosen as 51 cm (20 in.) which is approximately the length between grid spacers, and the specimen was heated using an internal electrical heater, tested in a steam environment, and prepressurized with helium to several initial pressures. The specimens were heated at rates from 5.6 to 28 C/sec to failure. A full description of the transient-heating burst test equipment and procedures is presented in Appendix D.

TEST RESULTS AND ANALYSIS (UNANNEALED SPECIMENS)

Tensile Tests

Unirradiated Sandvik Cladding

The tensile-test results for the unirradiated Sandvik material are listed in Table 16 and are plotted in Figures 17 and 18. Because no archive material was available for the H. B. Robinson reactor, the unirradiated Sandvik cladding material was acquired from Oak Ridge National Laboratory (ORNL) and was part of the material supplied to ORNL for their multirod burst tests. The Sandvik cladding was reactor-grade Zircaloy-4, cold reduced and stress relieved. The tensile-test results are representative of unirradiated cladding and are used as a nominal baseline for comparison with the irradiated H. B. Robinson Zircaloy-4 fuel-rod cladding tensile-test results.

The results in Table 16 show good agreement between the Sandvik-reported properties and the properties reported by BCL. At a test temperature of 27 C, the BCL ultimate stress of 737 MPa is equal to the lowest value obtained by Sandvik. However, the BCL yield stress and uniform strain are slightly lower (4 and 9 percent) than the respective Sandvik values. The BCL total strain value is between the Sandvik upper and lower total strain values. These small differences are attributed to normal scatter inherent in this material and the data are not sufficient for a statistical analysis.

TABLE 16. TENSILE TEST RESULTS FOR UNIRRADIATED SANDVIK FUEL-ROD CLADDING

Strain Rate 0.025/min.

Test Temperature, C	Stress, MPa		Strain, percent	
	Ultimate	Yield	Uniform	Total
27	759.7	570.1	7.1	20.3
27	763.0	564.7	7.3	27.5
27	758.6	559.2	6.7	20.3
27	737.0	557.1	9.1	23.7
27	741.0	552.8	7.6	22.4
27	737.0	531.0	6.1	22.3[a]
316	464.9	362.0	4.9	21.5[a]
371	434.6	344.7	4.1	31.8[a]
385	446.5	352.3	4.4	18.2
385	448.7	340.3	4.4	19.7
385	437.8	338.1	4.8	23.1
385	429.2	331.6	5.1	18.5
385	429.2	333.8	5.1	19.2
427	362.0	294.8	2.1	26.8[a]

(a) Tested at BCL on Tube 114-T, Lot 7FD12, during this testing program; remainder were tested at Sandvik on Tubes 1013 and 0276 and Lots 7FD12 and 7FD11.

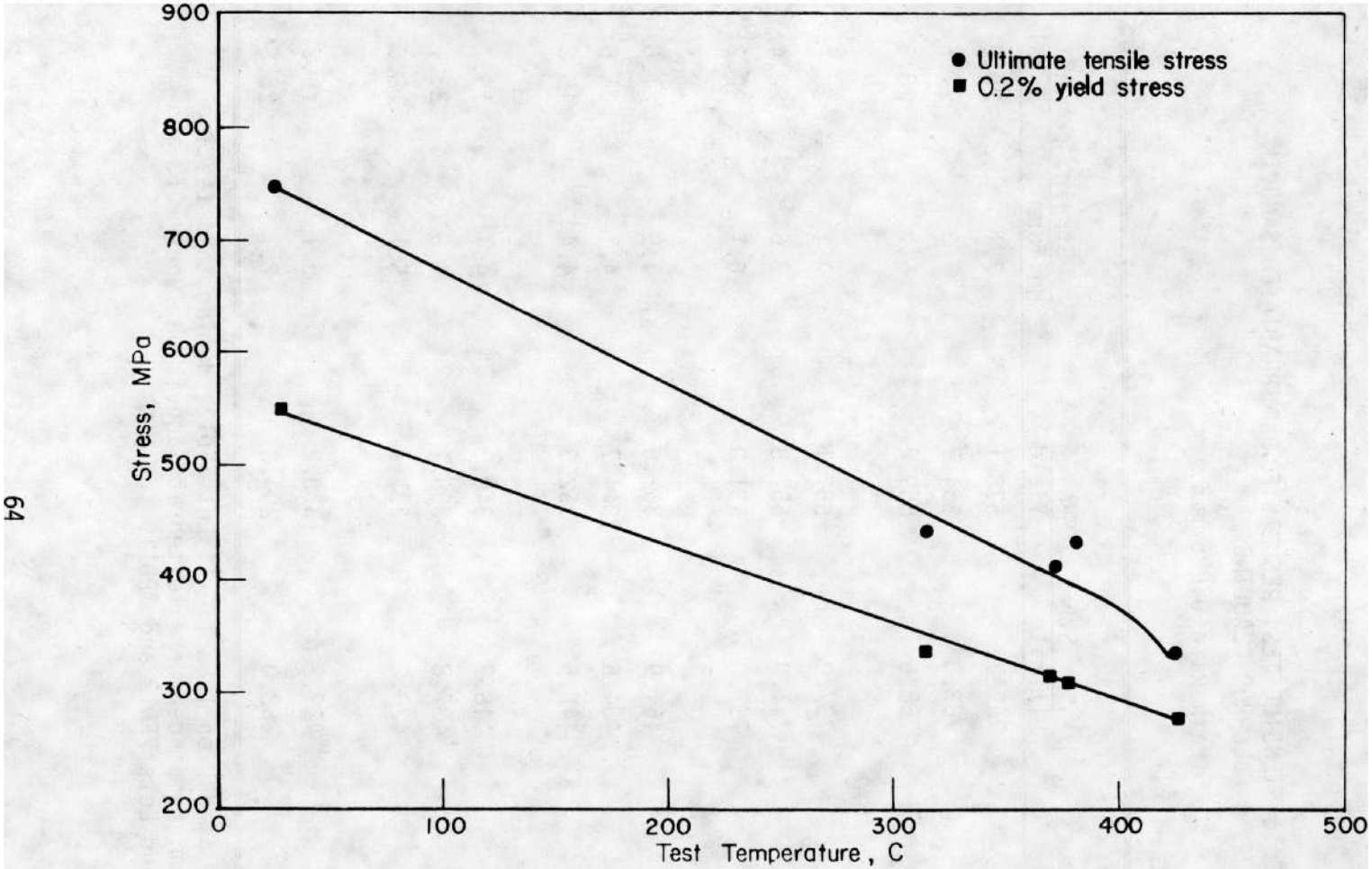

FIGURE 17. AVERAGE ENGINEERING TENSILE STRESS FOR UNIRRADIATED SANDVIK FUEL-ROD CLADDING AS A FUNCTION OF TEMPERATURE

Strain Rate 0.025/min.

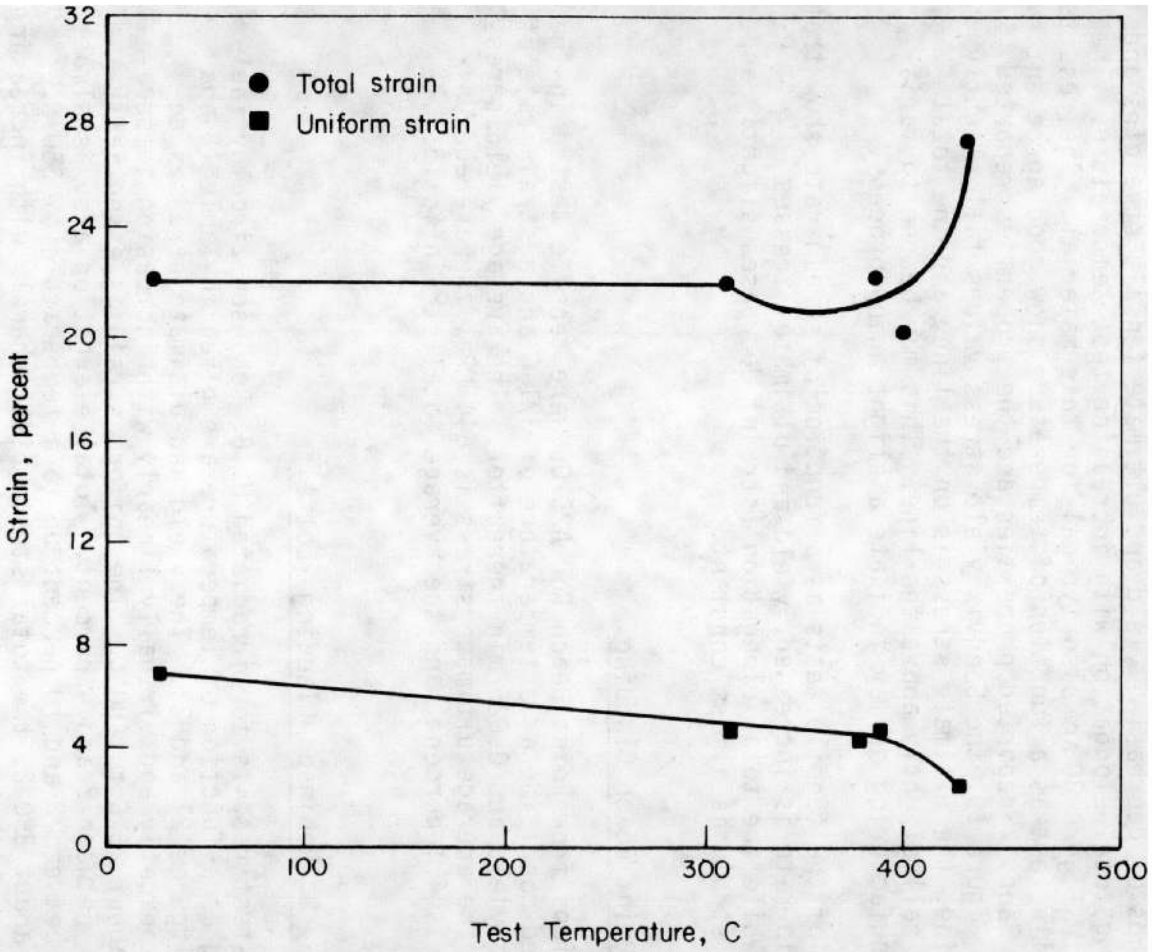

FIGURE 18. AVERAGE ENGINEERING TENSILE STRAIN FOR UNIRRADIATED SANDVIK FUEL-ROD CLADDING AS A FUNCTION OF TEMPERATURE

Strain Rate 0.025/min.

Unirradiated Oconee I Archive Cladding

Table 17 contains a tabulation of the tensile test results for the Oconee archive material. This data is graphically displayed in Figures 19 and 20 for the constant-strain-rate and constant-temperature tests, respectively. In general, the data in Figure 19 showed the typical trends of decreasing yield and ultimate tensile strengths and an increasing total elongation with increasing test temperature. The data shown in Figure 20 are also typical for this material. The results of the tensile test as a function of temperature show good agreement between the Sandvik-reported properties and the properties reported by BCL. In Figure 19, the Sandvik yield stress values fall slightly below the line, the ultimate stress is on the line, and the total elongations fall slightly above the line. This may be due to variations in manufacturing or may indicate a slight aging process.

The results of the tensile tests as a function of strain rate show that as the strain rate is increased, yield and ultimate stresses increases while the total elongation (strain) decreases slightly and the uniform strain is almost constant.

Irradiated Point Beach Cladding

Three specimens from Point Beach Rod A25-06 were tensile tested in the as-irradiated condition at a temperature of 371 C and a strain rate of 0.005/min to yield and 0.025/min thereafter. The average yield stress is 500 MPa, the average ultimate stress is 644 MPa, the average uniform strain is 4.1 percent, and the average total strain is 13.1 percent.

Irradiated H. B. Robinson Cladding (Lot 1)

The tensile-test results for irradiated H. B. Robinson Zircaloy fuel-rod cladding as a function of temperature are given in Table 18 and plotted in Figures 21 and 22. The yield and ultimate stresses decrease monotonically and virtually linearly with increasing temperature from about 25 C to 480 C. The uniform strain is essentially constant at between 2 and 4 percent. Total elongation also is almost constant at between 8 and 10 percent up to a temperature of 350 C. However, at about 350 C, the total strain rises sharply with increasing temperature to slightly over 16 percent. At about 420 C, the total strain drops sharply with increasing temperature to between 10 and 12 percent.

TABLE 17. TENSILE TEST RESULTS FOR UNIRRADIATED OCONEE I ZIRCALOY ARCHIVE FUEL-ROD CLADDING AS A FUNCTION OF TEMPERATURE AND STRAIN RATE

Specimen	Test Temp, C	Strain Rate /min	Strength, MPa		Elongation, percent	
			Ultimate	Yield	Uniform	Total
(a)	27	(a)	754	541	-	18.8
(a)	27	(a)	778	590	-	21.9
(a)	27	(a)	766	565	-	21.9
(a)	27	(a)	767	590	-	20.3
(a)	27	(a)	763	561	-	20.3
215-1-247-3-5	204	0.0025	566	485	2.9	13.2
80-2-249-1-1	204	0.025	549	427	5.0	16.0
36-2-248-1-1	316	0.0025	482	418	2.3	13.0
80-2-249-1-2	316	0.025	476	380	4.4	17.7
(a)	343	(a)	470	348	-	18.8
(a)	343	(a)	496	376	-	20.3
(a)	343	(a)	472	357	-	18.8
(a)	343	(a)	486	355	-	18.8
(a)	343	(a)	479	363	-	18.8
(b)	343	(b)	477	370	2.8	12.6
(b)	343	(b)	482	382	4.5	13.8
(b)	343	(b)	478	365	4.7	16.5
(b)	343	(b)	488	373	3.0	14.2
(b)	343	(b)	494	386	2.9	12.9
(b)	343	(b)	482	373	3.6	13.2
215-1-247-3-4	371	0.0025	423	384	1.8	14.6
36-2-248-1-2	427	0.0025	340	322	1.4	22.0
80-2-249-1-3	427	0.025	365	316	2.5	16.0
36-2-248-1-3	471	0.0025	274	268	1.2	29.9
36-2-248-1-5	371	0.025	446	400	1.9	13.6
34101-1	371	0.025	460	383	3.5	20.0

TABLE 17. (Continued)

Specimen	Test Temp, C	Strain Rate /min	Strength, MPa		Elongation, percent	
			Ultimate	Yield	Uniform	Total
34101-2	371	0.025	464	390	3.6	21.9
36-2-248-1-4	371	0.25	463	425	2.2	12.5

(a) Data provided by Sandvik as a certification for Lot 2 and Lot 3 Zircaloy-4 tubing.
(b) Preirradiation tube tensile data were made available by B&W; the tubes were tested at a strain rate of 0.005/min to the 0.2 percent of set yield and at 0.25/min thereafter.

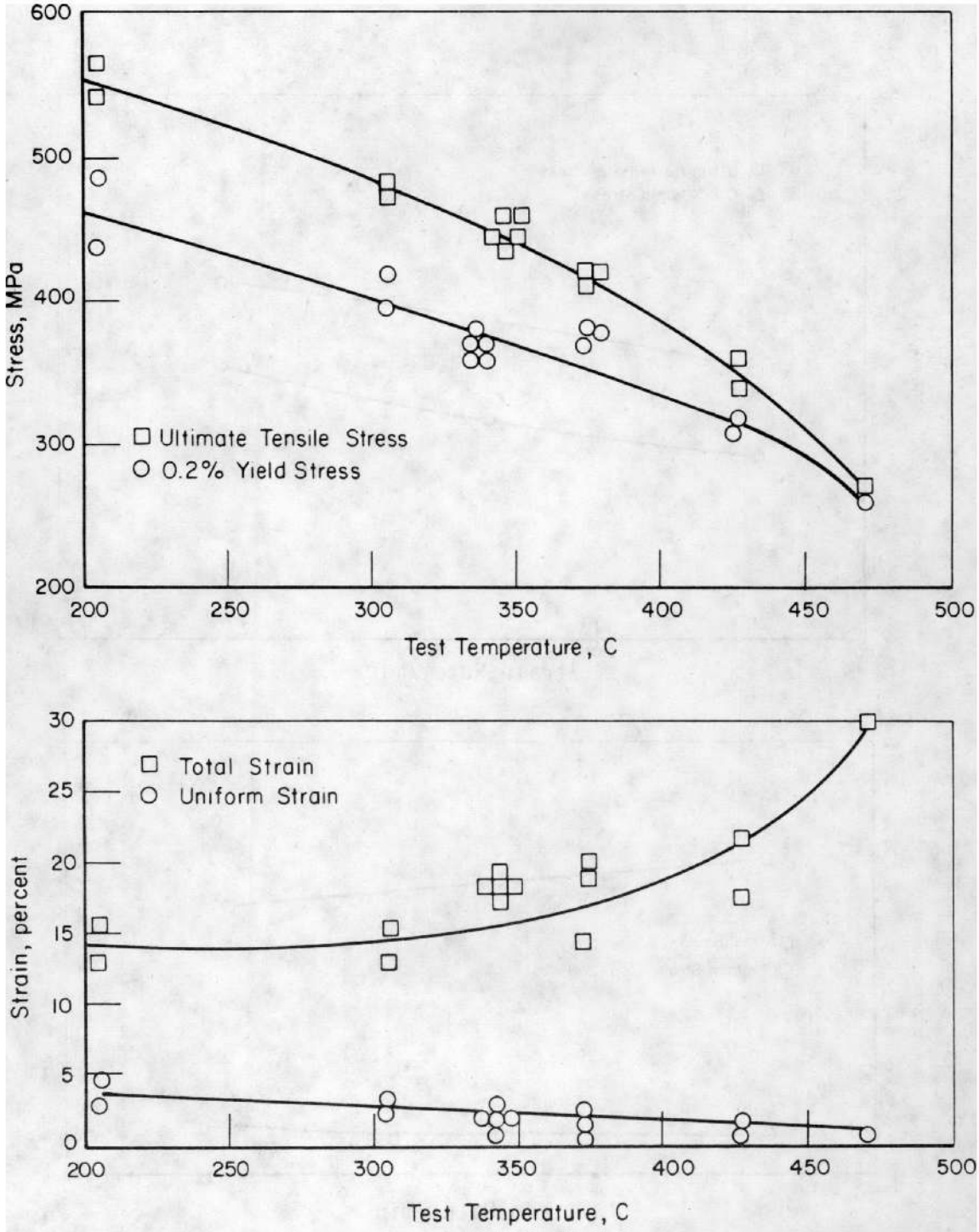

FIGURE 19. EFFECT OF TEST TEMPERATURE ON THE STRENGTH AND DUCTILITY OF OCONEE ARCHIVE MATERIAL AS MEASURED IN TENSILE TESTS

Strain Rate 0.0025/min.

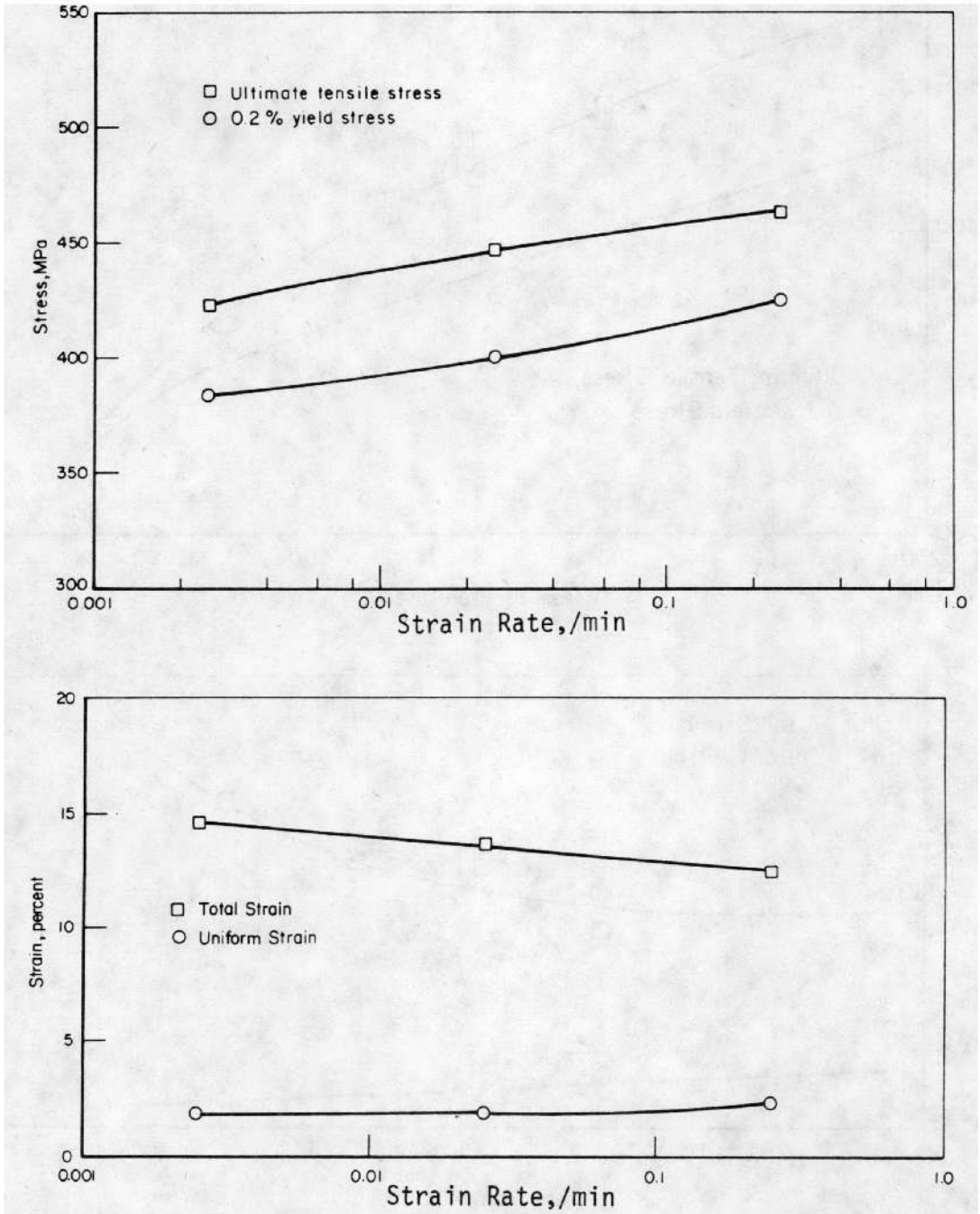

FIGURE 20. EFFECT OF STRAIN RATE ON STRENGTH AND DUCTILITY OF OCONEE ARCHIVE MATERIAL AS MEASURED IN TENSILE TESTS

Test Temperature 371 C.

TABLE 18. TENSILE TEST RESULTS FOR IRRADIATED H. B. ROBINSON ZIRCALOY FUEL-ROD CLADDING AS A FUNCTION OF TEMPERATURE

Strain Rate, 0.025/min.

Specimen	Test Temperature, C	Stress, MPa		Strain, percent	
		Ultimate	Yield	Uniform	Total
P8-7	26	937	810	2.1	3.7[a]
P8-21	26	985	807	4.2	10.2
P8-9	26	1000	830	3.9	8.5
P8-23	93	904	747	3.8	9.1
P8-37	93	899	740	3.6	9.1
P8-19	93	917	763	3.8	6.3
P8-8	204	822	667	3.9	6.5
P8-38	204	800	672	4.2	9.6
P8-47	204	777	639	4.0	9.5
P8-52	316	670	561	2.3	7.1
P8-51	316	685	571	2.7	8.1
P8-50	316	704	601	2.8	8.8
M12-11	329	708	591	3.0	9.4
M12-8	343	725	586	2.9	11.0
P8-20	371	623	485	4.1	18.9
P8-34	371	650	524	4.0	20.5
P8-46	371	661	540	2.8	12.2
H10-20	371	694	586	3.8	16.5
H10-15	427	565	506	2.0	16.3
H10-30	427	533	506	1.2	4.4[a]
P8-53	427	478	452	1.3	5.2[a]
G8-106-111	427	592	494	3.4	18.0
G8-111-116	482	441	379	2.8	9.8
M12-9	482	491	434	1.9	11.7

(a) Specimen appears to have fractured prior to reaching full maximum load and therefore exhibits a reduced total elongation.

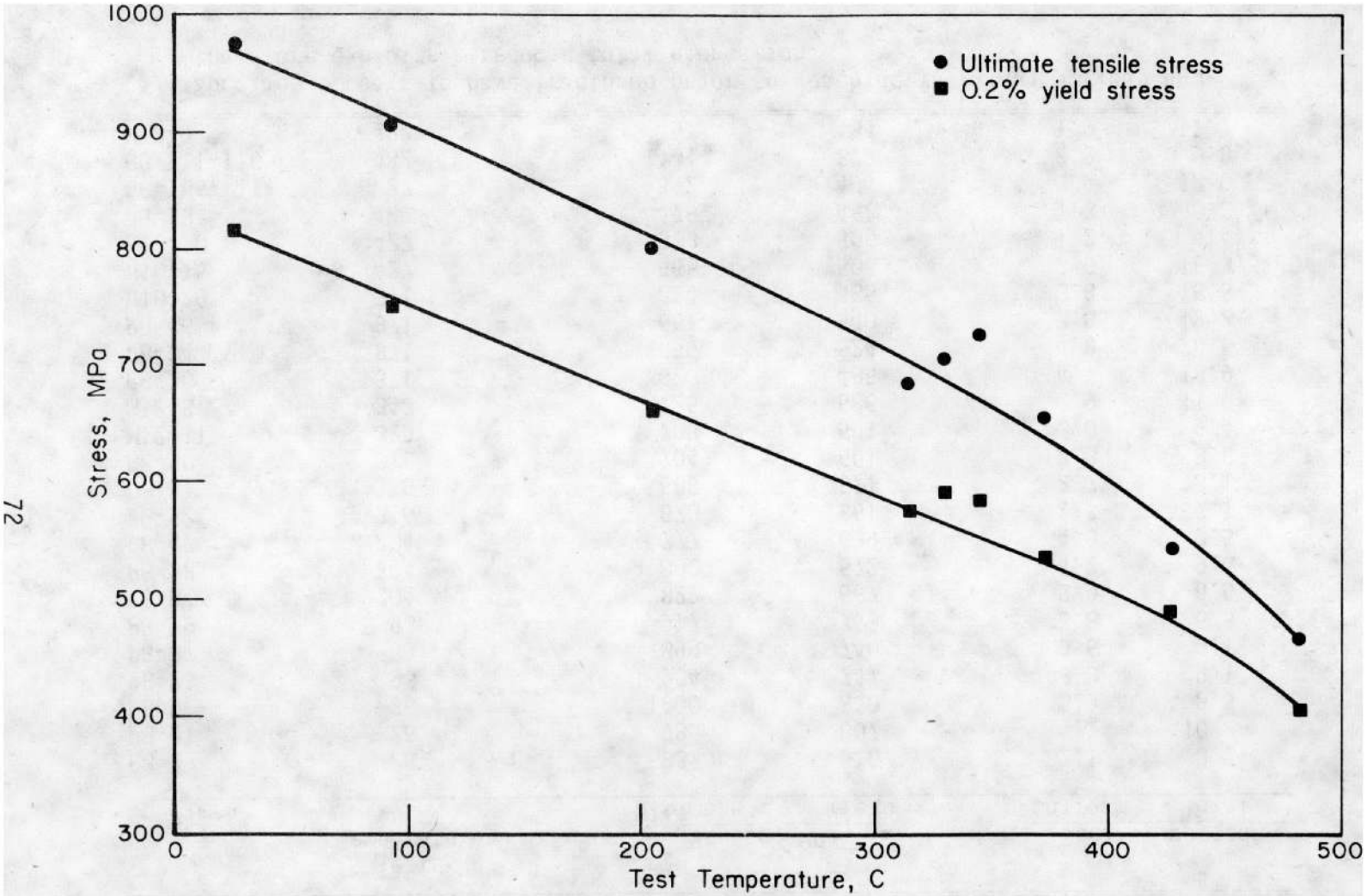

FIGURE 21. AVERAGE ENGINEERING TENSILE STRESS FOR IRRADIATED H. B. ROBINSON FUEL-ROD CLADDING AS A FUNCTION OF TEMPERATURE

Strain Rate 0.025/min

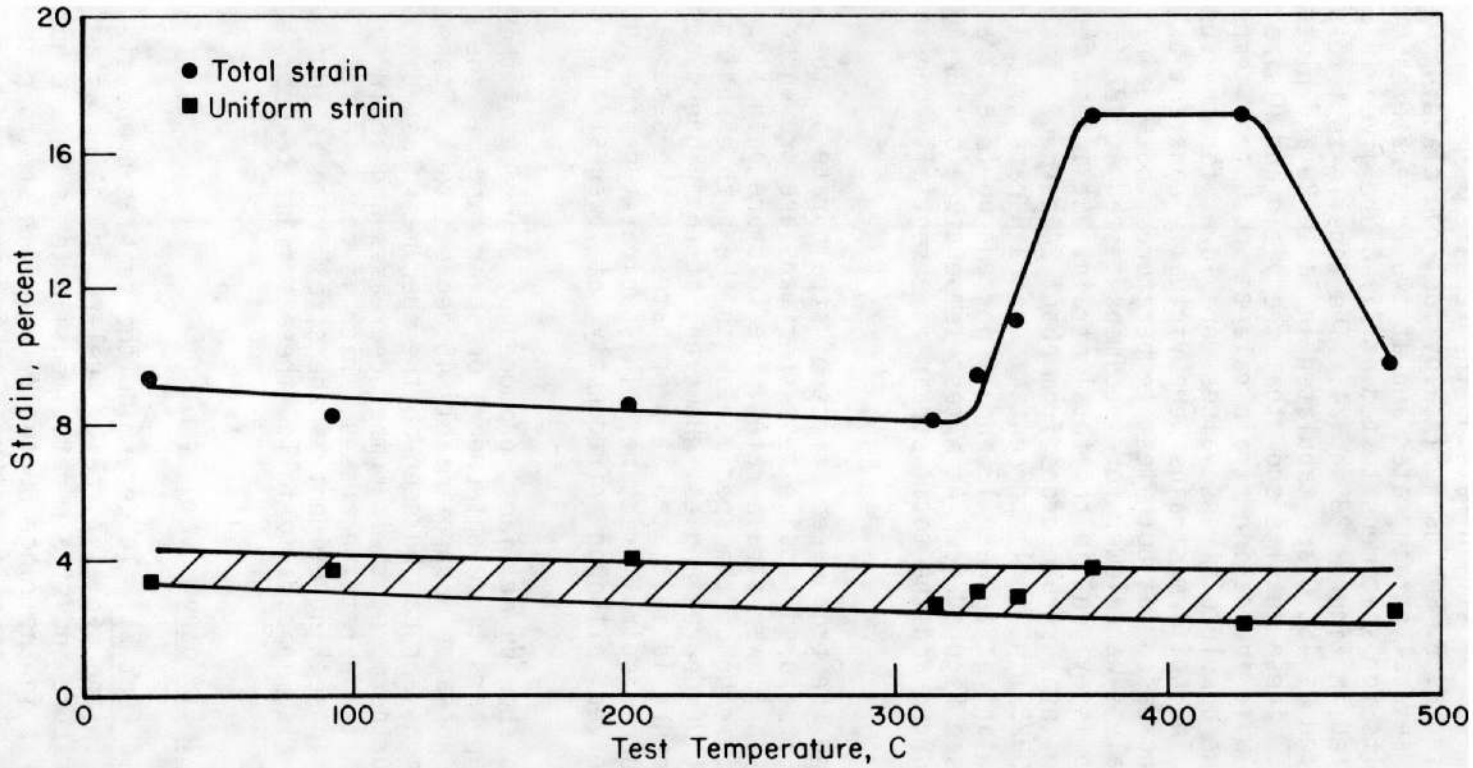

FIGURE 22. AVERAGE ENGINEERING TENSILE STRAIN FOR IRRADIATED H. B. ROBINSON FUEL-ROD CLADDING AS A FUNCTION OF TEMPERATURE

Strain Rate 0.025/min

To evaluate the effect of strain rate on the tensile properties, the irradiated H. B. Robinson Zircaloy fuel-rod cladding was tensile tested at several strain rates and at two temperatures. The tensile-test results for specimens tested at 371 C are given in Table 19 and plotted in Figures 23 and 24. The tensile-test results for specimens tested at 482 C are tabulated in Table 20 and plotted in Figures 25 and 26. These results show that the yield and ultimate stresses increase with increasing strain rate at both test temperatures, although the absolute stress values were lower for the specimens tested at 482 C. The uniform strains were virtually constant as the strain rate was increased at both test temperatures, but again the absolute strain values were lower for specimens tested at 482 C. The biggest difference is evident in the total strain. At a test temperature of 371 C, the total strain drops from about 24 percent at a strain rate of 0.0025/min to 12 percent at a strain rate of 0.1/min and is almost constant at between 12 and 15 percent up to a strain rate of 2.5/min (see Figure 24). At a test temperature of 482 C, annealing has occurred and the total strain is essentially constant at 9 to 10 percent.

Photographs showing the pronounced effect of strain rate on the appearance of the fractured tensile test specimens are presented in Figure 27. At the lower strain rates, the fracture path zigzags around the circumference of the specimen, with the path changing direction at about 90-degree angles. However, at the highest strain rates, once a fracture is initiated it propagates in the same direction to produce a spiral fracture. This spiral-type fracture also has been observed, although infrequently, at lower strain rates.

The specimens also show an artifact, produced by cracking of the surface oxide, that appears to reveal Lüders or shear bands in the specimens. These appear at approximately 45 degrees to the tensile axis of the specimens and can be seen on the specimens tested at both 371 and 427 C. Furthermore, their number decreases and their spacing increases as the strain rate increases, which is consistent with the decrease in necking evident as the strain rate is increased. The fracture path also appears to follow these surface traces.

Irradiated Oconee I Cladding

Oconee I, One Cycle (Lot 2). To determine the tensile properties of irradiated Oconee I (one cycle) Zircaloy fuel-rod cladding as a function of temperature and strain rate, tensile tests were conducted at test temperatures in the range 80 to 427 C and at strain rates of 0.0025 to 2.5/min. The tensile-test results for irradiated Lot 2,

TABLE 19. TENSILE TEST RESULTS FOR IRRADIATED H.B. ROBINSON ZIRCALOY FUEL-ROD CLADDING AS A FUNCTION OF STRAIN RATE AT 371 C

Specimen	Strain Rate, /min	Stress, MPa		Strain, percent	
		Ultimate	Yield	Uniform	Total
H10-33	0.0025	648	524	5.6	24.0
H10-20	0.025	694	586	3.8	16.5
H10-32	0.10	746	586	3.5	12.3
H10-34	0.50	750	609	4.2	11.8
H10-35	2.5	754	658	4.5	13.2
H10-38	2.5	761	678	4.2	12.8

TABLE 20. TENSILE TEST RESULTS FOR IRRADIATED H.B. ROBINSON ZIRCALOY FUEL-ROD CLADDING AS A FUNCTION OF STRAIN RATE AT 482 C

Specimen	Strain Rate, /min	Stress, MPa		Strain, percent	
		Ultimate	Yield	Uniform	Total
G8-111-116	0.025	442	370	2.8	9.8
G8-99-104	0.25	539	437	2.9	3.7
G8-121-126	2.5	575	471	2.9	9.3

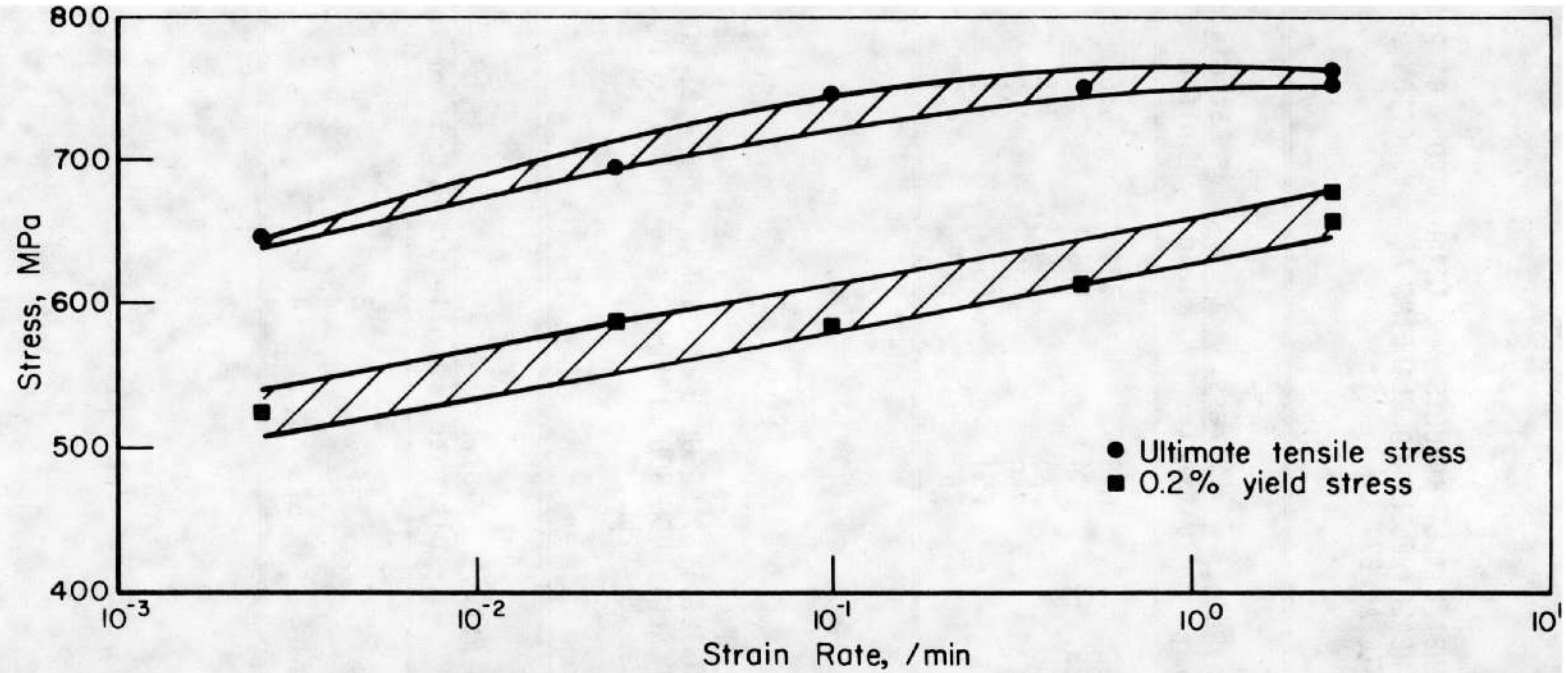

FIGURE 23. ENGINEERING TENSILE STRESS FOR IRRADIATED H.B. ROBINSON FUEL-ROD CLADDING AS A FUNCTION OF STRAIN RATE

Test Temperature 371 C

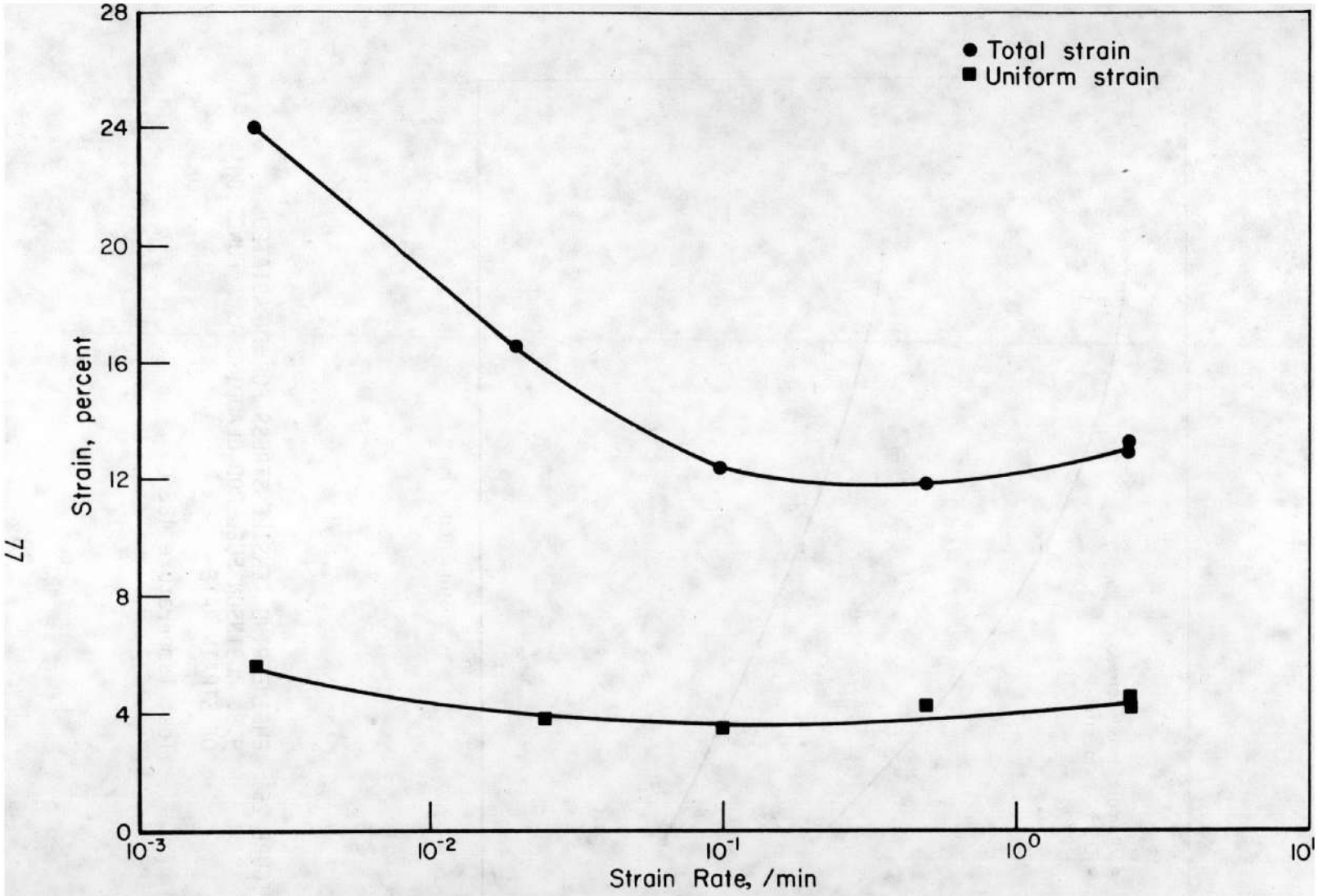

FIGURE 24. ENGINEERING TENSILE STRAIN FOR IRRADIATED H.B. ROBINSON FUEL-ROD CLADDING AS A FUNCTION OF STRAIN RATE

Test Temperature 371 C

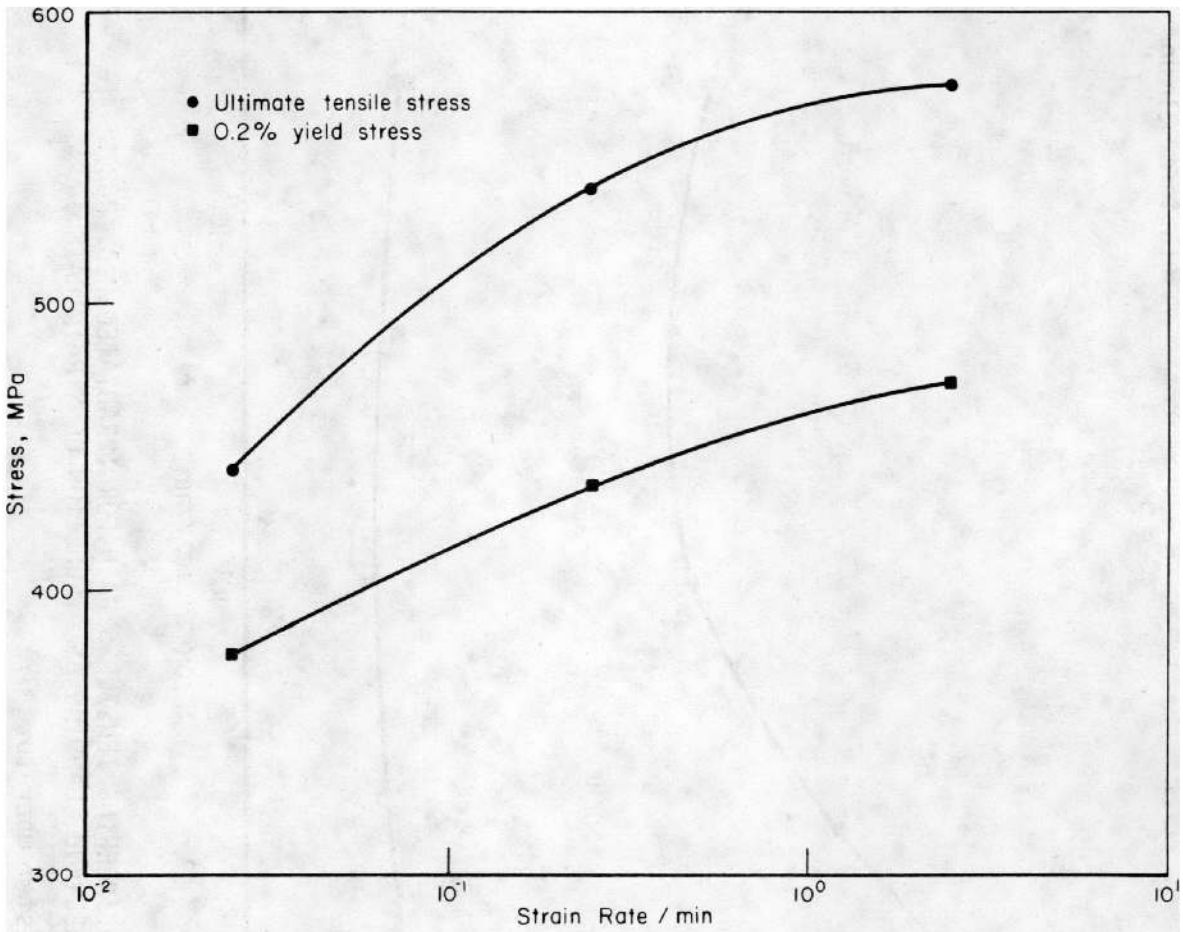

FIGURE 25. ENGINEERING TENSILE STRESS FOR IRRADIATED H.B. ROBINSON FUEL-ROD CLADDING AS A FUNCTION OF STRAIN RATE

Test Temperature 482 C

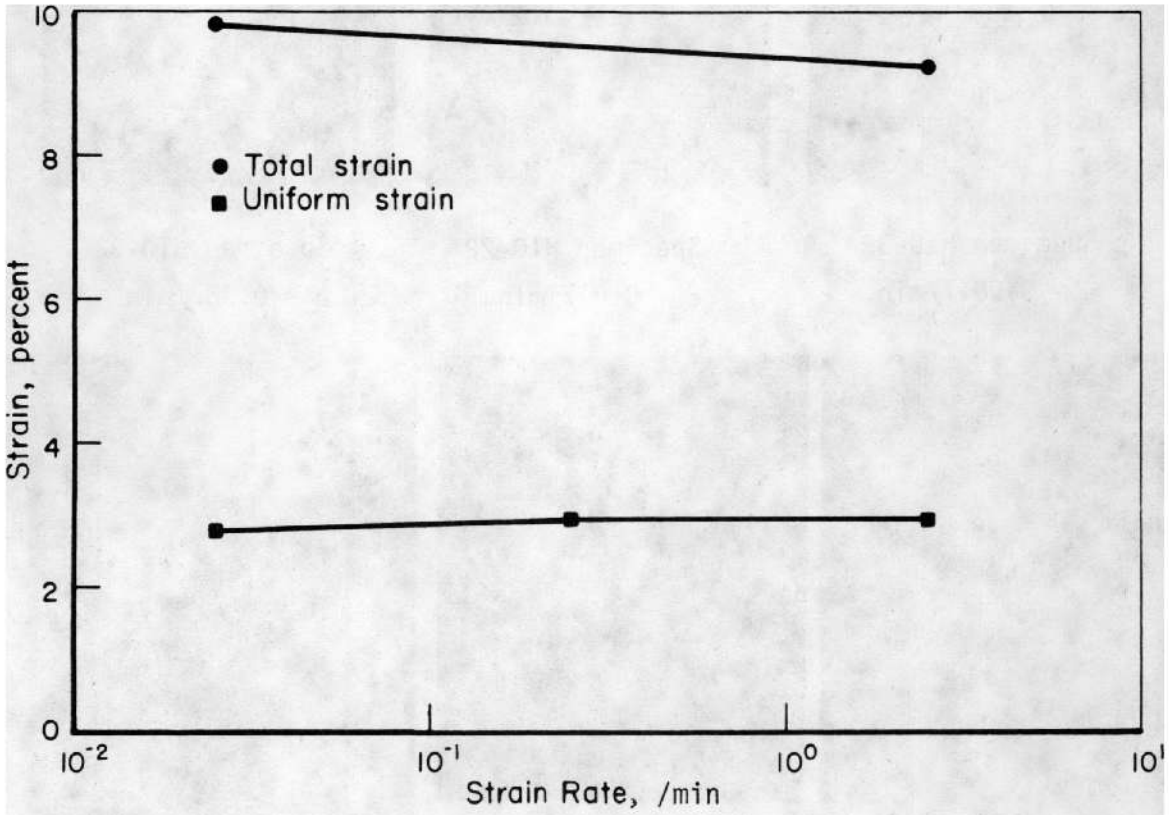

FIGURE 26. ENGINEERING TENSILE STRAIN FOR IRRADIATED H.B. ROBINSON FUEL-ROD CLADDING AS A FUNCTION OF STRAIN RATE

Test Temperature 482 C

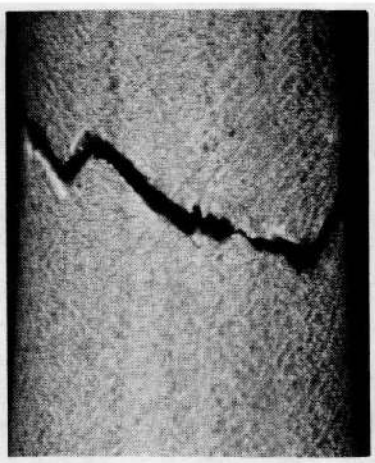

Specimen H10-33
$\dot{\varepsilon}$ = 0.0017/min.

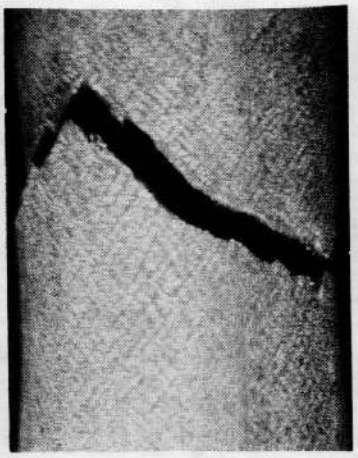

Specimen H10-22
$\dot{\varepsilon}$ = 0.017/min.

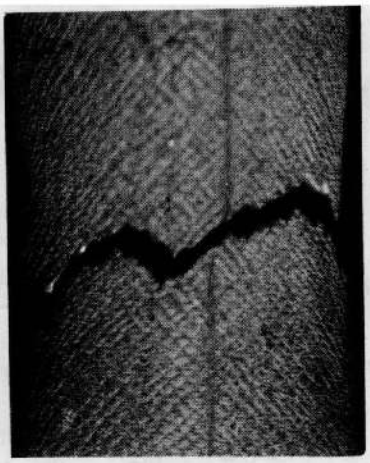

Specimen H10-32
$\dot{\varepsilon}$ = 0.067/min.

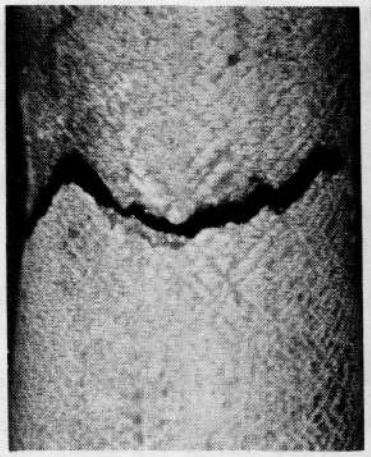

Specimen H10-34
$\dot{\varepsilon}$ = 0.33/min.

Specimen H10-38
$\dot{\varepsilon}$ = 1.7/min.

Specimen P8-69
$\dot{\varepsilon}$ = 6.7/min.

FIGURE 27. EFFECT OF STRAIN RATE ON THE APPEARANCE OF FRACTURED TENSILE TEST SPECIMENS OF H.B. ROBINSON IRRADIATED ZIRCALOY FUEL-ROD CLADDING

Test Temperature 371 C

Oconee I (one cycle), cladding are given in Table 21 and are plotted in Figures 28 and 29. The yield and ultimate stresses decrease monotonically and almost linearly with increasing temperature from 28 C to 427 C. The uniform strain is essentially constant at between 2 and 4 percent. The total elongation (strain) exhibits a decreasing trend in the test temperature range from 28 to almost 300 C. The total strain then increases sharply to a value of about 22 percent at a test temperature of 427 C. No tests were run at higher temperatures.

The tensile-test results for irradiated Lot 2 cladding are given in Table 22 and are plotted in Figures 30 and 31. The yield stress, ultimate stress, and uniform strain all exhibit almost no effect of increased strain rate in the range 0.0025 to 2.5/min. The stresses show a slight (4 to 6 percent) increasing trend and the uniform strain decreases slightly with increased strain rate. However, the total strain decreases about 50 percent from 0.0025 to 0.25/min and is about constant out to a strain rate of 2.5/min.

Oconee I, Two Cycle (Lot 3). The tensile-test results for the Oconee I (two cycle) as-irradiated fuel-rod cladding are given in Table 23. Included in this table are the tensile-properties variations as a function of both test temperature and strain rate. The constant strain-rate (varying test temperature) data are plotted in Figure 32. Trends in these data are normal for this two-cycle cladding with respect to the decreases in both yield and ultimate tensile stress and the increase in total strain, all with increasing test temperature. The data do show stress elevation throughout the entire test-temperature range over the Oconee I (one cycle) cladding.

The constant-temperature (varying strain rate) data for the two-cycle cladding are plotted in Figure 33. Except for the highest strain-rate data point, 0.5/min, the other data show the previously demonstrated strain-rate strength elevation and ductility depression effect. The strength at the 0.5/min strain rate appears low and no explanation except the possibility of scatter is apparent. An additional test was conducted at this strain rate and the stresses obtained verified these data.

Oconee I, Three Cycle (Lot 4). Table 24 gives the tensile-test results for the Oconee I (three cycle) as-irradiated spent-fuel cladding. Included in this table are the tensile-properties variations as a function of both test temperature and strain rate. The constant-strain (varying test temperature) data are plotted in Figure 34. Trends are as expected for the three-cycle cladding, with a decrease in both the yield and ultimate tensile stress and an increase in

TABLE 21. TENSILE TEST RESULTS FOR IRRADIATED OCONEE I (ONE CYCLE) ZIRCALOY FUEL-ROD CLADDING AS A FUNCTION OF TEMPERATURE

Strain Rate, 0.025/min

Specimen	Test Temp, C	Stress, MPa		Strain, Percent	
		Ultimate	Yield	Uniform	Total
47118/92-97	28	925	780	3.5	10.9
47118/14-19	204	734	618	3.3	8.0
47015/42-47	296	649	544	2.8	7.2
47118/26-31	316	616	506	3.9	15.0
47104/55-60	316	623	517	3.9	11.5
47015/37-42	316	620	492	5.3	12.3
47118/70-75[a]	343	609	511	3.7	13.9
47118/31-36[a]	343	636	516	3.4	12.9
46118/75-80[a]	343	603	494	3.6	14.1
47118/87-92[a]	343	605	487	3.3	14.4
47118/117-122[a]	343	610	492	3.3	14.3
47103/87-92[a]	343	599	482	3.5	13.9
47104/60-65[a]	343	605	494	3.5	14.4
47118/104-109	371	588	498	3.1	14.8
47118/122-127	427	484	443	2.4	23.3
47015/47-52	427	481	429	2.5	20.0

(a) Strain rate was 0.005/min to 2.0 percent offset yield strength and 0.025/min to failure.

TABLE 22. TENSILE TEST RESULTS FOR IRRADIATED OCONEE I (ONE CYCLE) ZIRCALOY FUEL-ROD CLADDING AS A FUNCTION OF STRAIN RATE

Test Temperature 371 C

Specimen	Strain Rate, /min	Stress, MPa		Strain, Percent	
		Ultimate	Yield	Uniform	Total
47103/111-116	2.5	591	503	<7.5	12.9
47103/74-79	0.25	594	492	3.6	13.6
47118/104-109	0.025	588	498	3.1	14.8
47103/11-16	0.0025	558	484	4.6	21.4

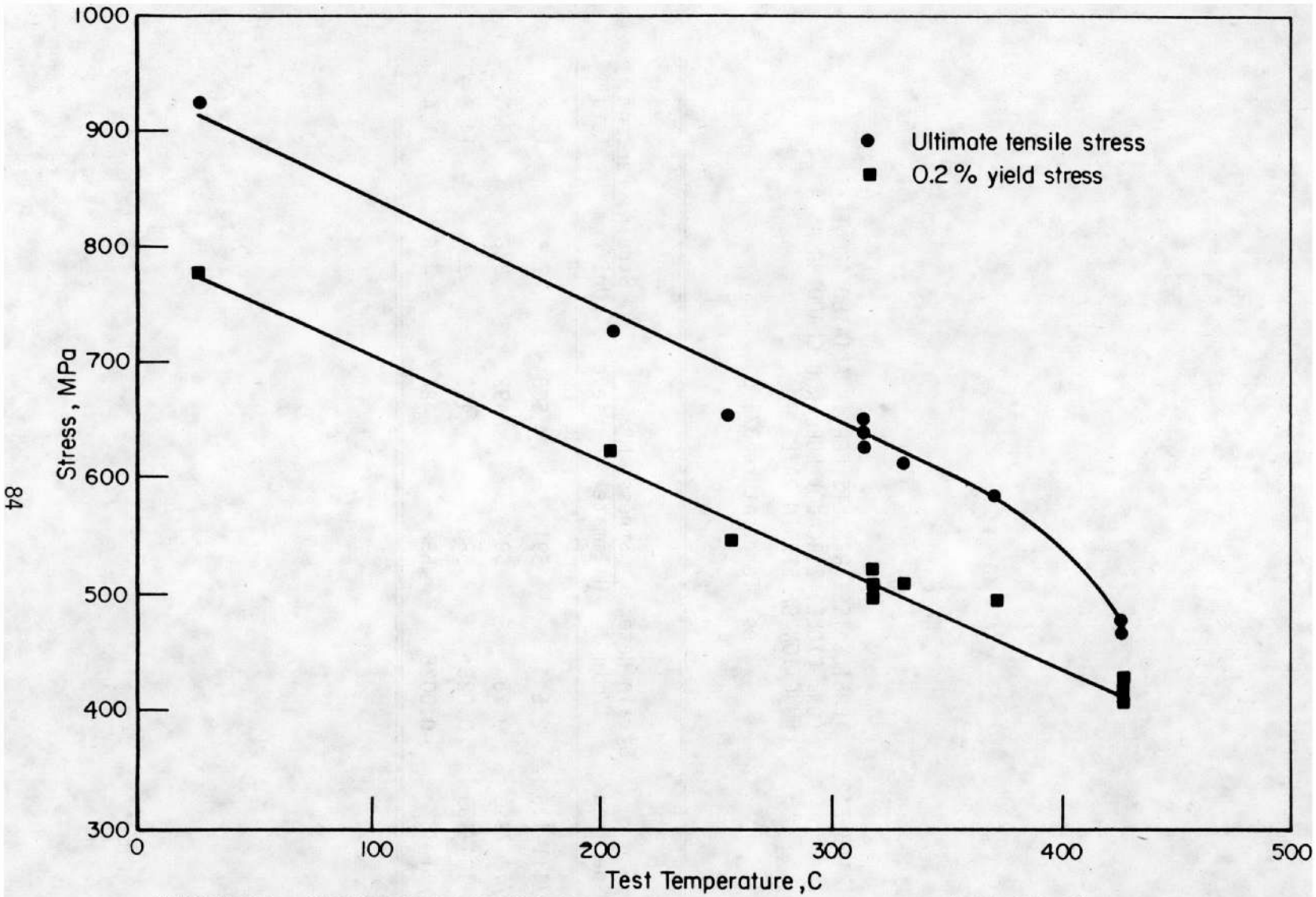

FIGURE 28. ENGINEERING TENSILE STRESS FOR IRRADIATED OCONEE I (ONE CYCLE) FUEL-ROD CLADDING AS A FUNCTION OF TEMPERATURE

Strain Rate 0.025/min

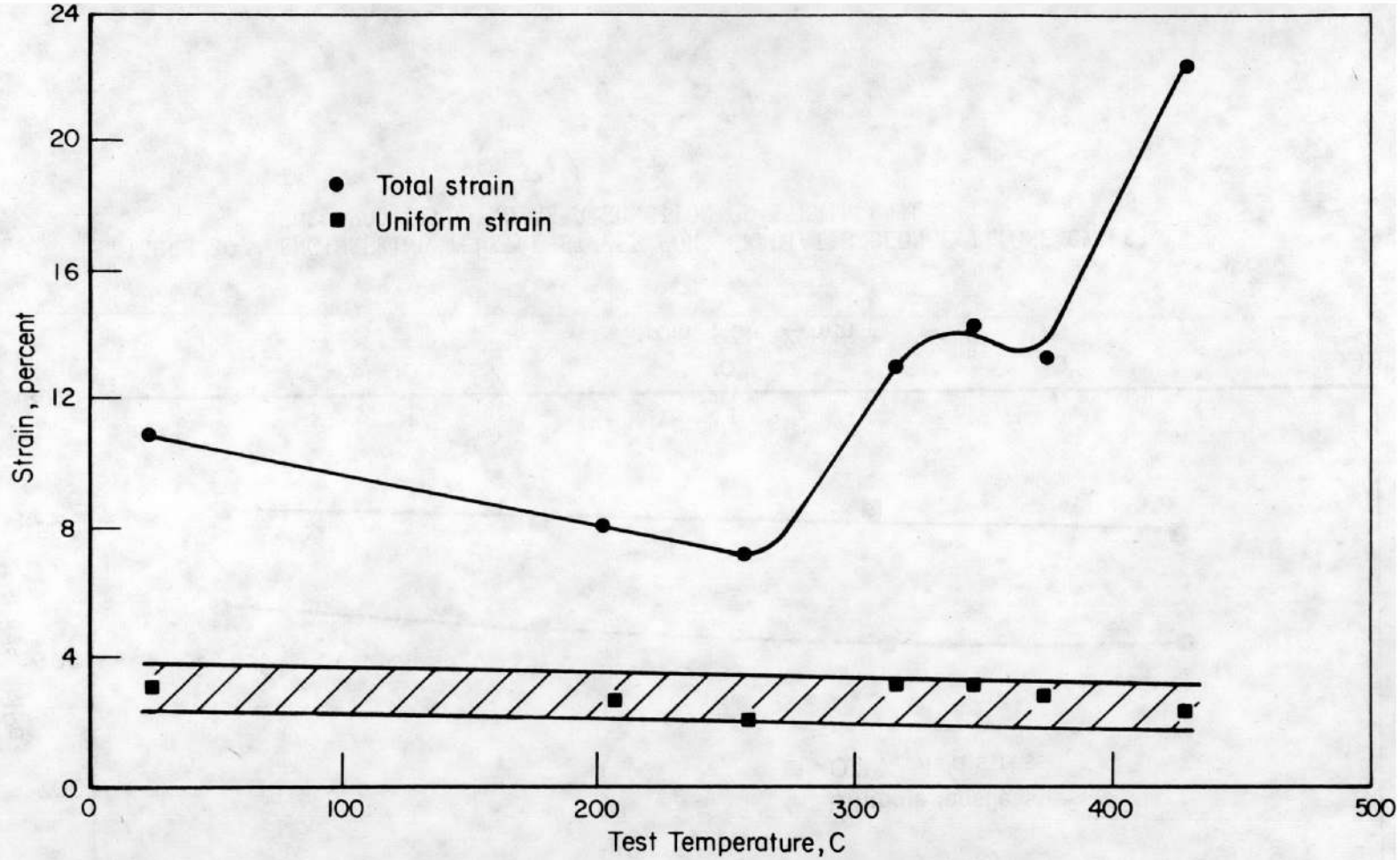

FIGURE 29. ENGINEERING TENSILE STRAIN FOR IRRADIATED OCONEE I (ONE CYCLE) FUEL-ROD CLADDING AS A FUNCTION OF TEMPERATURE

Strain Rate 0.025/min

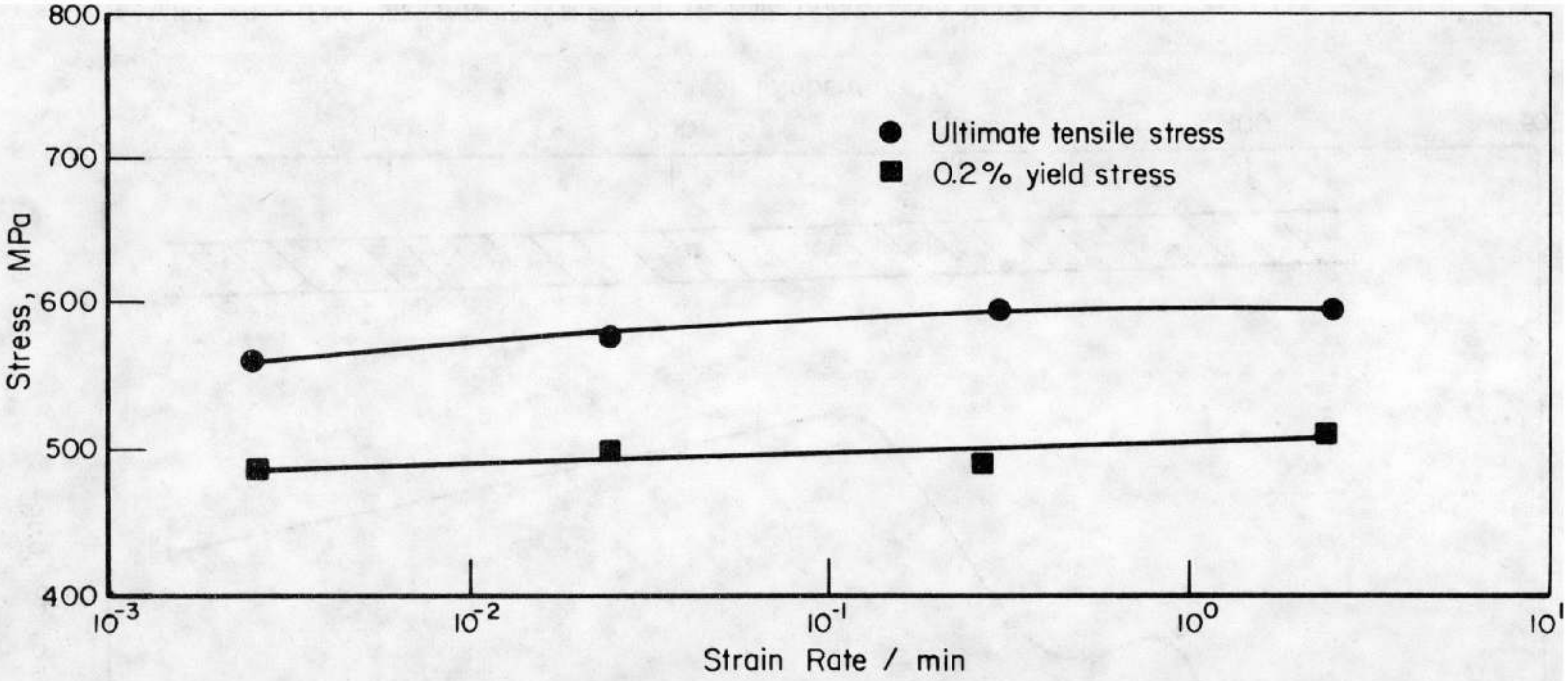

FIGURE 30. ENGINEERING TENSILE STRESS FOR IRRADIATED OCONEE I (ONE CYCLE) FUEL-ROD CLADDING AS A FUNCTION OF STRAIN RATE

Test Temperature 371 C

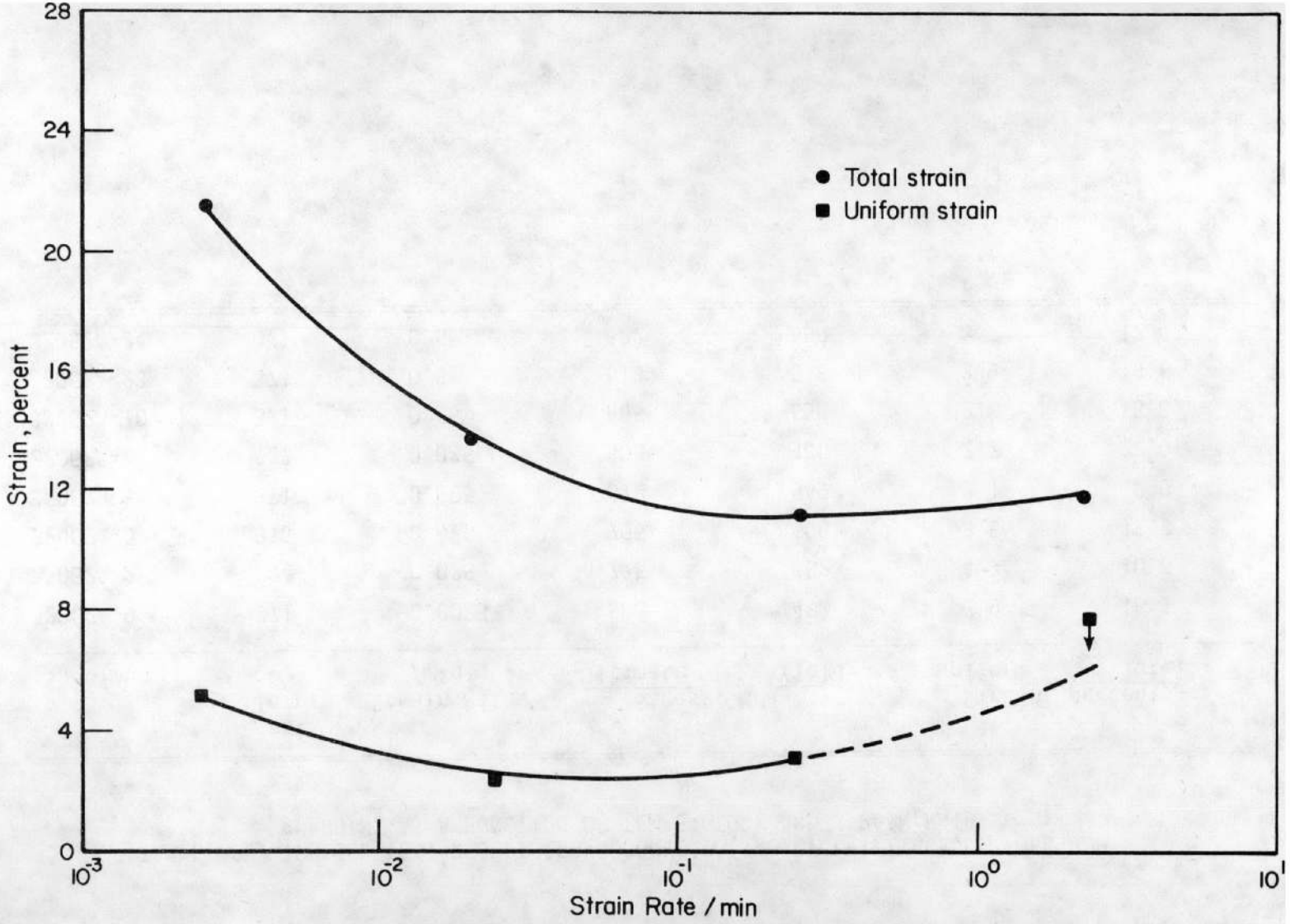

FIGURE 31. ENGINEERING TENSILE STRAIN FOR IRRADIATED OCONEE I (ONE CYCLE) FUEL-ROD CLADDING AS A FUNCTION OF STRAIN RATE

Test Temperature 371 C

TABLE 23. TENSILE TEST RESULTS FOR OCONEE I (TWO CYCLE) ZIRCALOY FUEL-ROD CLADDING AS A FUNCTION OF TEMPERATURE AND STRAIN RATE

Specimen	Test Temp, C	Strain Rate, /min	Stress, MPa		Strain, percent	
			Ultimate	Yield	Uniform	Total
32062A-9	371	0.0025	588	480	3.9	18.1
32062A-2	204	0.025	775	652	4.7	10.6
32062A-3	316	0.025	705	608	3.5	15.3
32062A-5	371	0.025	613	549	3.1	18.0
32062A-8	427	0.025	503	460	2.7	22.0
32062A-10	371	0.25	665	590	2.8	15.8
32062A-23	371	0.5	613	518	3.9	12.6
32062A-24	371	0.5	622	530	3.7	12.4

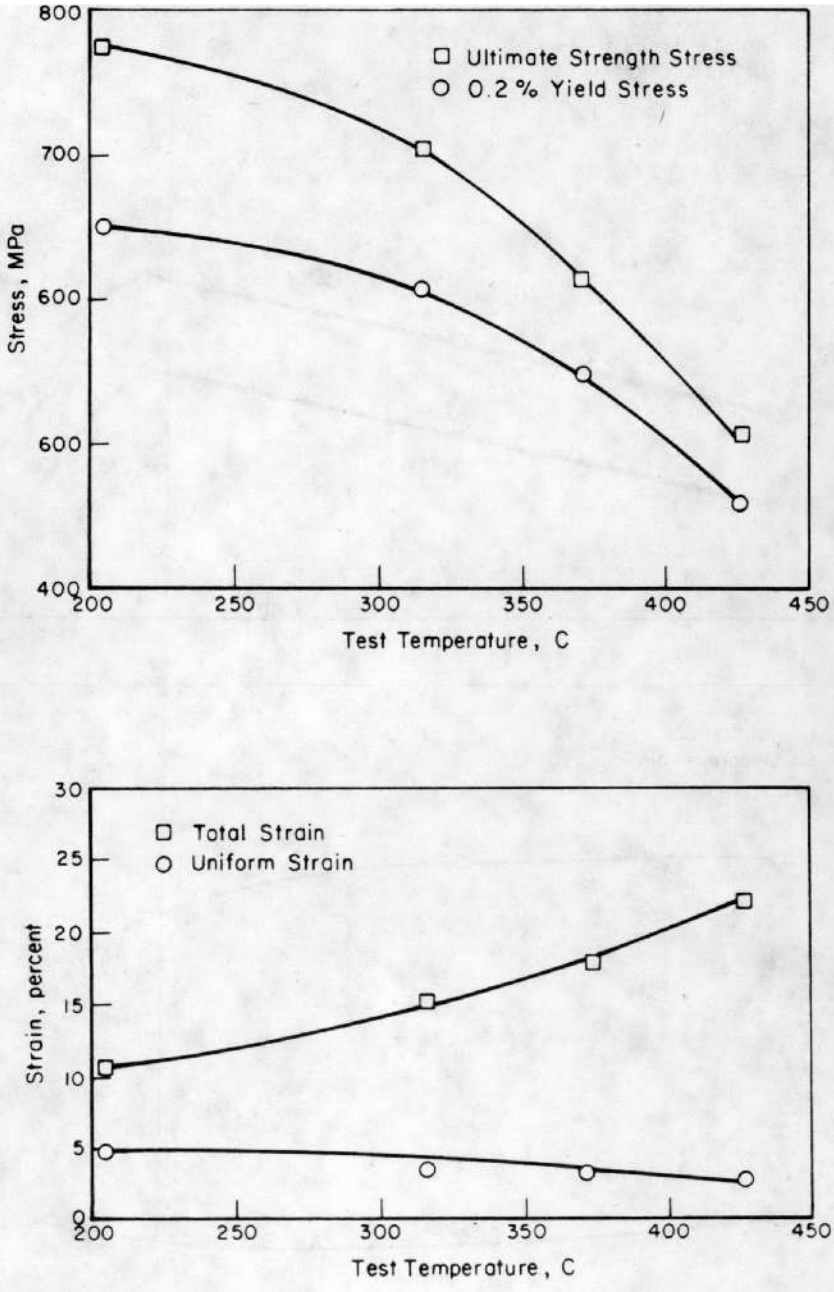

FIGURE 32. ENGINEERING TENSILE STRESS AND STRAIN FOR IRRADIATED OCONEE I (TWO CYCLE) FUEL ROD CLADDING AS A FUNCTION OF TEMPERATURE
Strain Rate 0.025/min

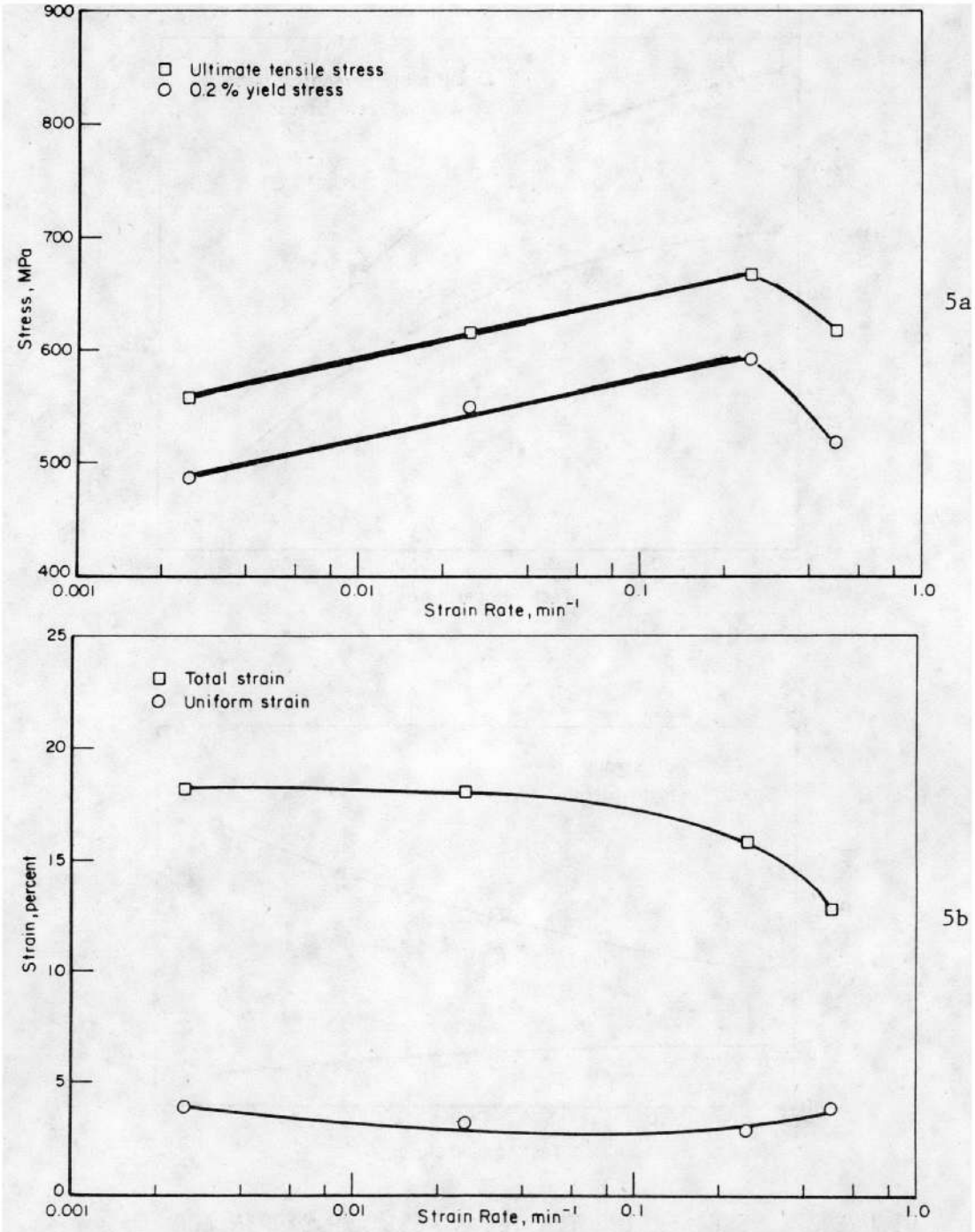

FIGURE 33. ENGINEERING TENSILE STRESS AND STRAIN FOR IRRADIATED OCONEE I (TWO CYCLE) FUEL-ROD CLADDING AS A FUNCTION OF STRAIN RATE
Test Temperature 371 C.

TABLE 24. TENSILE TEST RESULTS FOR OCONEE I (THREE CYCLE) ZIRCALOY FUEL-ROD CLADDING AS A FUNCTION OF TEMPERATURE AND STRAIN RATE

Specimen	Test Temp, C	Strain Rate, /min	Stress, MPa		Strain, percent	
			Ultimate	Yield	Uniform	Total
47080-5	371	0.0025	567	498	3.5	16.9
47082-6	204	0.025	780	647	3.7	8.4
47082-10	316	0.025	713	606	3.8	13.9
47082-16	371	0.025	606	534	3.0	14.8
47082-17	427	0.025	542	468	2.2	18.6
47080-11	371	0.25	585	498	3.5	10.4
47080-14	371	0.5	603	507	3.9	10.7

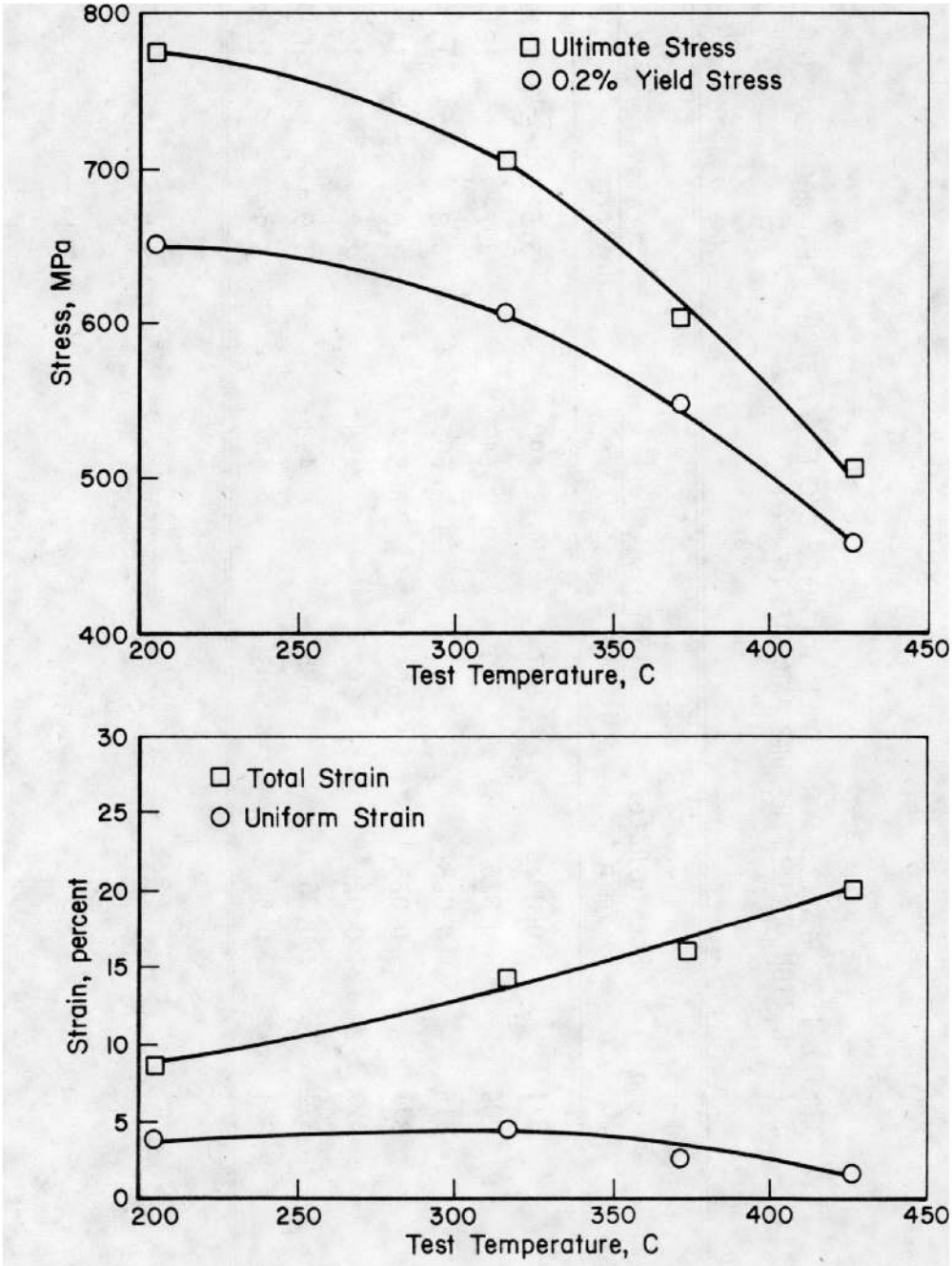

FIGURE 34. ENGINEERING TENSILE STRESS AND STRAIN FOR IRRADIATED OCONEE I (THREE CYCLE) FUEL ROD CLADDING AS A FUNCTION OF TEMPERATURE

Strain Rate 0.025/min

total tensile strain with increasing test temperature. The uniform tensile strain is almost constant at between 2 and 4 percent.

The constant-temperature (varying strain rate) data for the three-cycle cladding are plotted in Figure 35. Again the uniform tensile strain is almost constant at 2 to 4 percent. Both the yield and ultimate tensile stresses increase with increasing strain rate to 0.025/min and are virtually constant at 500 and 600 MPa, respectively. The total strain decreases with increasing strain rate to 0.25/min (10.4 percent) and increases only slightly at 0.5/min (10.7 percent).

Comparison of Tensile Data

A comparison of the unirradiated Oconee I archive material and the unirradiated tubing supplied to ORNL and BCL by Sandvik shows that there is no difference in either the stress or strain values within experimental error and material properties scatter. This is not surprising since both materials were fabricated by Sandvik. However, these data do indicate that the ultimate tensile stress varies about 3 percent and the yield stress varies almost 8 percent. The strains appear to vary as much as 30 percent. Therefore, when comparisons are made with the irradiated-specimen data where only one or two tests are possible, trends may appear. The experimental results are assumed to vary by at least the amounts stated above and therefore no meaningful statistical analysis is possible. The lines were drawn on each graph by hand and represent a best estimate for the available data.

The average tensile-properties values for the Point Beach Rod A25-06, the H.B. Robinson rods (see Table 18), and the Oconee I, three-cycle (see Table 21) rods are plotted in Figures 36 through 39. As can be seen, above 300 C the total strains for the unirradiated H.B. Robinson rods and the Oconee I (three-cycle) rods (Figure 39) indicate an increase with increased test temperature. Total strain for the H.B. Robinson rod drops again at 482 C. No trends are apparent in the uniform strain. However, when examining the average stresses more closely, a slight increase at about 300 C and a subsequent drop at about 375 C are seen in both the ultimate and yield stress for the unirradiated and irradiated H.B. Robinson cladding. There are not enough data for the Oconee I (three cycle) cladding at 300 to 371 C to determine whether the slight trends in stresses exist for the material. However, the total elongation does increase for the Oconee I cladding, but at a slightly lower temperature (between 200 and 300 C), and continues to increase up to 427 C. The slight trends in all the tensile-properties data except the total strain may be due to variations in the specimens, and the trends were examined only because of the large

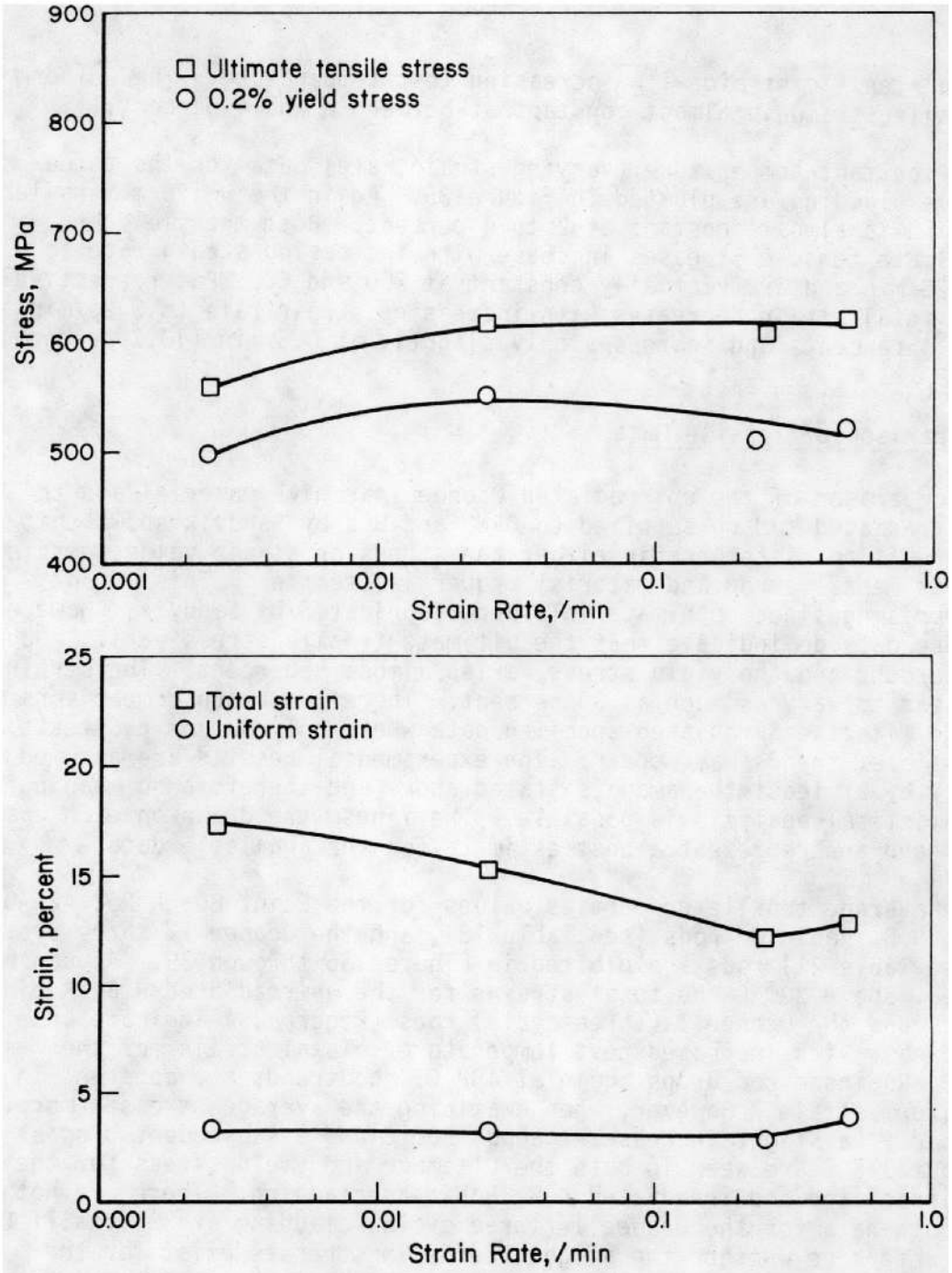

FIGURE 35. ENGINEERING TENSILE STRESS AND STRAIN FOR IRRADIATED OCONEE I (THREE CYCLE) FUEL-ROD CLADDING AS A FUNCTION OF STRAIN RATE

Test Temperature 371 C

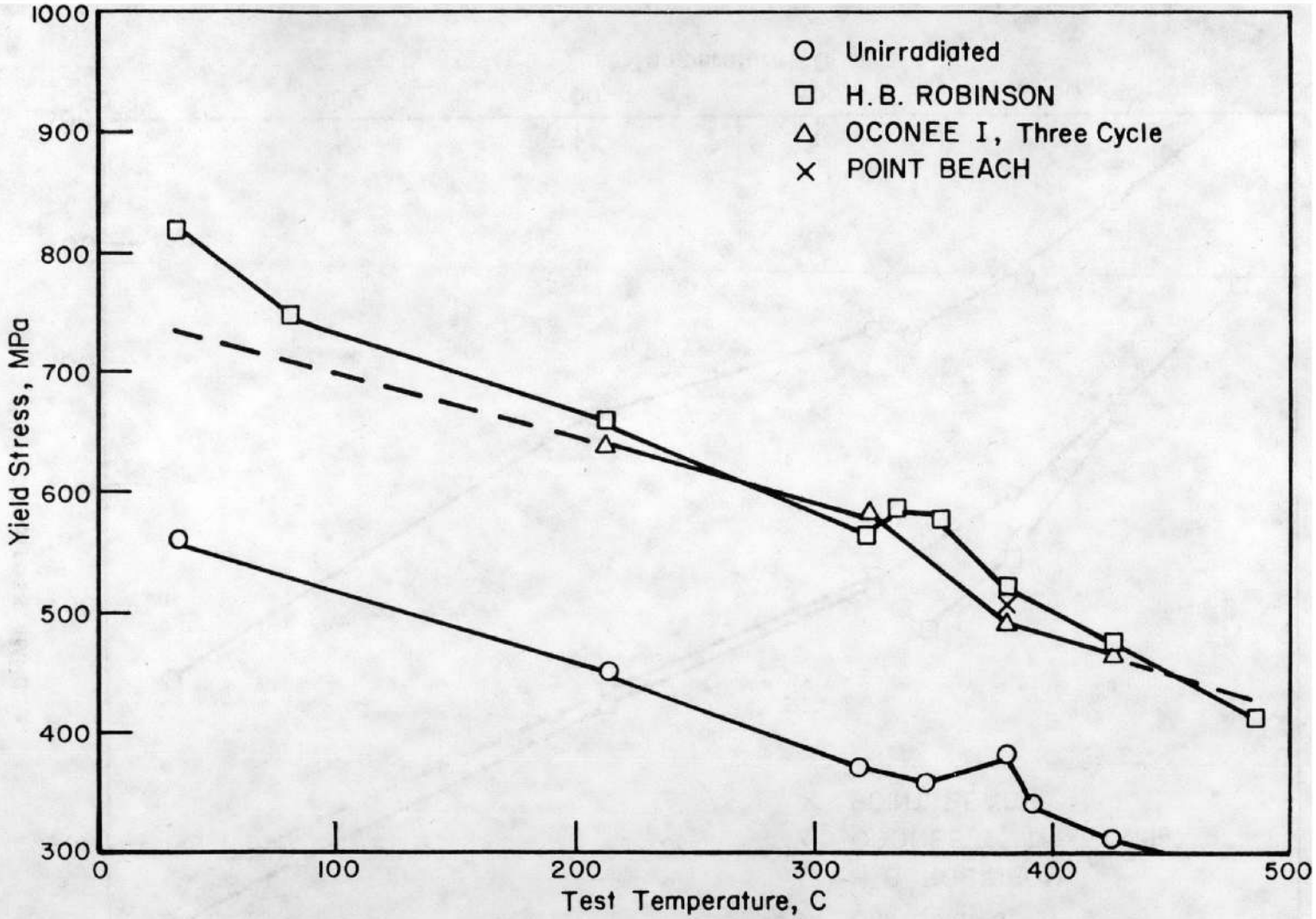

FIGURE 36. COMPARISON OF AVERAGE ENGINEERING 0.2% YIELD TENSILE STRESS FOR VARIOUS CLADDINGS AS A FUNCTION OF TEMPERATURE
Strain Rate 0.025/min

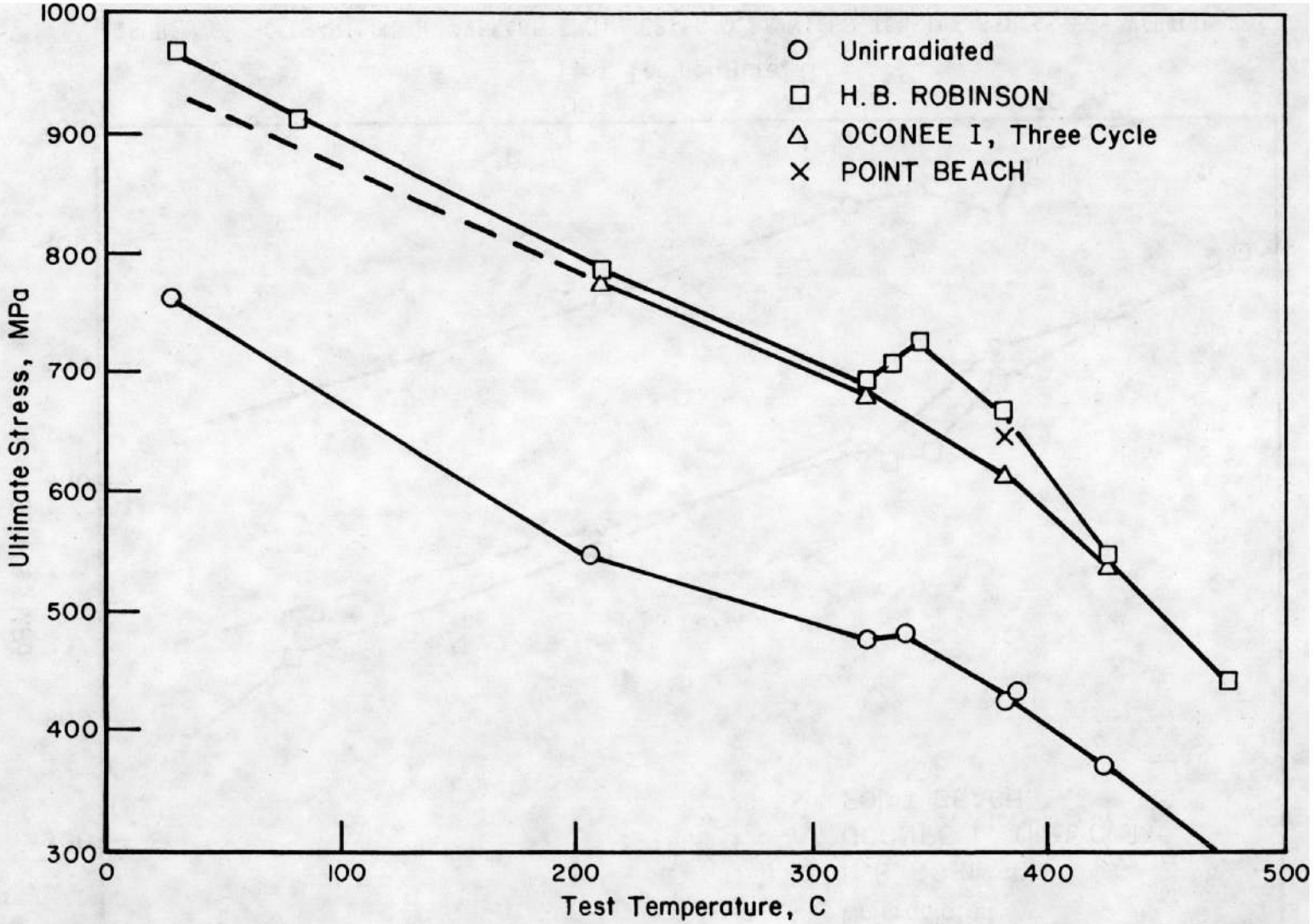

FIGURE 37. COMPARISON OF AVERAGE ENGINEERING ULTIMATE TENSILE STRESS FOR VARIOUS CLADDINGS AS A FUNCTION OF TEMPERATURE

Strain Rate 0.025/min

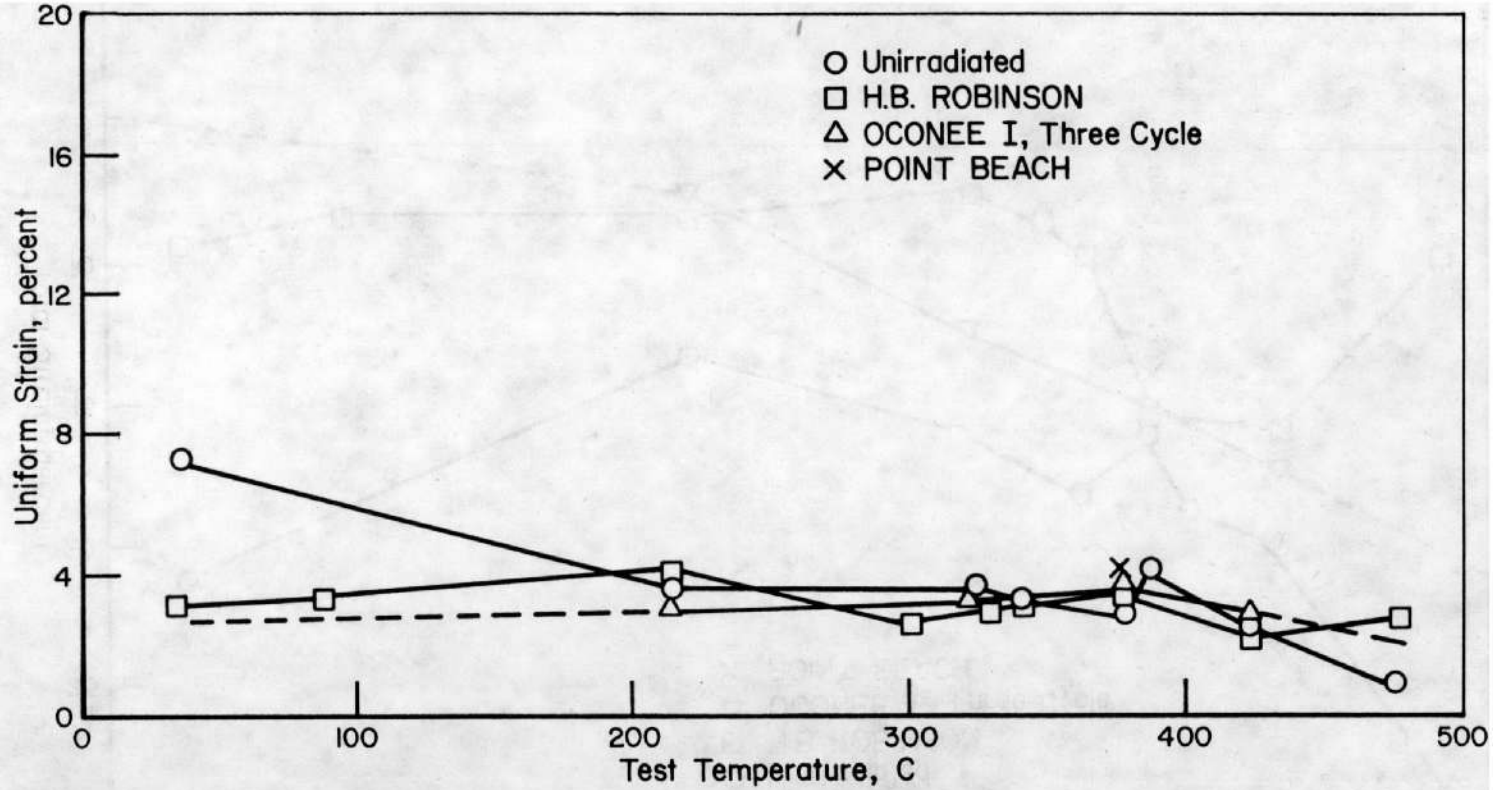

FIGURE 38. COMPARISON OF AVERAGE ENGINEERING UNIFORM TENSILE STRAIN FOR VARIOUS CLADDINGS AS A FUNCTION OF TEMPERATURE

Strain Rate 0.025/min

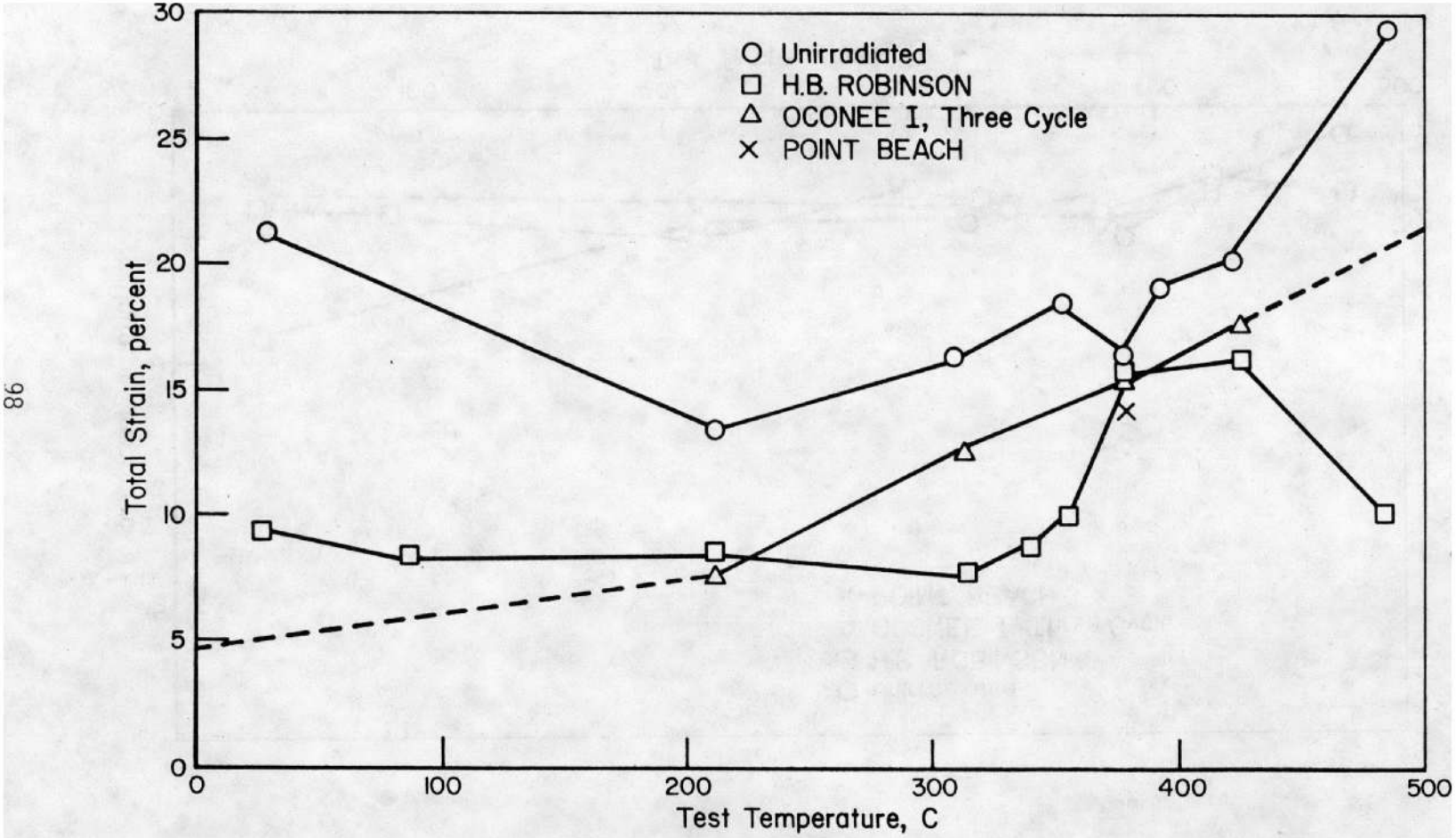

FIGURE 39. COMPARISON OF AVERAGE ENGINEERING TOTAL TENSILE STRAIN FOR VARIOUS CLADDINGS AS A FUNCTION OF TEMPERATURE

Strain Rate 0.025/min

increase in total strain exhibited by all the claddings, both unirradiated and irradiated.

Note that the temperature range 300 to 400 C is at or only slightly above the reactor operating temperature. Therefore, the irradiated Zircaloy-4 material exhibited an increased total strain between 300 and 400 C almost equal to that for the unirradiated material, even after the former material was irradiated to approximately 30,000 MWD/MTU. The exact reason for irradiation having almost no effect on the total strain in this temperature range is unknown. The yield and ultimate tensile strenghts (stresses) increased approximately 50 percent between 300 and 400 C because of irradiation; the uniform and total elongation (strain) values were approximately equal (possibly a 10 percent reduction) to those for the unirradiated material. This led to the surprising conclusion that, for the cladding materials tested, the tensile properties may be superior for irradiated cladding when the reactor is operated in the temperature range between 300 to 400 C.

Comparison of the tensile-test results for the Oconee I, one-, two-, and three-cycle material (from Tables 21, 23, and 24) showed that the ultimate and yield stresses increased about 100 to 150 MPa uniformly between 28 and 427 C after one cycle of irradiation (see Figure 40).

After two cycles of irradiation the strengths (stresses) again increased slightly but changed very little upon an additional cycle of irradiation. The uniform strain decreased after one cycle of irradiation and then remained almost constant at 2 to 4 percent. The total strain exhibited a similar trend, but above 300 C the decrease due to irradiation became less noticeable, and the total strain was almost equal to that for the unirradiated material at approximately 400 C. The tensile properties of the Oconee I Zricaloy-4 fuel-rod cladding again appeared to be improved after irradiation and during operation between about 350 and 427 C (see Figure 41).

Tube-Burst Tests

Unirradiated Oconee I Archive Cladding

Because very little Oconee I archive material remained, only four burst tests were conducted. Single tests were conducted at 316 and 427 C and two tests at 371 C; the strain rate was 0.004/min for all tests. The results of these tests are included with the

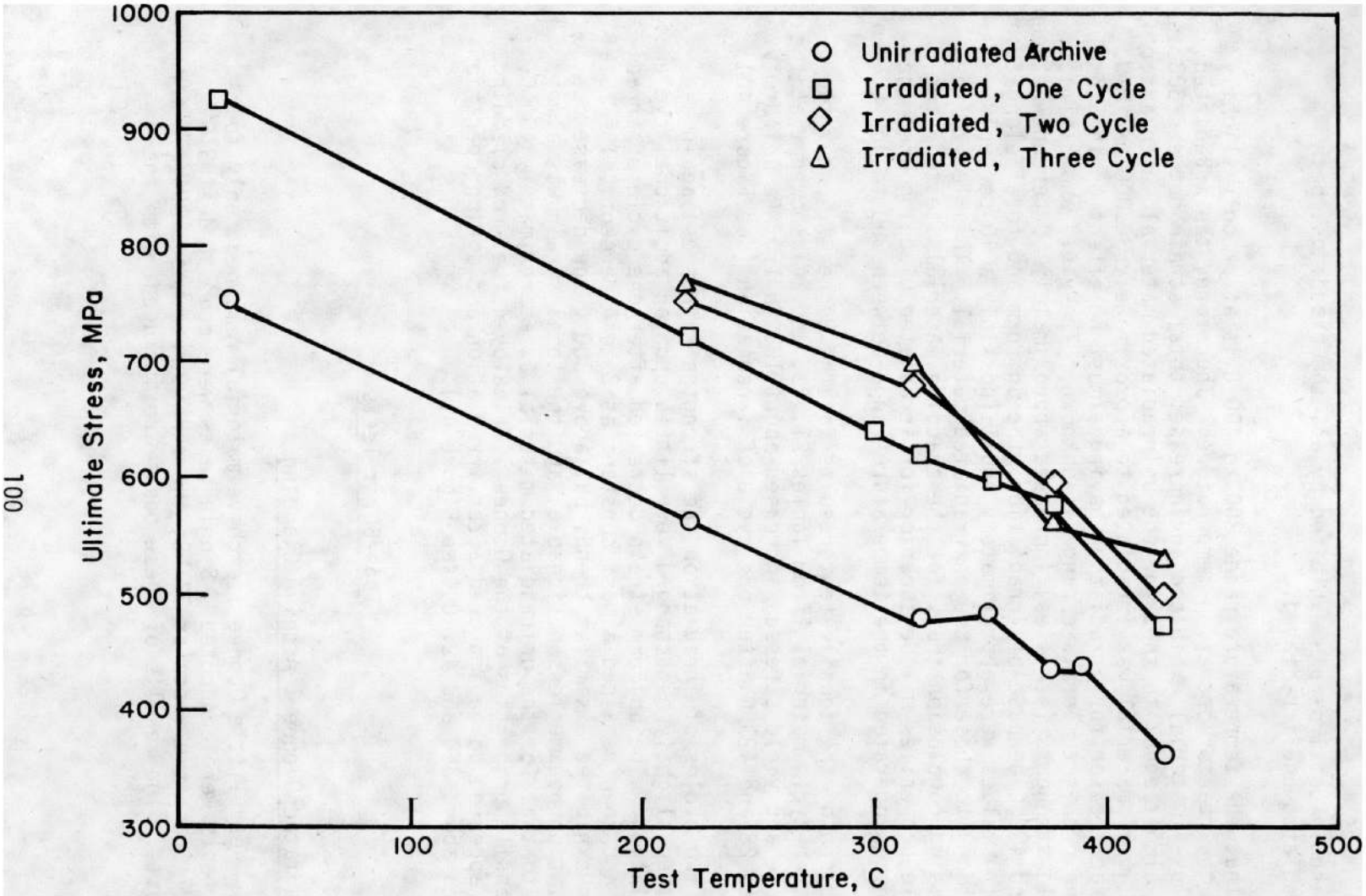

FIGURE 40. COMPARISON OF AVERAGE ENGINEERING ULTIMATE TENSILE STRESS FOR OCONEE I FUEL-ROD CLADDING AS A FUNCTION OF TEMPERATURE

Strain Rate 0.025/min

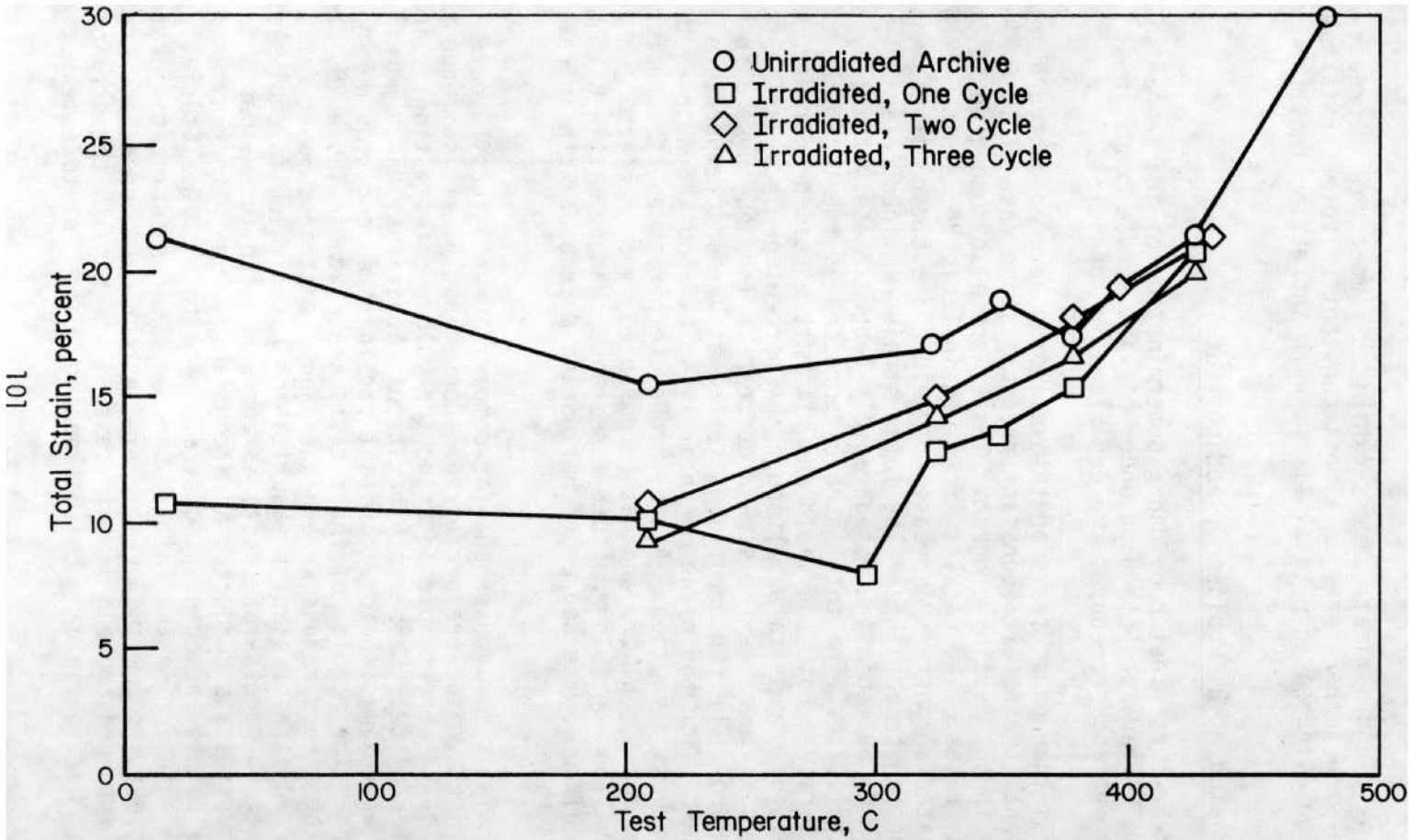

FIGURE 41. COMPARISON OF AVERAGE ENGINEERING TOTAL TENSILE STRAIN FOR OCONEE I FUEL-ROD CLADDING AS A FUNCTION OF TEMPERATURE

Strain Rate 0.025/min

irradiated Oconee I data in Table 26.

The yield and ultimate stress exhibited a monotonic decrease with increasing temperature, an almost constant uniform strain, and a monotonic increase in total strain with increasing temperature.

Irradiated H. B. Robinson Cladding (Lot 1)

The tube-burst test provided a determination of the mechanical properties of irradiated cladding under biaxial stress conditions. The test equipment and procedures are described in Appendix C.

Several tube-burst tests on this cladding were conducted using a constant strain rate (constant pressurization rate of 13.8 MPa/min) early in the testing program. Tests were also conducted at three stress rates. The results are given in Table 25. This material exhibited a constant decrease in yield and ultimate stress with increasing temperature. The total strain remained relatively constant to 316 C, but then increased rapidly (approximately tripled) between 316 and 427 C. The total strain decreased as the logarithm of stress rate. Both the yield and ultimate stresses increased with increasing stress rate, although the percentage increase in stress was not as great as the strain decrease. The toughness also increased. The ruptured tubes tested at various temperatures failed in shear, with the plane of shear lying at about 45 degrees to the hoop-stress direction. At the higher temperatures, the rupture became more localized and was accompanied by a greater degree of tube ballooning. The rupture appearance changed little with stress rate, although the degree of ballooning decreased with increase in stress rate.

For analytical purposes and for comparison with tensile data, constant strain rate data were preferred. Consequently, all subsequent tube-burst tests were conducted using the volume-rate testing feature of the BCL Hot Cell Laboratory burst-test apparatus, which permits a close approximation to a constant strain rate condition during testing. The results of these tests are given in Table 25. Note that the stress values were higher and the strains lower for a test conducted at a constant pressurization rate (which is equivalent to an engineering stress-rate test) as compared with the values obtained in tube-burst tests conducted at a constant volume rate (which is equivalent to an engineering strain-rate test). Qualitatively, the strain rate during the initial portion of a pressurization rate tube-burst test was low and relatively constant but increased extremely rapidly toward the end of this test. As a result, the strain rate was highest during yielding and ballooning, which let to somewhat higher

TABLE 25. TUBE-BURST TEST RESULTS FOR IRRADIATED H. B. ROBINSON ZIRCALOY FUEL-ROD CLADDING AS A FUNCTION OF TEMPERATURE AND STRAIN RATE

Specimen	Test Temp, C	Strain Rate, /min	Stress, MPa			Strain, percent	
			Yield	Ultimate	Failure	Uniform	Total
A8-25	204	0.0024	866	913	913	-	2.3
014-63	316	0.0024	763	803	803	-	2.5
014-17	371	0.0024	680	749	749	-	4.9
A8-17	427	0.0024	601	664	664	-	6.6
A1-17	371	0.0004	582	675	675	-	7.2
A1-72	371	0.024	739	797	797	-	1.8
G8/55-62	204	0.004	734	765	765	2.4	2.4
M12-16	204	0.004	678	749	749	2.5	2.6
G8/27-34	316	0.004	698	723	723	3.0	3.0
H6/62-69	371	0.001	507	583	574	3.8	4.4
M12-4	371	0.001	579	665	659	2.9	5.2
G8/20-27	371	0.004	625	647	637	3.4	6.6
M12-14	371	0.004	581	660	660	2.4	3.5
H6/10	371	0.035	586	657	657	2.4	2.5
M12-15	371	0.035	643	685	685	2.7	2.8
G8/13-20	427	0.004	498	566	554	2.9	7.3
M12-2	427	0.004	542	598	590	2.4	5.7

stresses and lower strains than would be obtained in a constant strain rate (volume rate) test. Therefore, only the last eight tests in Table 25 were used for comparison.

The yield and ultimate stresses exhibited a nonlinear decrease that accelerated with increase in temperature. The uniform strain remained constant with temperature, while the total strain increased sharply at 371 and 427 C. At lower temperatures, 204 and 316 C, the uniform and total strains were essentially identical. This was reflected in the coincidence of the ultimate and burst strengths, recorded in Table 25, for tests conducted at these temperatures.

Increases in strain rate produced a gradual increase in both ultimate and yield strengths. These increases in strength were accompanied by corresponding decreases in both the circumferential uniform and failure strains. The changes in uniform strain tended to be fairly minimal.

At strain rates of 0.001, 0.004, and 0.035/min, there were slight trends toward increased stresses and decreased strains with increasing strain rate.

Irradiated Oconee I Cladding

Oconee 1, One Cycle (Lot 2). The tube-burst results for Lot 2 material are given in Table 26, along with the Oconee I archive tube-burst data. These data are for burst stress and strain of irradiated Lot 2 fuel-rod cladding as a function of temperature and strain rate. The tube-burst yield and ultimate (engineering) stress and the uniform and total (engineering) strain are plotted versus temperature in Figure 42. These exhibited the expected trends. The burst mechanical properties also appeared to follow the expected trend with increasing strain rate, with both the stresses and strains coverging at about 0.5/min.

Oconee I, Two Cycle (Lot 3). The tube-burst results for Lot 3 material are given in Table 27. These data are for burst stress and strain of irradiated Lot 3 fuel-rod cladding as a function of temperature and strain rate. The expected trends were exhibited with respect to the effects of increasing temperature and strain rate.

Oconee I, Three Cycle (Lot 4). The tube-burst results for Lot 4 material are given in Table 28. These data are for burst stress and strain of irradiated Lot 4 fuel-rod cladding as a function of temperature and strain rate. The data again exhibited the expected

TABLE 26. TUBE-BURST TEST RESULTS FOR IRRADIATED OCONEE I (ONE CYCLE) ZIRCALOY FUEL-ROD CLADDING AS A FUNCTION OF TEMPERATURE AND STRAIN RATE

Specimen	Test Temp, C	Strain Rate, /min	Stress, MPa			Strain, percent	
			Yield	Ultimate	Failure	Uniform	Total
3[a]	316	0.004	499	565	560	2.7	9.2
2[a]	371	0.004	439	498	493	2.6	9.6
34020	371	0.004	410	476	456	2.6	10.0
1[a]	427	0.004	330	419	406	3.2	15.4
4/104-27	260	0.004	596	688	688	2.4	6.4
47101-2	260	0.004	732	797	797	1.8	5.7
47104-19	316	0.004	622	664	664	2.4	4.5
47101-7	316	0.004	622	687	687	1.8	4.0
47104-28	371	0.004	537	610	610	2.7	6.8
47104-2	427	0.004	420	525	495	4.7	18.0
47104-22	371	0.001	493	595	564	2.7	8.1
47118-4	371	0.035	679	725	725	2.3	2.5

(a) Unirradiated archive specimens.

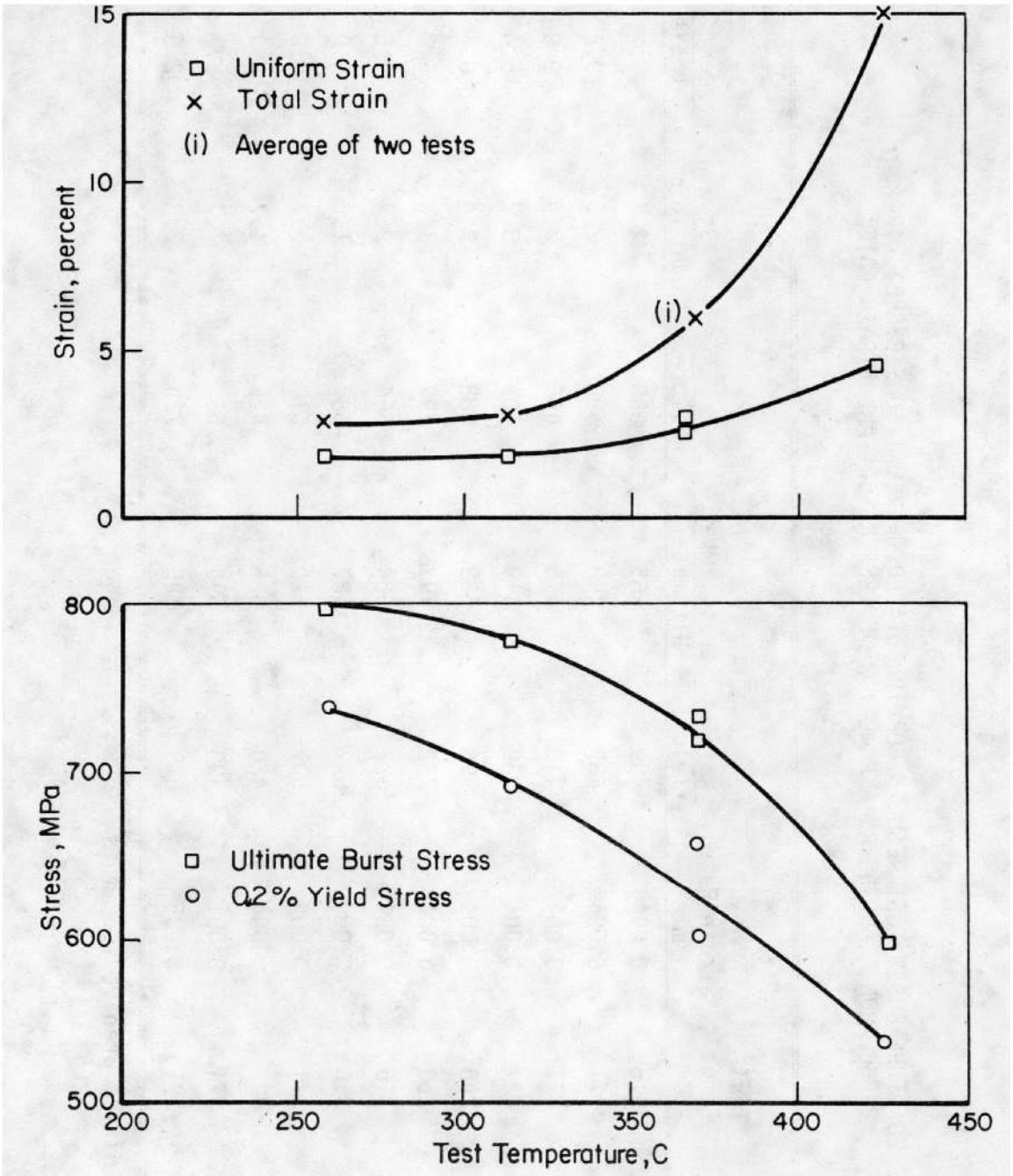

FIGURE 42. EFFECT OF TEST TEMPERATURE ON IRRADIATED OCONEE I (ONE CYCLE) FUEL ROD CLADDING BURST STRESS AND STRAIN (ENGINEERING)

Strain Rate 0.004/min

TABLE 27. TUBE-BURST TEST RESULTS FOR IRRADIATED OCONEE I (TWO CYCLE) ZIRCALOY FUEL-ROD CLADDING AS A FUNCTION OF TEMPERATURE AND STRAIN RATE

Specimen	Test Temp, C	Strain Rate, /min	Stress, MPa			Strain, percent	
			Yield	Ultimate	Failure	Uniform	Total
32062A-12	260	.004	737	794	794	1.7	4.0
32062A-11	316	.004	688	774	774	1.9	2.7
32062A-4	371	.004	654	727	727	2.7	4.0
31778A-9	371	.004	595	714	709	2.7	7.7
32002A-13	427	.004	532	593	583	4.4	14.9
32062A-16	371	.001	598	658	658	2.2	5.5
32062A-17	371	.035	725	725	725	0.8	2.7

TABLE 28. TUBE-BURST TEST RESULTS FOR IRRADIATED OCONEE I (THREE CYCLE) ZIRCALOY FUEL-ROD CLADDING AS A FUNCTION OF TEMPERATURE AND STRAIN RATE

Specimen	Test Temp, C	Strain Rate, /min	Stress, MPa			Strain, percent	
			Yield	Ultimate	Failure	Uniform	Total
47082-4	204	0.004	728	880	880	0.9	7.5
47082-13	316	0.004	678	776	776	1.7	1.7
47080-8	371	0.001	546	626	626	1.0	1.5
47082-21	371	0.004	588	680	680	2.3	3.9
47080-26	371	0.035	649	675	675	1.0	2.9
47080-10	427	0.004	485	553	544	2.8	5.3

with respect to the effects of increasing temperature and strain rate.

Comparison of Tube-Burst Data

The irradiated H. B. Robinson and Oconee I (three cycle) materials had almost identical stresses and strains as a function of test temperature.

The unirradiated Oconee archive and irradiated Oconee I materials exhibited decreasing strengths with increasing test temperature. The strains decreased to a minimum at about 371 C and then increased with increasing temperature to 427 C.

The effect of irradiation on the engineering burst (hoop) stress for Oconee I Zircaloy-4 fuel-rod cladding is illustrated in Figure 43, and the test results are given in Tables 26, 27, and 28. At a test temperature of 260 C, the yield stress increased 11 percent and the ultimate burst stress increased 7 percent for specimens irradiated for two cycles over those for specimens irradiated for one cycle. After an additional cycle of irradiation (three cycles), the yield stress value appeared to be the same as that for the specimens irradiated for two cycles, and the ultimate stress increased an additional 7 percent.

The yield and ultimate burst stress increased about 25 percent after one cycle of irradiation at test temperatures of 316, 371, and 427 C. At the test temperature of 316 C and after two cycles of irradiation, the yield stress increased an additional 11 percent (a total of 36 percent) and the ultimate stress increased an additional 14 percent (a total of 34 percent) as compared with the one-cycle test results. At the test temperature of 371 C and after two cycles of irradiation, the yield stress increased an additional 16 percent (a total of 42 percent) and the ultimate stress increased an additional 18 percent (a total of 43 percent) as compared with the one-cycle test results. However, after three cycles of irradiation, the yield and ultimate burst stresses were unchanged from those after two cycles of irradiation at those same temperatures. Finally, at 427 C and after two cycles of irradiation, the yield stress increased an additional 27 percent (a total of 54 percent) and the ultimate stress increased an additional 13 percent (a total of 38 percent) as compared with the one-cycle test results. Both stresses appeared to decrease after three cycles of irradiation at 427 C. These results indicate that the yield and ultimate burst stresses for Oconee I reactor Zircaloy-4 fuel-rod cladding, as compared with those for unirradiated archive Zircaloy-4 cladding material, increased about 25 percent after one cycle of irradiation, increased approximately an additional 15 percent

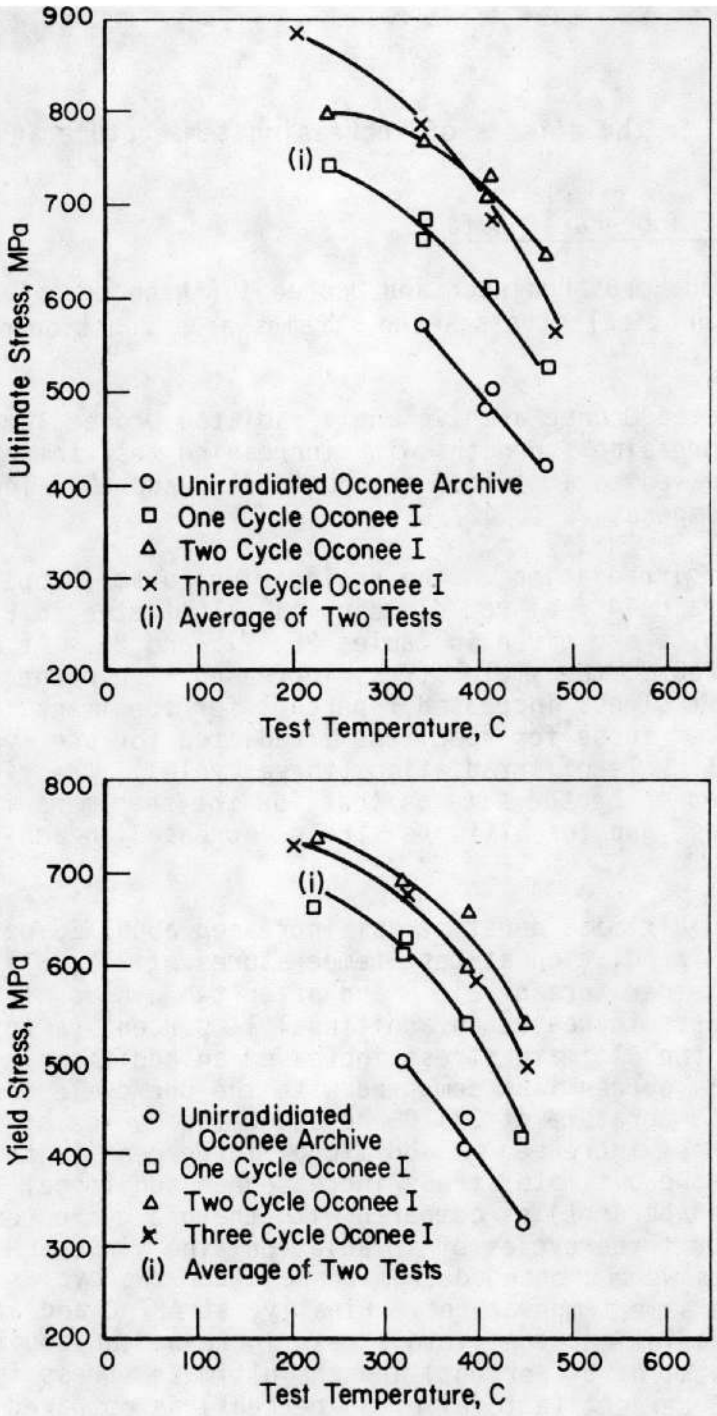

FIGURE 43. ENGINEERING BURST ULTIMATE AND YIELD STRESS FOR UNIRRADIATED OCONEE I ARCHIVE AND IRRADIATED OCONEE I (LOTS 2, 3 and 4) FUEL-ROD CLADDING AS A FUNCTION OF TEMPERATURE

Strain Rate 0.004/min

after a second cycle of irradiation, increased an additional 7 percent at 204 C, remained unchanged at 316 and 371 C, and decreased about 7 percent at 427 C. This halting (or reversal) of the increase in stress indicated that saturation or peaking of radiation damage had occurred.

The uniform and total burst (hoop) strains decreased after one cycle of irradiation and experienced an additional, smaller decrease after two cycles of irradiation for test temperatures of 260 and 371 C (see Figure 44). A small decrease also appeared after three cycles of irradiation. At 427 C, the uniform strain increased from about 3 percent to about 4.5 percent, which was expected as the burst stresses increased and the modulus changed slightly. Also at 427 C, the total strain showed little or no change, with the unirradiated, one-cycle, and two-cycle specimens all exhibiting total strains in the range 15 to 18 percent. However, after a third cycle of irradiation, the uniform strain dropped from 4.5 percent to 2.8 percent and the total strain dropped from 15 percent to 5 percent.

In the burst tests, increased total strain was exhibited by the H. B. Robinson and Oconee I (Lots 2 and 3) materials. This appeared to be a strain-aging (4) effect similar to that seen in steels in narrow temperature ranges. However, after three cycles, the Oconee I material appeared to exhibit little or no such effect. This might be because the fuel-cladding reaction observed at high burnups (30,000 MWD/MTU) was reducing the ductility, thus nullifying the strain aging effect.

As-irradiated tube-burst specimens of Lots 1, 2, 3, and 4 (H. B. Robinson and Oconee I) were tested at three strain rates--0.001, 0.004, and 0.035/min; all tests were conducted at 371 C (see Tables 25 through 28). The stress and strain results for the Lot 1 material were almost identical to those for Lot 3 material. The Oconee I, one-cycle, two-cycle, and three-cycle tube-burst-test results are plotted in Figures 45 and 46 as a function of strain rate. Note that as the strain rate was increased, the irradiation had less effect until one-cycle and three-cycle results converged at about 0.05/min. The biggest effect is seen at the lowest strain rate, 0.001/min, where the total strain dropped from 8 percent after one cycle, to 5.5 percent after two cycles, and to 1 percent after three cycles.

Expanding Mandrel Tests

The expanding mandrel test description is contained in Appendix C. Prior to testing, the outside diameters of a number of unirradiated specimens were scribe marked axially at 3-degree intervals around their

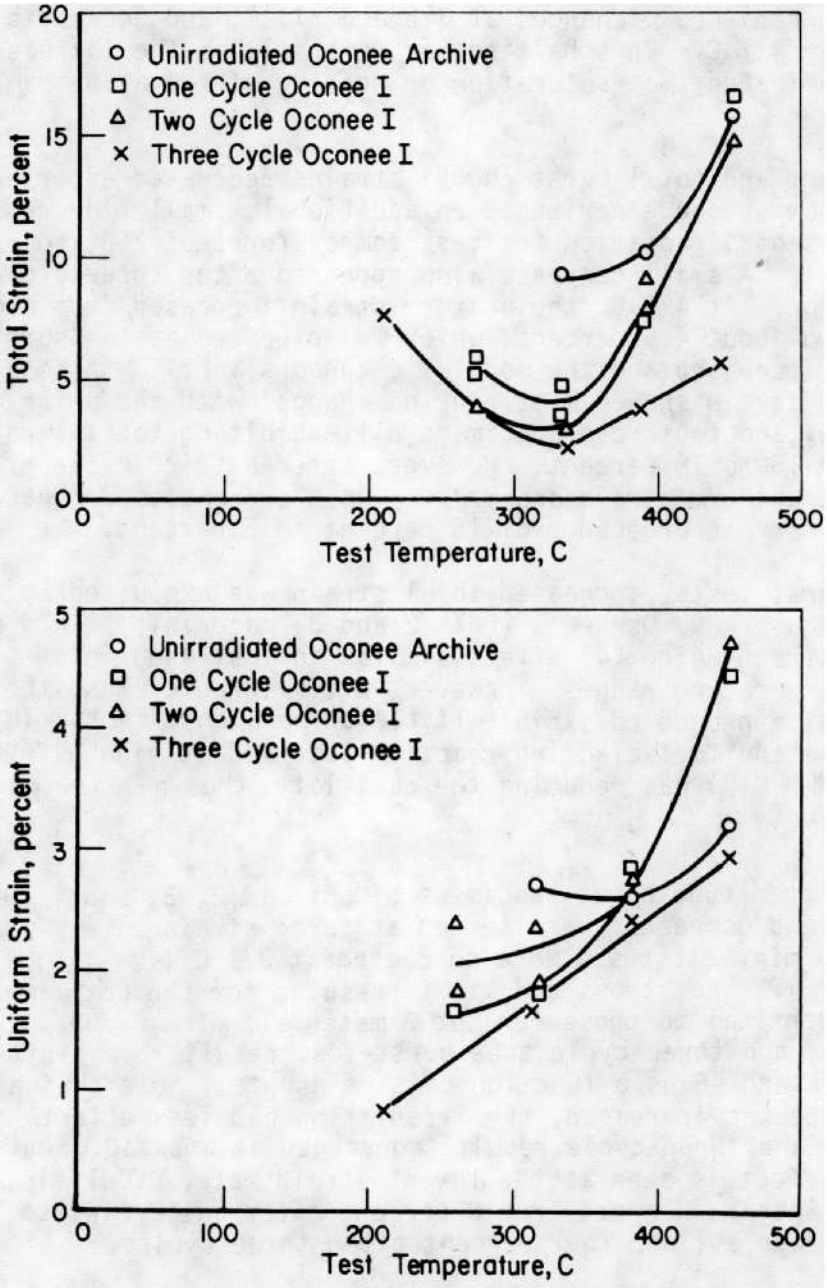

FIGURE 44. ENGINEERING UNIFORM AND TOTAL BURST STRAIN FOR OCONEE I FUEL-ROD CLADDINGS AS A FUNCTION OF TEMPERATURE

Strain Rate 0.004/min

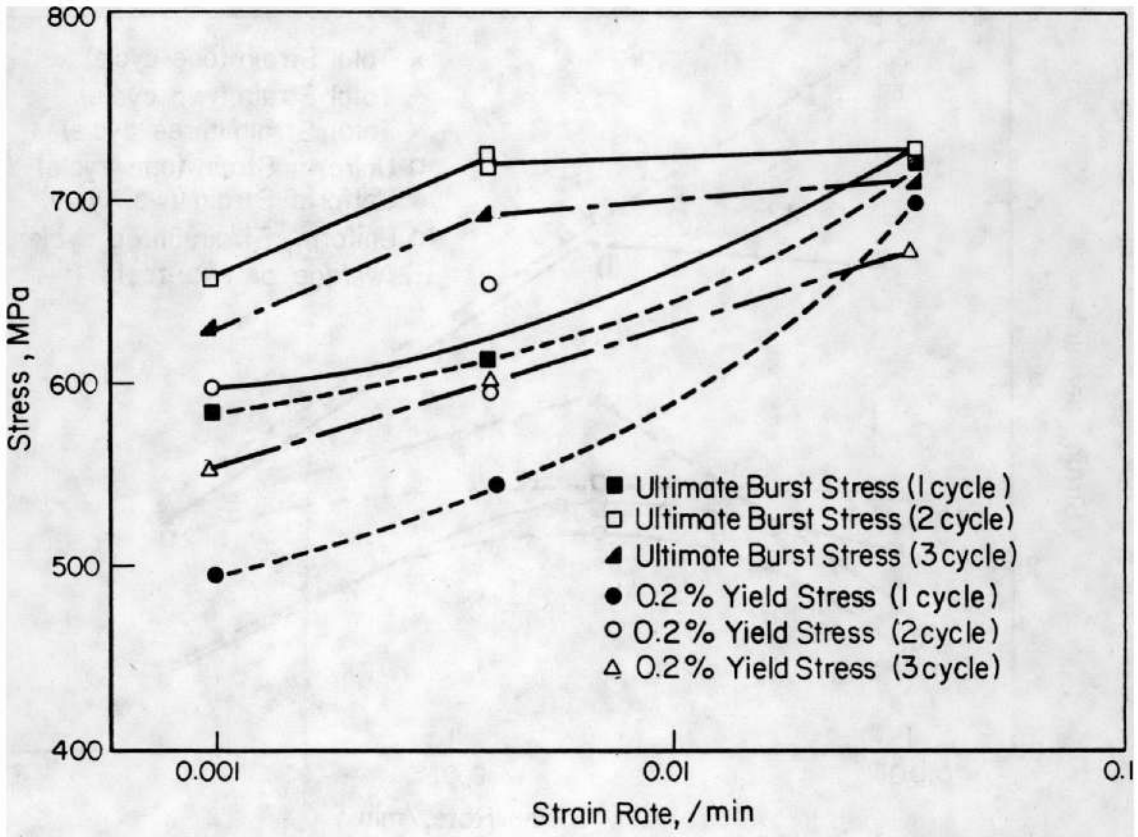

FIGURE 45. ENGINEERING BURST ULTIMATE AND YIELD STRESS FOR IRRADIATED OCONEE I (LOTS 2, 3, AND 4) FUEL-ROD CLADDING AS A FUNCTION OF STRAIN RATE

Test Temperature 371 C

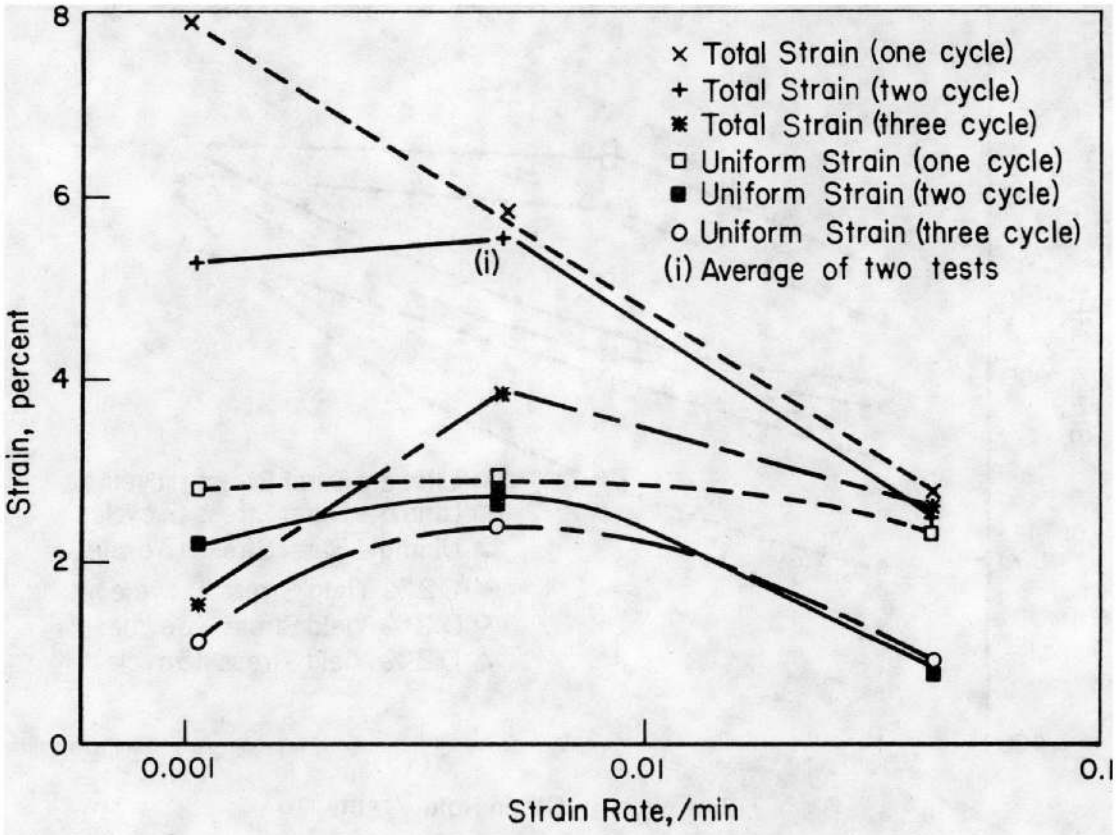

FIGURE 46. ENGINEERING UNIFORM AND TOTAL BURST STRAIN FOR IRRADIATED OCONEE I (LOTS 2, 3, AND 4) FUEL-ROD CLADDING AS A FUNCTION OF STRAIN RATE

Test Temperature 371 C

circumference, producing scribe mark spacings of approximately 280 microns. Visual examination of these specimens after testing revealed no obvious areas of significant localized deformation, and subsequent spacing measurements, while indicating some spacing variability, confirmed the absence of concentrated large deformations at locations corresponding to the mandrel apparatus.

From the scribe-mark observations and measurements, it was concluded that it was reasonable to base the expanding mandrel strain data on the complete specimen circumference.

Unirradiated Oconee I Archive Cladding

The effects of test temperature and strain rate in expanding mandrel tests conducted on the Oconee archive material are listed in Table 29, and are plotted in Figures 47 and 48.

As can be seen in Figure 47, the ultimate strength showed a moderate, approximately linear decrease with increasing test temperature. The failure stress occurred at either the ultimate strength or slightly below it. The uniform failure strains remained relatively constant, showing no effect of test temperature.

The strain-rate tests conducted at 371 C showed a slight increase in both the ultimate and failure stresses and almost no change in strain with increasing strain rate (see Figure 48).

Irradiated H. B. Robinson Cladding (Lot 1)

The effects of test temperature and of strain rate in expanding mandrel tests conducted on H. B. Robinson irradiated fuel-rod cladding are listed in Table 30 and plotted in Figures 49 and 50.

The uniform strain remained constant, showing no effect of temperature. Up to 371 C, the failure and uniform strain limits coincided since failure occurred at maximum load. At higher temperatures, failure occurred at reduced load and the failure strain rose sharply.

The ultimate strength showed a gradual decrease with increase in test temperature, the rate of decrease becoming greater as the temperature increased.

In strain-rate tests conducted at 371 C, both the ultimate stress and uniform strain--which also were the failure stress and failure strain

TABLE 29. EXPANDING MANDREL TEST RESULTS FOR OCONEE ZIRCALOY ARCHIVE MATERIAL AS A FUNCTION OF TEMPERATURE AND STRAIN RATE

Specimen	Test Temp, C	Strain Rate, /min	Stress, MPa			Strain, Percent	
			Ultimate	Yield	Failure	Uniform	Total
88-2-312-3-1	371	0.0064	214	85	203	14.5	20.9
215-1-247-3-6	204	0.064	330	118	325	18.8	22.3
36-2-248-1-6	316	0.064	258	82	258	12.6	12.6[b]
203-1-311-3-1	343	0.064	270	99	268	16.1	18.6
88-2-312-3-2	371	0.064	232	88	223	15.1	20.4
13-1-246-3-6	427	0.064	184	75	179	16.0	20.3
80-2-249-1-1	371	0.64	245	89	245	14.7	14.7[b]
203-1-311-3-2	371	1.28	257	93	255	15.9	20.8

(a) Circumferential strain based on original OD of 1.1 cm (0.43 in.).
(b) Failure occurred at maximum load.

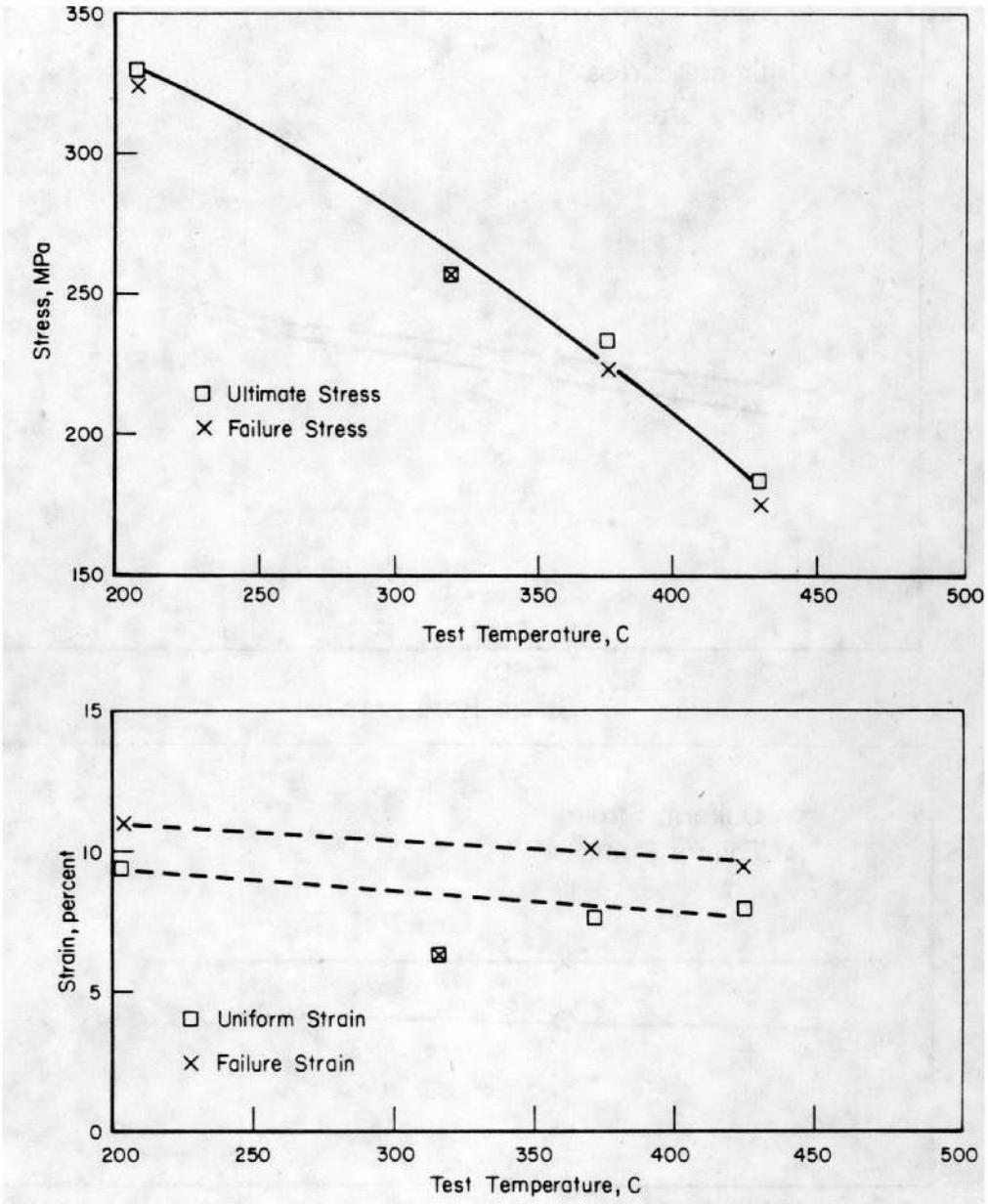

FIGURE 47. EFFECT OF TEST TEMPERATURE ON THE STRENGTH AND DUCTILITY OF OCONEE ARCHIVE FUEL-CLADDING MATERIAL AS MEASURED IN THE EXPANDING MANDREL TEST

Strain Rate 0.064/min

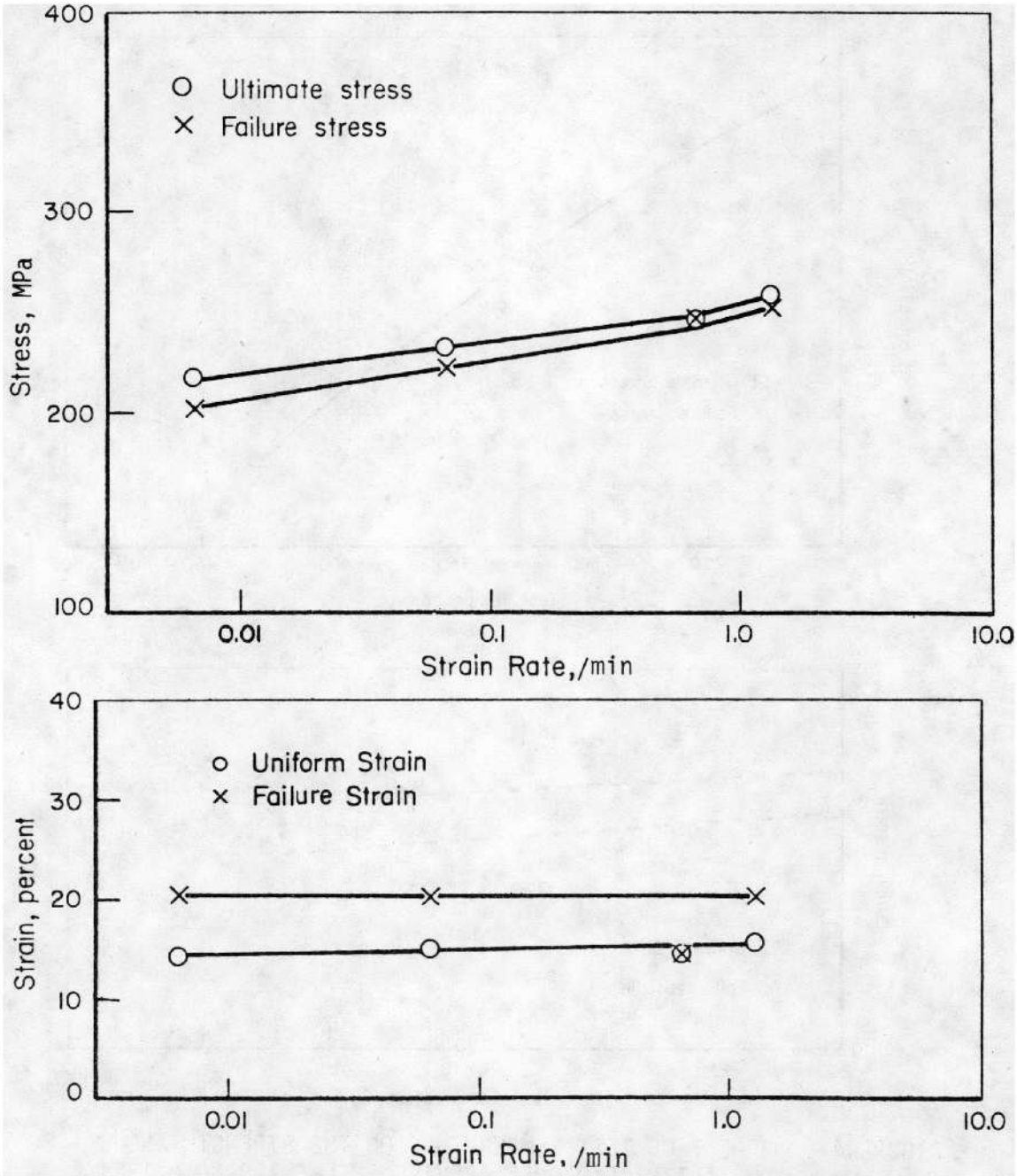

FIGURE 48. EFFECT OF STRAIN RATE ON THE STRENGTH AND DUCTILITY OF OCONEE ARCHIVE FUEL CLADDING MATERIAL AS MEASURED IN THE EXPANDING MANDREL TEST

Strain Rate 0.074/min

TABLE 30. EXPANDING MANDREL TEST RESULTS FOR IRRADIATED H. B. ROBINSON ZIRCALOY FUEL-ROD CLADDING AS A FUNCTION OF TEMPERATURE AND STRAIN RATE

Specimen	Test Temp, C	Strain Rate, /min	Stress, MPa			Strain, percent	
			Ultimate	Yield	Failure	Uniform	Total
C8-2	204	0.0063	431	146	431	16.0	16.0
C8-3	316	0.0063	388	163	388	13.5	13.4
C8-7	316	0.0063	381	135	381	14.2	14.2
C8-4	371	0.0063	335	142	335	16.4	16.4
C8-8	371	0.0063	358	125	358	18.2	18.2
C8-5	427	0.0063	253	108	195	13.4	33.6
C8-9	427	0.0063	299	135	299	15.4	15.4
C8-6	482	0.0063	160	68	97	16.2	58.6
C8-11	371	0.063	279	135	279	8.8	8.8
K10-20	371	0.063	252	50	250	11.2	11.3
C8-12	371	0.63	240	127	240	8.0	8.0
K10-23	371	0.63	246	119	246	9.4	9.4
K10-29	371	6.3	322	274	322	~0	~0

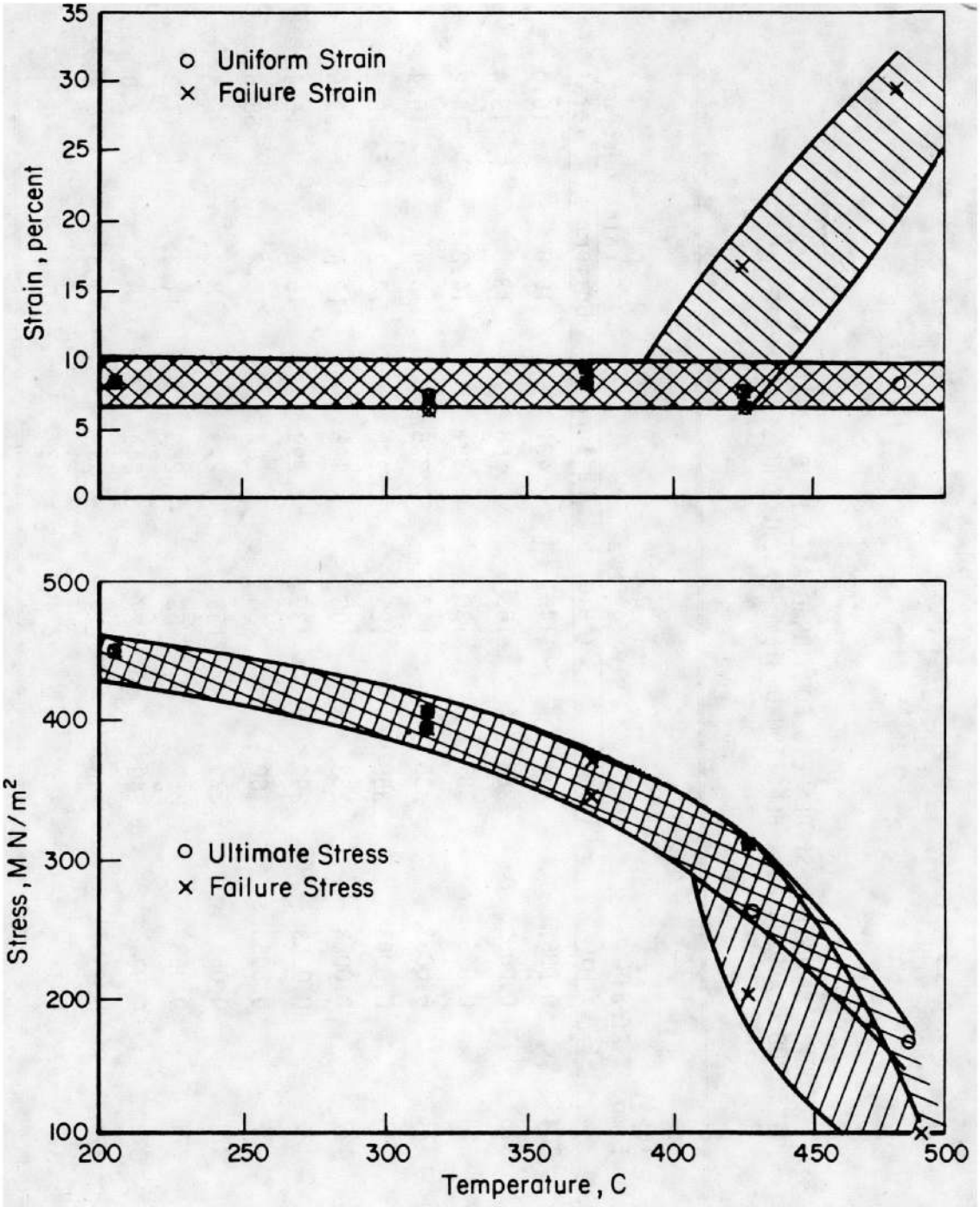

FIGURE 49. ENGINEERING ULTIMATE HOOP STRESS AND UNIFORM CIRCUMFERENTIAL STRAIN FOR IRRADIATED H.B. ROBINSON FUEL-ROD CLADDING AS A FUNCTION OF TEMPERATURE

Strain Rate 0.0063/min

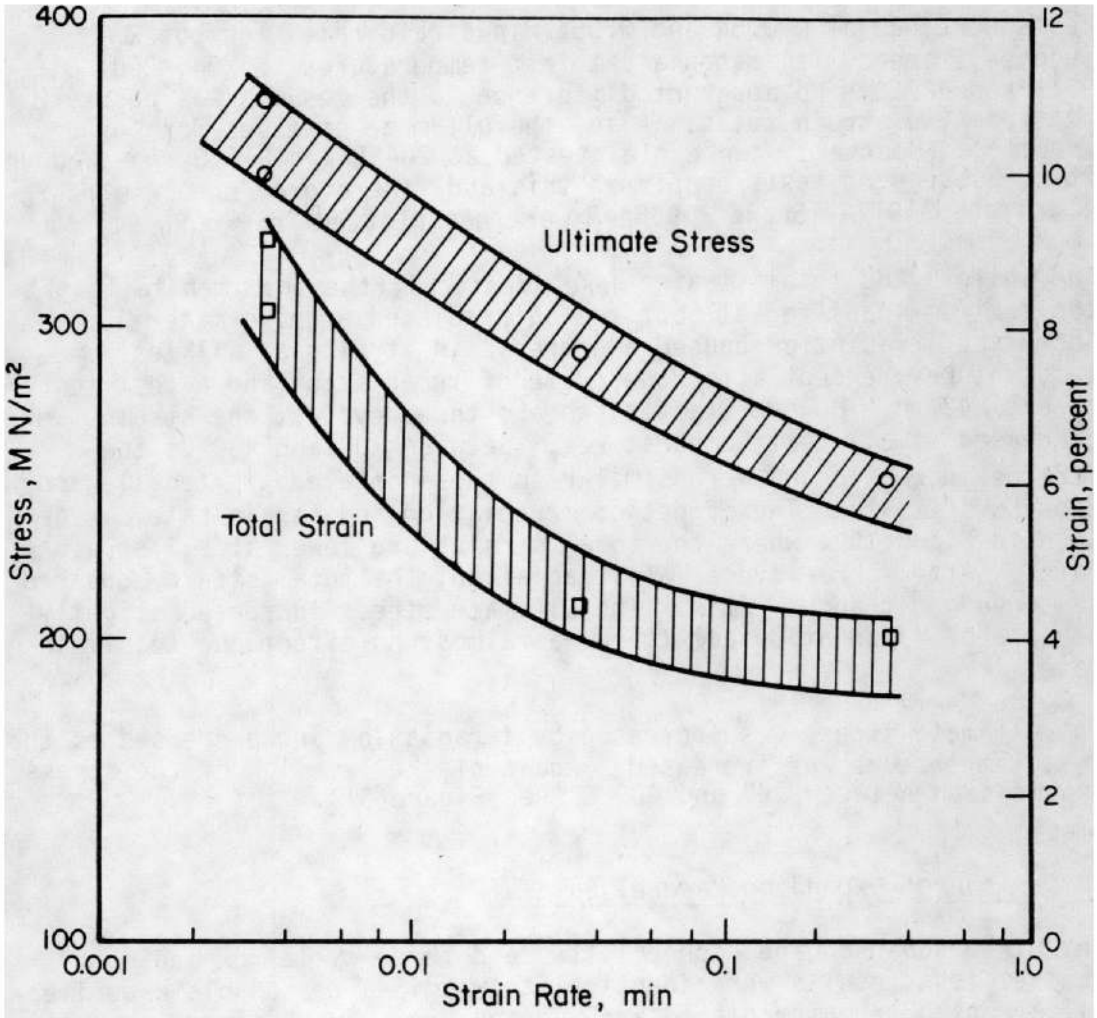

FIGURE 50. ENGINEERING EXPANDING MANDREL ULTIMATE HOOP STRESS AND UNIFORM CIRCUMFERENTIAL STRAIN FOR IRRADIATED H.B. ROBINSON FUEL ROD CLADDING AS A FUNCTION OF STRAIN RATE

Test Temperature 371 C

at this temperature--decreased with increase in strain rate. The strains were particularly sensitive to strain rate.

Irradiated Oconee I Cladding

The effects of test temperature and strain rate in expanding-mandrel tests conducted utilizing Oconee I irradiated fuel-rod cladding are listed in Tables 31 through 33 and plotted in Figures 51 and 52.

Tests were run at 0.0064 and 0.064/min strain rates for Lot 2 (Oconee I one cycle) material at test temperatures of 204, 260, 316, 371, and 427 C. No apparent difference in the results was observed at these two strain rates. Also, the ultimate stresses for Lot 3 specimens (Oconee I, two cycle) tested at 204 C and 316 C appeared very low. Subsequent tests confirmed this and, therefore, the results for Specimens 31917A-15 and 31965A-8 were not plotted in Figure 51.

The uniform and total strains were identical (the specimen failed at the maximum load) for all but the unirradiated archive material. Increased irradiation caused a decrease in strains at all test temperatures, except after one cycle of irradiation and a test temperature of 427 C. However, after two and three cycles, the strains were decreased at all test temperatures. Between 300 and 400 C, the strains increased and were similar to those obtained in tensile and tube-burst tests. The effect of irradiation and strain rate can be seen in Figure 52, where the total strains are lower at all strain rates. After three cycles of irradiation, the total strain appeared to converge at about 2/min. The ultimate stress increased slightly because of irradiation but there was almost no effect due to strain rate.

The ultimate stress was increased by irradiation and decreased as the test temperature was increased. Again slight leveling of the stress can be seen between 300 and 400 C (see Figure 51).

Comparison of Expanding Mandrel Data

The H. B. Robinson and Oconee I (two and three cycle) expanding mandrel test results were identical to within a reasonable experimental error. The unirradiated archive and one-, two-, and three-cycle Oconee I expanding mandrel test results are plotted in Figures 51 and 52, and are discussed and compared in the preceding section.

TABLE 31. EXPANDING MANDREL TEST RESULTS FOR IRRADIATED OCONEE I (ONE CYCLE) ZIRCALOY FUEL-ROD CLADDING AS A FUNCTION OF TEMPERATURE AND STRAIN RATE

Specimen	Test Temp, C	Strain Rate, /min	Stress, MPa			Strain, percent	
			Ultimate	Yield	Failure	Uniform	Total
47104-9	260	0.0064	350	136	350	13.7	13.7
47111-13B	204	0.064	347	165	347	9.9	9.9
47104-10	316	0.0064	319	104	319	16.5	16.5
47111-13E	316	0.064	293	119	293	9.8	9.8
47104-15	371	0.0064	270	86	261	15.2	28.9
47125-12A	371	0.0064	266	104	266	13.5	13.4
47111-13C	427	0.064	281	118	281	13.0	13.0
47118-2	427	0.0064	220	84	181	14.5	27.8
47118-11	371	0.064	313	114	313	14.3	14.3
47125-12B	371	0.064	280	120	280	12.5	12.5
47118-27	371	0.64	328	209	328	≈0	≈0
47125-12C	371	0.64	285	152	285	1.2	1.2
47111-13B	371	1.28	280	146	280	9.8	9.8
47125-12D	371	6.4	311	235	311	1.6	1.6

TABLE 32. EXPANDING MANDREL TEST RESULTS FOR OCONEE I (TWO CYCLE) ZIRCALOY FUEL-ROD CLADDING AS A FUNCTION OF TEMPERATURE AND STRAIN RATE

Specimen	Test Temp, C	Strain Rate, /min	Stress, MPa			Strain,[a,b] percent	
			Ultimate	Yield	Failure	Uniform	Total
31917A-4	371	0.0064	312	134	312	13.7	13.7
31917A-15	204	0.064	235	148	235	8.1	8.1
31965A-11	204	0.064	400	160	400	11.7	11.7
31965A-8	316	0.064	240	142	240	9.3	9.3
31965A-21	316	0.064	327	132	327	10.1	10.1
31917A-5	371	0.064	299	146	299	10.0	10.0
31965A-4	371	0.064	274	171	274	7.4	7.4
31965A-10	427	0.064	290	98	290	15.5	15.5
31917A-6	371	0.64	235	146	235	9.4	9.4
31917A-14	371	1.28	187	123	187	7.0	7.0

(a) Circumferential strain based on original OD of 1.1 cm.
(b) All failures occurred at maximum load.

TABLE 33. EXPANDING MANDREL TEST RESULTS FOR IRRADIATED OCONEE I (THREE CYCLE) ZIRCALOY FUEL-ROD CLADDING AS A FUNCTION OF TEMPERATURE AND STRAIN RATE

Specimen	Test Temperature, C	Strain Rate, /min	Stress, MPa			Strain, percent	
			Ultimate	Yield	Failure	Uniform	Total
47082-2	204	0.064	374	184	374	9.0	9.0
47082-3	316	0.064	314	167	314	9.2	9.2
47082-11	371	0.0064	311	114	311	11.8	11.8
47082-5	371	0.064	312	138	312	10.0	10.0
47082-18	371	0.64	271	136	271	9.9	9.9
47082-25	371	1.28	312	158	312	10.3	10.3
47082-9	427	0.064	292	115	287	15.6	17.9

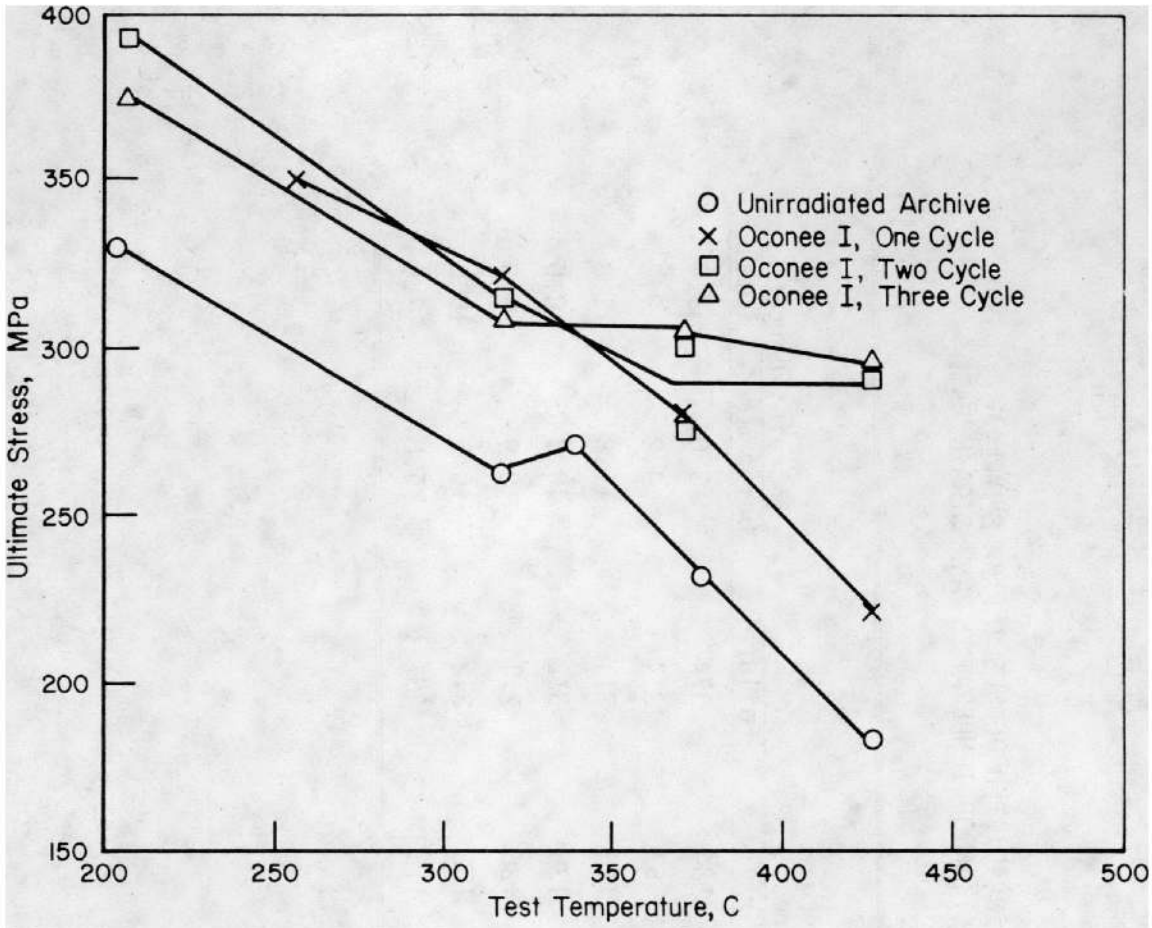

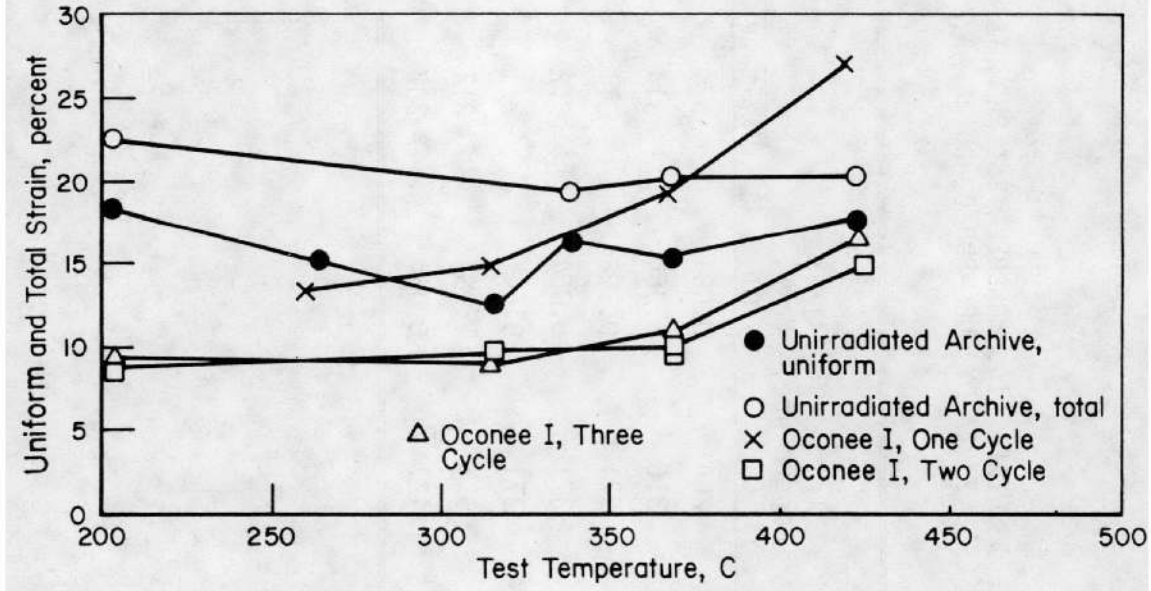

FIGURE 51. EFFECT OF TEST TEMPERATURE ON THE STRENGTH AND DUCTILITY ON OCONEE I FUEL-ROD CLADDING AS MEASURED IN THE EXPANDING MANDREL TESTS

Strain Rate 0.064/min

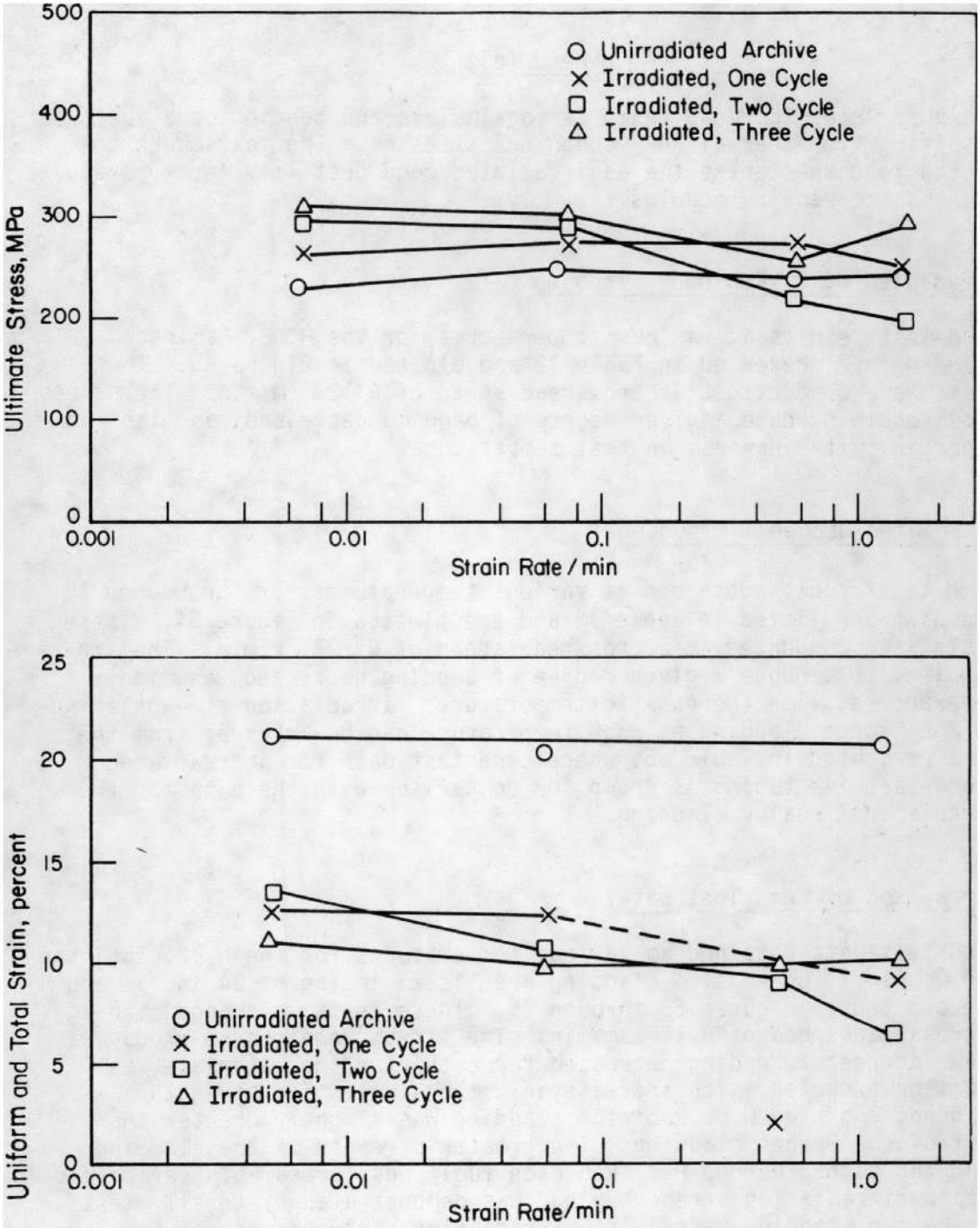

FIGURE 52. EFFECT OF STRAIN RATE ON THE STRENGTH AND DUCTILITY OF OCONEE I FUEL-ROD CLADDING AS MEASURED IN EXPANDING MANDREL TESTS

Test Temperature 371 C

Bend Tests

The purpose of the bend tests is to simulate the bending of a fuel rod resulting from thermal and mechanical stresses. The tests were conducted to characterize the as-irradiated bend ductility and to evaluate the elastic bending modulus.

Irradiated H. B. Robinson Cladding

Bend-test results at various temperatures for the H. B. Robinson cladding are presented in Table 34 and plotted in Figure 53. These tests were conducted at a crosshead speed of 0.127 cm/min. The stress required to produce a given degree of bending decreased, as might be expected, with increase in test temperature.

Irradiated Oconee I Cladding

Bend-test results obtained at various temperatures for the Oconee I cladding are listed in Table 35 and are plotted in Figure 54. These tests were conducted at a crosshead speed of 0.127 cm/min. The stress required to produce a given degree of bending decreased, as might be expected, with increase in temperature. Irradiation strengthening of the Oconee cladding at room temperature can be inferred from the data presented in Table 35, where bend-test data for unirradiated Oconee archive tubing is shown for comparison with the data for the irradiated Zircaloy cladding.

Comparison of Bend Test Data

Bend-test data obtained at various temperatures for the H. B. Robinson and Oconee I (one-cycle) cladding are listed in Tables 34 and 35 and are plotted in Figures 53 through 55. These tests were conducted at a crosshead speed of 0.127 cm/min. The stress required to produce a given degree of bending decreased for both cladding materials, as might be expected, with increase in temperature. The strength in bending of the H.B. Robinson cladding was slightly greater than that of the Oconee cladding. The greater strength of the cladding from the higher burnup H.B. Robinson fuel rods, presumably reflecting greater irradiation strengthening, was demonstrated by tensile tests of the two cladding materials. Irradiation strengthening of the Oconee I, one cycle, cladding at room temperature can be inferred from the data presented in Table 35, where bend-test data for unirradiated Oconee archive tubing is shown for comparison with the data for the irradiated Zircaloy cladding.

TABLE 34. BEND-TEST RESULTS AT VARIOUS TEMPERATURES FOR H. B. ROBINSON SPENT-FUEL CLADDING

Specimen	Test Temp, C	Stress, $N/m^2 \times 10^{-9}$		Modulus in Bending, $N/m^2 \times 10^{-10}$
		0.02 Percent Maximum Fiber Strain	At 10.2-Cm (4-in.) Radius of Curvature	
014/29-34	25	1.57	1.64	13.3
A1/62-67	204	1.37	1.51	18.1
A8/37-42	316	1.32	1.37	13.3
014/116-121	316	1.21	1.33	13.1
A8/62-67	371	1.14	1.25	11.6
H6/15-20	371	1.07	1.21	12.1
014/24-29	427	1.01	1.06	7.7
H6/20-25	427	0.95	1.06	7.1
04/100-105[a]	371	1.27	1.33	9.5

(a) Tested at a crosshead speed of 12.7 cm/min.

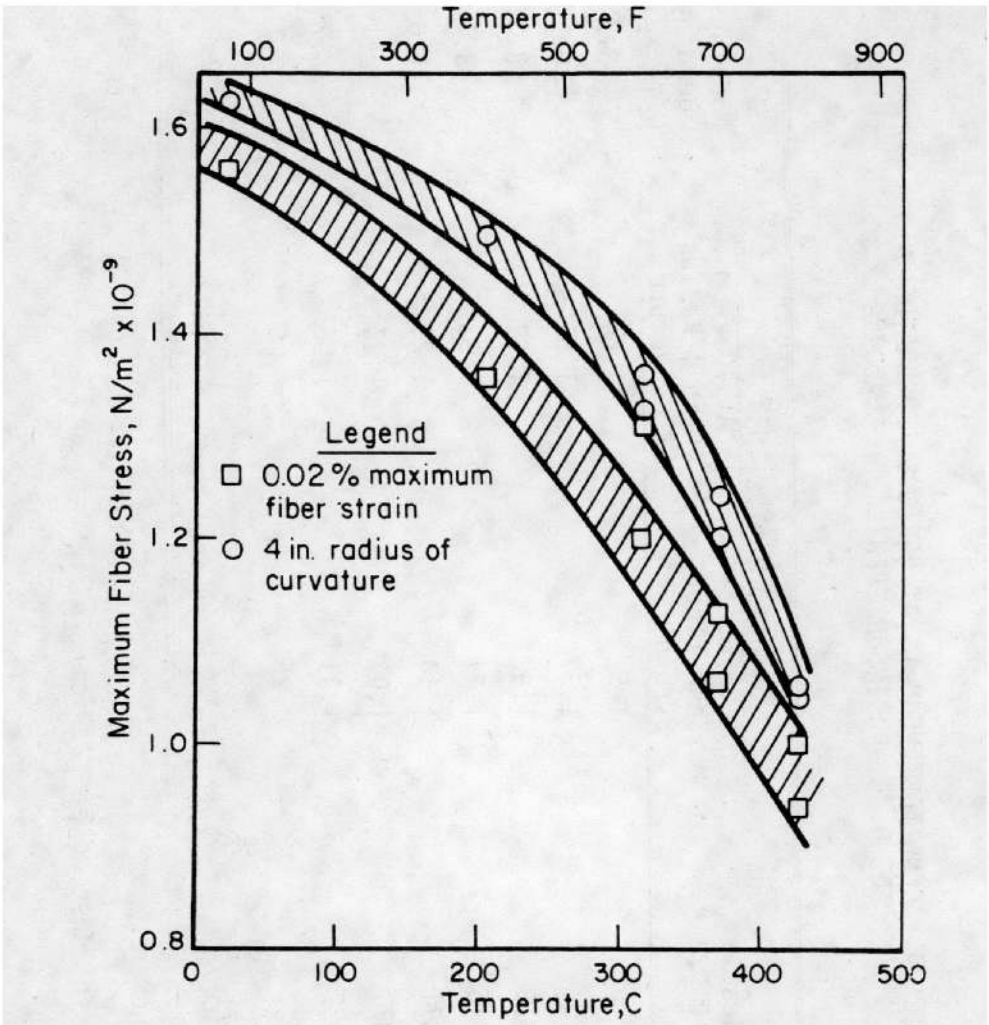

FIGURE 53. EFFECT OF TEMPERATURE ON THE MAXIMUM FIBER STRESS REQUIRED FOR 0.02 PERCENT MAXIMUM FIBER STRAIN AND A 10 CM RADIUS OF CURVATURE IN BENDING FOR IRRADIATED H.B. ROBINSON SPENT-FUEL CLADDING

TABLE 35. BEND-TEST RESULTS AT VARIOUS TEMPERATURES FOR OCONEE SPENT-FUEL CLADDING

Specimen	Test Temp, C	Stress, $N/m^2 \times 10^{-9}$ 0.02 Percent Maximum Fiber Strain	Stress, $N/m^2 \times 10^{-9}$ At 10.2-Cm (4-In.) Radius of Curvature	Modulus in Bending, $N/m^2 \times 10^{-10}$
47104-7	204	1.26	1.39	19.8
47104-16	316	1.10	1.23	16.6
47110-21	371	1.02	1.13	16.7
47104-21	427	0.90	0.95	12.7
47104-23	25	1.53	1.61	15.8
Unirradiated[a]	25	1.03	1.14	15.1
Ditto	25	1.06	1.16	-
47104-24[b]	371	1.08	1.14	10.2

(a) Oconee archive tubing.
(b) Tested at a crosshead speed of 12.7 cm/min.

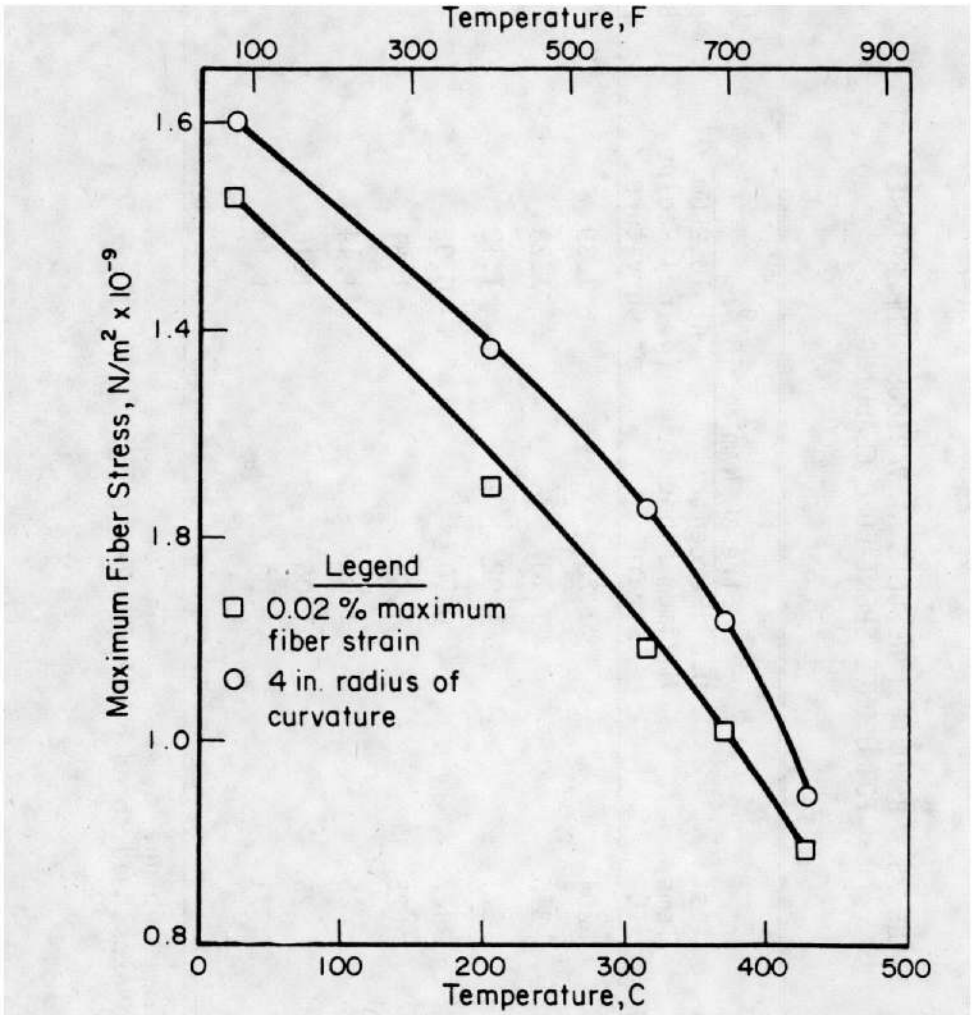

FIGURE 54. EFFECT OF TEMPERATURE ON THE MAXIMUM FIBER STRESS REQUIRED FOR 0.02 PERCENT MAXIMUM FIBER STRAIN AND A 10-CM RADIUS OF CURVATURE IN BENDING FOR OCONEE I (ONE-CYCLE) IRRADIATED SPENT-FUEL CLADDING

The bending modulus was determined from the initial linear portion of the load-deflection curve for each test. As seen in Figure 55, the modulus increased slightly between room temperature and 200 C and then decreased. No effect of irradiation on the bending modulus of the Oconee cladding was indicated by the modulus measurements recorded in Table 35. No effect on strength values was observed at the higher rate of testing for the one H. B. Robinson specimen and one Oconee I specimen tested at a strain rate of 12.7 cm/min.

Bend-test strength values show effects similar to those obtained in tube-burst and expanding mandrel tests when the test temperature was increased. A greater degree of irradiation strengthening for the cladding from the higher burnup H.B. Robinsonspent-fuel cladding as compared with that for Oconee spent fuel was also evident from the bend-test results. However, little information concerning cladding ductility was available from the tests except for the significant observation that the cladding was highly ductile in bending. Specimens were routinely bent to a 10-cm radius of curvature, and smaller, without producing failure. Therefore, no further bend tests were conducted.

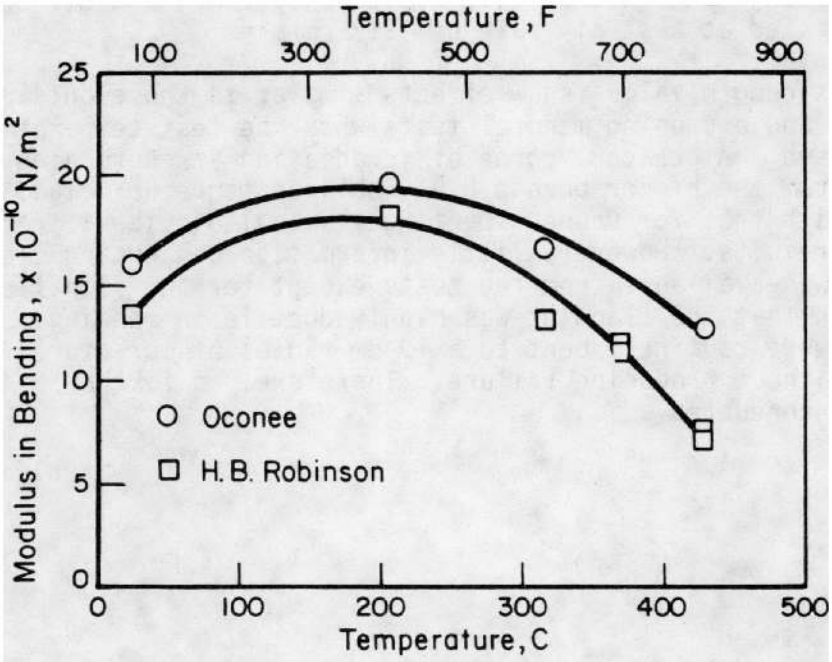

FIGURE 55. EFFECT OF TEMPERATURE ON THE ELASTIC MODULUS IN BENDING FOR IRRADIATED H.B. ROBINSON AND OCONEE SPENT-FUEL CLADDING

TEST RESULTS AND ANALYSIS (ANNEALED SPECIMENS)

Tensile Tests

Unirradiated Sandvik

A limited study to determine the tensile property changes caused by transient annealing was conducted using unirradiated, stress-relieved, Sandvik fuel-rod tubing. The tests were designed to determine whether the unirradiated Sandvik tubing exhibited the same recovery characteristics as the irradiated H.B. Robinson cladding. Tensile specimens were transient annealed to temperatures between 538 and 704 C and at heating rates of 5.6 and 28 C/sec. The specimens were then tensile tested at a test temperature of 371 C and at a strain rate of 0.025/min. The transient annealed tensile test results are given as the first eight data sets in Table 38. At the heating rate of 28 C/sec, both the yield and ultimate stresses and uniform strains were nearly constant until the maximum transient annealing temperature of 704 C was reached. The total strain data suggested a slight minimum value at 593 C but this may only be scatter in the data.

With a heating rate of 5.6 C/sec, the yield stress, ultimate stress, and uniform strain were again constant until the maximum temperature of 621 C in the transient anneal was reached. Both yield and ultimate strain exhibited a significant drop between transient annealing temperatures of 593 and 704 C, while the uniform strain increased to 4.8 percent at 593 C and 24.3 percent at 704 C. However, with a heating rate of 5.6 C/sec, the total strain was almost constant at about 24.5 percent for the maximum transient annealing temperatures of 538 and 593 C but indicated a reduced total strain to 19.3 percent at 621 C and a subsequent large rise to 49.1 percent at the maximum transient annealing temperature of 704 C. Note that whenever a reduction in stress was registered at a specific transient annealing temperature, an increase in strain was also registered, i.e., the recovery of strength and ductility occurred at the same transient temperature.

Unirradiated Oconee I Archive

Tensile tests were also performed on Oconee archive tubing specimens after undergoing transient annealing to temperatures between 482 and 871 C. These anneals were performed from just above the reactor operating temperature (482 C) to 871 C and at a heating rate of 28 C/sec. The specimens were subsequently tested at 371 C and a strain rate of 0.0025/min. The results are given in Table 36 and plotted

TABLE 36. TENSILE-TEST RESULTS FOR UNIRRADIATED OCONEE I ARCHIVE TRANSIENT ANNEALED FUEL ROD MATERIAL
Test Temperature 371 C

Strain Rate 0.025/min

Specimen[a]	Transient Annealing Condition		Stress, MPa		Strain, percent	
	Heating Rate, C/sec	Maximum Temp, C	Ultimate	Yield	Uniform[b]	Total[c]
215-1-247-3-2	28	482	427	394	1.8	19.7
215-1-247-3-1	28	538	403	392	1.9	16.0
13-1-246-3-5	28	592	406	371	2.0	17.1
13-1-246-3-4	28	621	412	374	2.2	14.1
13-1-246-3-3	28	704	408	371	2.2	20.8
13-1-246-3-2	28	760	405	377	2.0	12.7
13-1-246-3-1	28	871	408	369	2.1	10.5

(a) Test temperature of 371° C and strain rate of 0.0025/min.
This strain rate is based on crosshead speed and 2-in. gage length between the bullet ends.

(b) Based on strain measured by an extensometer.

(c) Based on uniform from note 2 and crosshead movement beyond maximum load over a 2-in. gage length between the bullet ends.

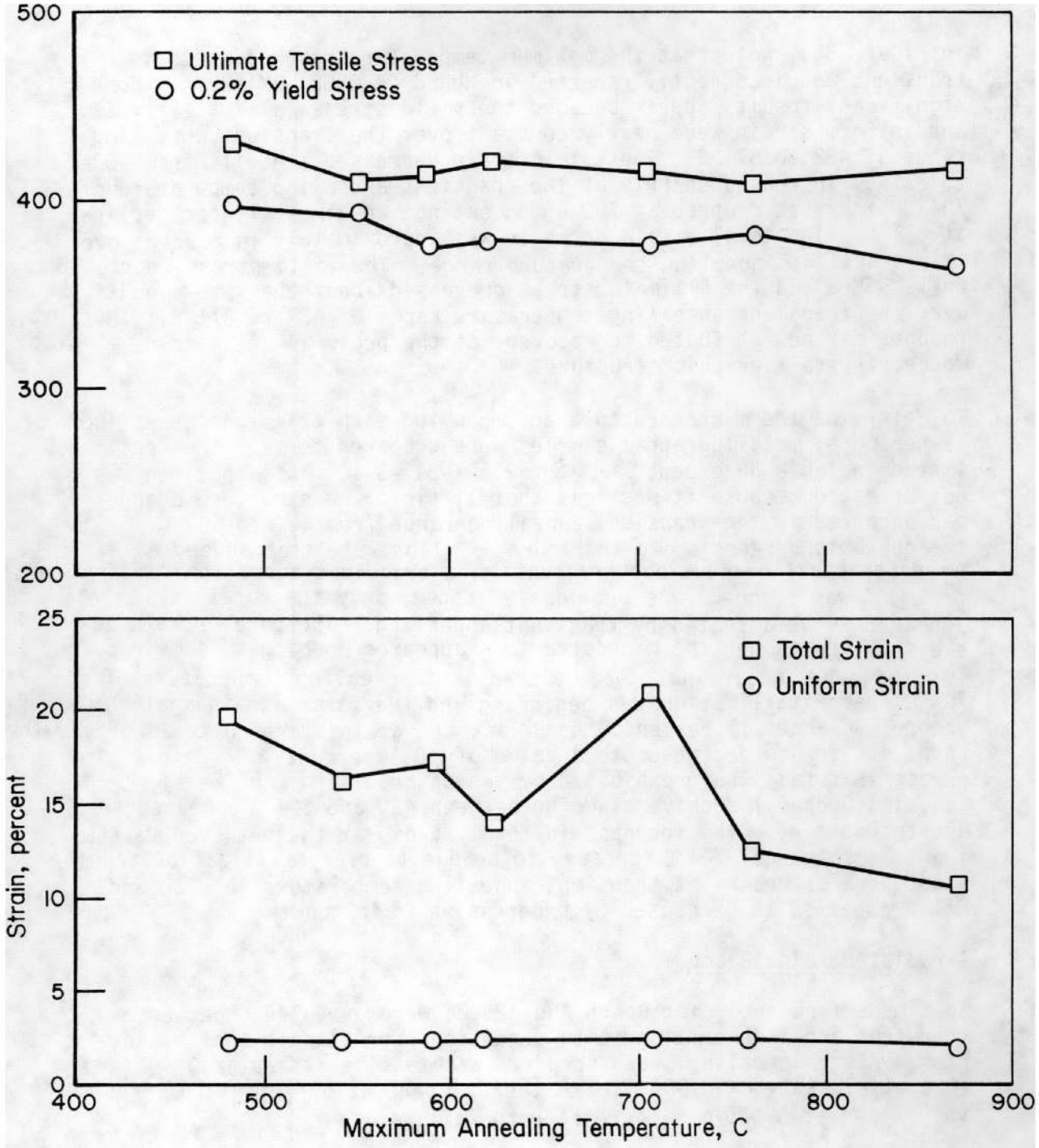

FIGURE 56. EFFECT OF TRANSIENT HEATING ON THE STRENGTH AND DUCTILITY OF OCONEE ARCHIVE FUEL CLADDING MATERIAL AS MEASURED IN TENSILE TESTS Strain Rate 0.025/min, Heating Rate = 28 C/sec, Test Temperature 371 C

in Figure 56. Note that the maximum temperature reached in the transient was incorrectly reported in NUREG/CR-0982, BMI-2034. Some significant results appear because the yield stress, ultimate stress, and uniform strain were nearly constant over the transient annealing range of 482 to 871 C. The total strain decreased steadily from 482 to 621 C, increased sharply at the transient annealing temperature of 704 C, and then dropped at 760 C to continue an almost linear decline at 871 C. The total strain decrease was approximately 10 percent over this transient annealing temperature range. The yield stress decreased only 25 MPa and the ultimate stress decreased about the same amount over the transient annealing temperature range of 482 to 871 C. These changes may be attributed to recovery of the preirradiation cold-worked crystallographic structure.

To determine the microstructure accompanying each transient annealing temperature, metallographic samples were prepared for all the specimens listed in Table 36 except Specimen 215-1-247-3-1. This specimen was not prepared because it was felt that little or no structure change had occurred in the transient annealing range from 482 to 592 C. The photomicrographs shown in Figure 57 illustrate that indeed no microstructual changes occurred until the transient annealing temperature of 704 C was reached. As previously stated, only the total strain appeared to be affected by transient annealing. The total strain decreased even though the microstructure appeared unchanged; some recovery was, however, occurring. At the transient annealing temperature of 704 C, recrystallization was beginning and the total strain again had dropped to about 13 percent. At 871 C, the grains were quite large and the total strain had decreased to a value of 10.5 percent. Therefore, the decrease in total strain exhibited by the unirradiated and transient annealed Oconee I archive cladding between 482 and 621 C appeared to be due to recovery. The increase in total strain at the transient annealing temperature of 704 C appeared to be due to recrystallization and the subsequent decreases at transient annealing temperatures of 760 and 871 C appeared to be caused by progressive grain growth.

Irradiated Point Beach

Specimens from the Point Beach Rod A25-06 were annealed under both transient and isothermal heating conditions for tensile test evaluation. After annealing, each specimen was tensile tested at 371 C and at a strain rate of 0.005/min to the 0.2 percent offset yield stress value, and at 0.025/min thereafter to failure.

Only two transient anneals were performed, one at 0.56 C/sec and one at 0.12 C/sec. The isothermal anneals were for periods of 15, 30, and 60 minutes and for temperatures in the range from 427 to 704 C. The tensile test results are given in Table 37 and show that all the

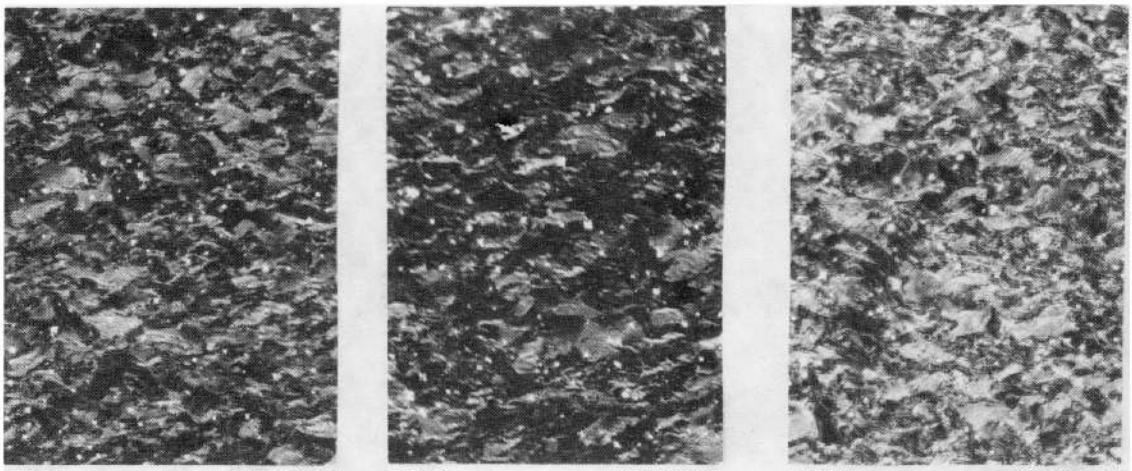

500X HC49604 482 C

500X HC49606 592 C

500X HC49608 621 C

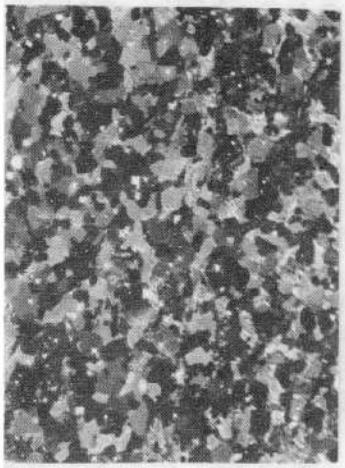

500X HC49605 704 C

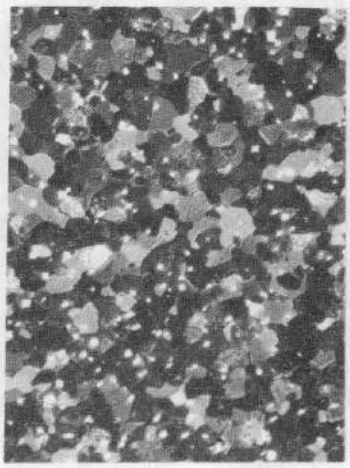

500X HC49607 760 C

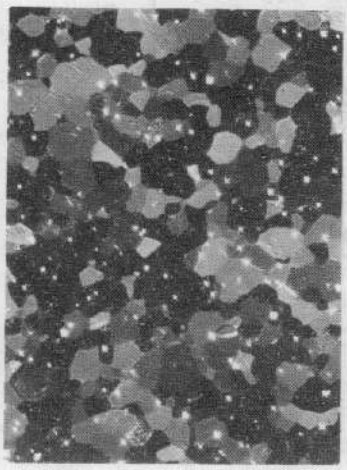

500X HC49599 871 C

FIGURE 57. MICROSTRUCTURE OF UNIRRADIATED AND TRANSIENT ANNEALED OCONEE I ARCHIVE TENSILE SPECIMENS

Test temperature 371 C, strain rate 0.025/min.

TABLE 37. TENSILE-TEST RESULTS FOR AS-RECEIVED TRANSIENT AND ISOTHERMAL ANNEALED POINT BEACH IRRADIATED ZIRCALOY FUEL ROD A25-06 CLADDING

Test temperature 371 C, strain rate 0.025/min.

Specimen	Annealing Conditions			Stress		Strain	
	Heating Rate, C/sec	Maximum Temp, C	Holding Time, min.	Ultimate MPa	Yield MPa	Uniform Percent	Total Percent
				As-Irradiated			
T-2	-	-	-	651	511	4.6	13.9
T-5	-	-	-	651	509	4.0	14.2
T-7	-	-	-	630	480	3.8	11.3
				Transient Anneals			
T-1	0.56	593	0	480	378	3.5	8.4
85-90	0.12	538	0	459	352	3.7	7.7
				Isothermal Anneals			
95-100	0.56	427	60	644	535	3.4	11.4
90-95	0.56	454	60	575	449	3.5	8.5
T-4	0.56	482	15	568	445	4.0	9.8
T-3	0.56	482	30	542	418	4.0	14.5
T-8	0.56	593	15	297	176	12.6	23.4
T-6	0.56	593	30	283	166	10.1	32.7
T-9	0.56	704	30	273	152	16.8	25.0

anneals except the isothermal anneal at 427 C exhibited reduced stresses However, only after the annealing temperature exceeded 15 minutes at 593 C did the strains indicate an appreciable increase.

Irradiated H. B. Robinson Cladding (Lot 1)

Specimens from the irradiated H. B. Robinson fuel rods A1, A8, H7, H10, and P4 were prepared and tensile tested. The 12.7-cm-long specimens were defueled and annealed under both transient and isothermal conditions as described in Appendix B. The annealed specimens were fitted with end plugs as shown in Appendix C and tensile tested at a test temperature of 371 C and at a strain rate of 0.025/min. Transient anneals included heating rates from 0.56 C/sec to ∿ 100 C/sec and to maximum temperatures reached in the transient in the range of 482 C to 982 C. Upon reaching the maximum temperature, the specimen was immediately cooled in a jet of helium. The isothermally annealed specimens were heated at a rate of 28 C/sec until the desired temperature was reached, held at that temperature for periods from 0.1 to 60 minutes, and quenched in a jet of helium.

The effects of transient heating anneals on the tensile properties of the irradiated H. B. Robinson Zircaloy-4-fuel-rod cladding are shown in Figures 58, 59, 60, and 61; the tensile test results are given in Tables 38 and 39. For clarity, only the ultimate stress is plotted for all four heating rates. The tensile properties for unirradiated and transient annealed (28 C/sec) specimens are also plotted for comparison. It should be noted that the properties of the irradiated cladding were influenced both by the heating rate and by the maximum temperature reached in the transient.

The transient annealing studies showed the expected recovery of strength properties (ultimate and yield stress) as the heating rate was decreased and the maximum temperature reached in the transient was increased. In general, stress changes followed the trends exhibited by the hardness measurements in transient annealing tests (see Figure 2 of this report). The hardness peak observed in transients to 482 C was reflected in the stress peaks obtained in transient annealing tensile tests at heating rates greater than or equal to 14 C/sec. The stress peaks observed in both microhardness and tensile test results suggest a thermal aging process possibly involving interactions between impurity atoms and irradiation-induced defects. However, overaging occurred rapidly as recovery processes associated with defect agglomeration proceeded at temperatures below about 600 C. At higher temperatures time-dependent recrystallization and grain growth occurred.

TABLE 38. TENSILE TEST RESULTS FOR IRRADIATED H.B. ROBINSON TRANSIENT ANNEALED ZIRCALOY FUEL ROD CLADDING.

Test temperature 371 C; strain rate 0.025/min.

Specimen	Heating Rate, C/sec	Maximum Temperature, C	Stress		Strain	
			Ultimate MPa	Yield MPa	Uniform Percent	Total Percent
0781-8 (a)	5.6	538	435	347	4.1	24.1
0781-7	5.6	593	432	343	4.1	24.6
0781-6	5.6	621	409	308	4.8	19.3
0781-5	5.6	704	252	141	24.3	49.1
0781-4	28	538	435	347	3.6	19.4
0781-3	28	593	438	353	3.3	16.2
0781-2	28	621	433	347	3.6	17.5
0781-1	28	704	422	326	4.6	17.4
P4-50-55	0.56	427	674	579	2.1	12.7
P4-55-60	0.56	482	633	508	2.7	12.7
P4-89-94	0.56	538	575	454	2.3	12.8
H10-40	0.56	593	570	423	4.1	14.7
P4-94-99	0.56	621	286	168	9.6	26.8
P4-99-104	0.56	704	269	148	9.2	28.8
P4-111-116	5.6	427	653	554	2.0	12.7
P4-45-50	5.6	482	676	592	2.4	11.8
P4-35-46	5.6	538	595	493	2.4	10.4
P4-70-75	5.6	593	349	271	2.9	12.6
P4-75-80	5.6	621	314	207	4.8	17.2
P4-84-89	5.6	704	287	164	10.6	29.8
014-106-111	14	482	717	600	2.4	11.8
A8-120-125	14	538	653	525	2.3	17.0
P4-16-21	14	593	578	464	2.5	9.5
P4-21-26	14	621	456	363	2.2	9.9
P4-26-31	14	704	305	188	5.7	19.6
P4-65-70	28	482	671	586	2.1	14.0
A1-29-34	28	538	722	614	2.7	15.6
A8-105-110	28	593	671	554	2.7	12.4
A8-110-115	28	621	598	492	2.1	9.8
A8-115-120	28	704	348	263	3.5	12.7

TABLE 38. (CONTINUED)

Specimen	Heating Rate, C/sec	Maximum Temperature, C	Stress		Strain	
			Ultimate MPa	Yield MPa	Uniform Percent	Total Percent
P4-116-121	28	760	329	236	4.7	15.7
014-111-116	28	871	338	195	8.6	25.1
014-37-42	28	982	340	188	10.5	34.5
H7-17	103	482	695	604	2.9	8.1
H7-18	108	538	700	621	2.7	8.6
H7-19	86	593	694	590	2.9	10.4
H7-20	114	649	698	594	2.7	11.2
H7-21	142	704	600	485	2.0	9.0
H7-22	87	816	354	221	11.2	25.6
H7-26	89	816	351	219	10.7	29.5

(a) The first seven specimens are unirradiated Sandvik tubing and the remainder are irradiated H.B. Robinson cladding.

TABLE 39. ADDITIONAL TENSILE-TEST RESULTS FOR IRRADIATED AND ANNEALED H.B. ROBINSON ZIRCALOY FUEL-ROD CLADDING

Specimen	Heating Rate, C/sec	Maximum Temperature, C	Time at Temp., C	Test Temperature, C	Strain Rate, /min	Stress		Strain	
						Ultimate MPa	Yield MPa	Uniform Percent	Total Percent
M12-12	14	593	0	27	0.025	865	694	4.0	12.1
M12-13	14	593	0	371	0.025	662	558	2.4	11.5
F8-13-18	28	482	10	27	0.025	898	683	5.0	10.5
F8-99-104	28	482	30	371	0.0025	579	453	3.1	8.8
F8-106-111	28	482	10	371	0.25	639	499	3.0	5.9
F8-121-126	28	704	30	371	0.0025	270	146	8.6	30.5
F8-94-99	28	593	5	371	0.0025	466	346	3.3	11.0
F8-116-121	28	583	30	371	0.25	345	212	2.8	5.1
F8-111-116	28	593	30	371	0.0025	305	190	6.4	15.7
F8-23-28	28	704	30	482	0.025	212	135	8.0	63.0
F8-18-23	28	593	30	482	0.025	333	271	3.5	21.5
F8-89-94	28	521	0	371	0.0025	517	379	3.0	11.4
G8-89-94	28	482	10	371	0.0025	589	460	2.6	15.0
G8-94-99	28	482	10	371	0.25	481	630	2.7	6.0

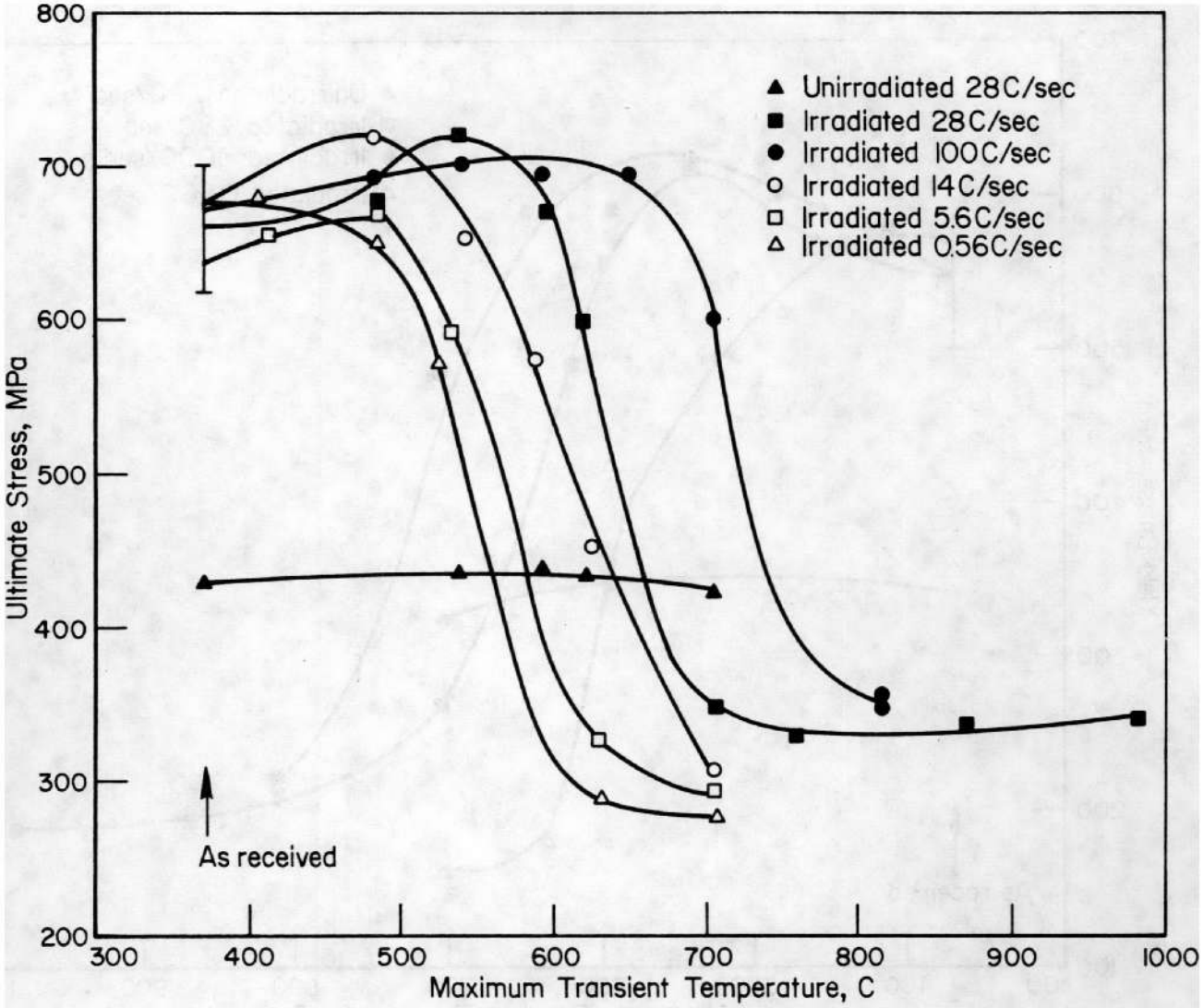

FIGURE 58. EFFECT OF TRANSIENT HEATING RATE AND MAXIMUM TEMPERATURE ACHIEVED IN TRANSIENT ON IRRADIATED H. B. ROBINSON FUEL-ROD CLADDING ULTIMATE TENSILE STRESS

Test temperature 371 C; strain rate 0.025/min.

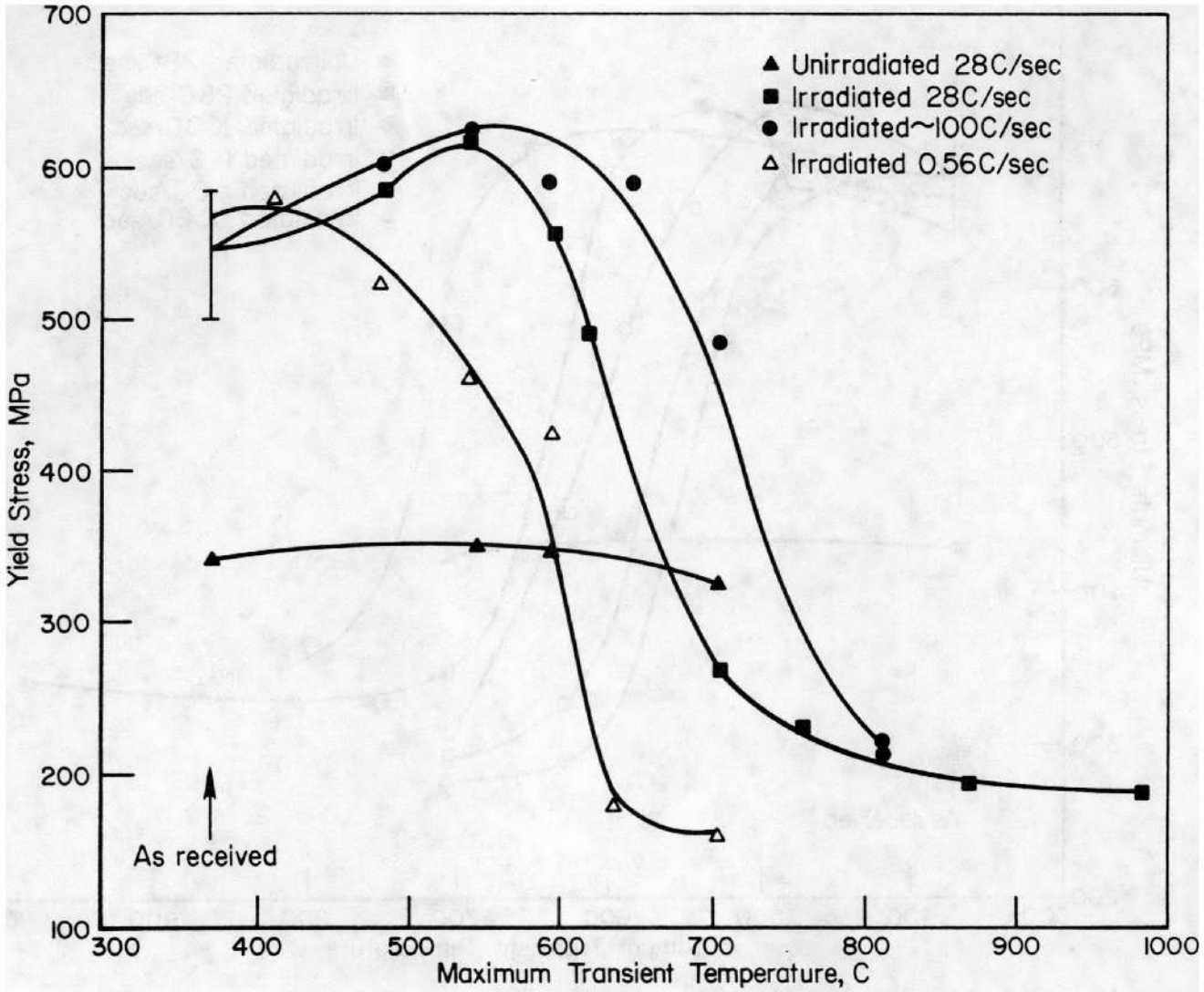

FIGURE 59. EFFECT OF TRANSIENT HEATING RATE AND MAXIMUM TEMPERATURE ACHIEVED IN TRANSIENT ON IRRADIATED H. B. ROBINSON FUEL-ROD CLADDING YIELD TENSILE STRESS

Test temperature 371 C; strain rate 0.025/min.

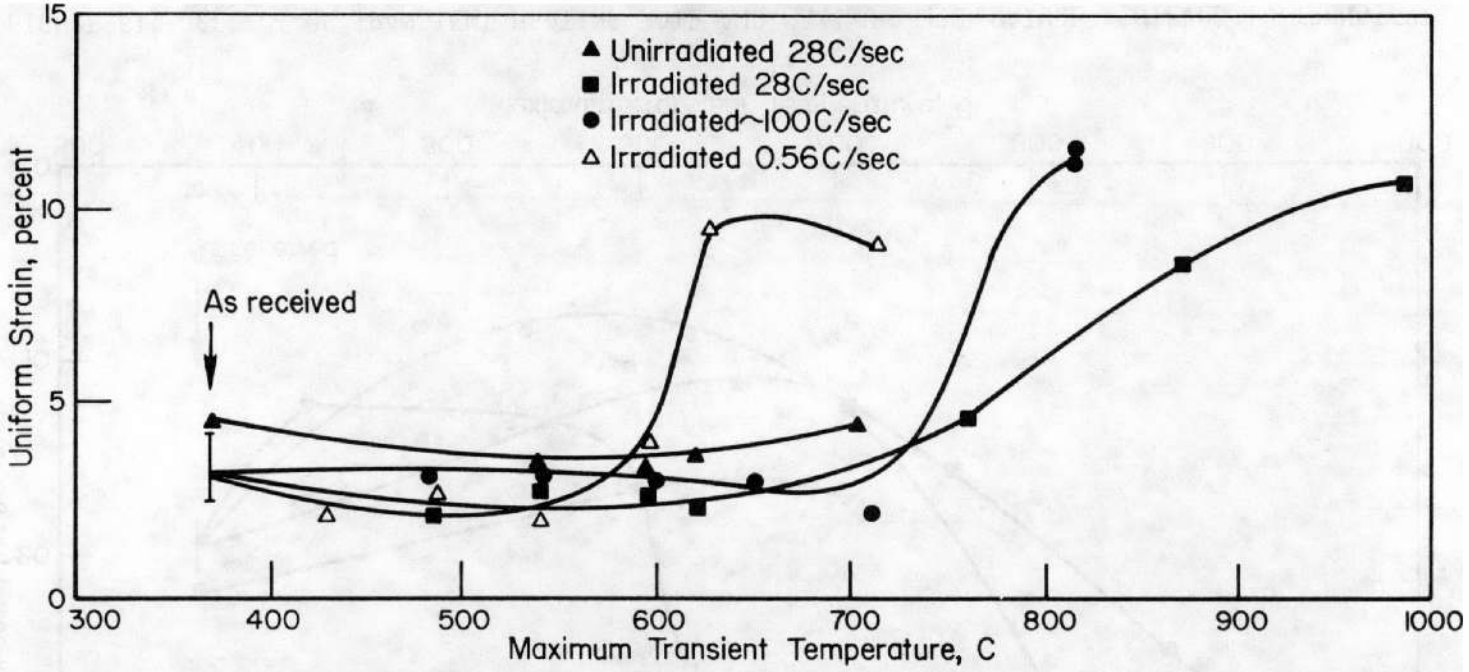

FIGURE 60. EFFECT OF TRANSIENT HEATING RATE AND MAXIMUM TEMPERATURE ACHIEVED IN TRANSIENT ON IRRADIATED H. B. ROBINSON FUEL ROD CLADDING UNIFORM TENSILE STRAIN

Test temperature 371 C; strain rate 0.025/min.

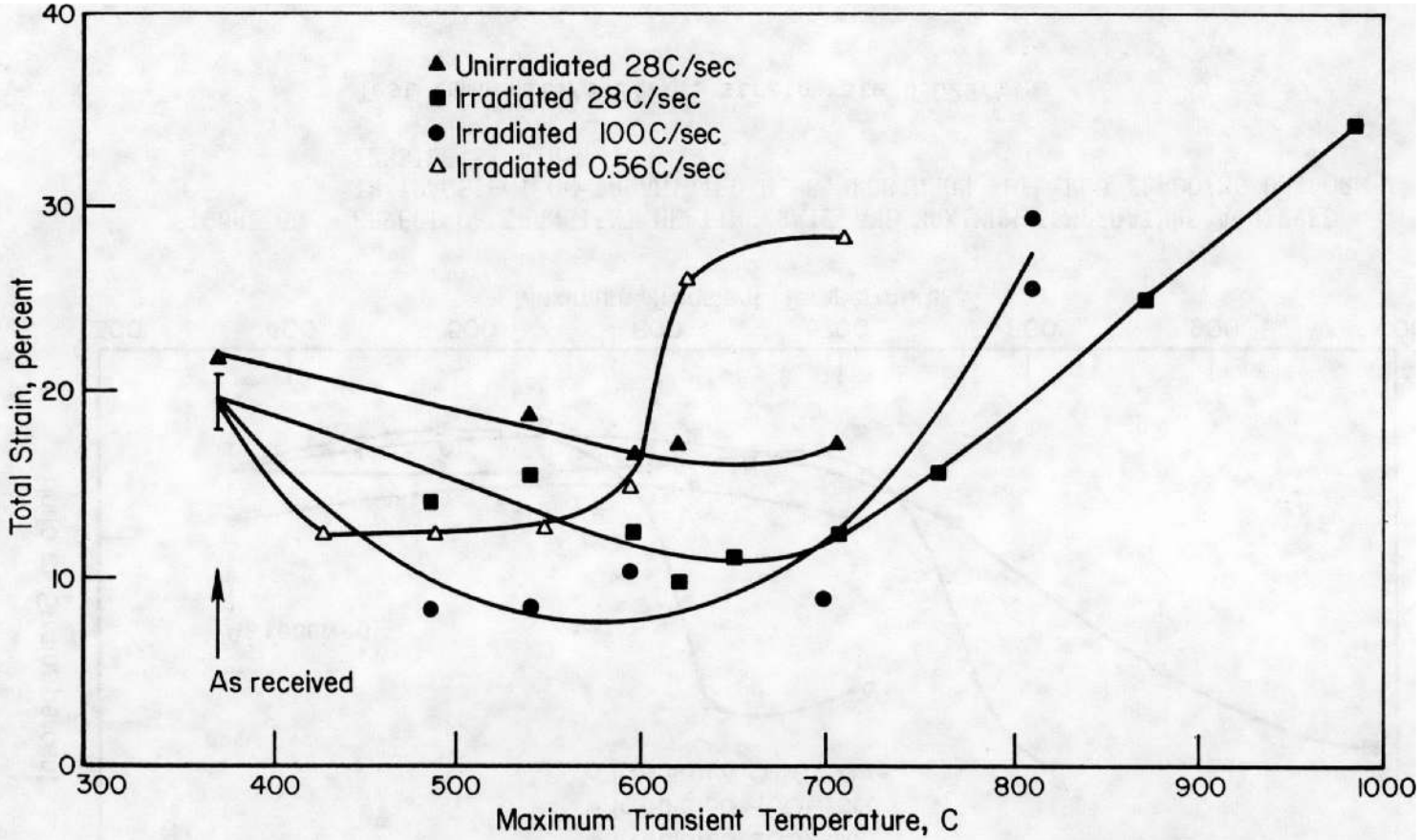

FIGURE 61. EFFECT OF TRANSIENT HEATING RATE AND MAXIMUM TEMPERATURE ACHIEVED IN TRANSIENT ON IRRADIATED H. B. ROBINSON-FUEL ROD CLADDING TOTAL TENSILE STRAIN

Test temperature 371 C; strain rate 0.025/min.

Ductility recovery, as evidenced by changes in uniform strain, lagged the stress changes. Initially, while stresses decreased, the uniform strain remained almost constant. Only after substantial stress loss occurred did the uniform strain increase.

The total strain, a measure of necking strain, showed a severe effect. The initial effect of annealing (between 400 and 600 C) was to degrade the necking strain to about one-half the as-received value and total strain goes through a minimum that moved to an increasingly higher maximum transient temperature as the rate of heating was increased. Normally, the recovery process (reduced stress) was accompanied by an increase in strain rather than the decrease noted in these experiments. However, only after recovery, as measured by stress decreases, was essentially complete did the total strain values recover to those characteristic of the as-irradiated condition. Subsequent increases in both uniform and total strains were accompanied by little or no change in stress. In fact, the total strain was still below the as-received value when the maximum transient temperature was 600 C for the lowest heating rate of 0.56 C/sec.

The severe effect on total strain suggested that the defect arrays produced during irradiation and possibly defect agglomeration during annealing at temperatures between 400 and 600 C serve as crack nuclei to initiate permature failure during plastic straining. Whether this was the mechanism for decreased ductility is uncertain, but such an explanation was consistant with the fact that ductility recovery significantly lagged the recovery in strength properties.

The effects of isothermal annealing on the tensile properties of irradiated H. B. Robinson Zircaloy fuel-rod cladding are shown in Figures 62, 63, 64, and 65; the results are tabulated in Tables 39 and 40. Recovery of tensile stress proceeded extremely rapidly at isothermal annealing temperatures above 593 C, with little change occurring for annealing times greater than 1 minute. Strain increases, as with transient anneals, tended to lag behind the stress decreases. Again, as with the transient anneals, significant decreases in necking ductility were evidenced by decreases in measured total strain. The apparent minimum in the total strain curves for 593 C and 621 C was displaced to longer times for the lower isothermal annealing temperature.

It should be noted that since the tensile properties are platted on semilog paper, the transient annealing results (0 time in Table 40) were plotted at the left margin (annealing time of 0.001 min).

TABLE 40. TENSILE TEST RESULTS FOR IRRADIATED H.B. ROBINSON ISOTHERMAL ANNEALED ZIRCALOY CLADDING.

Test Temperature 371 C; strain rate 0.025/min.

Specimen	Maximum Temperature, C	Time at Temperature, min	Stress		Strain	
			Ultimate MPa	Yield MPa	Uniform Percent	Total Percent
H10-5	427	60	616	487	3.4	16.0
H10-41	482	10	591	441	2.9	8.1
H10-17	482	60	556	365	3.1	9.2
A1-29-34	538	0	722	614	2.7	15.6
H7-2	538	0.5	617	514	2.3	5.6
P4-60-65	538	1.0	561	446	2.9	12.7
A1-24-29	538	10	363	237	3.2	9.4
H10-18	538	30	371	237	5.1	16.0
A8-105-110	593	0	671	554	2.7	12.4
H7-3	593	0.1	558	446	2.5	6.9
H7-4	593	0.25	499	434	1.5	7.1
H7-5	593	0.5	481	422	1.4	7.7
H7-6	593	0.75	473	422	1.4	9.5
A1-105-110	593	1.0	332	291	4.5	14.3
A1-99-104	593	5.0	311	175	8.0	23.6
H10-3	593	30	322	176	10.1	35.6
A8-110-115	621	0	598	492	2.1	9.8
H7-9	621	0.1	459	430	1.2	6.1
H7-10	621	0.25	426	409	1.1	7.4
H7-11	621	0.5	383	321	2.1	8.9
H7-12	621	0.75	415	304	4.8	11.6
A1-110-115	621	1.0	308	168	7.9	25.1
H10-4	621	30	319	169	13.9	32.7
A8-115-120	704	0	348	263	3.5	12.7
H7-13	704	0.1	330	196	9.3	25.0
H7-27	704	0.5	302	235	10.8	27.3
A1-116-131	704	1.0	306	170	9.4	20.3
H10-16	704	30	311	165	11.8	28.8

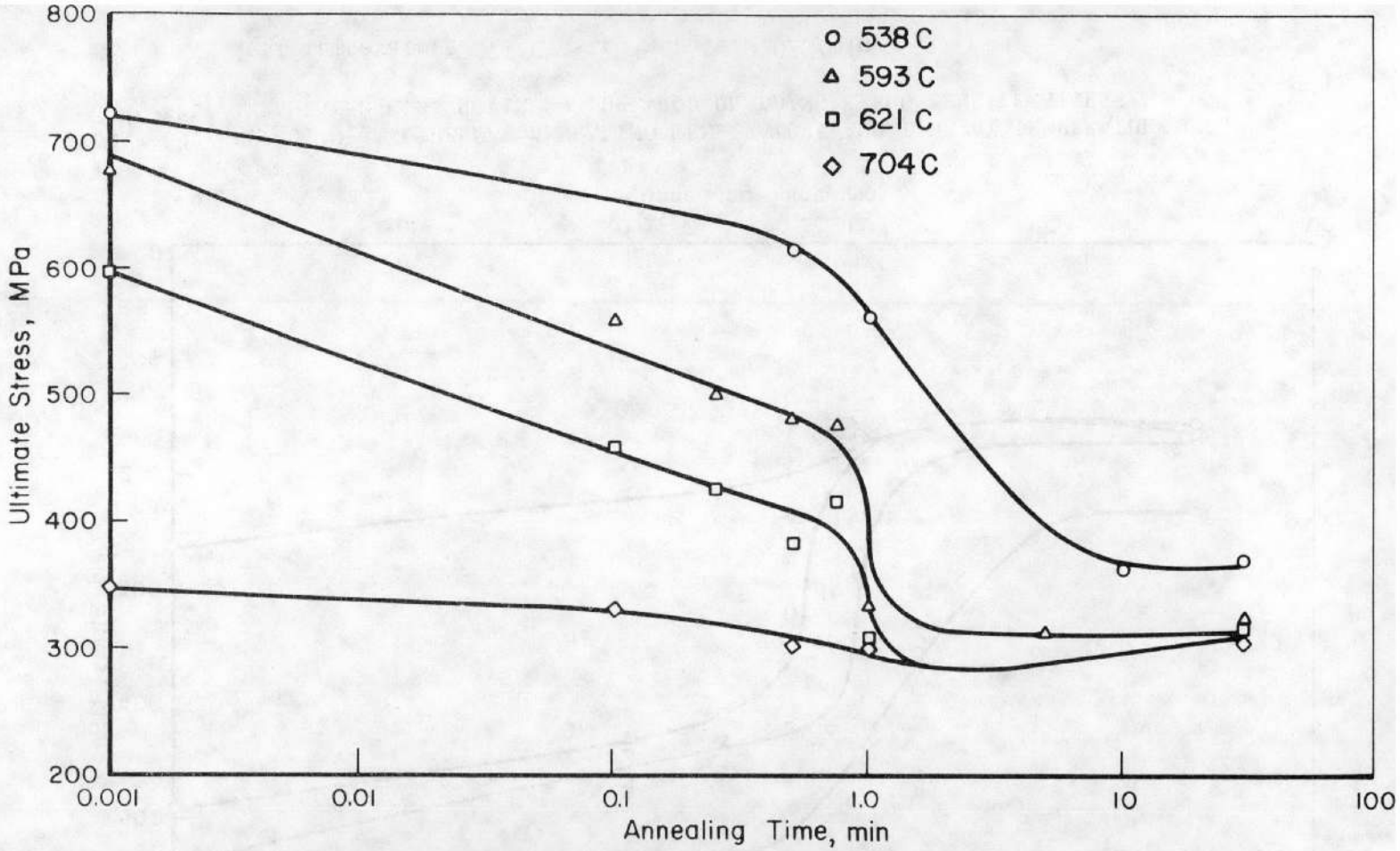

FIGURE 62. EFFECT OF ISOTHERMAL ANNEALING TEMPERATURE AND TIME AT TEMPERATURE ON IRRADIATED H.B. ROBINSON FUEL-ROD CLADDING ULTIMATE TENSILE STRESS

Test temperature 371 C; strain rate 0.025/min.

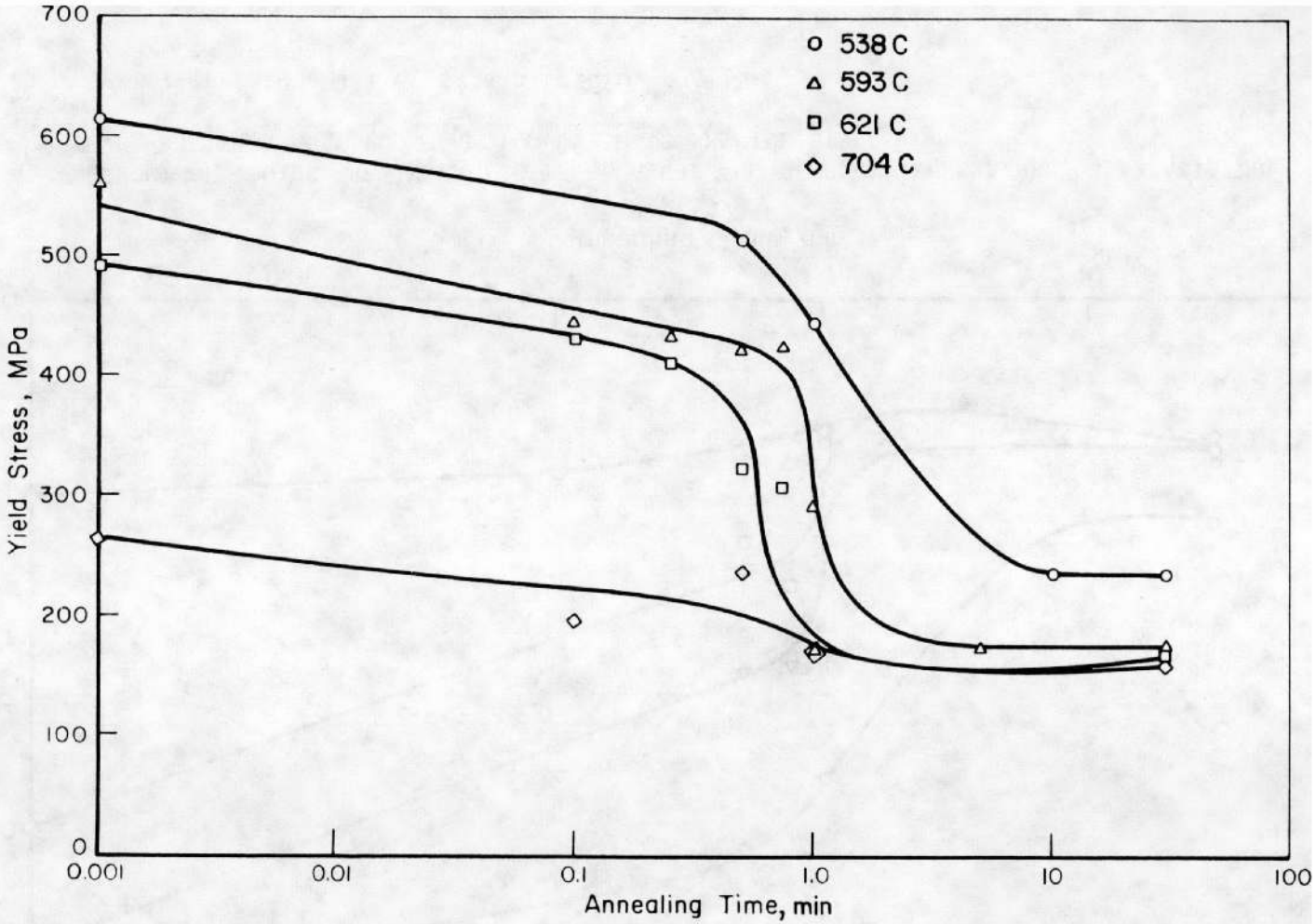

FIGURE 63. EFFECT OF ISOTHERMAL ANNEALING TEMPERATURE AND TIME AT TEMPERATURE ON IRRADIATED H.B. ROBINSON FUEL-ROD CLADDING YIELD TENSILE STRESS

Test temperature 371 C; strain rate 0.025/min.

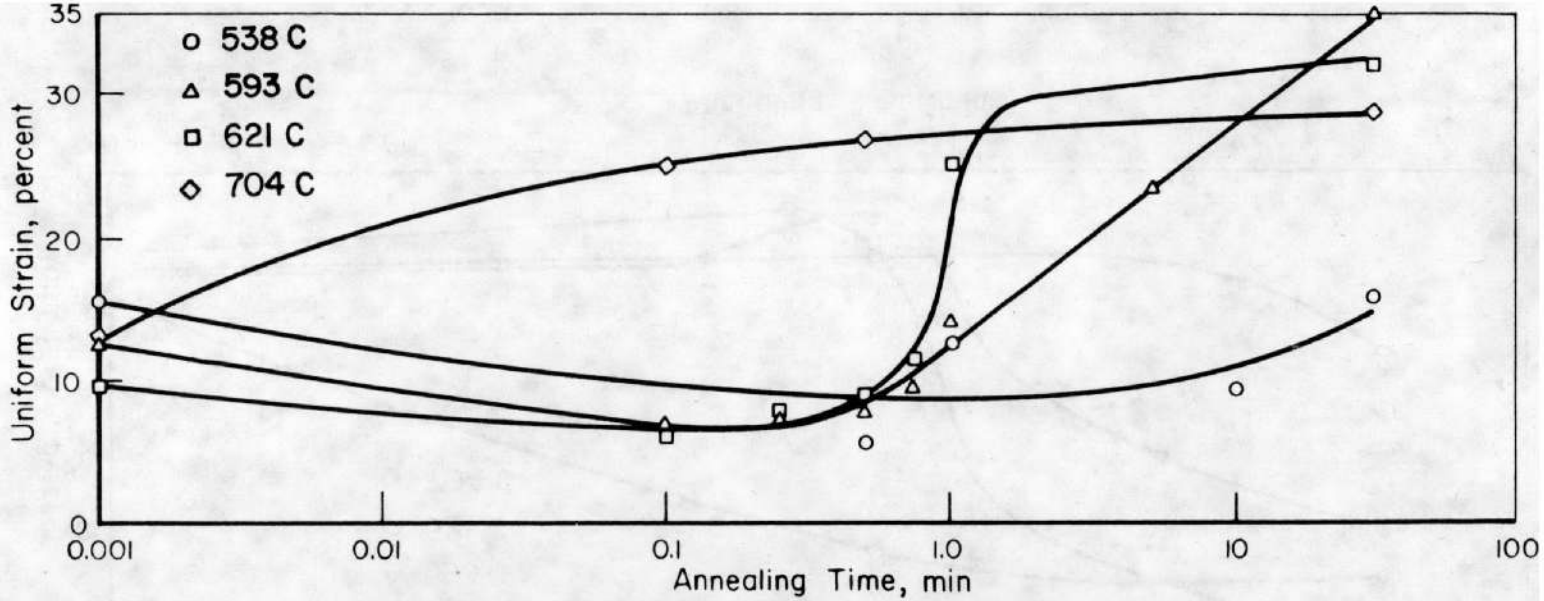

FIGURE 64. EFFECT OF ISOTHERMAL ANNEALING TEMPERATURE AND TIME AT TEMPERATURE ON IRRADIATED H.B. ROBINSON FUEL-ROD CLADDING UNIFORM TENSILE STRAIN

Test temperature 371 C; strain rate 0.025/min.

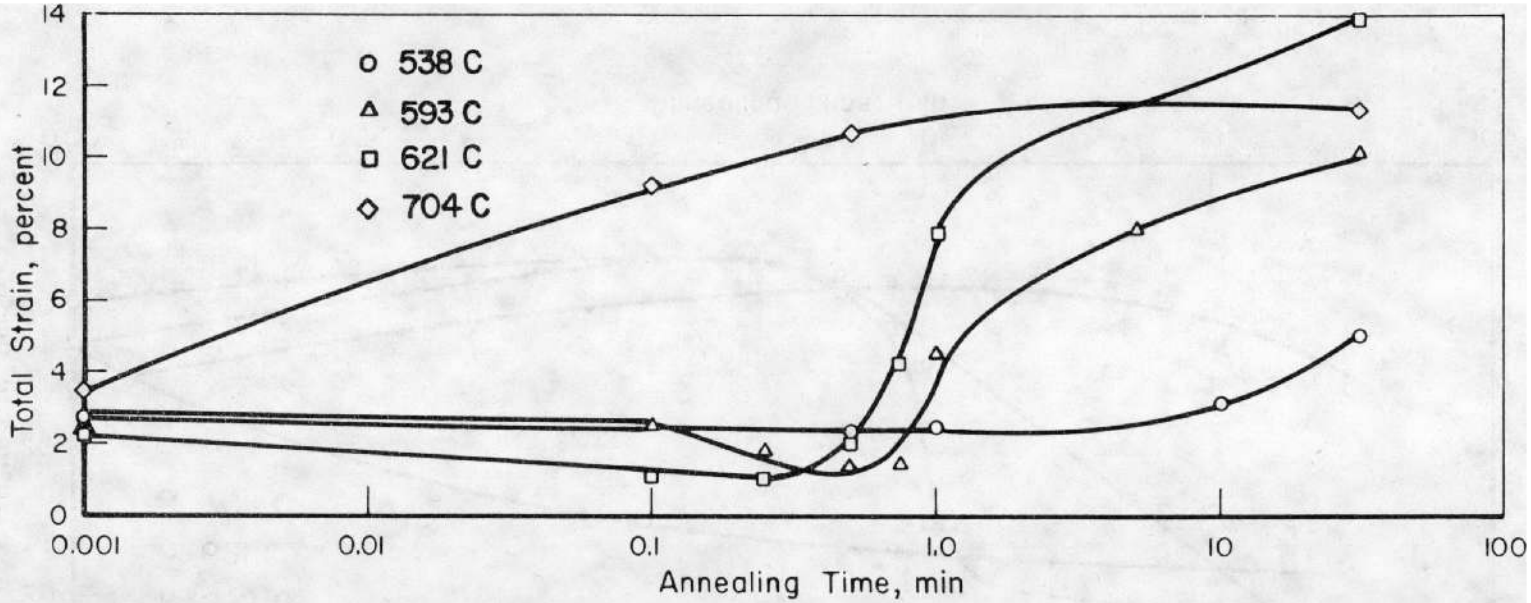

FIGURE 65. EFFECT OF ISOTHERMAL ANNEALING TEMPERATURE AND TIME AT TEMPERATURE ON IRRADIATED H.B. ROBINSON FUEL-ROD CLADDING TOTAL TENSILE STRAIN

Test temperature 371 C; strain rate 0.025/min.

The cause of the loss of strength and increase in ductility appeared to be the same for both transient and isothermal annealed specimens. However, the isothermal annealed tensile specimen test results showed the time-temperature relationship. For instance, at 593 C, the stress changes had stabilized at a minimum value within 1 minute but strains were only beginning to increase from their minimum values

Tube-wall reductions as a function of distance from the fracture surface were characterized for a number of annealed and tested tensile specimens by measuring the wall thickness of transverse sections of metallographically mounted test specimens as they were ground to successive depths from the initial fracture surface. These test data helped define the amount of wall thinning and the region of nonuniform plastic strain (localized necking region). If the wall thinning was attributed to axial elongation and tube diameter reduction to radial reduction, these data may be used to infer anisotropy of the test specimens. Tables 41 and 42 list the specimens measured, along with the test conditions and measured results for wall thickness, tube diameter, and cross-sectional area reductions; total strain values are also listed.

A variety of details concerning the tensile deformation of tubing was obtained by measurement of tube-wall reductions as a function of distance from the fracture. It was found that low total strains were associated with limited and highly localized wall necking, a characteristic that may be caused by dislocation channeling in both irradiated and partially recovered, annealed material. In general, an increase in total strain was accompanied by an increase in reduction in area. However, this was not a universal trend and there was no clear relationship between the two measures of ductility.

More notable is the apparent change in anisotropy that accompanied annealing. In comparing irradiated and irradiated-and-annealed tubing behavior, the fracture characteristics were found to be unaffected by annealing, with both irradiated and annealed tubing exhibiting shear-type ductile fractures. However, tube-wall and tube-diameter reduction measurements indicated a change in the isotropy of deformation at fracture when the tubing was annealed. Comparison of the tube-wall and tube-diameter necking reductions for the as-irradiated and irradiated-and-annealed tubing, showed that, whereas the wall reduction exceeded the diametral reduction in the irradiated tubing, this relationship was reversed after annealing. Thus, irradiation appeared to produce a less anisotropic material and annealing caused a return to the anisotropic behavior characteristic of unirradiated Zircaloy-4 tubing.

TABLE 4i. TUBE WALL AND DIAMETER DATA FOR IRRADIATED H.B. ROBINSON FUEL-ROD CLADDING IN TENSILE TESTS

Specimen	Test Conditions		Necking Reductions, percent			Total Strain, percent
	Temperature, C	Strain Rate, /min	Wall Thickness	Tube Diameter	Cross-Sectional Area	
P8-51	316	0.025	25.0	20.9	40.1	8.1
H10-20	371	0.025	25.0	15.4	36.6	16.5
H10-15	427	0.025	40.0	30.7	58.2	16.3
H10-33	371	0.0025	$\leq$27	14.0	$\leq$37	24.0
H10-38	371	2.5	$\leq$15	11.1	$\leq$24	12.8

TABLE 42. TUBE WALL AND DIAMETER DATA FOR IRRADIATED AND ANNEALED H.B. ROBINSON FUEL ROD-CLADDING IN TENSILE TESTS

Test temperature 371 C; strain rate 0.025/min.

Specimen	Annealing Conditions		Necking Reductions, percent			Total Strain, percent
	Temp, C	Time, min	Heating Rate, C/sec	Wall Thickness	Tube Diameter	Cross-Sectional Area
H10-17	482	60	28	18.1	19.0	33.7	9.2
H10-18	538	30	28	37.5	29.3	55.8	16.0
H10-3	593	30	28	37.1	39.1	61.7	35.6
H10-4	621	30	28	33.5	39.3	59.6	32.7
H10-16	704	30	28	33.1	28.8	52.4	28.8
A1-29-34	538	0	0.56	16.1	24.0	36.2	15.6
P4-89-94	538	0	28	19.4	23.0	37.9	12.8
P4-94-99	621	0	0.56	38.1	43.7	65.2	26.8
A8-110-115	621	0	28	16.1	26.1	38.0	9.8
P4-99-104	704	0	0.56	30.9	41.9	59.9	28.8
P4-84-89	704	0	5.6	36.9	43.6	64.4	29.8
P4-26-31	704	0	14	33.1	42.6	61.6	19.6
A8-115-120	704	0	28	41.1	33.7	60.9	12.7
H10-20	371	0	-	25.0	15.4	36.6	16.5
H10-40	593	0	0.56	19.7	35.2	48.7	14.7
P4-75-80	621	0	5.6	33.2	39.3	59.7	17.2
A8-105-110	593	0	28	18.7	27.1	25.1	12.4
0276-4	385	0	-	28.0	31.5	50.8	19.2

Irradiated Oconee I Cladding

Oconee I, One Cycle (Lot 2). Specimens from irradiated Oconee I fuel rods (One Cycle, Lot 2) were tensile tested at a test temperature of 371 C and at a strain rate of 0.025/min after being annealed under transient and isothermal conditions. For the transient anneals, 12.7-cm-long specimens were defueled and then heated at either 5.6 or 28 C/sec to specified maximum temperatures, from which they were quenched in a jet of helium. In the case of isothermal anneals, the specimens were heated at 28 C/sec to the required annealing temperature where they were held for the prescribed time before quenching with helium. The annealing procedures are outlined in Appendix B and the test procedures are given in Appendix C.

The tensile test results for specimens transient annealed are given in Table 43 and plotted in Figures 66 and 67. Note that the Oconee I (Lot 2) material tensile properties were also influenced both by the heating rate and by the maximum temperature reached in the transient. The transient annealing studies revealed the expected decrease in stress and increase in strain as the heating rate was decreased and the maximum temperature reached in the transient was increased. A peaking of stress was observed at the lower heating rate (5.6 C/sec) at a transient temperature of about 500 C. This appeared to suggest a thermal aging process possibly involving interactions between impurity atoms and irradiation induced defects. At higher temperatures, time-dependent recrystallization and grain growth occurred.

Ductility recovery, as evidenced by changes in uniform strain, lagged the stress changes. Initially, while the stresses decreased, the uniform strain for the 28 C/sec heating rate remained almost constant, but the uniform strain for the 5.6 C/sec heating rate exhibited a minimum at 600 C. Only after substantial stress loss occurred did the uniform strain increase.

The total strain, a measure of the necking strain, showed a minimum in the curve which was displaced to a higher temperature as the heating rate was increased. Only after recovery, as measured by stress decreases, was essentially complete did the total strain values recover. Subsequent changes (both increases and decreases) in uniform and total strains were accompanied by little or no change in stress. This minimum in total strain suggested that the defect arrays produced during irradiation and possibly defect agglomeration during annealing at temperatures between 400 and 700 C serve as crack nuclei to initiate premature failure during plastic straining. However, for Oconee I (Lot 2) material, the agglomeration did not occur at the higher heating rate of 28 C/sec, and therefore the effect was not as pronounced.

TABLE 43. TENSILE TEST RESULTS FOR IRRADIATED OCONEE I (ONE CYCLE) TRANSIENT ANNEALED ZIRCALOY FUEL ROD CLADDING

Test temperature 371 C; strain rate 0.025/min.

Specimen	Heating Rate, C/sec	Maximum Temperature, C	Stress		Strain	
			Ultimate MPa	Yield MPa	Uniform, percent	Total, percent
47015/81-86	28	482	570	475	3.1	13.7
47015/116-121	28	538	568	466	2.4	13.4
47015/111-116	28	593	550	445	2.3	8.4
47021/37-42	28	621	526	433	2.5	7.7
47015/86-91	28	704	338	272	3.9	8.7
47015/31-36	28	760	296	183	11.4	33.0
47015/23-28	28	871	310	150	7.9	32.3
47015/11-16	28	982	310	148	9.8	30.9
47010/10-15	5.6	482	632	554	3.5	14.4
47021/67-72	5.6	538	566	464	3.1	15.9
47010/116-121	5.6	593	530	441	2.1	8.9
47021/47-52	5.6	704	288	177	9.3	26.1

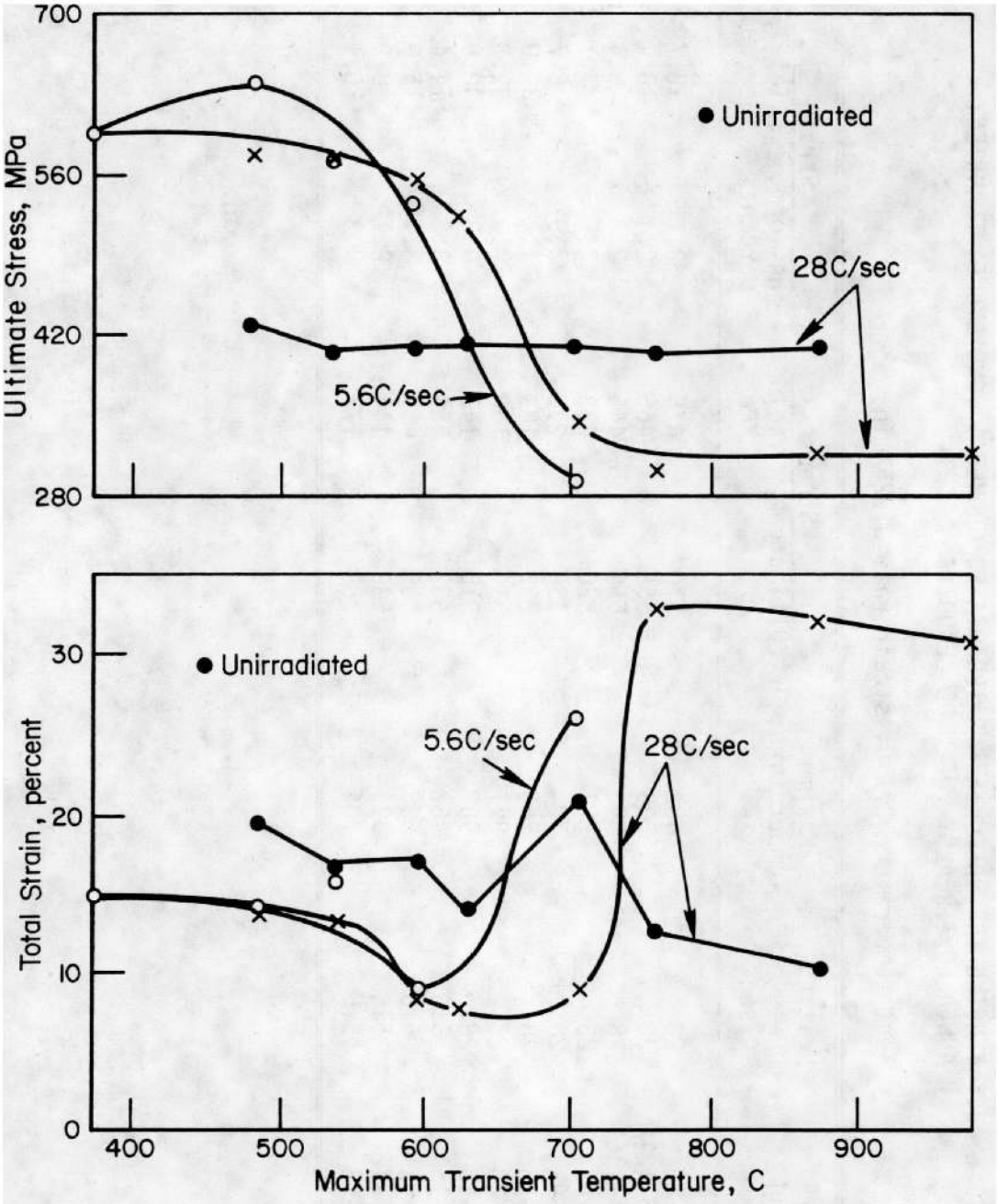

FIGURE 66. EFFECT OF TRANSIENT HEATING RATE AND MAXIMUM TEMPERATURE ACHIEVED IN TRANSIENT ON IRRADIATED OCONEE I (ONE CYCLE) FUEL ROD CLADDING ULTIMATE TENSILE STRESS AND TOTAL STRAIN Test Temperature, 371 C, Strain Rate 0.025/min.

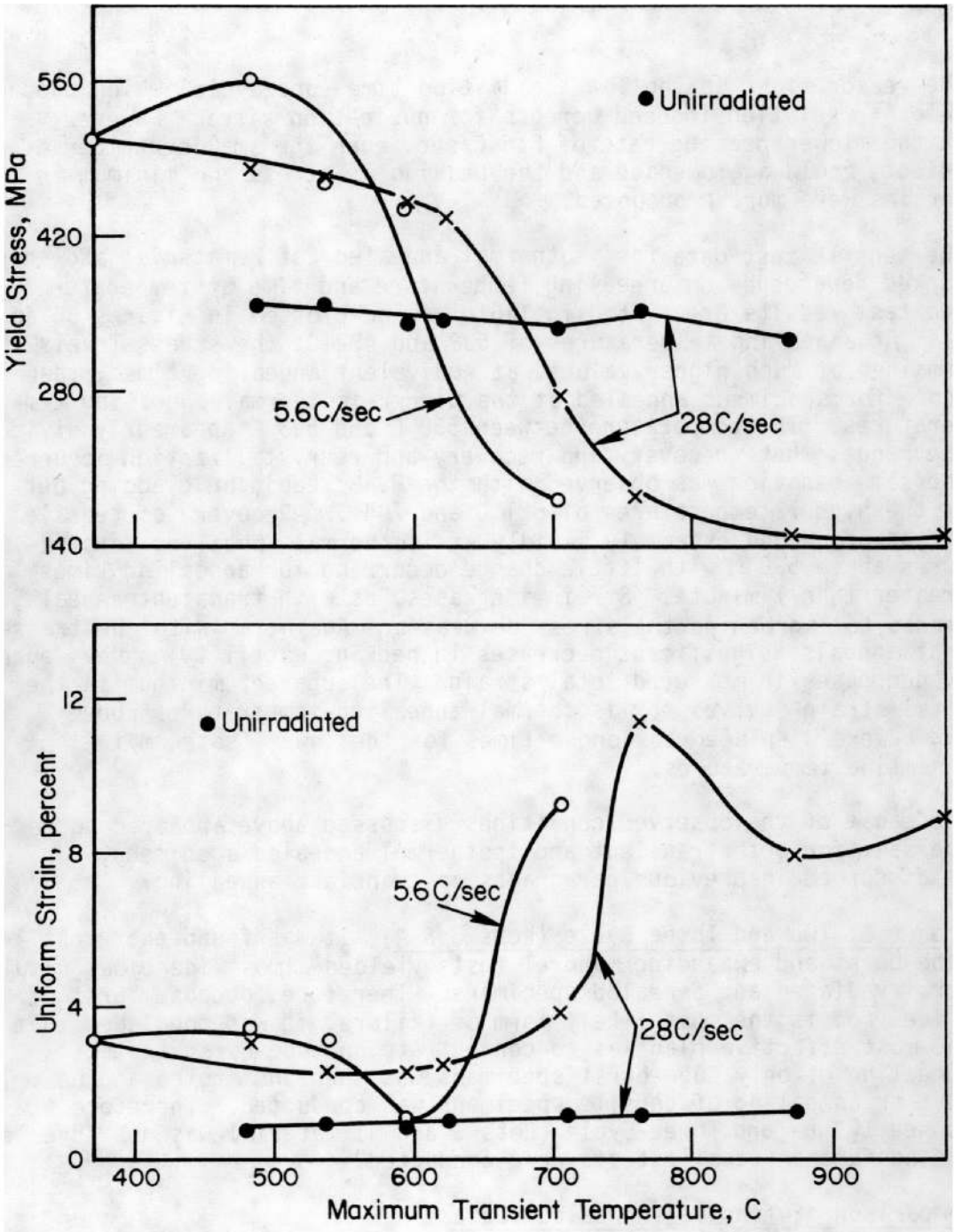

FIGURE 67. EFFECT OF TRANSIENT HEATING RATE AND MAXIMUM TEMPERATURE ACHIEVED IN TRANSIENT ON IRRADIATED OCONEE I (ONE CYCLE) FUEL ROD CLADDING YIELD TENSILE STRESS AND UNIFORM STRAIN Test Temperature 371 C; Strain Rate 0.025/min.

The reason might be the low irradiation time (one cycle) which produces fewer irradiation induced defects for nucleation sites. However, at the lower heating rate of 5.6 C/sec, even the smaller number of defects could agglomerate and the peaking of stress and minimum in the strains were more pronounced.

The tensile-test data for isothermal annealed Lot 2 material showed marked dependence on annealing temperature and time at temperature. The test results are listed in Table 44 and plotted in Figures 68 and 69. At annealing temperatures of 538 and 482 C, the stress levels remained at much higher values, at equivalent annealing times, than those for specimens annealed at the higher isothermal annealing temperatures. The temperature between 538 C and 593 C apparently divided the ranges where recovery and recovery-and-recrystallization occurred. The same behavior was observed with the H. B. Robinson cladding but at the higher temperatures of 621 C and 704 C. Recovery of tensile stress proceeded extremely rapidly at isothermal annealing temperatures above 538 C, with little change occurring for annealing times greater than 1 minute. Strain increases, as with transient anneals, tended to lag behind the stress decreases. Again, as with the transient anneals, significant decreases in necking ductility were evidenced by decreases in measured total strain. The apparent minimum in the total strain curves for isothermal annealing temperatures above 482 C were displaced to longer times for the lower isothermal annealing temperatures.

The cause of the observed conditions discussed above appeared to be the same for both transient and isothermal annealed specimens, as discussed in previous paragraphs on transient annealing.

Oconee I, Two and Three Cycle (Lots 3 & 4). It was found that tensile, tube-burst and expanding mandrel tests yielded almost identical results for irradiated and annealed specimens. Therefore, because burst of a fuel rod is the most likely form of failure, it was concluded that the most effective plan was to concentrate on tube-burst tests. Annealing of only tube-burst specimens was then instituted and no further annealing of tensile specimens was conducted. Therefore, Oconee I, Two- and Three-Cycle (Lots 3 and 4) material was not annealed and no further tensile tests were conducted.

Comparison of Tensile (Annealed) Data

Comparison of the tensile-test data for the unirradiated Oconee I archive material and the unirradiated tubing, supplied to ORNL and BCL by Sandvik, after transient annealing at 28 C/sec showed similarities but also some distinct differences (see Tables

TABLE 44. TENSILE-TEST RESULTS FOR IRRADIATED OCONEE I (ONE CYCLE) ISOTHERMAL ANNEALED ZIRCALOY CLADDING

Test temperature 371 C; strain rate 0.025/min.

Specimen	Maximum Temperature, C	Time at Temperature, min	Stress		Strain	
			Ultimate MPa	Yield MPa	Uniform, percent	Total, percent
47021/31-36	482	10	565	424	2.9	12.5
47021/9-14	482	60	532	420	3.5	16.0
47021/84-89	538	1	521	426	2.2	6.2
47021/79-84	538	5	505	410	2.2	9.0
47021/52-57	593	1	339	283	2.5	9.8
47021/19-24	593	30	279	163	13.1	22.8
47021/74-79	621	1	296	205	5.2	17.7
47021/14-19	704	1	270	151	11.9	32.1

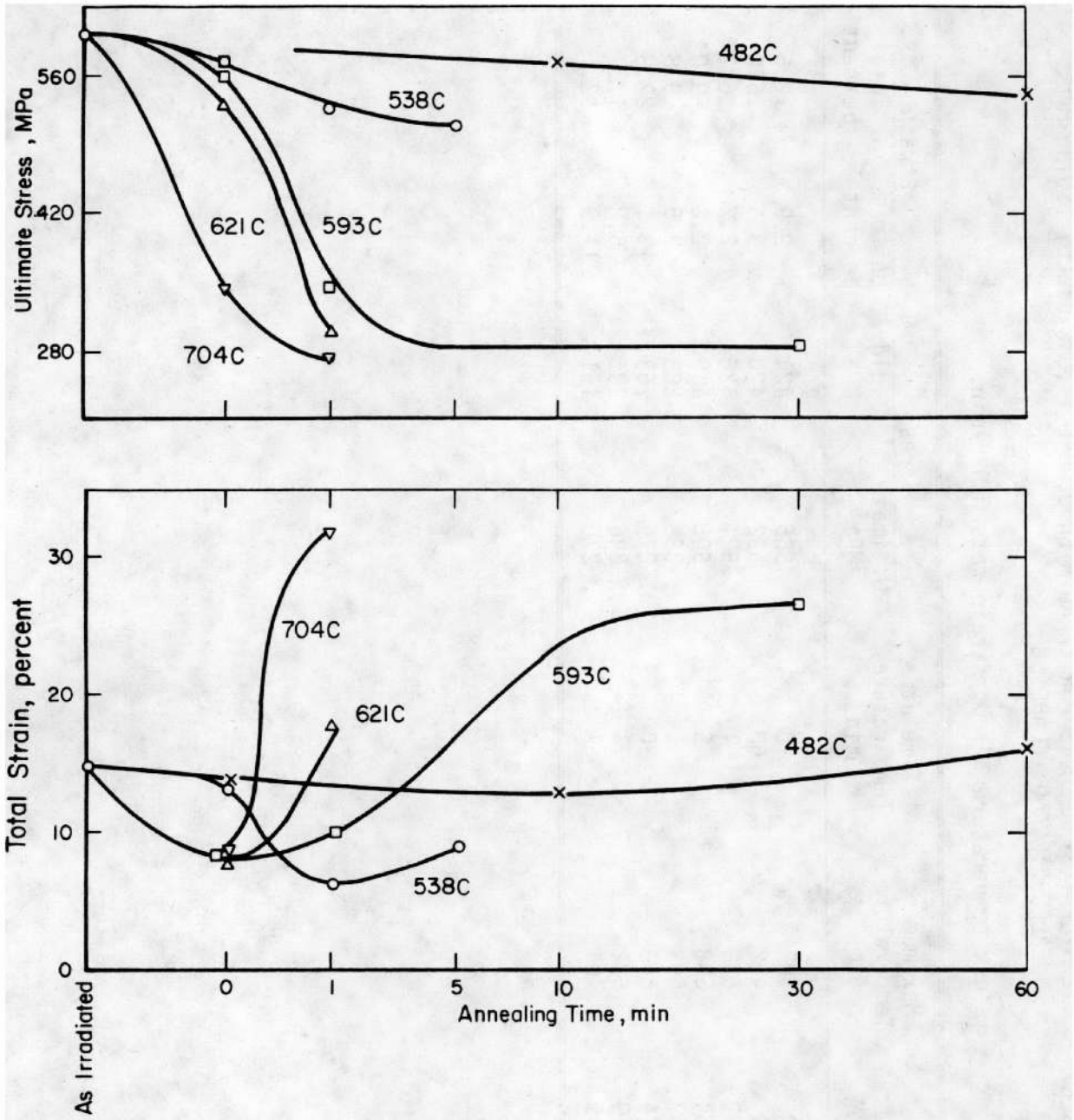

FIGURE 68. EFFECT OF ISOTHERMAL ANNEALING TEMPERATURE AND TIME AT TEMPERATURE ON IRRADIATED OCONEE I (ONE CYCLE) FUEL-ROD CLADDING ULTIMATE TENSILE STRESS AND TOTAL STRAIN

Test Temperature 371 C; strain rate 0.025/min.

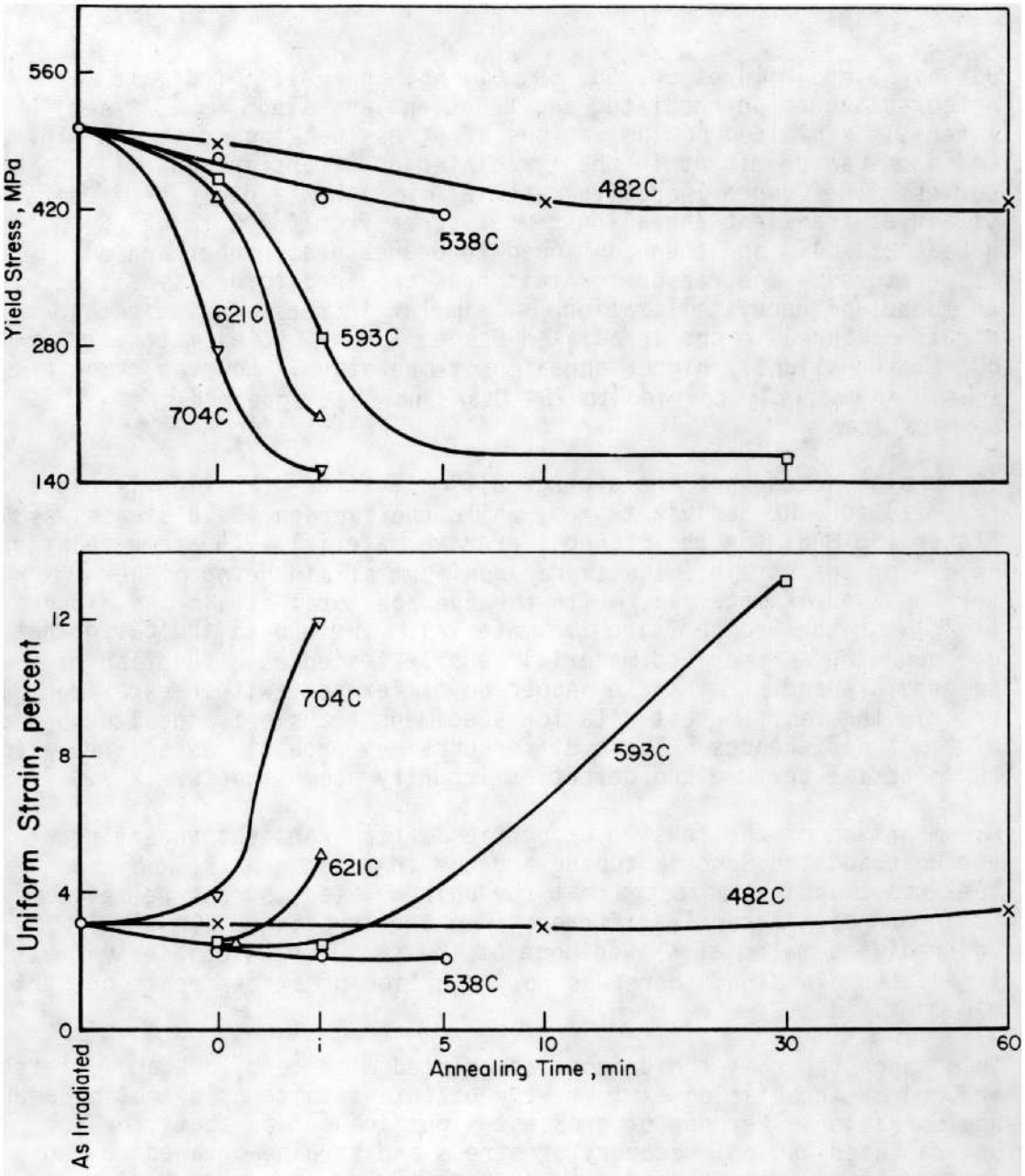

FIGURE 69. EFFECT OF ISOTHERMAL ANNEALING TEMPERATURE AND TIME AT TEMPERATURE ON IRRADIATED OCONEE I (ONE CYCLE) FUEL-ROD CLADDING YIELD TENSILE STRESS AND UNIFORM STRAIN

Test temperature 371 C; strain rate 0.025/min.

36 and 38 and Figures 56, 58, 59, 61, 66, and 67). First, it was noted that both unirradiated and transient annealed (at 28 C/sec) materials exhibited no indications of stress peaking or strain minimums which were so prominent in the irradiated and transient annealed data curves. The Oconee I archive material did show a decrease in total strain at transient annealing temperatures from 482 C to 621 C, a peak at 704 C, and then continued to decrease at higher annealing temperatures. The reason for this peak appeared to be associated with the onset of recrystallization, and similar increase in the total strain occurred in the irradiated Oconee I (One Cycle) material, but at the slightly higher annealing temperature. However, transient annealing was only carried to 704 C and no peak appeared up to this temperature.

It was also noted that the average ultimate stress was slightly higher (20 MPa) for the Sandvik tubing, while the average yield stress was higher (35 MPa) for the Oconee I archive material. The same relation held for the strains, the average uniform strain being higher (1.8%) for the Sandvik material, while the average total strain was higher (1.8%) for the Oconee I archive material. These data indicated that although the as-received material tensile tested as a function of temperature and strain rate showed no difference (within experimental error), the tensile test data for specimens transient annealed showed distinct differences. These differences were probably associated with the material texture and defect or impurity atom structure.

A comparison of the tensile properties after transient annealing of the unirradiated Sandvik tubing and the irradiated H. B. Robinson fuel rod cladding indicated that the unirradiated, stress-relieved tubing was significantly different from the irradiated cladding. The unirradiated material showed none of the features associated with the irradiated cladding; there was no indication of stress peaks or strain minimums.

This suggested that the defects associated with cold work and defects induced by irradiation exhibit very different patterns of motion and agglomeration. Perhaps of greatest significance was that, for the unirradiated tubing, recovery of stress and strain appeared to begin at the same transient temperature, with no lag in recovery of the ductility behind that of the strength, whereas the irradiated fuel-rod cladding recovery of strain lagged the stress recovery. Another significant observation was that, at least for the transient annealing temperature range chosen for these tensile tests, once the recovery occurred, the ultimate and yield stresses dropped below, and the uniform and total strain increase rose above the unirradiated

tubing values at equivalent transient annealing temperatures. This suggested that because of increased nucleation sites produced by irradiation-induced defects the grain structure of the irradiated and annealed material was finer and, therefore, of somewhat lower strength and higher ductility after annealing. Another explanation is that if the unirradiated tubing were annealed to higher temperatures the strength would drop and ductility, would increase to those values exhibited by the irradiated cladding.

A comparison of the tensile properties of unirradiated and transient annealed Oconee I archive material and of the irradiated Oconee I (One Cycle) fuel-rod cladding showed the same trends discussed in the previous paragraph,and the same discussion and observations hold for the Oconee I cladding. The transient annealing of the Oconee I archive material, however, was extended to a temperature of 871 C which is very close to the alpha-to-beta transition temperature. Even at these higher annealing temperatures, the irradiated-and-transient annealed stresses remained below the unirradiated-and-transient annealed stresses. The tensile strains for irradiated-and-transient annealed specimens remained much higher than tensile strains for unirradiated-and-transient annealed material. This confirmed that the structural differences were the probable cause for the lower strength and higher ductilities associated with the irradiated, transient annealed and tensile tested fuel-rod cladding.

When comparing the tensile data for the Oconee I and H. B. Robinson irradiated, transient annealed and subsequently tensile tested 371 C and at a strain rate of 0.025/min, it must be noted that the average burnup for the H. B. Robinson fuel rods is about 28,000 MWD/MTU and the average burnup for the Oconee I (One Cycle) fuel rods is 10,000 MWD/MTU. However, because of concentrated emphasis on tube-burst tests, no data were generated for the Oconee I (three cycle) fuel rods, which have a burnup of about 30,000 MWD/MTU.

While the two sets of cladding material exhibited fairly similar behavior, there are some notable instances of deviation. Thus, while both exhibited radiation-induced strengthening, the amount of the increase of the higher burnup H.B. Robinson cladding was slightly above that of the Oconee cladding. Also, the irradiated H.B. Robinson cladding exhibited a pronounced stress peak when the transient annealing heating rate was 28 C/sec to temperatures between 500 and 600 C. However, while the Oconee irradiated fuel-rod cladding exhibited a strength peak at about 500 C when the transient annealing heating rate was 5.6 C/sec, none was evidenced in the irradiated Oconee cladding results when the transient annealing heating rate was 28 C/sec. Again these differences were probably caused by differences in manufacturing, stress relieving, microstructure, and the number of irradiation-induced defects.

Another significant difference in behavior between the H.B. Robinson and Oconee Zircaloy claddings was in the effect of annealing on uniform elongation. While the uniform elongation of the H.B. Robinson cladding tended to remain essentially constant during initial recovery annealing stages, the Oconee cladding showed a pronounced decrease in uniform elongation before the increase occurs. The same behavior is observed in the course of isothermal annealing. This decrease in ductility at intermediate recovery stages was characteristic of both materials in measurements of total elongation.

Below 704 C, the rate of recovery of strength and ductility were very similar for both materials. Above 750 C, ductility increased much more rapidly in the Oconee cladding than in the H. B. Robinson cladding as a result of the transient anneals. However, both showed pronounced increases in strains above 750 C and this suggested the possibility of a spontaneous recovery above a critical temperature.

Tube-Burst Tests

Irradiated H. B. Robinson Cladding (Lot I)

The tube-burst test provided a determination of the mechanical properties of irradiated cladding under biaxial stress conditions. The test equipment and procedures for annealing specimens are outlined in Appendix B. The test equipment and procedures for tube-burst testing are given in Appendix C. The tube-burst tests were conducted on specimens of irradiated H. B. Robinson fuel-rod cladding after various transient and isothermal annealing treatments. The specimens were first sectioned from irradiated fuel rods, the fuel removed and the cladding sections were then annealed. After annealing, the specimens were burst tested at a test temperature of 371 C and at a strain rate of 0.004/min.

The results of the burst tests for specimens transient annealed are tabulated in Table 45. The effect of transient annealing on the tube-burst stresses and strains is shown in Figures 70 and 71. The yield and ultimate stresses exhibited very similar behavior. Both showed a peak at the two lower heating rates of 0.56 and 5.6 C/sec but not at the 14 and 23 C/sec transient annealing heating rates. The stress values dropped rapidly when the temperature achieved in the transient exceeded about 550 C and all evidence of irradiation strengthening disappeared when the transient temperature reached 700 C, regardless of the heating rate. The uniform and total strain increases tended to lag the drop in stresses. This was most evident in the case of the uniform strain which showed an initial decrease as annealing proceeded such that, at the point that the initial as-irradiated ductility values was recovered, complete annealing of the irradiation induced strengthening had occurred.

A decrease in uniform strain accompanied the initial stages of recovery during the transient annealing. A similar decrease in the failure strain may have occurred, but is less obvious and less pronounced.

It is believed that similar mechanisms described in the preceding Tensile Test Section apply and adequately explain the peaks in stresses and minimums in strains observed in these tube-burst tests results.

The results of the burst tests for specimens isothermally annealed to temperatures in the range from 538 to 704 C are tabulated in Table 46. After heating at a rate of 28 C/sec, the specimens were held at the isothermal annealing temperature for periods from 1 to 30 minutes and subsequently burst tested. The effect of isothermal annealing on the irradiated tube-burst stresses and strains is shown in Figures 72 and 73. As the annealing

TABLE 45. TUBE-BURST TEST RESULTS FOR IRRADIATED H.B. ROBINSON TRANSIENT ANNEALED ZIRCALOY FUEL-ROD CLADDING

Test temperature 371 C; strain rate 0.004/min.

Specimen	Circumferential Strain Rate/min	Anneal		Yield Strength MPa	Burst Strength, MPa		Circumferential Strain, percent	
		Heating Rate C/sec	Maximum Temperature, C		Ultimate	Failure	Uniform	Failure
D9-2	0.004	0.56	427	680	747	736	2.5	5.9
D9-3	0.004	0.56	482	632	675	654	2.2	9.6
D9-4	0.004	0.56	538	532	582	569	2.2	7.2
D9-6	0.004	0.056	593	330	393	372	3.4	26.4
D9-7	0.004	0.56	621	282	367	356	5.9	21.2
D9-8	0.004	0.56	704	265	361	351	6.8	20.4
D9-9	0.004	5.6	427	662	733	718	2.9	7.6
D9-10	0.004	5.6	482	654	691	681	2.0	6.1
D9-11	0.004	5.6	538	584	597	579	1.9	8.6
D9-12	0.004	5.6	593	460	479	457	1.7	20.7
D9-13	0.004	5.6	621	316	372	361	2.9	22.5
D9-14	0.004	5.9	704	278	368	335	5.4	29.2
D4/7	0.004	14	427	564	645	642	3.3	> 2.5
D4/9	0.004	14	482	571	637	630	2.8	> 2.6
D4/2	0.004	14	538	574	603	603	2.4	2.4
D4/3	0.004	14	593	510	539	537	1.6	3.4
D4/8	0.004	14	621	368	396	390	2.2	14.8
D4/5	0.004	14	704	272	334	314	4.7	23.8
D4/6	0.004	28	538	572	638	638	2.7	2.7
D4/13	0.004	28	593	527	550	549	1.8	2.8
D4/12	0.004	28	621	456	471	466	1.6	7.6
D4/11	0.004	28	704	274	325	319	3.0	14.2
D4/17	0.004	28	760	260	332	331	5.5	18.8

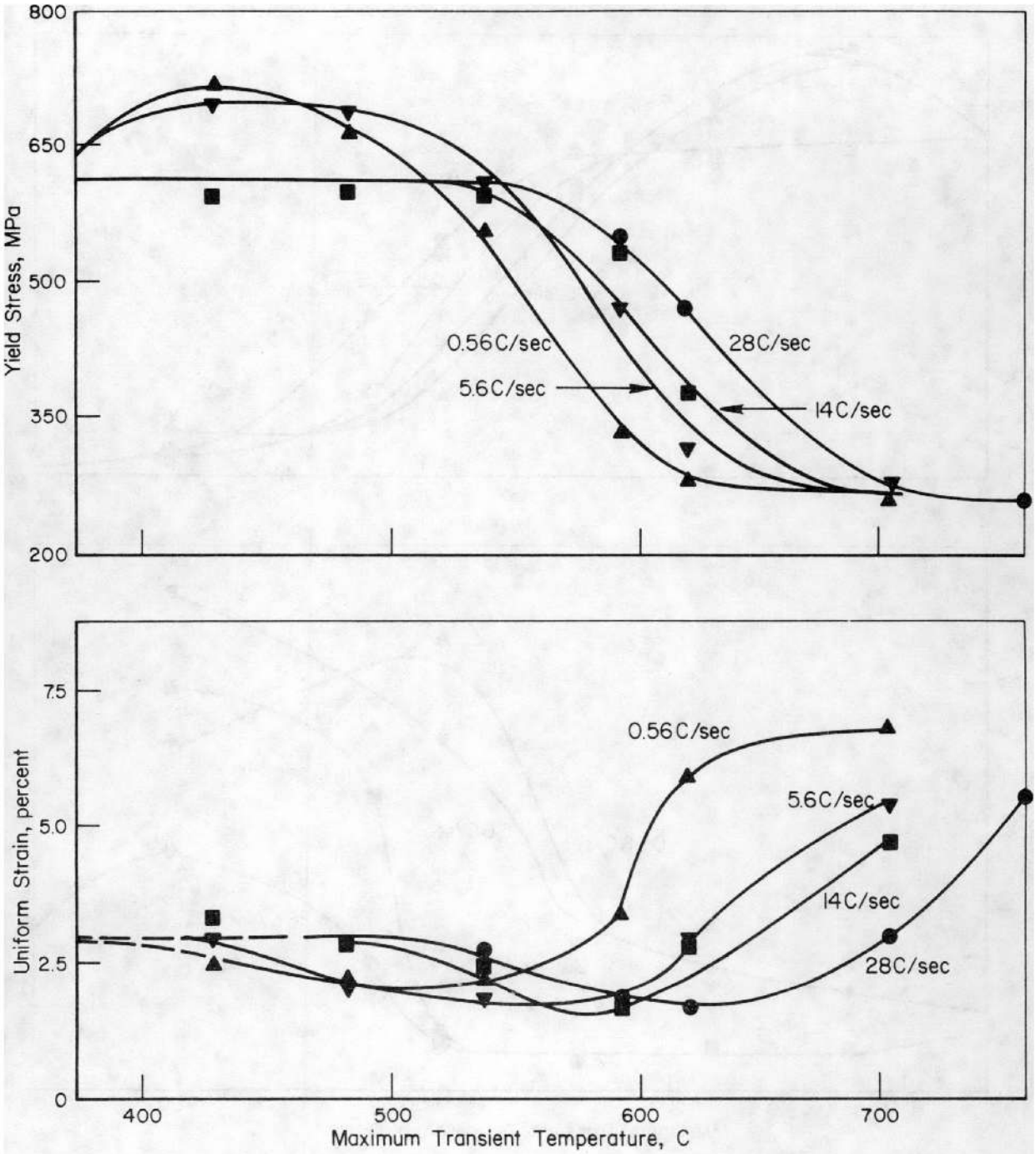

FIGURE 70. EFFECT OF TRANSIENT ANNEALING ON YIELD STRENGTH AND UNIFORM CIRCUMFERENTIAL STRAIN IN ISOTHERMAL TUBE-BURST TESTS OF H. B. ROBINSON SPENT-FUEL CLADDING Test Temperature, 371 C.

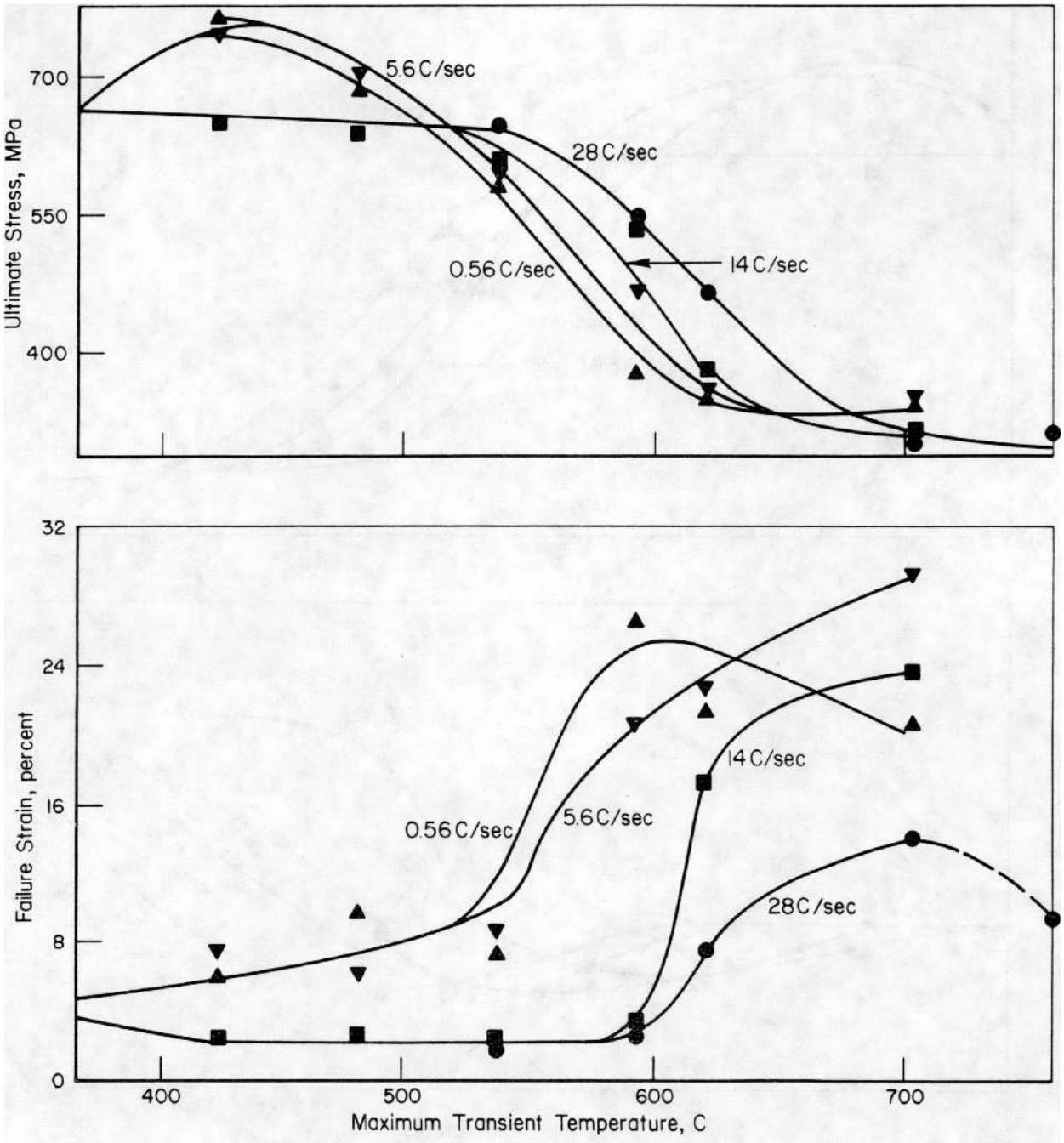

FIGURE 71. EFFECT OF TRANSIENT ANNEALING ON ULTIMATE STRENGTH AND CIRCUMFERENTIAL FAILURE STRAIN IN ISOTHERMAL TUBE-BURST TESTS OF H. B. ROBINSON SPENT-FUEL CLADDING Test Temperature, 371 C.

TABLE 46. TUBE-BURST TEST RESULTS FOR IRRADIATED H. B. ROBINSON ISOTHERMAL ANNEALED ZIRCALOY FUEL-ROD CLADDING

Test temperature 371 C; strain rate 0.004/min.

Specimen	Anneal			Yield Strength, MPa	Burst Strength MPa		Circumferential Strain, percent	
	Heating Rate, C/sec	Maximum Temperature, C	Time at Temperature, min		Ultimate	Failure	Uniform	Failure
D4/15[a]	28	482	10	516	549	547	2.2	5.5
D4/14	28	482	10	507	564	554	2.3	4.8
D4/16[b]	28	482	10	515	570	566	1.9	5.6
K8/13	28	538	10	472	505	481	2.3	5.9
F8/28-35	28	593	1	316	339	319	2.6	24.7
K8/5	28	593	10	342	368	358	1.7	15.1
K8/6[b]	28	593	10	335	372	372	2.3	6.6
F8/55-62	28	621	1	252	300	274	2.7	32.5
K8/14	28	621	30	236	299	296	5.5	14.0
F8/55-62	28	704	1	221	290	279	4.9	27.6
K8/10[b]	28	704	30	239	316	306	7.4	18.1
H6/6A	28	704	30	208	296	288	6.1	14.4

(a) Tested at a strain rate of 0.001/min.

(b) Tested at a strain rate of 0.035/min.

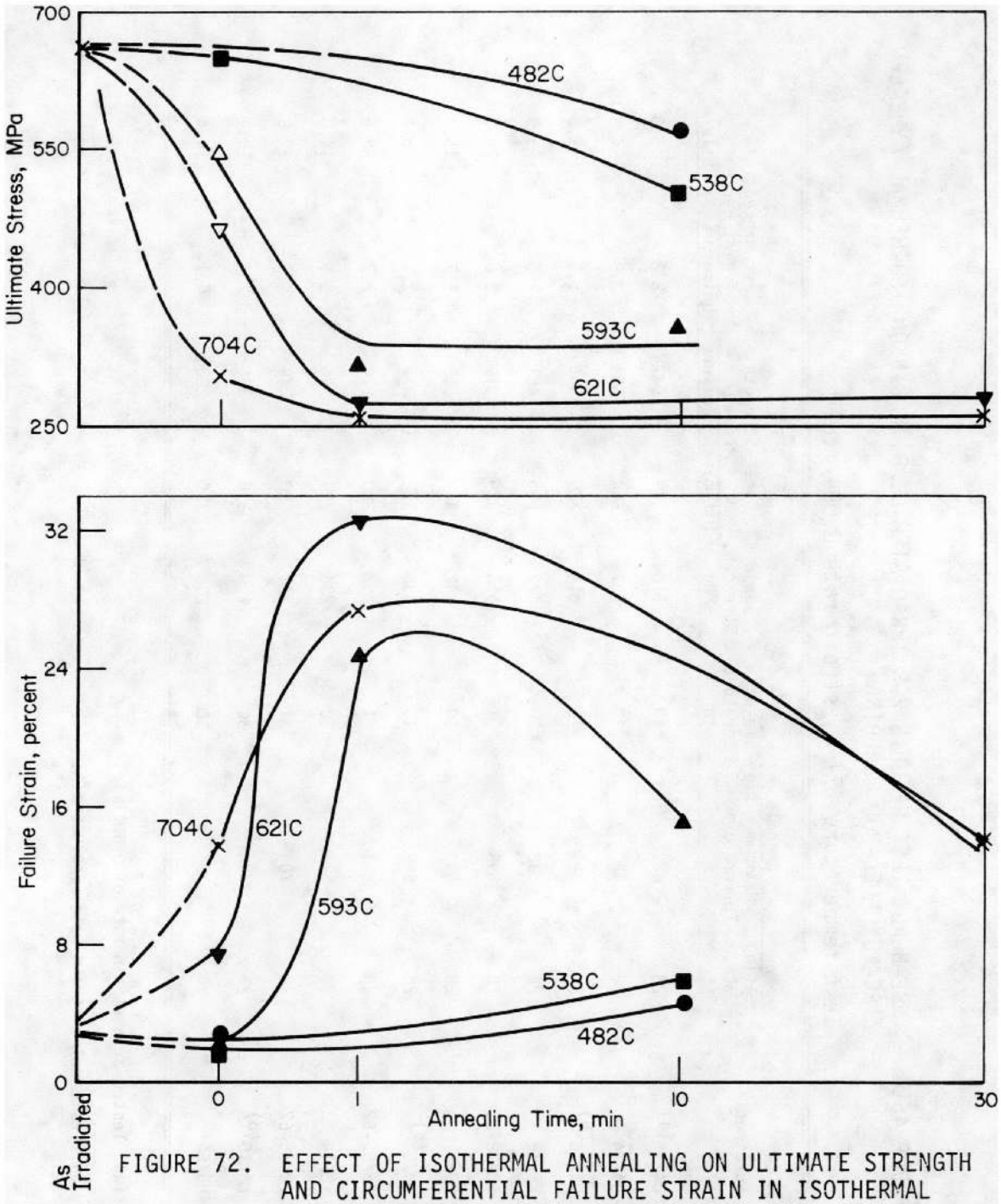

FIGURE 72. EFFECT OF ISOTHERMAL ANNEALING ON ULTIMATE STRENGTH AND CIRCUMFERENTIAL FAILURE STRAIN IN ISOTHERMAL TUBE-BURST TESTS OF H. B. ROBINSON SPENT-FUEL CLADDING

Test temperature 371 C.

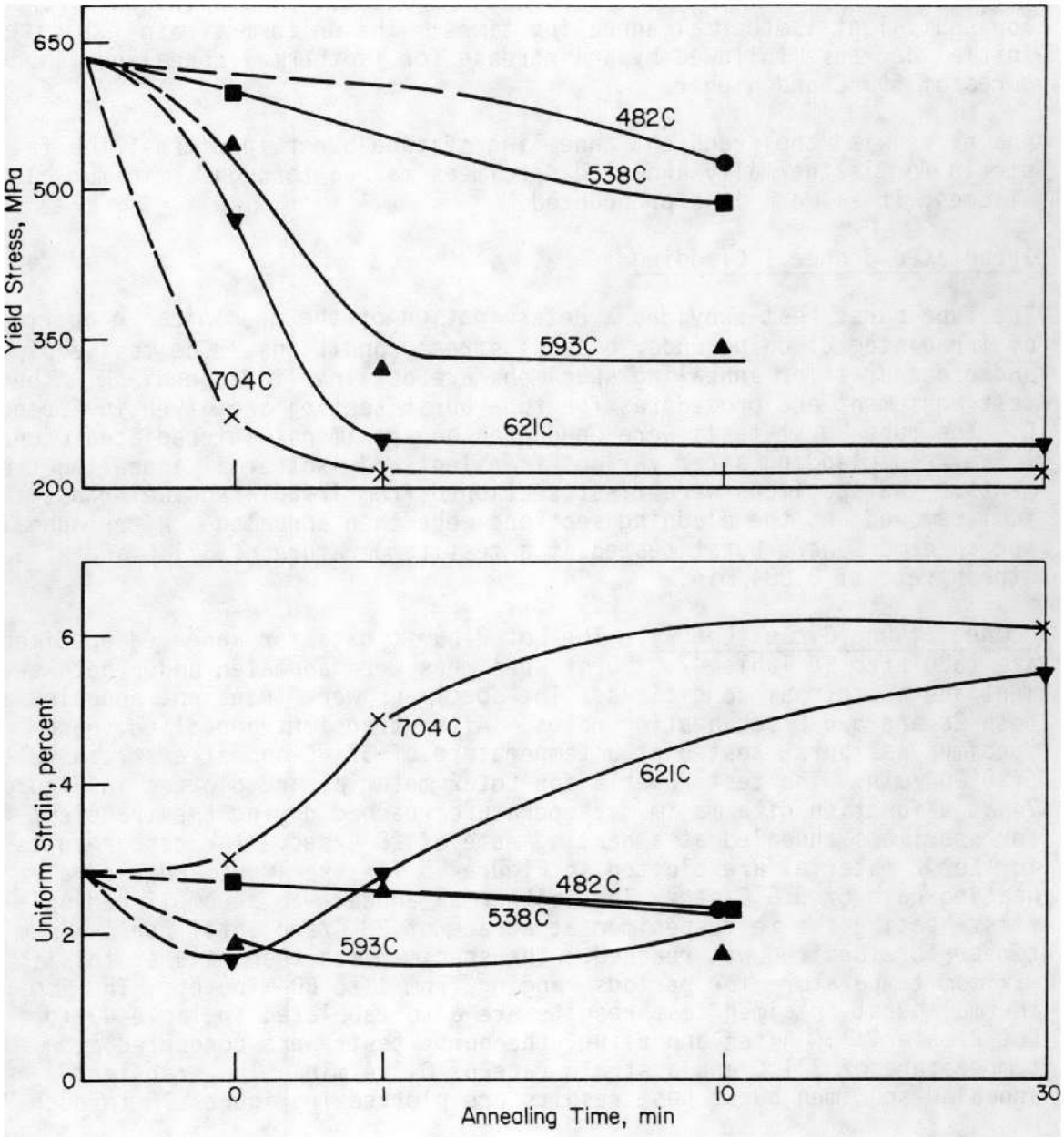

FIGURE 73. EFFECT OF ISOTHERMAL ANNEALING ON YIELD STRENGTH AND UNIFORM CIRCUMFERENTIAL STRAIN IN ISOTHERMAL TUBE-BURST TESTS OF H. B. ROBINSON SPENT-FUEL CLADDING

Test temperature 371 C.

temperature was increased, the extent of annealing of irradiation damage, as evidenced by the decrease in ultimate and yield stress values, increased for equivalent isothermal annealing times. The uniform strain exhibited an initial decrease followed by an increase for isothermal annealing temperatures of 593 C and higher.

Again, as with the transient annealing of tube-burst specimens, the failure strain for isothermally annealed specimens may go through a minimum but if it does, it is much less pronounced.

Irradiated Oconee I Cladding

The tube-burst test provided a determination of the mechanical properties of irradiated cladding under biaxial stress conditions. The test equipment and procedures for annealing specimens are outlined in Appendix B. The test equipment and procedures for tube-burst testing are given in Appendix C. The tube-burst tests were conducted on specimens of irradiated Oconee I fuel-rod cladding after various transient and isothermal annealing treatments. The specimens were first sectioned from irradiated fuel rods, the fuel removed and the cladding sections were then annealed. After annealing the specimens were burst tested at a test temperature of 371 C and at a strain rate of 0.004/min.

Oconee I, One Cycle (Lot 2). The Lot 2 burst data for annealed specimens are tabulated in Table 47. Burst specimens were annealed under both transient and isothermal conditions. The specimens were transient annealed at both 28 and 5.6 C/sec heating rates. After transient annealing, each specimen was burst tested at a temperature of 371 C and at a strain rate of 0.004/min. The test resutls for Lot 2 material are plotted in Figure 74 as a function of a maximum temperature reached during the transient for specimens annealed at a heating rate of 28 C/sec. The test results for Lot 2 material are plotted in Figure 75 for specimens annealed at a heating rate of 5.6 C/sec. The isothermal anneal was accomplished by first heating the test specimen at a rate of 28 C/sec until the maximum temperature desired was reached. The specimen was then held at this maximum temperature for periods ranging from 1 to 60 minutes. The isothermal burst specimen test results are also tabulated in Table 47 for Lot 2 material. After annealing, the burst tests were conducted at a temperature of 371 C and a strain rate of 0.004/min. The transient annealed specimen burst test results are plotted in Figures 76 through 79.

It was noted that if the ultimate stress for as-irradiated tests at 371 C were used (Tables 26, 27 and 28), peaking of the stress was apparent and similar to that observed in the H. B. Robinson cladding transient annealed at heating rates of 0.56 and 5.6 C/sec and subsequently burst tested at the same test conditions. However, the Lot 2 tube-burst results indicated no minimum in the strains which was previously noted in the uniform strains

TABLE 47. TUBE-BURST TEST RESULTS FOR IRRADIATED OCONEE I (ONE CYCLE) ANNEALED ZIRCALOY FUEL ROD CLADDING.

Test temperature 371 C; strain rate 0.004/min.

Specimen Number	Maximum Temperature C	Heating Rate C/sec	Holding Time Min	STRESS			STRAIN	
				Yield MPa	Ultimate MPa	Failure MPa	Uniform Percent	Total Percent
			Transient Anneals					
47118-7	482	28	0	561	640	640	2.7	2.7
47118-17	538	28	0	556	621	619	2.6	2.9
47118-20	593	28	0	559	622	622	2.7	3.6
47118-22	621	28	0	557	627	627	2.5	4.0
47103-23	704	28	0	255	377	377	6.5	8.8
47101-8	816	28	0	250	376	371	7.2	16.0
47101-17	538	5.6	0	586	609	609	1.6	3.6
47101-12	593	5.6	0	554	587	587	2.1	5.0
47101-13	621	5.6	0	515	530	530	1.9	5.9
47010-8	621	5.6	0	254	371	367	6.6	11.8
47010-11	704	5.6	0	272	338	338	2.6	14.8
			Isothermal Anneals					
47010-13	538	28	1	537	600	576	1.7	5.7
47015-12	593	28	1	327	376	361	4.6	21.7
47015-14	621	28	1	256	326	326	3.2	6.7
47015-17	704	28	1	239	338	315	9.4	22.8
47015-3	538	28	15	339	383	378	2.7	12.4
47015-13	593	28	15	220	326	318	6.3	10.8
47015-12	482	28	60	505	543	539	2.4	5.0

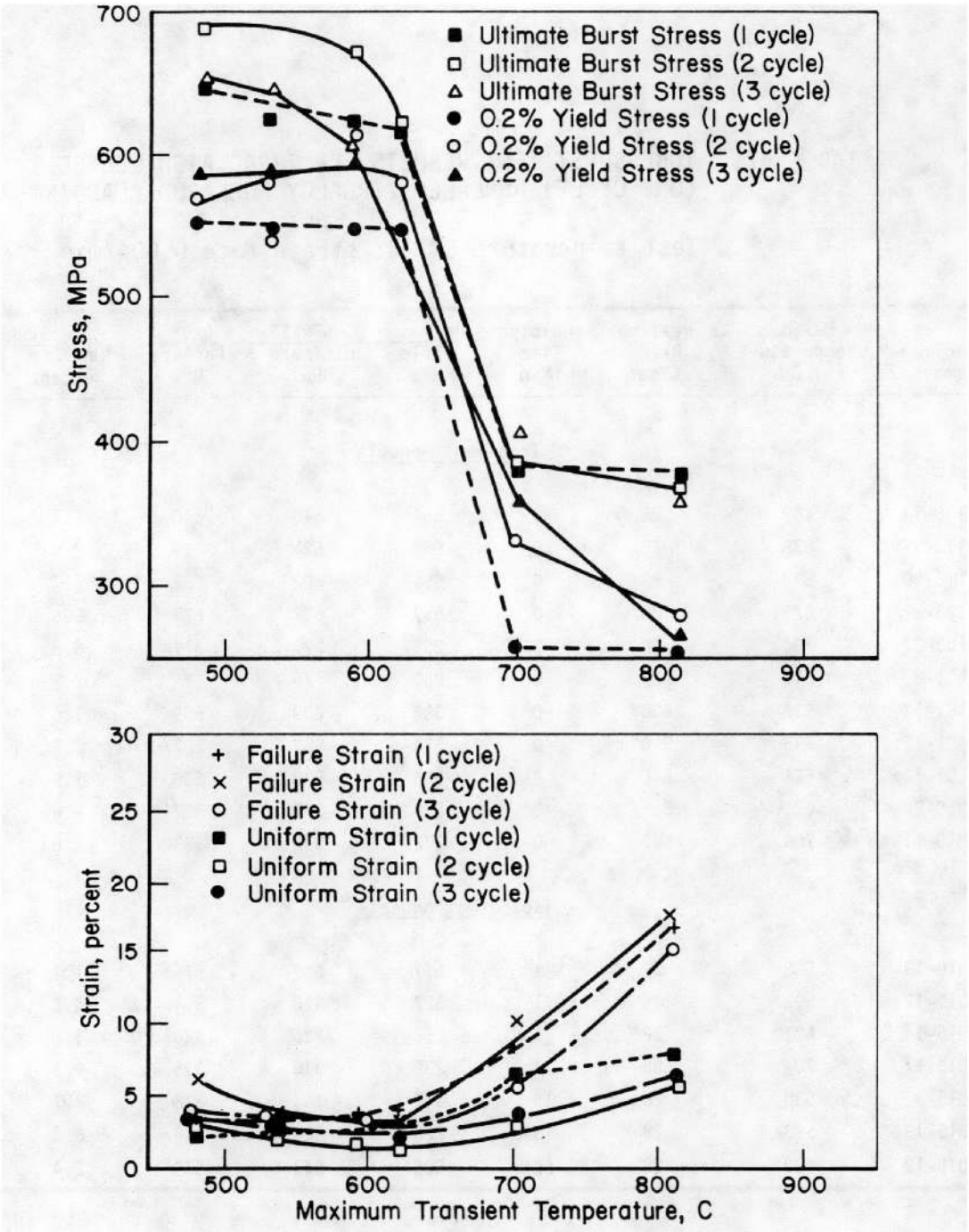

FIGURE 74. EFFECT OF MAXIMUM TEMPERATURE ACHIEVED IN TRANSIENT ON IRRADIATED OCONEE I (LOTS 2, 3, AND 4) FUEL ROD CLADDING STRESS AND STRAIN AT A HEATING RATE OF 28 C/SEC

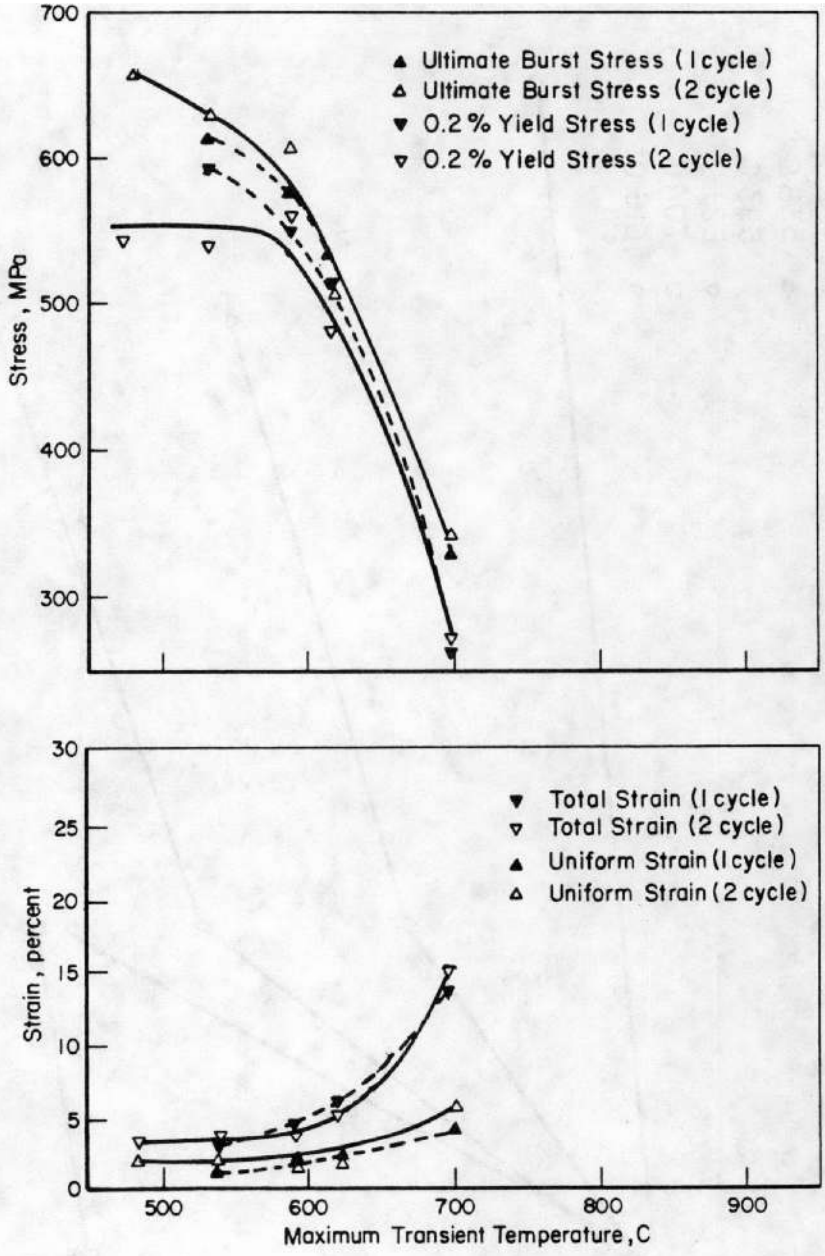

FIGURE 75. EFFECT OF MAXIMUM TEMPERATURE ACHIEVED IN TRANSIENT ON IRRADIATED OCONEE I (ONE AND TWO CYCLE) FUEL ROD CLADDING STRESS AND STRAIN AT A HEATING RATE OF 5.6C/SEC

Test temperature 371 C; strain rate 0.004/min.

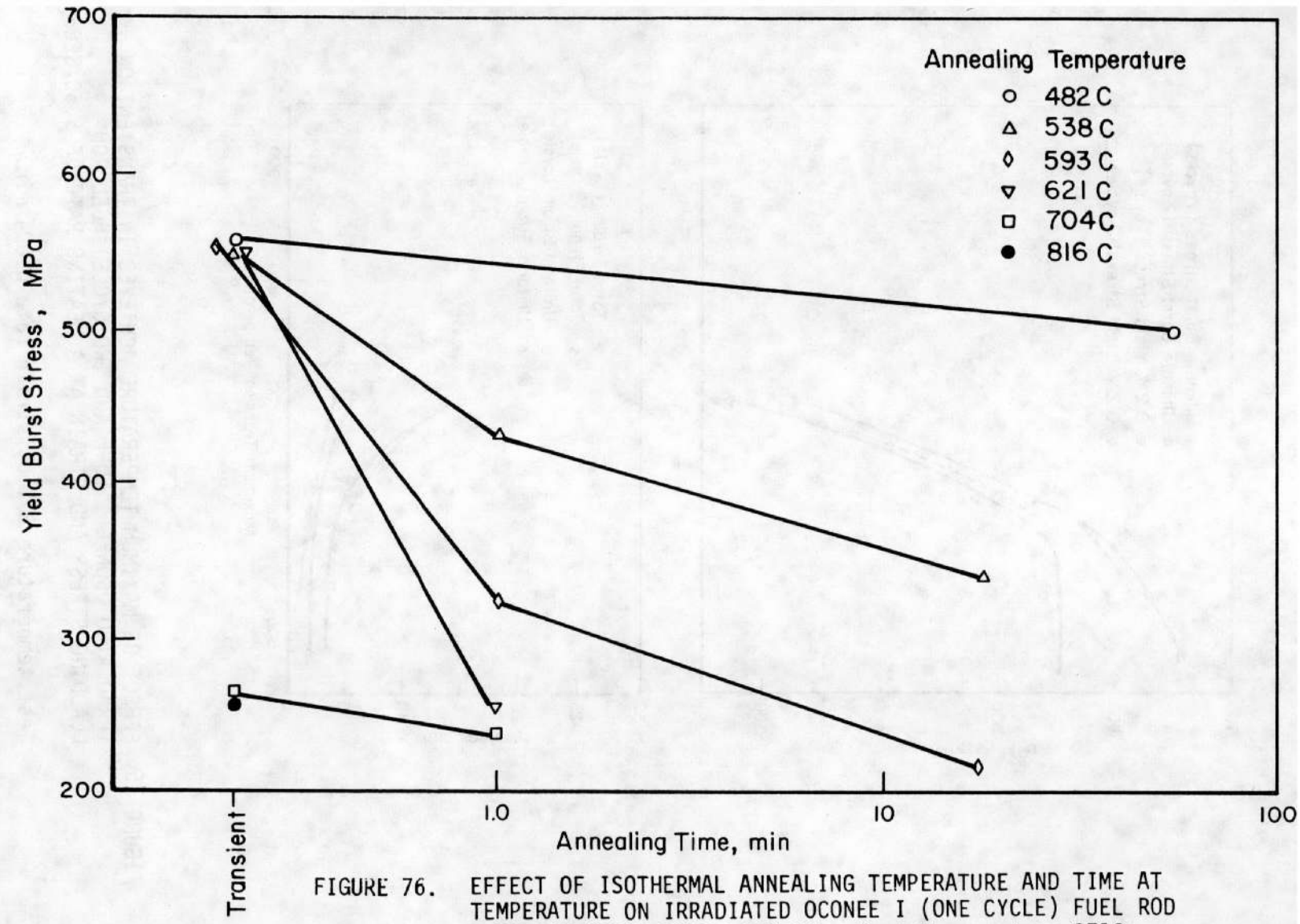

FIGURE 76. EFFECT OF ISOTHERMAL ANNEALING TEMPERATURE AND TIME AT TEMPERATURE ON IRRADIATED OCONEE I (ONE CYCLE) FUEL ROD CLADDING YIELD BURST STRESS Test Temperature 371C; Strain Rate, 0.004/min.

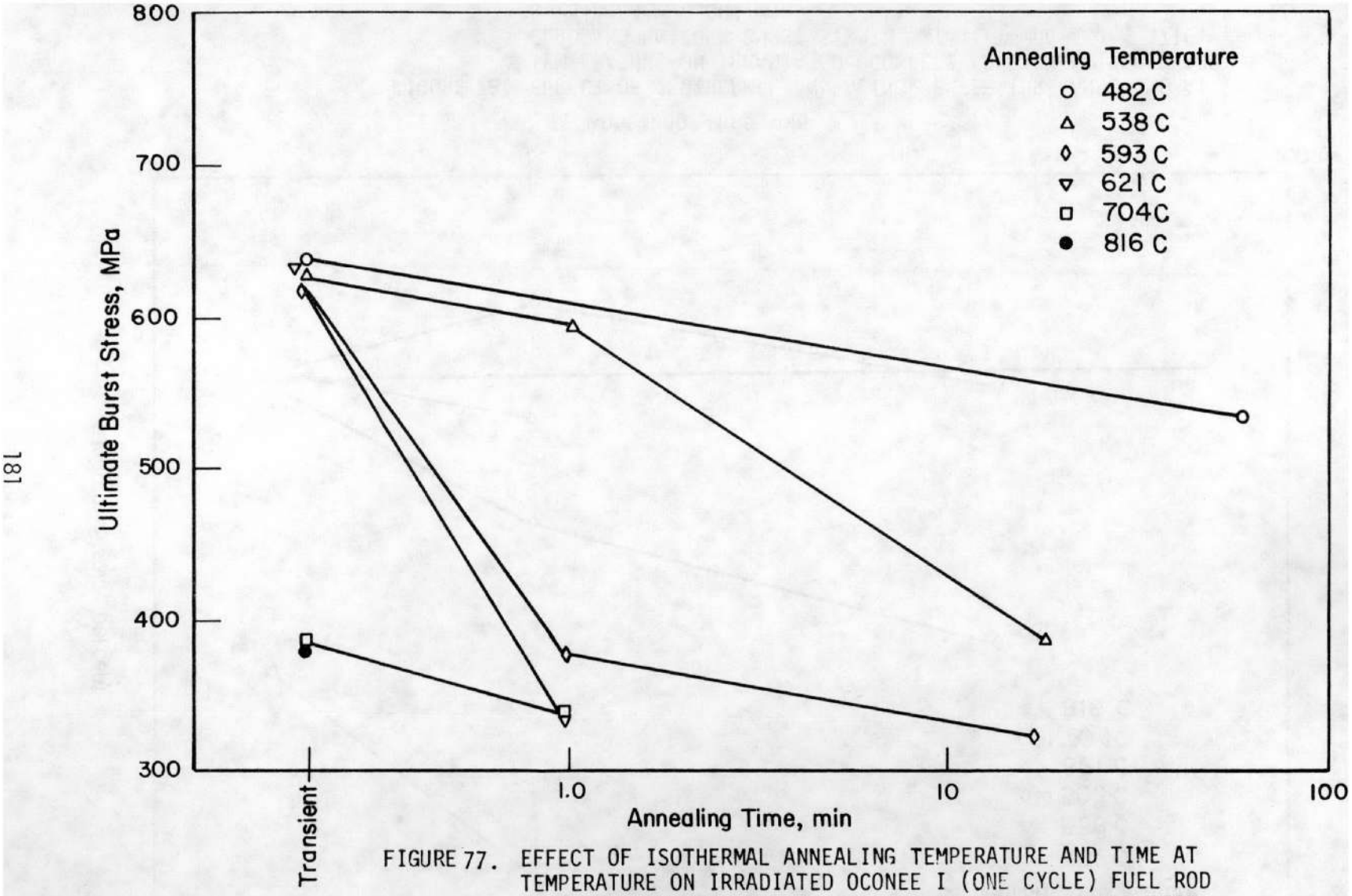

FIGURE 77. EFFECT OF ISOTHERMAL ANNEALING TEMPERATURE AND TIME AT TEMPERATURE ON IRRADIATED OCONEE I (ONE CYCLE) FUEL ROD CLADDING ULTIMATE BURST STRESS Test Temperature 371C; Strain Rate 0.004/min.

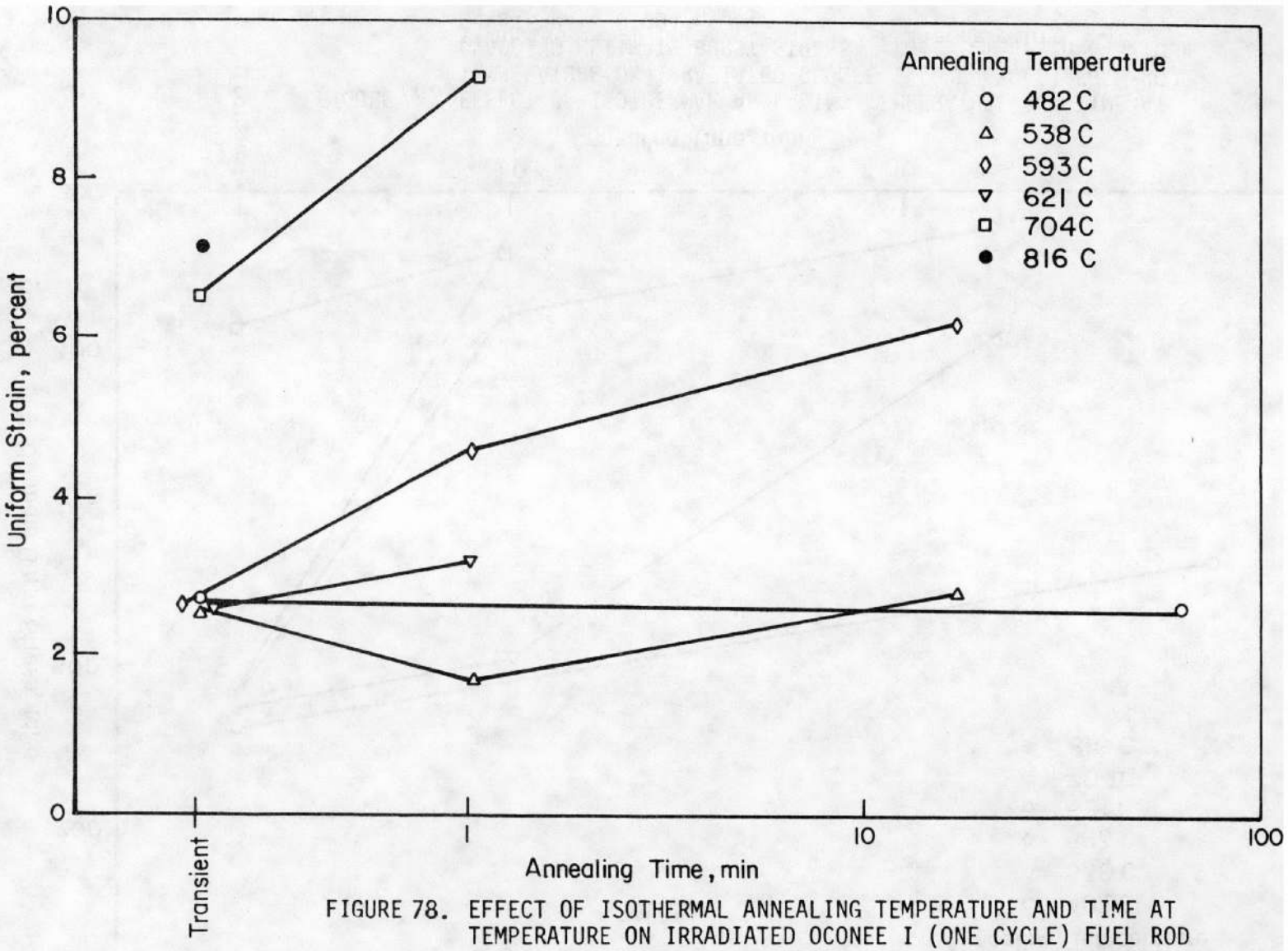

FIGURE 78. EFFECT OF ISOTHERMAL ANNEALING TEMPERATURE AND TIME AT TEMPERATURE ON IRRADIATED OCONEE I (ONE CYCLE) FUEL ROD CLADDING UNIFORM BURST STRAIN Test Temperature 371C; Strain Rate 0.004/min.

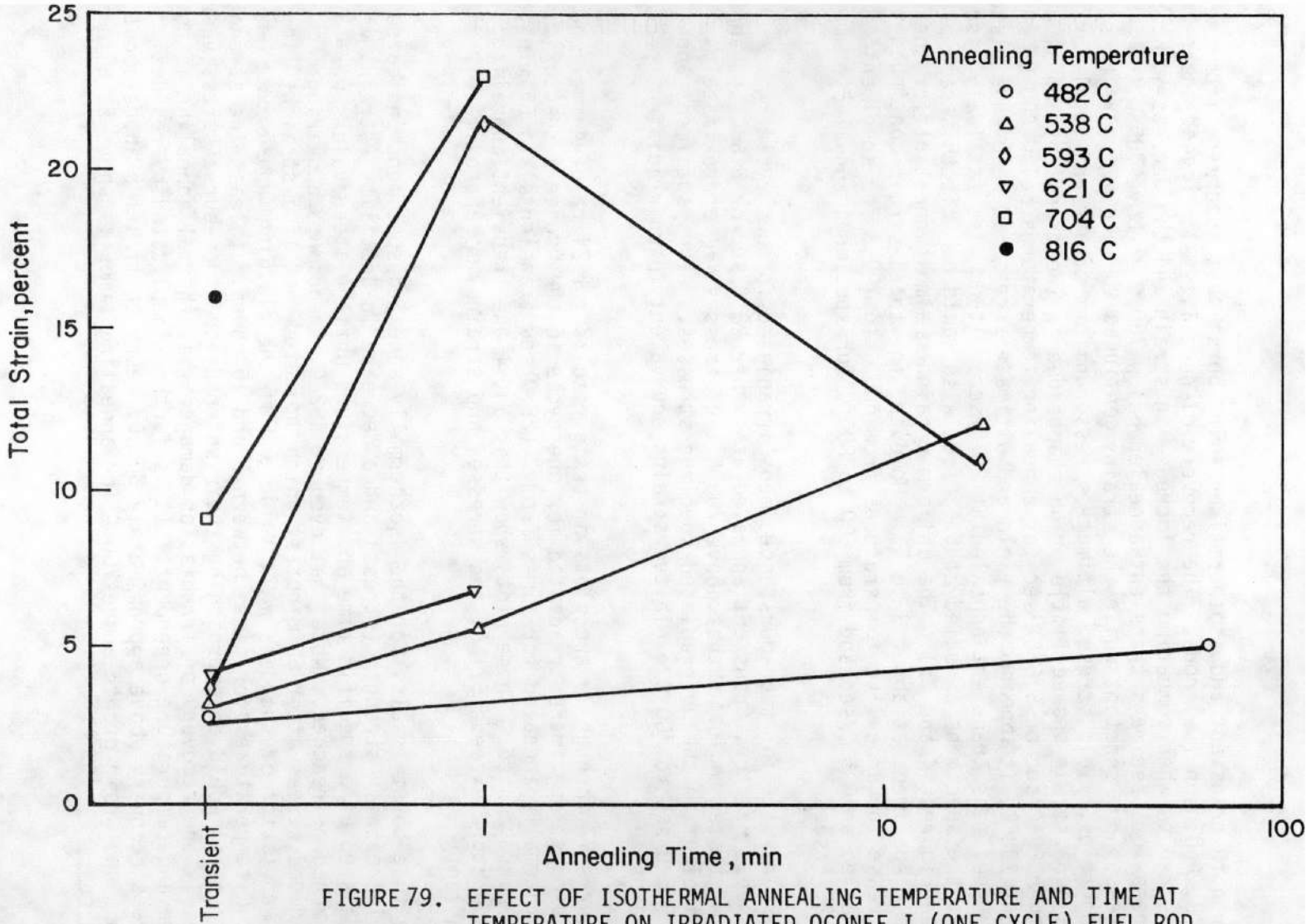

FIGURE 79. EFFECT OF ISOTHERMAL ANNEALING TEMPERATURE AND TIME AT TEMPERATURE ON IRRADIATED OCONEE I (ONE CYCLE) FUEL ROD CLADDING TOTAL BURST STRAIN Test Temperature 371C; Strain Rate 0.004/min.

for both transient and isothermal annealed burst test specimens from the H. B. Robinson fuel rods. The recovery of ductility also lagged the recovery of strength when comparing the increase in strain and the decrease in stress for specimens transient annealed below 700 C. Above 700 C the stresses were constant while the strains continued to increase. The burst properties, yield stress, ultimate stress, uniform strain and total (or failure) strain showed little or no change due to the transient anneal at either 28 C/sec or 5.6 C/ sec for annealing temperatures below 600 C. At about 700 C, it appeared the yield and ultimate stress had reached a plateau for specimens transient annealed at 28 C/sec. It was also tactfully assumed that the specimens annealed at 5.6 C/sec also would exhibit this same plateau (see Figures 74 and 75). The uniform strain was almost constant for the one cycle specimens at about 3 to 5%. However, the total strain continued to increase for annealing temperatures from 600 to 700 C for specimens annealed at 6.5 C/sec and from 600 to 800 C for specimens annealed at 28 C/sec.

These results for tube-burst specimens irradiated for one cycle in the Oconee I reactor, transient annealed at either 28 C/sec or 5.6 C/sec and burst tested indicated that above 700 C the stresses were approximately equivalent to the unirradiated specimen stresses. Also, specimens annealed at 5.6 C/sec to 700 C exhibited strains equivalent to unirradiated specimen strains.

Figures 77 through 79 are plots of tests results for Zircaloy-4 fuel-rod tube-burst specimens irradiated for one cycle in the Oconee I reactor, isothermally annealed for times from 0 (28 C/sec transients) to 60 minutes and burst tested. These plots show that until the transient annealing temperature exceeds 621 C, the stresses and strains were approximately constant.

The tube-burst results for the isothermally annealed specimens indicated an increase in strength (stress) and a decrease in ductility (strain) which persisted at a specific time and temperature until plateau values were approached or reached. Note that even at 482 C, trends were appearing (reduced stress after 60 minutes) which indicated that if a straight line extrapolation of the data were valid and if the cladding were exposed to 482 C temperatures for times between 5 and 10 hours, at least the strengths (stresses) would be approaching their unirradiated tube-burst stress values. Clearly the recovery of irradiation damage by isothermal annealing is both time and temperature dependent. It is further complicated by residual stress recovery above approximately 500 C, recrystallization above about 700 C and grain growth above 700 C for annealing times as short as a few minutes.

Oconee I, Two Cycle (Lot 3). The Lot 3 burst data for annealed specimens are tabulated in Table 48. Burst specimens were annealed under both transient and isothermal conditions. The specimens were transient annealed at both 28 and 5.6 C/sec heating rates. After transient annealing, the burst specimens were tested at a temperature of 371 C and a strain rate of 0.004/min. The test results for Lot 3 material are plotted in Figure 74 as a function of maximum temperature reached during the transient for specimens annealed at a heating rate of 28 C/sec. The test results for Lot 3 material are plotted in Figure 75 for specimens annealed at a heating rate of 5.6 C/sec. After annealing, the burst specimens were tested at a temperature of 371 C and at a strain rate of 0.004/min. The isothermal annealed specimen burst test results are also listed in Table 48 and are plotted in Figures 80 through 83.

The burst properties, yield stress, ultimate stress, uniform strain and total (or failure) strain showed little or no change due to the transient anneal at either 28 C/sec or 5.6 C/sec for annealing temperatures below 600 C. At about 700 C, it appeared the burst yield and ultimate stresses had reached a plateau for specimens transient annealed at 28 C/sec. The uniform strains were almost constant for the two cycle specimens at about 3 to 5%. However, the total strain continued to increase for annealing temperatures from 600 to 700 C for specimens annealed at 6.5 C/sec and from about 600 to 800 C for specimens annealed at 28 C/sec.

These results for tube-burst specimens irradiated for two cycles in the Oconee I reactor, transient annealed at either 28 C/sec or 5.6 C/sec and burst tested indicated that above 700 C the stresses were approximately equivalent to unirradiated specimen stresses. Also, tube-burst specimens annealed at 5.6 C/sec to 700 C exhibited strains equivalent to unirradiated specimen strains.

Figures 80 through 83 are plots of tests results for Zircaloy-4 fuel rod tube-burst specimens irradiated for two cycle in the Oconee I reactor, isothermally annealed for times from 28 C/sec transients to 60 minutes and burst tested. The tube-burst tests were conducted at a test temperature of 371 C and a strain rate of 0.004/min. These plots showed that after the transient annealing temperature exceeded 621 C, the stresses (both yield and ultimate) decreased rapidly and the strains (both uniform and total) increased rapidly. Above 704 C, the stresses and strains were again approximately constant.

The results of the isothermmaly annealed specimens indicated an increase in strength (stress) and a decrease in ductility (strain) which persisted at a specific time and temperature until plateau values was approached or reached. Note that again at 482 C, trends were appearing (reduced stress after 60 minutes) which indicated that if a straight line extrapolation of

TABLE 48. TUBE-BURST TEST RESULTS FOR IRRADIATED OCONEE I (TWO CYCLE) ANNEALED ZIRCALOY FUEL ROD CLADDING. Test Temperature 371C; Strain Rate 0.004/min.

Specimen Number	Maximum Temperature C	Heating Rate C/sec	Holding Time Min	STRESS			STRAIN	
				Yield MPa	Ultimate MPa	Failure MPa	Uniform Percent	Total Percent
			Transient Anneals					
31778A-2	482	28	0	570	690	690	2.7	6.3
31778A-4	538	28	0	540	579	579	2.1	3.5
31778-10	593	28	0	617	671	671	1.9	3.0
31778-14	621	28	0	582	625	625	1.3	3.1
31778-15	704	28	0	330	385	348	2.8	10.0
31778-18	816	28	0	279	367	348	5.5	16.1
32062A-18	482	5.6	0	545	660	660	1.3	3.3
32062A-19	538	5.6	0	540	630	630	1.9	4.1
32062A-20	593	5.6	0	561	608	608	1.4	3.2
32211A-18	621	5.6	0	482	505	505	1.6	4.8
32013A-4	704	5.6	0	274	342	340	5.5	25.4
			Isothermal Anneals					
32013A-10	538	28	1	585	620	620	1.4	3.3
32211A-14	593	28	1	463	484	481	1.8	7.7
32013A-22	621	28	1	339	378	358	2.0	14.4
32013A-25	704	28	1	236	331	330	6.3	12.9
32013A-11	538	28	10	505	562	554	1.5	6.3
32013A-21	593	28	10	268	331	331	3.8	17.9
32013A-9	482	28	60	540	579	579	1.8	4.8

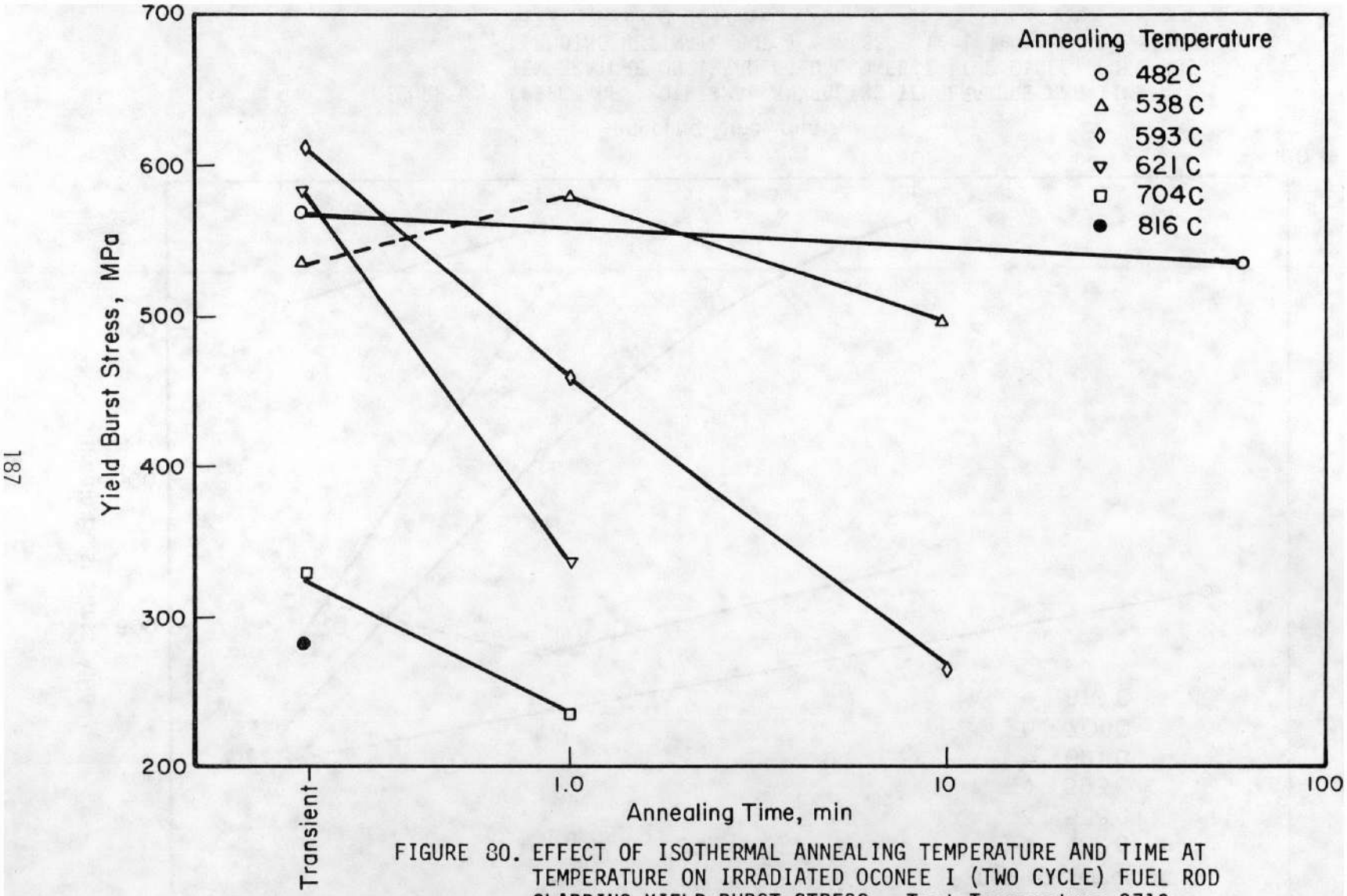

FIGURE 80. EFFECT OF ISOTHERMAL ANNEALING TEMPERATURE AND TIME AT TEMPERATURE ON IRRADIATED OCONEE I (TWO CYCLE) FUEL ROD CLADDING YIELD BURST STRESS Test Temperature 371C; Strain Rate 0.004/min.

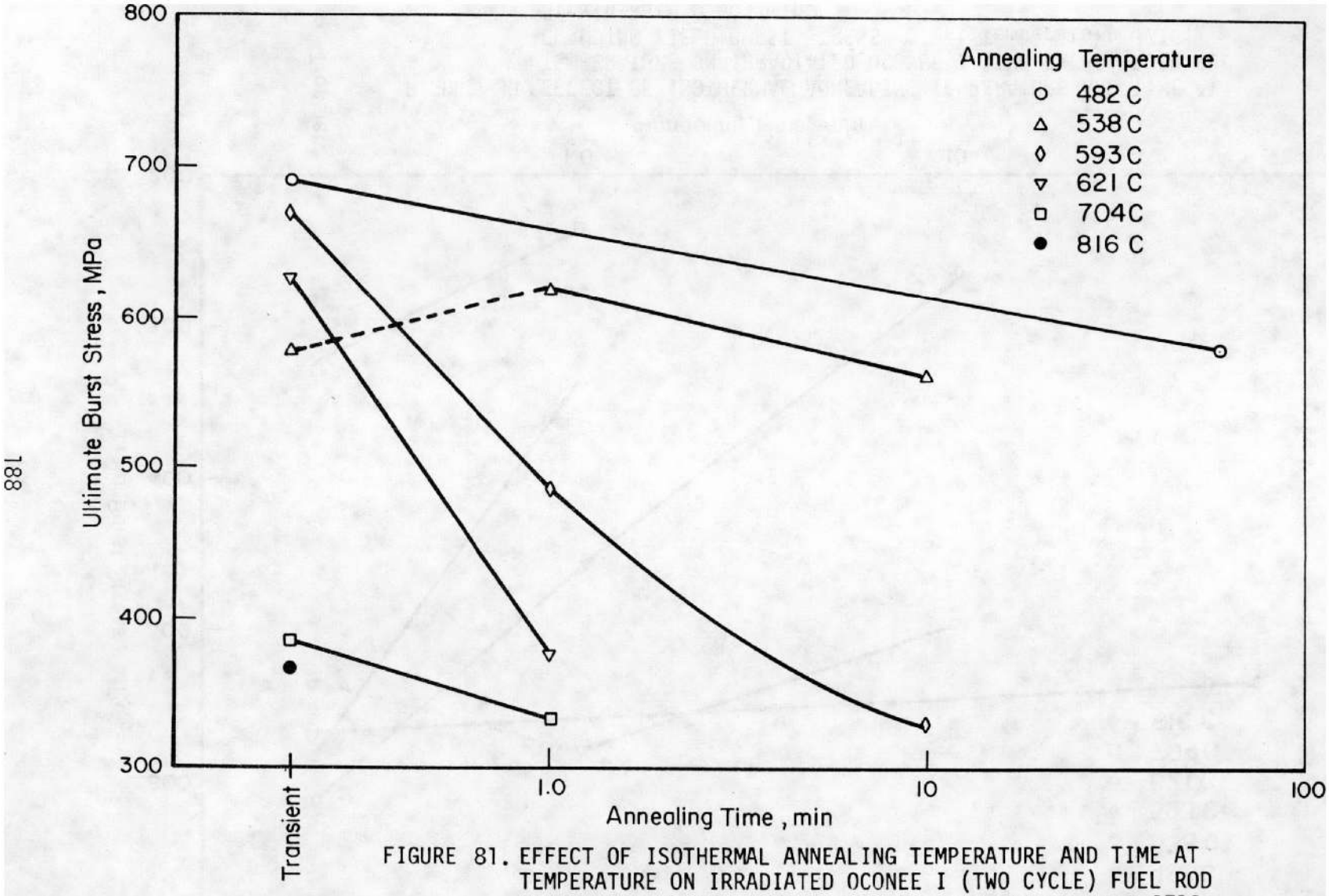

FIGURE 81. EFFECT OF ISOTHERMAL ANNEALING TEMPERATURE AND TIME AT TEMPERATURE ON IRRADIATED OCONEE I (TWO CYCLE) FUEL ROD CLADDING ULTIMATE BURST STRESS Test Temperature 371C; Strain Rate 0.004/min.

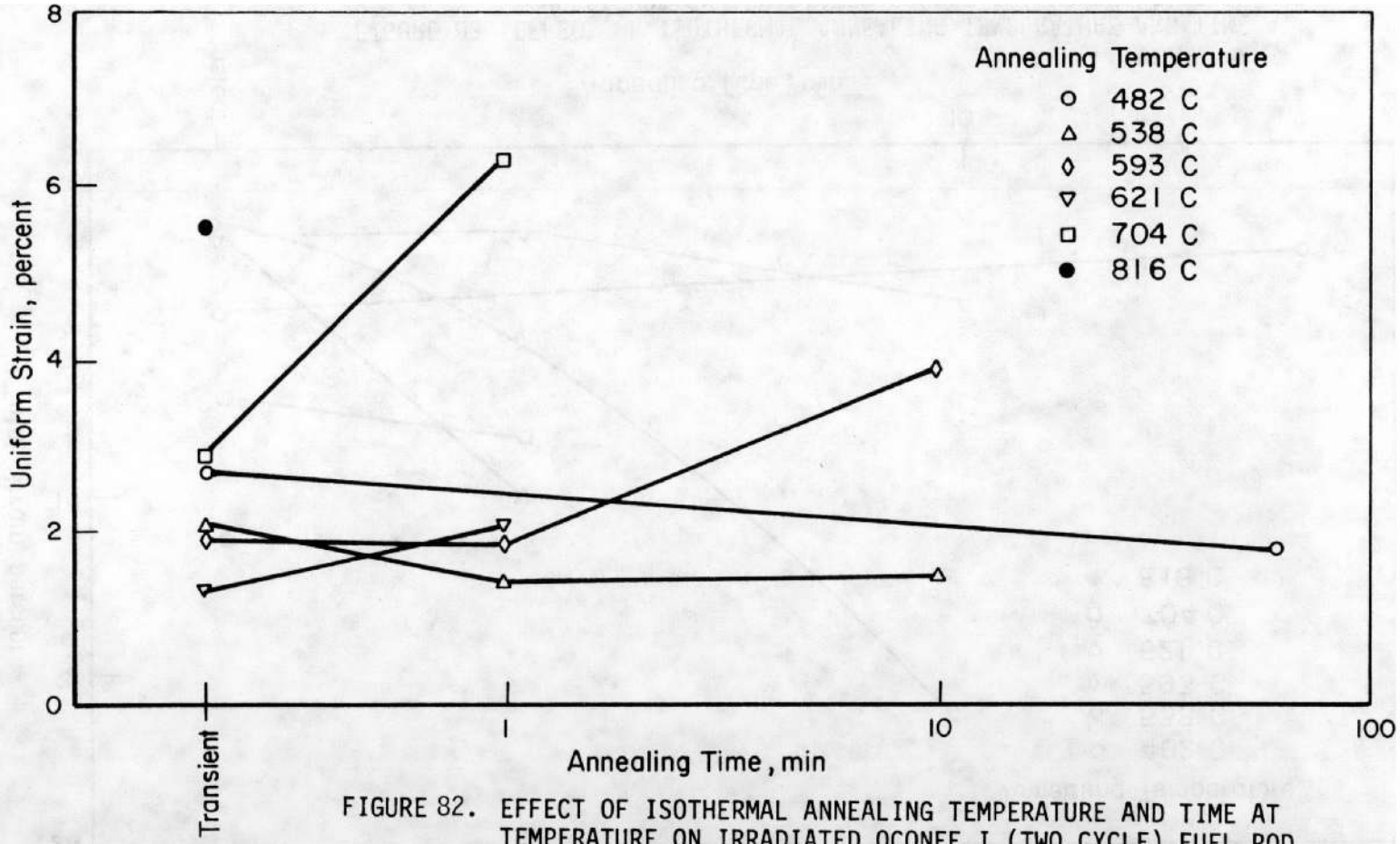

FIGURE 82. EFFECT OF ISOTHERMAL ANNEALING TEMPERATURE AND TIME AT TEMPERATURE ON IRRADIATED OCONEE I (TWO CYCLE) FUEL ROD CLADDING UNIFORM BURST STRAIN Test Temperature 371C; Strain Rate 0.004/min.

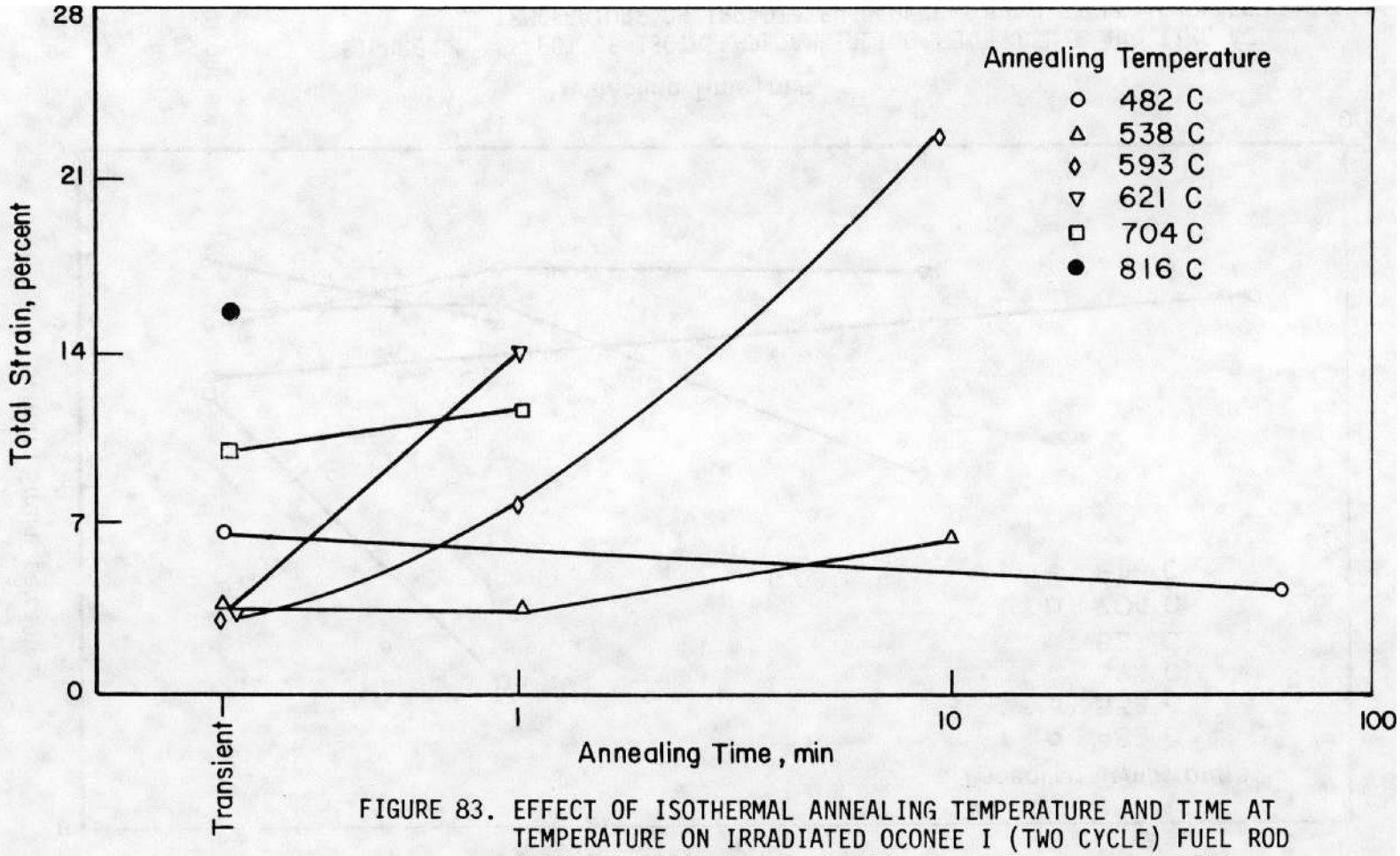

FIGURE 83. EFFECT OF ISOTHERMAL ANNEALING TEMPERATURE AND TIME AT TEMPERATURE ON IRRADIATED OCONEE I (TWO CYCLE) FUEL ROD CLADDING TOTAL BURST STRAIN Test Temperature 371C; Strain Rate 0.004/min.

the data were valid and if the cladding were exposed to 482 C temperatures for times between 5 and 10 hours, the strengths (stresses) would be approaching their unirradiated tube-burst stress values. Clearly the recovery of irradiation damage by isothermal annealing is both time and temperature dependent. It is further complicated by residual stress recovery above approximately 500 C, recrystallization above 600 C and grain growth above 700 C for annealing times as short as a few minutes.

Oconee I, Three Cycle (Lot 4). The Lot 4 burst test data for annealed specimens are tabulated in Table 49. Burst specimens were annealed under both transient and isothermal conditions. The specimens were transient annealed at a heating rate of 28 C/sec. After transient annealing, each specimen was burst tested at a temperature of 371 C and a strain rate of 0.004/min. The test results for Lot 4 material are plotted in Figure 74 as a function of maximum temperature reached during the transient for specimens annealed at a heating rate of 28 C/sec. The isothermal anneal was accomplished by first heating the test specimen at a rate of 28 C/sec until the maximum temperature desired was reached. The specimen was then held at this maximum temperature for periods ranging from 0.1 to 30 minutes. After annealing, the burst tests were conducted at a temperature of 371 C and a strain rate of 0.004/min. The isothermal burst specimen test results are also tabulated in Table 49 for the Lot 4 material. The isothermally annealed specimen tube-burst test results are plotted in Figures 84 through 87.

The burst properties, yield stress, ultimate stress, uniform strain and total (or failure) strain showed little or no change due to the transient anneal at 28 C/sec for annealing temperatures below 600 C. At about 700 C, it appeared the burst yield and ultimate stresses had reached a plateau. The uniform strains werealmost constant for both one, two and three cycle specimens at about 3 to 5%. However, the total strain continued to increase for annealing temperatures from 600 to 800 C for specimens annealed at 28 C/sec.

Figures 84 through 87 are plots of test results for Zircaloy-4 fuel rod tube-burst specimens irradiated for three cycle in the Oconee I reactor, isothermally annealed four times from 0 (28 C/sec transients) to 60 minutes and burst tested. The tube-burst tests were conducted at a test temperature of 371 C and a strain rate of 0.004/min. These plots showed that until the transient annealing temperature exceeded 593 C, the stresses were approximately constant. Between 593 and 704 C, the stresses continued to decrease but at a reduced rate. The strains, however, for Lot 4 material remained quite low and exhibited a large increase only at a transient temperature of 816 C. The results of the isothermally annealed Lot 4 tube-burst specimens indicated a reduced strength (yield and ultimate stress) for all the annealing temperatures. Note that at 538 C, the stresses were decreasing

TABLE 49. TUBE-BURST TEST RESULTS FOR IRRADIATED OCONEE I (THREE-CYCLE) ANNEALED ZIRCALOY FUEL ROD CLADDING

Test temperature 371 C; strain rate 0.004/min.

Specimen Number	Maximum Temperature C	Heating Rate C/sec	Holding Time Min	STRESS			STRAIN	
				Yield MPa	Ultimate MPa	Failure MPa	Uniform Percent	Total Percent
			Transient Anneals					
47079-18	482	28	0	580	652	652	2.2	2.2
47079-19	538	28	0	569	647	647	1.7	1.7
47079-21	593	28	0	574	609	608	1.9	2.8
47079-24	704	28	0	382	410	410	2.0	4.6
47079-9	816	28	0	265	374	365	5.9	15.5
			Isothermal Anneals					
47079-10	593	28	0.1	550	591	591	2.1	3.2
47079-2	538	28	1	586	607	603	2.0	5.4
4079-12	593	28	1	341	403	385	3.3	15.1
4079-16	704	28	1	358	358	358	1.8	15.0
4079-3	538	28	10	525	585	585	2.0	3.9
4079-13	593	28	10	293	353	343	2.2	16.5
4079-9	538	28	30	472	527	524	1.8	4.7

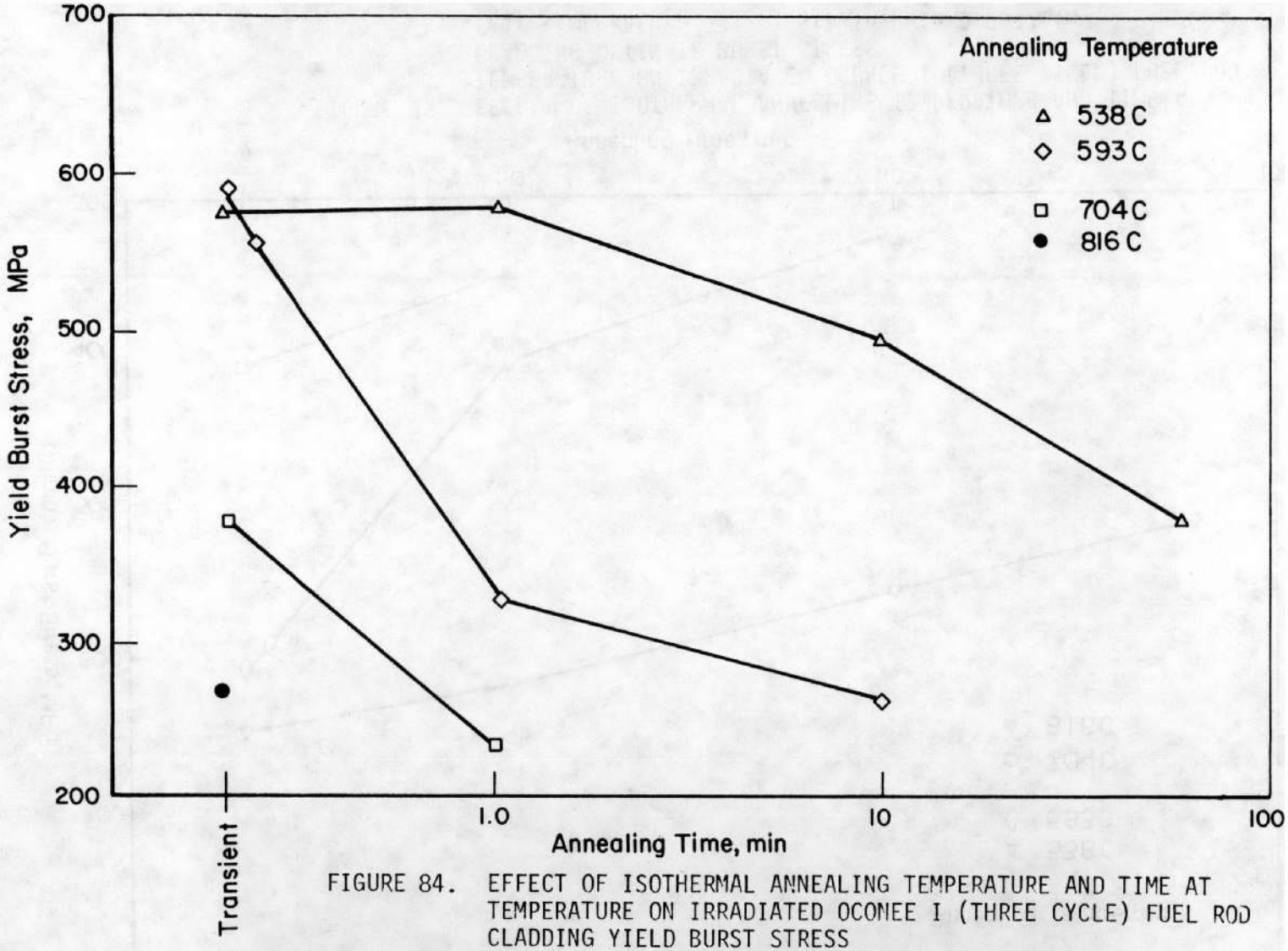

FIGURE 84. EFFECT OF ISOTHERMAL ANNEALING TEMPERATURE AND TIME AT TEMPERATURE ON IRRADIATED OCONEE I (THREE CYCLE) FUEL ROD CLADDING YIELD BURST STRESS
Test temperature 371 C; Strain Rate 0.004/min

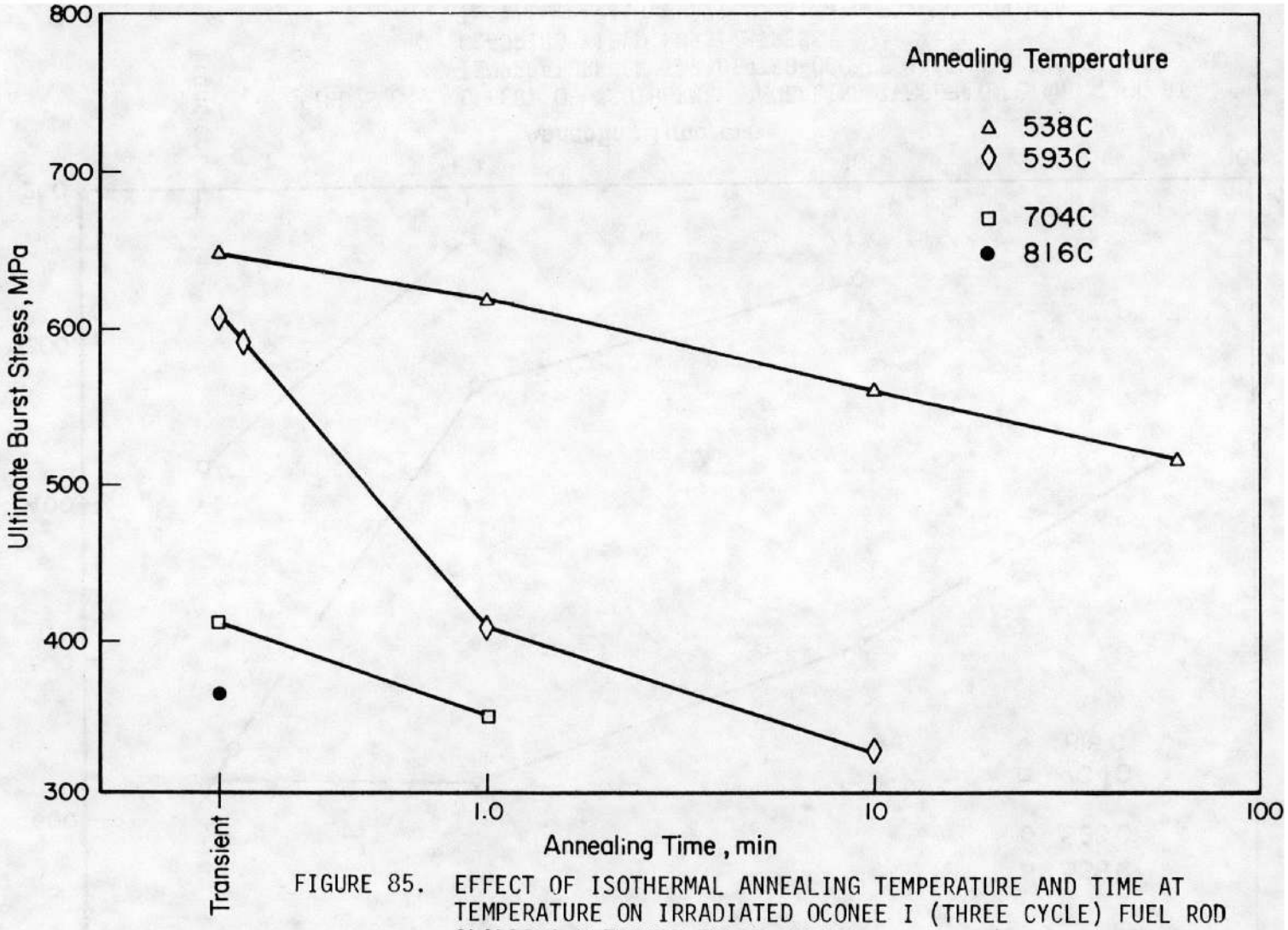

FIGURE 85. EFFECT OF ISOTHERMAL ANNEALING TEMPERATURE AND TIME AT TEMPERATURE ON IRRADIATED OCONEE I (THREE CYCLE) FUEL ROD CLADDING ULTIMATE BURST STRESS
Test temperature 371 C; Strain Rate 0.004/min

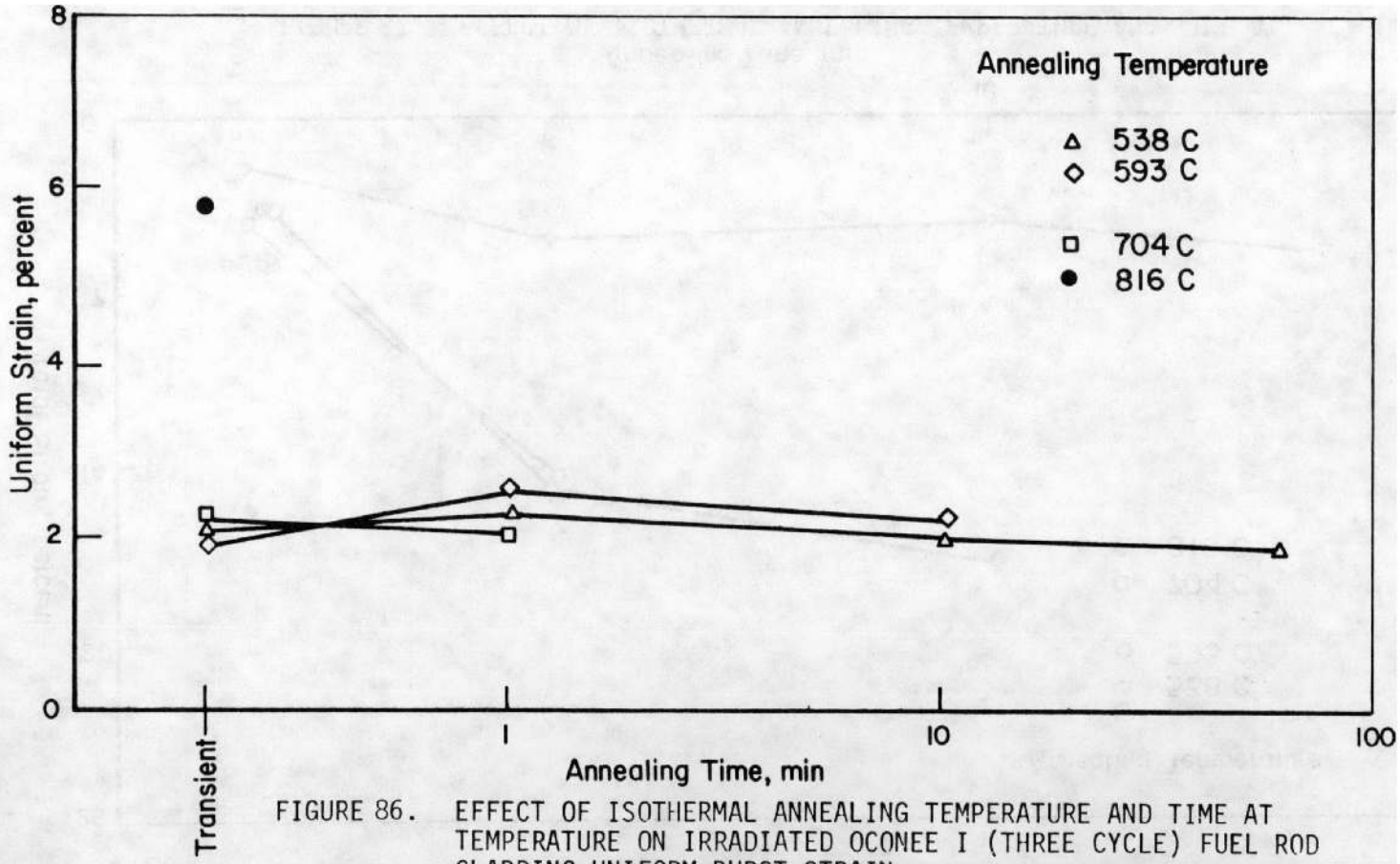

FIGURE 86. EFFECT OF ISOTHERMAL ANNEALING TEMPERATURE AND TIME AT TEMPERATURE ON IRRADIATED OCONEE I (THREE CYCLE) FUEL ROD CLADDING UNIFORM BURST STRAIN
Test Temperature 371 C; Strain Rate 0.004/min

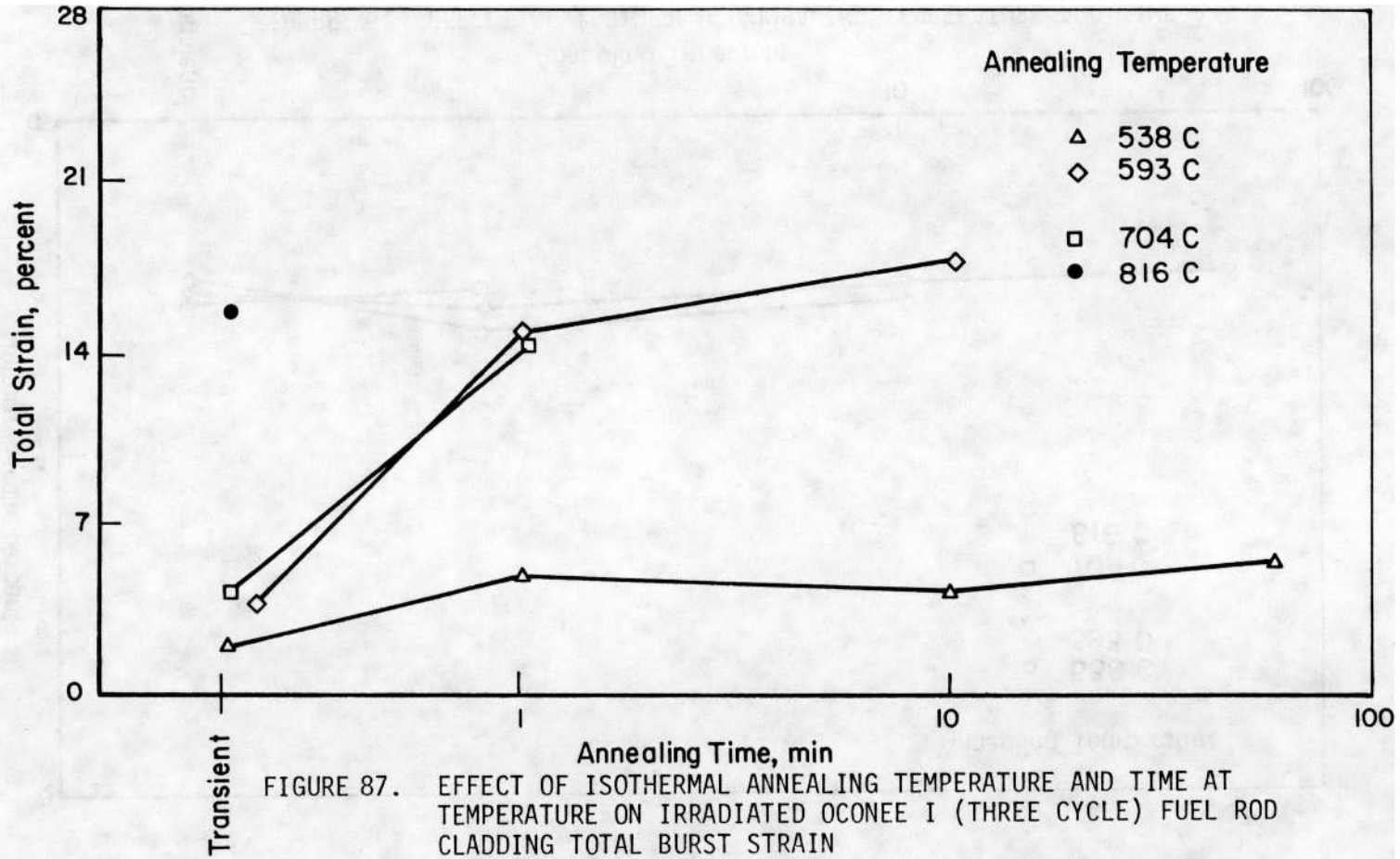

FIGURE 87. EFFECT OF ISOTHERMAL ANNEALING TEMPERATURE AND TIME AT TEMPERATURE ON IRRADIATED OCONEE I (THREE CYCLE) FUEL ROD CLADDING TOTAL BURST STRAIN
Test Temperature 371 C; Strain Rate 0.004/min

with increased annealing time and would probably reach the unirradiated value in a few hours at 538 C. The uniform strain showed essentially no change with annealing for any of the annealing times and temperatures. The total strain also showed no change at an annealing temperature of 538 C and annealing times to 60 minutes. The total strainwas, however, appreciably increased for isothermal annealing temperatures above 538 C for annealing times of 1 and 10 minutes.

Comparison of Tube-Burst (Annealed) Data

A comparison of the H. B. Robinson burst test data for specimens annealed under both transient and isothermal annealing conditions and the Oconee I burst test data for specimens similarly annealed and tested was made (see Tables 45, 46 and 49). It was first noted that only Oconee I three cycle (Lot 4) fuel rod material test results and the H. B. Robinson (Lot 1) results would provide a good comparison because these specimens were irradiated to approximately the same burnup levels (∿30,000 MWD/MTU).

The results of the burst tests, yield stress, ultimate stress, uniform strain and total or failure strain for the H. B. Robinson cladding were taken from Table 45 and 49 for the Oconee I, three cycle cladding. These test results were for specimens annealed at a transient annealing rate of 28 C/sec and are plotted in Figures 88 and 89. These plots showed that for both Lot 1 and Lot 4 material, the general trends and the transient temperature at which the changes occurred are very similar with the ultimate stresses almost equal at the annealing temperature of 538 C. The ultimate stress was beginning to decrease at almost 550 C for both the Oconee I and H. B. Robinson material. Both material ultimate stresses decreased between 600 and 700 C with the H. B. Robinson ultimate stress attaining a constant value at 700 C and the Oconee I ultimate stress reaching about the same value at 816 C. The yield stresses followed the same pattern. The uniform and total strains for the Lot 1 and Lot 4 material were almost identical with the uniform strains showing a slight decrease between 500 and 600 C before beginning a slow, gradual increase above 600 C. Again it was noticed that the ductility increases appeared to lag the strength decreases with the stresses at almost their minimum values before the strains increased appreciably.

The tube-burst data, yield stress, ultimate stress, uniform strain and total or failure strain for the H. B. Robinson cladding was taken from Table 46 and Table 49 for the Oconee I, three cycle cladding. These test results were for specimens isothermally annealed at 538 C, 593 and 704 C and are plotted in Figures 90, 91, 92 and 93. These plots showed some similarities and some dissimilarities. The ultimate and yield burst stresses for the Oconee I material were approximately equal to the H. B.

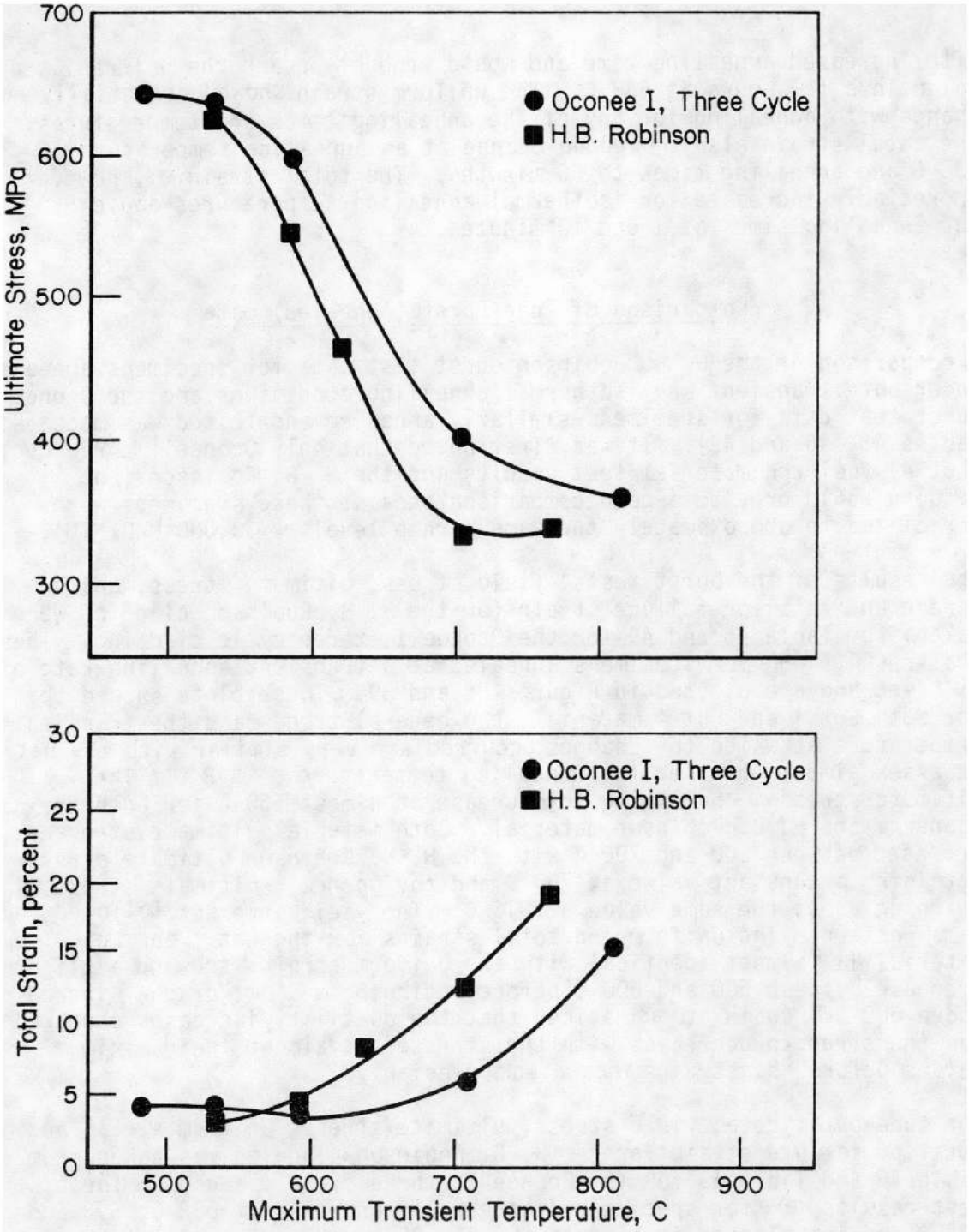

FIGURE 88. EFFECT OF MAXIMUM TEMPERATURE ACHIEVED IN TRANSIENT ON IRRADIATED LOT 1 AND LOT 4 ULTIMATE STRESS AND TOTAL STRAIN AT A HEATING RATE OF 28 C/SEC

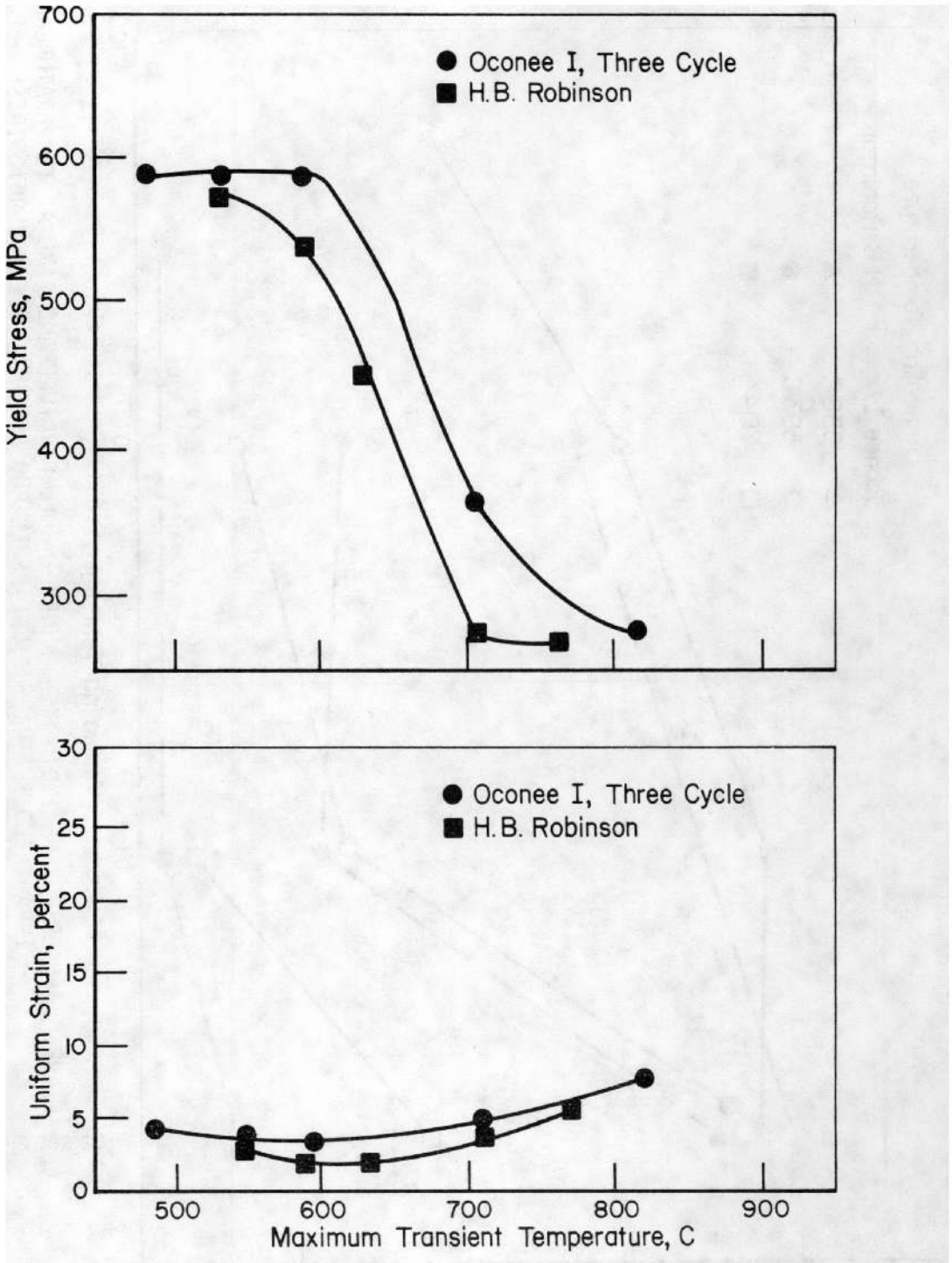

FIGURE 89. EFFECT OF MAXIMUM TEMPERATURE ACHIEVED IN TRANSIENT ON IRRADIATED LOT 1 AND LOT 4 YIELD STRESS AND UNIFORM STRAIN AT A HEATING RATE OF 28 C/SEC

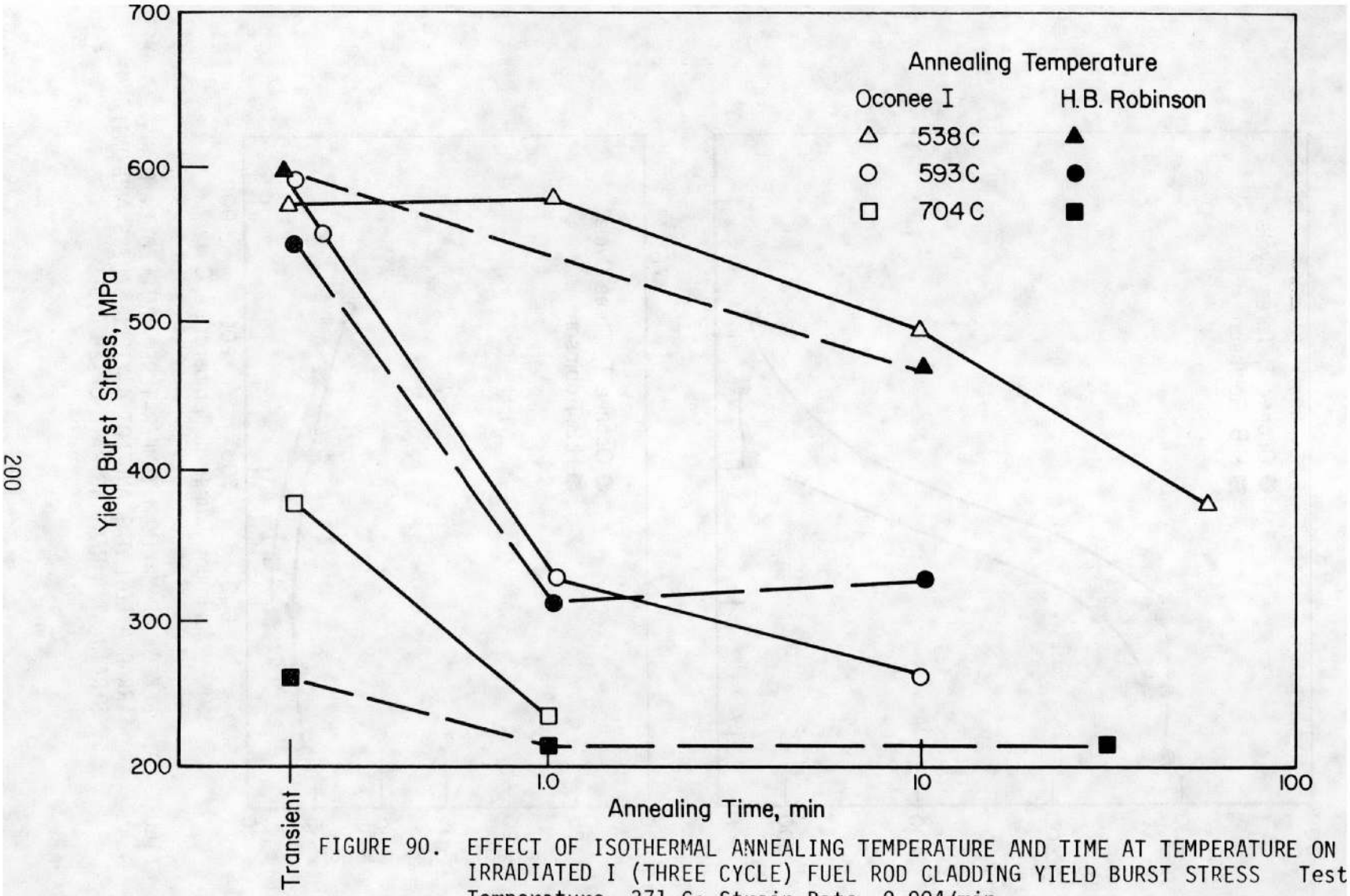

FIGURE 90. EFFECT OF ISOTHERMAL ANNEALING TEMPERATURE AND TIME AT TEMPERATURE ON IRRADIATED I (THREE CYCLE) FUEL ROD CLADDING YIELD BURST STRESS Test Temperature, 371 C; Strain Rate, 0.004/min.

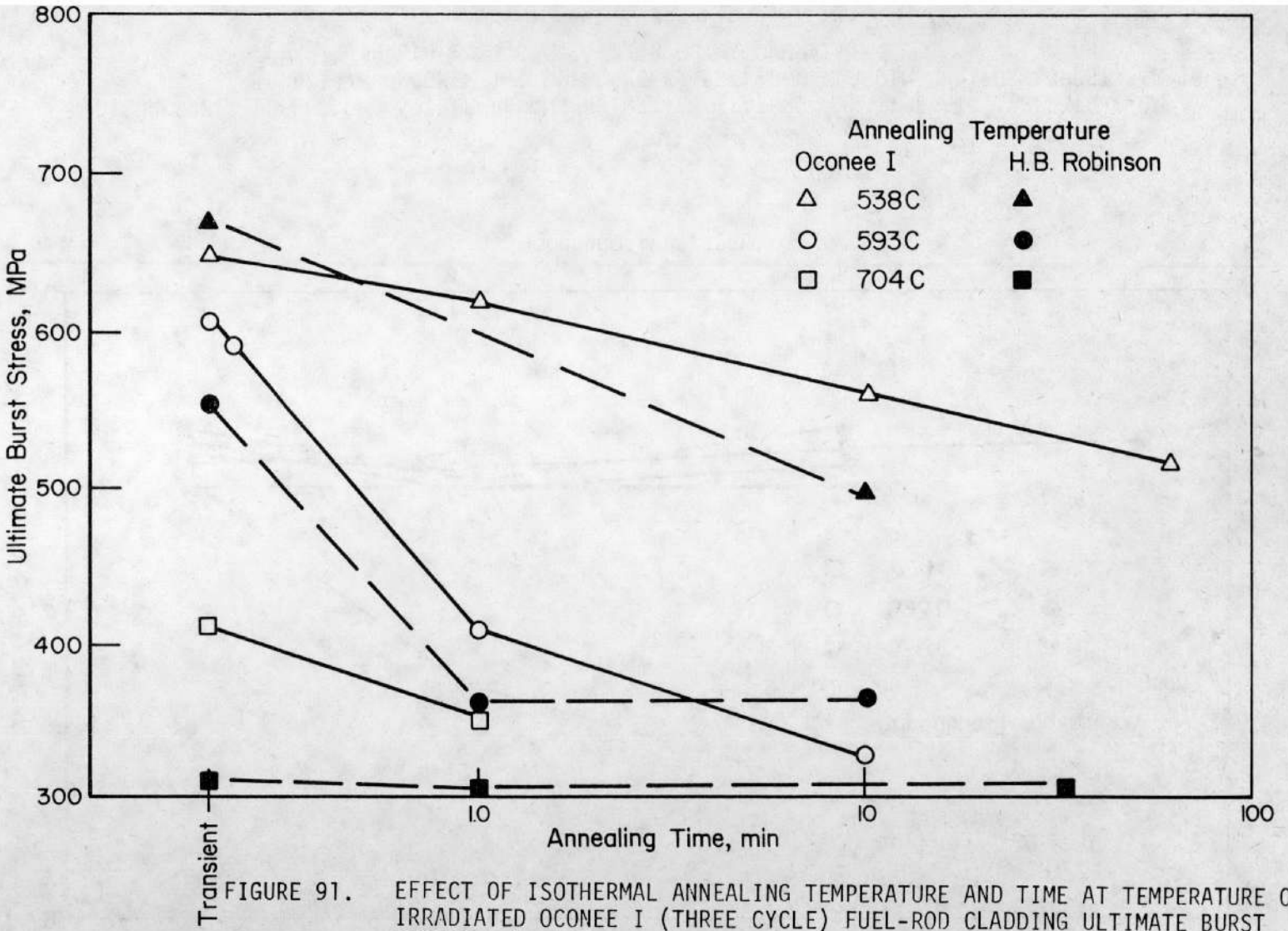

FIGURE 91. EFFECT OF ISOTHERMAL ANNEALING TEMPERATURE AND TIME AT TEMPERATURE ON IRRADIATED OCONEE I (THREE CYCLE) FUEL-ROD CLADDING ULTIMATE BURST STRESS Test Temperature, 371 C; Strain Rate, 0.004/min.

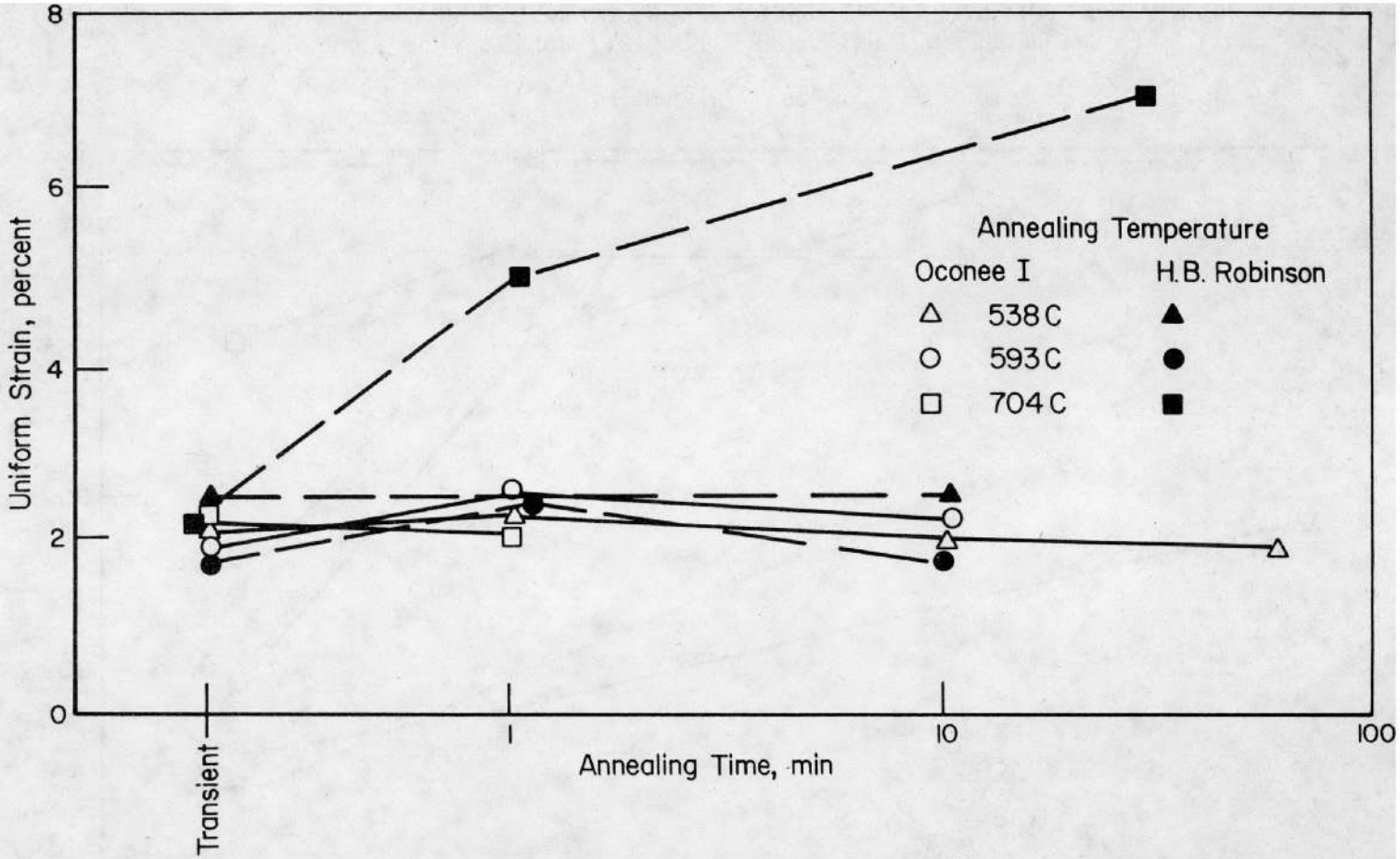

FIGURE 92. EFFECT OF ISOTHERMAL ANNEALING TEMPERATURE AND TIME AT TEMPERATURE ON IRRADIATED OCONEE I (THREE CYCLE) FUEL-ROD CLADDING UNIFORM BURST STRAIN
Test Temperature, 371 C; Strain Rate, 0.004/min.

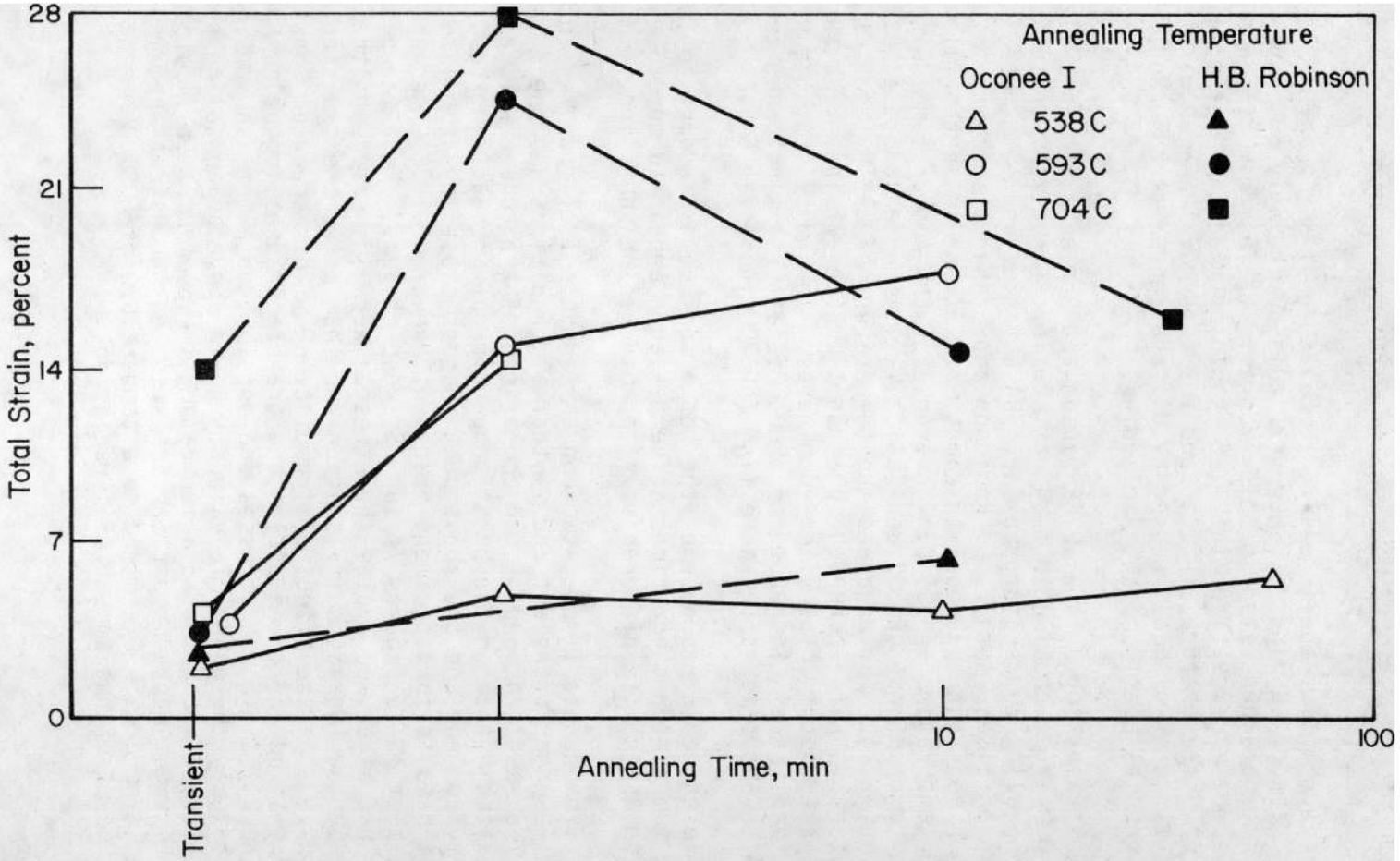

FIGURE 93. EFFECT OF ISOTHERMAL ANNEALING TEMPERATURE AND TIME AT TEMPERATURE ON IRRADIATED OCONEE I (THREE CYCLE) FUEL-ROD CLADDING TOTAL BURST STRAIN
Test Temperature, 371 C; Strain Rate, 0.004/min.

Robinson cladding for the annealing temperature of 593 C with an isothermal annealing time of 10 minutes. However, this was the only occurance of this type for the data generated in this program. The uniform strain was constant at about 2% except for the H. B. Robinson cladding isothermally annealed at a temperature of 704 C and for times of 1 and 30 minutes. This difference was probably caused by differences in texture and grain size between the Lot 1 and Lot 4 cladding.

The total strains for both H. B. Robinson and Oconee I, three cycle material were about equal at 3 to 4% at the left (transient) position for all annealing temperatures except 704 C. At 1 and 10 minute isothermal annealing times, both H. B. Robinson and Oconee I specimen total strains were constant and equal to about 3 to 5% for an isothermal annealing temperature of 538 C. However, for the longer times, isothermal annealing temperatures of 593 and 704 C produced increased total strains for both material. For an annealing temperature of 593 C, the Lot 4 cladding total strain increased to about 14% after 1 minute and continued to increase to about 16.5% after 10 minutes. In comparison, the H. B. Robinson total strain increased to about 25% after 1 minute and then decreased to about 15% after annealing for 10 minutes at 593 C.

These differences in response of the Lot 1 and Lot 4 cladding to isothermal annealing temperatures and times at temperature appear to be caused by texture and grain size differences after undergoing annealing.

Specimens from Oconee I, one, two and three cycle fuel rods were prepared and annealed under transient and isothermal conditions and the data tabulated in Tables 47, 48 and 49. A comparison of the tube-burst test results illustrate the effect on the burst properties of increasing exposure to an neutron environment and the subsequent changes caused by annealing. The tube-burst results for specimens transient annealed at 28 C/sec and 5.6 C/sec are plotted in Figures 74 and 75, respectively. From the plots it was noted that after two cycles the stresses were increased and the strains decreased by the increased irradiation and that after the transient annealing exceeds 600 C, the effect of irradiation had disappeared. However, after irradiation for three cycles and transient annealing below 600 C, (see Figure 74) the burst stresses and possibly total strain had decreased to approximately the one cycle values. Again above an annealing temperature of 600 C, the effect of irradiation damage disappeared. It should also be noted that the burst properties for specimens transient annealed at either 28 C/sec or 5.6 C/sec and to a temperature of 800 C were equal and were independent of the amount of irradiation.

A comparison of tube-burst properties of Oconee I, one-, two-, and three-cycle fuel-rod cladding specimens (Lots, 2, 3 and 4) isothermally annealed (see Figures 76, 77, 80, 81, 84 and 85) indicated that even at the annealing temperature of 482 C, recovery of the strength was occurring if the annealing time was long enough. But in general, the effect of isothermal annealing on the tube-burst properties was the same as the effect described for transient annealing, with the two-cycle material exhibiting the pronounced increases in strength and decreases in dutilities. These data indicated that a peaking or saturating of irradiation damage had occurred after two cycles in the Oconee I reactor. This apparent saturation might be caused by a combination of irradiation time, operating temperature and other reactor conditions. These data, however, did not clearly indicate what effect extended burnups (> 30,000 MWD/MTU) would have on the fuel rod mechanical properties; the properties might improve but are just as likely to deteriorate.

The burst test data for isothermally annealed Lots 2, 3, and 4 material also indicated that the responses of the fuel-rod tube-burst mechanical properties depended on a complicated combination of cladding condition at manufacture, irradiation time, reactor environmental history, annealing temperature, and annealing time. The condition of fuel-rod cladding after an off-normal or transient reactor condition could only be generalized from these data.

Expanding Mandrel Tests

Expanding mandrel tests were conducted in an attempt to simulate the interaction of longitudinally cracked fuel pellets with the restraining Zircaloy fuel-rod cladding (PCI). The test apparatus is described and the test procedures outlined in Appendix C.

Specimens 6.5 to 7.5 cm in length were cut from irradiated fuel rods. The irradiated samples were defueled, annealed, and tested. The unirradiated specimens required only annealing and testing. The annealing apparatus is described and the test procedures outlined in Appendix B.

Irradiated H. B. Robinson Cladding (Lot 1)

Specimens from the irradiated H. B. Robinson fuel rod C8 were prepared and expanding-mandrel tested. The specimens were defueled and annealed under both transient and isothermal conditions. Transient anneals included heating the specimens at 5.6 and 28 C/sec to maximum temperatures reached in the transient of from 482 to 816 C and immediately quenching in a jet of helium. The isothermally annealed specimens were heated at a rate of 28 C/sec until the desired temperature was reached, held at that temperature for periods from 1 to 60 min and quenched in a jet of helium. After annealing, the specimens were expanding mandrel tested at a test temperature of 371 C and at a strain rate of 0.0063/min.

The effects of transient heating anneals on the expanding mandrel properties, ultimate stress and uniform strain, of irradiated H. B. Robinson Zircaloy-4 fuel-rod cladding are shown in Figure 94 and the data are listed in Table 50. Only the ultimate stress and uniform strain values are shown as these are illustrative of the general trends in strength and ductility changes.

The stress values showed no significant influence of heating rate from 5.6 to 28 C/sec. While the results showed some scatter, the stress showed essentially no change until the maximum temperature reached in the transient exceeded about 600 C, at which point the stress decreased substantially, regardless of heating rate.

The effects of isothermal annealing on the expanding mandrel properties, ultimate stress and uniform strain, of irradiated H. B. Robinson fuel-rod cladding are plotted in Figure 95, and serve to illustrate general trends. The expanding mandrel test data are shown in Table 51.

The stress values showed a distinct temperature and time-at-temperature dependence. The strength dropped very quickly at the highest annealing temperature of 704 C but there was little or no decrease in strength at an annealing temperature of 482 C even after an isothermal anneal of 60 minutes. The minimum value of the ultimate hoop stress ($\sim$200 MPa) reached after several minutes for isothermal annealing temperatures above 593 C, appeared to be independent of temperature. However, the minimum value of the ultimate hoop stress ($\sim$300 MPa) for the 583 C annealing temperature and the minimum value of the ultimate hoop stress ($\sim$370 MPa) for the 482 C annealing temperature showed a pronounced temperature dependence. It was not apparent what the response would be if the specimens were held for long periods (several hours) at

TABLE 50. EXPANDING MANDREL TEST RESULTS FOR IRRADIATED AND TRANSIENT ANNEALED H. B. ROBINSON ZIRCALOY FUEL-ROD CLADDING

Test temperature, 371 C; strain rate 0.0063/min.

Specimen	Annealing Conditions		Ultimate Stress MPa	Yield Stress MPa	Failure Stress MPa	Uniform Strain, Percent	Total Strain, Percent
	Heating Rate, C/sec	Maximum Temp, C					
C8-13	5.6	482	332	122	332	12.0	12.0
C8-14	5.6	538	322	148	322	10.2	10.2
C8-15	5.6	593	253	117	253	8.8	8.8
C8-18	5.6	593	341	116	351	16.2	16.2
C8-16	5.6	621	336	108	336	10.6	10.6
C8-17	5.6	704	237	106	237	9.4	9.4
C8-19	5.6	704	274	81	274	19.0	19.0
C8-20	28	482	363	127	362	15.6	15.6
C8-21	28	538	344	114	344	13.6	13.6
C8-22	28	593	354	108	354	16.2	16.2
C8-23	28	621	343	122	343	15.2	15.2
C8-24	28	704	168	38	152	20.0	42.2
C8-25	28	816	226	58	213	19.0	28.6

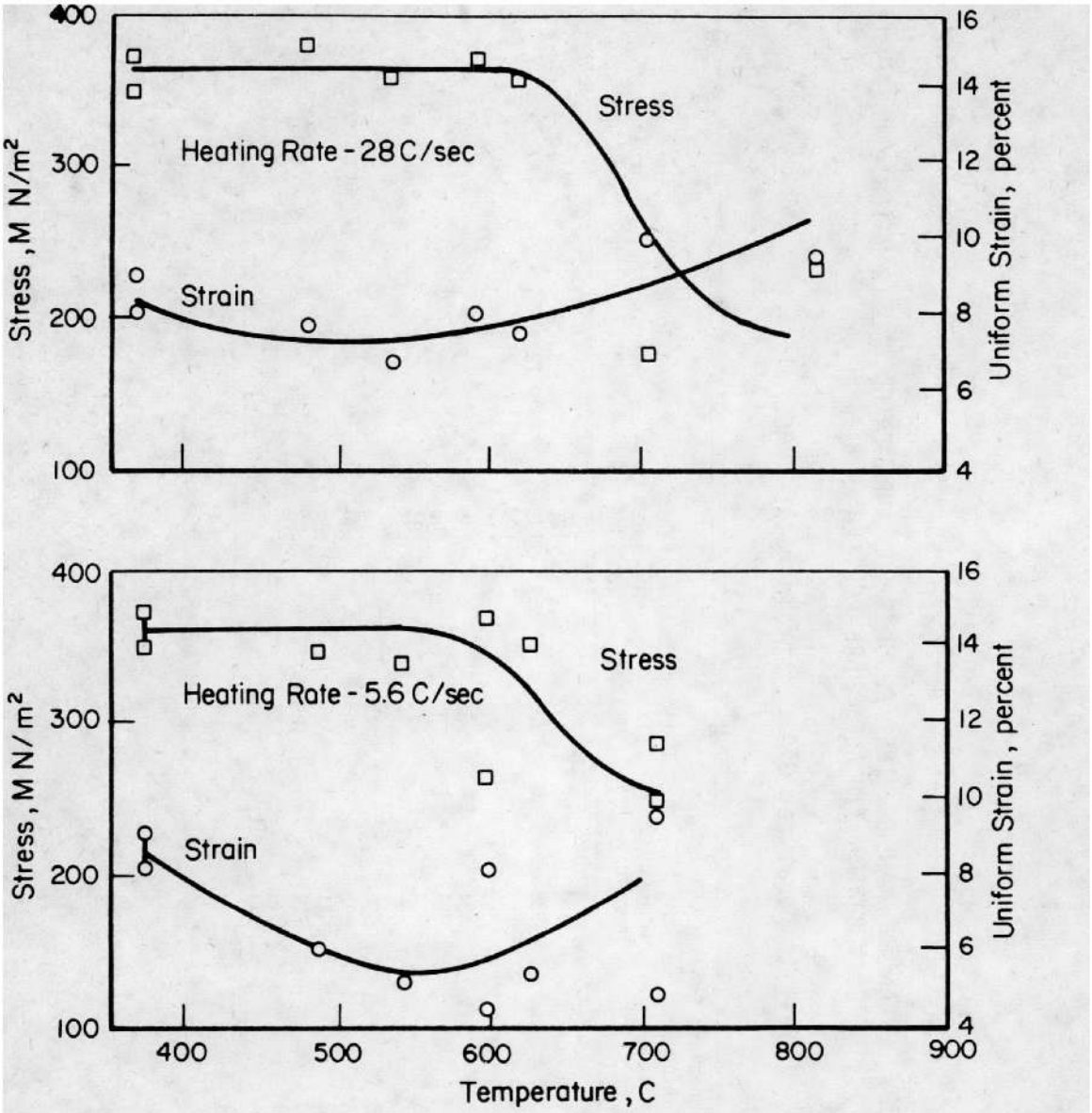

FIGURE 94. EFFECT OF TRANSIENT HEATING RATE AND MAXIMUM TEMPERATURE ACHIEVED IN TRANSIENT ON IRRADIATED H.B. ROBINSON FUEL-ROD CLADDING ULTIMATE HOOP STRESS AND UNIFORM STRAIN AS MEASURED IN EXPANDING MANDREL TESTS

Test temperature 371 C.

TABLE 51. EXPANDING MANDREL TEST RESULTS FOR IRRADIATED AND ISOTHERMAL ANNEALED H.B. ROBINSON ZIRCALOY FUEL-ROD CLADDING

Test temperature 371 C; strain rate 0.0063/min.

Specimen	Annealing Conditions[a]		Ultimate Stress, MPa	Yield Stress, MPa	Failure Stress, MPa	Uniform Strain, percent	Total Strain, percent
	Maximum Temp, C	Holding Time, min					
C8-31	482	10	291	108	291	12.0	12.0
C8-33	482	60	293	121	293	12.6	12.6
C8-34	482	60	293	102	291	15.6	18.4
C8-26	538	1	292	119	292	11.8	11.8
C8-30	538	5	289	100	279	15.6	23.2
C8-27	593	1	278	75	274	17.6	20.8
C8-32	593	30	195	34	192	21.4	27.4
C8-28	621	1	268	86	260	17.6	24.2
C8-29	704	1	195	50	184	30.4	41.2

(a) Nominal heating rate, 28 C/sec.

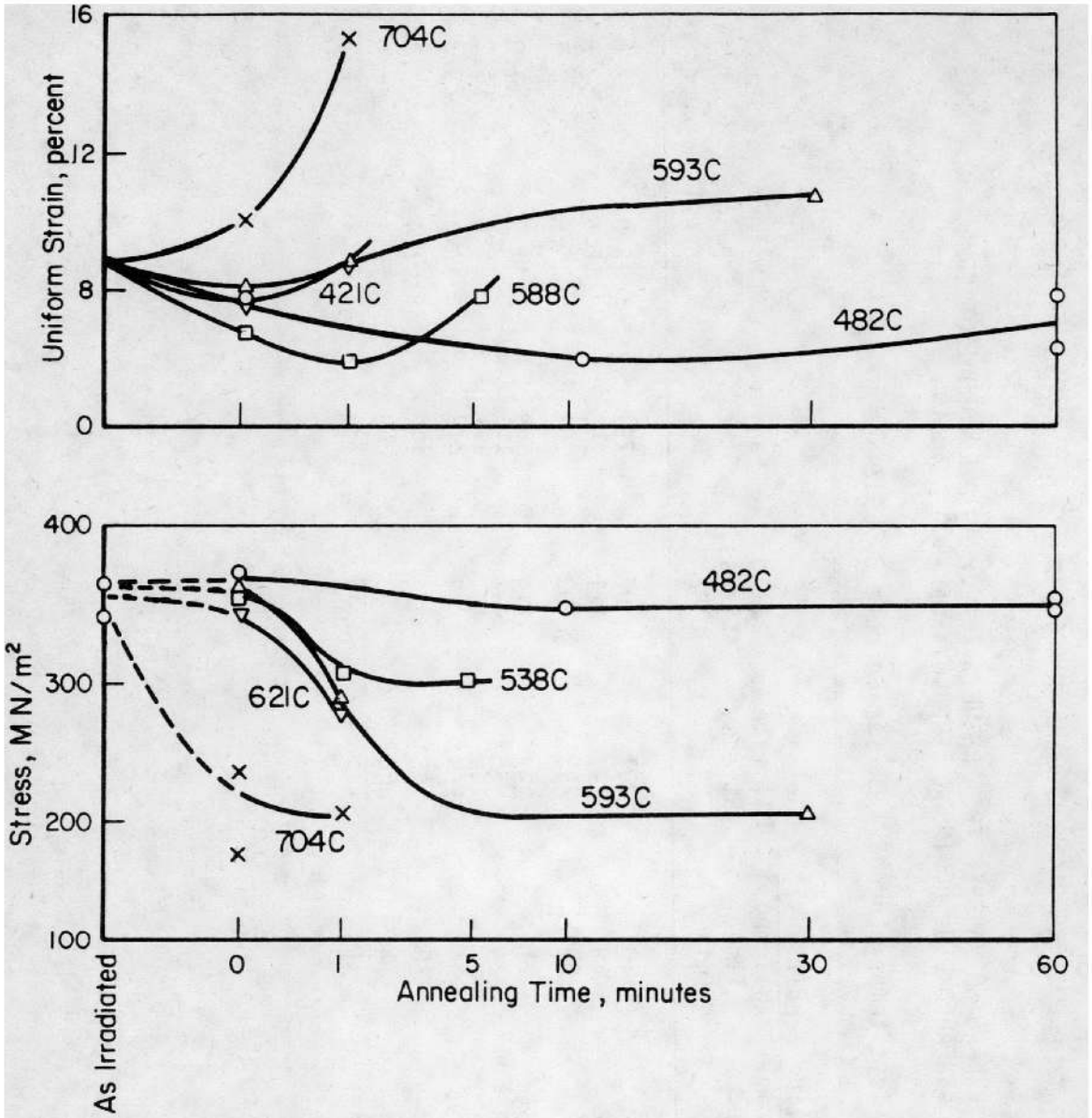

FIGURE 95. EFFECT OF ISOTHERMAL ANNEALING TEMPERATURE AND TIME AT TEMPERATURE ON IRRADIATED H.B. ROBINSON FUEL-ROD CLADDING ULTIMATE HOOP STRESS AND UNIFORM STRAIN AS MEASURED IN EXPANDING MANDREL TESTS

Test temperature 371 C.

temperatures below 538 C but the expanding mandrel mechanical properties appeared to be stabilized after 1 minute of isothermal annealing time.

The strain values showed a pronounced temperature dependence at all the isothermal annealing temperatures examined. It should be noted that the uniform strain appeared to exhibit a minimum for all isothermal temperatures except 704 C and also exhibited a lag in recovery of ductility behind recovery of the strength. These results were consistent with those recorded in the tensile and tube-burst tests.

Irradiated Oconee I Cladding

Specimens from the Oconee I fuel rods were prepared and expanding mandrel tested. The specimens were defueled and annealed under both transient and isothermal conditions. The transient anneals included heating the specimens at 5.6 and 28 C/sec to maximum temperatures reached in the transient of from 482 C to 816 C; the specimens were then immediately quenched in a jet of helium. The isothermally annealed specimens were heated at a rate of 28 C/sec until the desired temperature was reached, held at that temperature for periods from 1 to 60 min and quenched to room temperature in a jet of helium. After annealing, the specimens were expanding mandrel tested at a test temperature of 371 C and at a strain rate of 0.0063/min.

Oconee I, One Cycle (Lot 2). The data for specimens transient annealed and expanding mandrel tested at 371 C and a strain rate of 0.0063/min are listed in Table 52. The ultimate stress values for the heating rate of 5.6 C/sec showed a drop between annealing temperatures of 482 C and 538 C, were constant to 621 C, and showed a second drop at 704 C. The yield and failure stresses for the heating rate of 5.6 C/sec exhibited a similar behavior. The uniform strain appeared to have a minimum at about 593 C but never rose above the strain value of 19.2 percent. The total strain was constant until the annealing temperature or 704 C was reached and then showed a pronounced increase.

TABLE 52. EXPANDING MANDREL TEST RESULTS FOR IRRADIATED AND TRANSIENT ANNEALED OCONEE I (ONE CYCLE) ZIRCALOY FUEL-ROD CLADDING.

Test temperature 371 C; strain rate 0.0063/min.

Specimen	Annealing Conditions		Ultimate Stress, MPa	Yield Stress, MPa	Failure Stress, MPa	Uniform Strain, percent	Total Strain, percent
	Heating Rate, C/sec	Maximum Temp, C					
47010-10	5.6	482	335	113	327	19.2	22.9
47010-14	5.6	538	282	101	282	19.2	19.3
47010-18	5.6	593	277	94	271	14.4	20.4
47010-19	5.6	621	276	101	261	16.8	25.3
47010-20	5.6	704	212	67	208	21.1	39.8
47103-2	28	482	286	104	264	19.3	34.4
47103-8	28	563	282	100	277	18.9	24.8
47103-18	28	593	270	101	276	18.6	20.3
47103-27	28	621	280	110	273	13.8	14.3
47103-28	28	704	273	90	264	14.9	21.3
47010-9	28	816	233	69	217	22.3	42.0

The transient annealing results for the Lot 2 material annealed at a heating rate of 28 C/sec showed similar behavior. However, the ultimate stress was constant from an annealing temperature of 482 C to 704 C. At 816 C the ultimate stress value dropped 50 MPa (from 273 to 233 MPa). The yield and failure stresses showed an identical behavior. The uniform strain exhibited a minimum at an annealing temperature of 621 C but only rose to 22.3 percent at an annealing temperature of 816 C. The total strain also appeared to show a minimum at 621 C but began with a total strain of 34.4 percent at an annealing temperature of 482 C and ended with a total strain of 42 percent at an annealing temperature of 816 C.

A similar explanation was suggested for the minima in the expanding mandrel ductilities, as discussed under previous tensile and tube-burst sections, i.e., agglomeration of defects during annealing.

The results of the expanding mandrel tests after isothermal annealing are given in Table 53. The expanding mandrel tests were conducted at 371 C and at a strain rate of 0.0063/min.

The data showed the expected decreases in stresses and increases in strains as the annealing temperatures were increased and as the time-at-temperature was increased for annealing temperatures above 538 C. The stresses and strains appeared uneffected by annealing time at 482 C, at least up to a 1-hour anneal.

Oconee I, Two Cycle (Lot 3). The data for specimens annealed under both transient and isothermal conditions and subsequently expanding-mandrel tested at 371 C and at a strain rate of 0.0063/min are listed in Table 54. The results followed the exact behavior described for the Lot 2 material. However, it was noted that two-cycle material had in general approximately 10 percent higher stress values and somewhat lower strain values.

The discussion in the previous section for both transient and isothermally annealed Lot 2 materials is equally valid for the Lot 3 material.

TABLE 53. EXPANDING MANDREL TEST RESULTS FOR IRRADIATED AND ISOTHERMAL ANNEALED OCONEE I (ONE CYCLE) ZIRCALOY FUEL-ROD CLADDING

Test temperature 371 C; strain rate 0.0063/min.

Specimen	Annealing Condition[a]		Ultimate Stress, MPa	Yield Stress, MPa	Failure Stress, MPa	Uniform Strain, percent	Total Strain, percent
	Maximum Temp, C	Holding Time, min					
47010-21	482	60	263	108	108	9.8	9.8
47010-22	538	1	270	101	259	15.9	26.3
47010-23	538	15	234	65	222	16.7	33.2
47010-28	593	1	256	99	254	18.2	23.1
47010-29	593	15	166	36	158	44.9	58.2
47010-26	621	1	220	79	202	17.3	38.0
47015-5	704	1	167	58	166	49.1	49.7

(a) Nominal heating rate, 28 C/sec.

TABLE 54. EXPANDING-MANDREL TEST RESULTS FOR TRANSIENT AND ISOTHERMAL ANNEALED OCONEE (TWO CYCLE) ZIRCALOY FUEL-ROD CLADDING

Test temperature 371 C; strain rate 0.064/min.

Specimen Number	Annealing Conditions: Heating Rate C/sec	Annealing Conditions: Maximum Temperature C	Annealing Conditions: Holding Time, min	Ultimate Stress, MPa	Yield Stress, MPa	Failure Stress, MPa	Uniform Strain,[a] percent	Total Strain,[b] percent
			TRANSIENT ANNEALS					
31778A-3	5.6	482	-	352	129	350	17.4	19.1[b]
37778A-5	5.6	538	-	354	119	354	15.8	15.8[b]
32211A-2	5.6	593	-	298	99	298	15.5	15.5[b]
32211A-5	5.6	621	-	280	98	280	15.8	15.8[b]
32211A-6	5.6	704	-	184	57	178	23.5	47.5
32013A-2	28	482	-	293[c]	138	293	14.4	14.4[b]
32013A-5	28	538	-	340	115	340	12.8	12.8[b]
32013A-8	28	593	-	321	108	321	17.1	17.1[b]
32013A-12	28	621	-	322	114	322	12.9	12.9[b]
32013A-18	28	704	-	202	62	191	21.1	38.0
32013A-20	28	816	-	201	43	196	32.7	39.0
			ISOTHERMAL ANNEALS					
32211A-8	28	482	60	293	145	293	12.4	12.4[b]
32211A-11	28	538	1	303	114	303	12.7	12.7[b]
32211A-12	28	538	10	281	93	280	17.4	18.5
32211A-15	28	593	1	257	121	257	13.8	20.0
32211A-23	28	593	10	194	86	186	28.7	40.0
32211A-35	28	621	1	218	77	194	21.3	34.5
31917A-2	28	704	1	171	48	167	33.9	49.0

(a) Circumferential strain based on the original OD of 1.1 cm (0.43 in.).
(b) Failures occurred at maximum load.
(c) Appears to have broken before reaching maximum load and may have had a defect.

Oconee I, Three Cycle (Lot 4). It was found that tensile, tube-burst and expanding mandrel tests yielded almost identical results for irradiated and annealed specimens. Therefore, because burst of a fuel rod is the most likely form of failure, it was concluded that the most effective plan was to concentrate on tube-burst tests. Annealing of tube-burst specimens only was then instituted and no further annealing of expanding mandrel specimens was conducted. Therefore, Oconee I, three cycle (Lot 4) material was not annealed and no further expanding mandrel tests were conducted.

Comparison of Expanding Mandrel (Annealed) Data

A comparison was made of the H. B. Robinson expanding mandrel test data for specimens annealed under both transient and isothermal annealing conditions and the Oconee I expanding mandrel data for specimens similarly annealed and tested. (See Tables 50 through 54.) Since only specimens from one-, and two-cycle irradiations in the Oconee I reactor were annealed and tested, the expanding mandrel results for all three data sets, H. B. Robinson, Oconee I, one-cycle, and Oconee I, two-cycle, were included in the comparison.

The results of the expanding mandrel tests for ultimate stress and uniform strain for the annealed H.B. Robinson cladding were taken from Tables 50 and 51 and those for the Oconee I cladding were taken from Tables 52, 53, and 54. These tests results are for specimens annealed at transient heating rates of 5.6 and 28 C/sec and isothermally annealed at 482 to 704 C for periods from 1 to 60 minutes.

The ultimate stress and uniform strain for expanding mandrel specimens transient annealed at 28 C/sec and subsequently tested at 371 C and a strain rate of 0.063/min are plotted in Figure 96 for Lots 1, 2 and 3 materials. As can be seen from these plots, the Lot 2 stress values were lower than the Lots 1 and 3 stress values for maximum temperatures reached in the transient below 621 C. However, above 621 C the strength of the Lot 2 cladding remained higher than either of the Lot 1 or Lot 3 strengths. This was consistent with the tensile results recorded after annealing of unirradiated Oconee I archive cladding as compared with irradiated and similarly annealed Oconee I fuel-rod cladding tensile test results. The strengths of both Lots 1 and 3 are almost the same for transient annealing temperatures above 538 C.

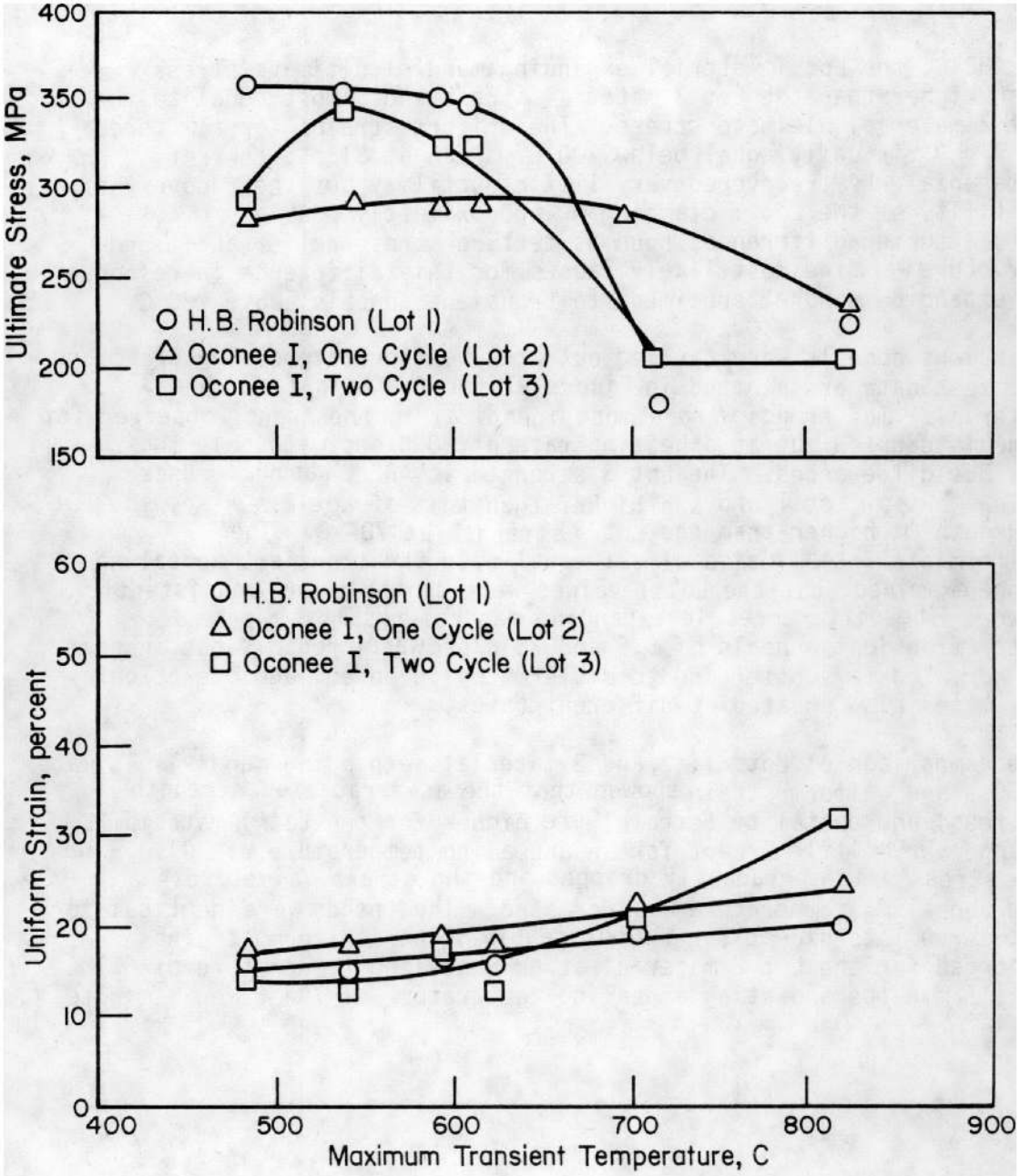

FIGURE 96. EFFECT OF TRANSIENT ANNEAL AT 28 C/SEC ON THE STRENGTH AND DUCTILITY OF SPENT-FUEL CLADDING AS MEASURED IN EXPANDING MANDREL TESTS

Test temperature 371 C; strain rate 0.025/min.

At 482 C, the Lot 1 material expanding-mandrel ultimate stress was much higher than the Lot 3 material stress and almost equal to the Lot 2 material ultimate stress. The uniform strains for all three lots were virtually equal below 700 C. Even at 816 C, the Lots 2 and 3 material had recovered very little ductility, but the recovery of ductility of the Lot 1 cladding was approximately doubled. Manufacturing differences such as texture stress relief and microstructure were the most likely causes for this difference in response of expanding mandrel specimens to transient anneals above 700 C.

Transient anneals were carried out at a heating rate of 5.6 C/sec and the test data are plotted in Figure 97 for the Lots 1, 2, and 3 material. The trends were almost identical to the trends observed for anneals carried out at a heating rate of 28 C/sec, with only two obvious differences. The Lot 3 strength at 482 C was not reduced below that of Lot 1 and was higher than that of Lot 2. Also, the Lot 1 strength was higher than the Lot 3 strength at 704 C. The uniform strains were also almost equal over the transient annealing range examined, but the Lot 1 values were slightly and consistently lower. The differences in expanding mandrel results after transient anneals of 5.6 and 28 C/sec were probably due in part to normal data scatter and to differences in defect agglomeration as the material was heated at different rates.

The comparison of Lots 1, 2, and 3 materials expanding mandrel ultimate stress and uniform strain showed that the as-irradiated strength (stress) and ductility (strain) were higher for the Lot 1 material, change very little except for an annealing temperature of 704 C, where the stress values gradually dropped and the strain values rose as the annealing temperature was increased. The trends were identical for all three lots except for the noticeably higher uniform strains recorded for the Lot 2 material at an annealing temperature of 621 C for 15 minutes and at an annealing temperature of 704 C for 1 minute.

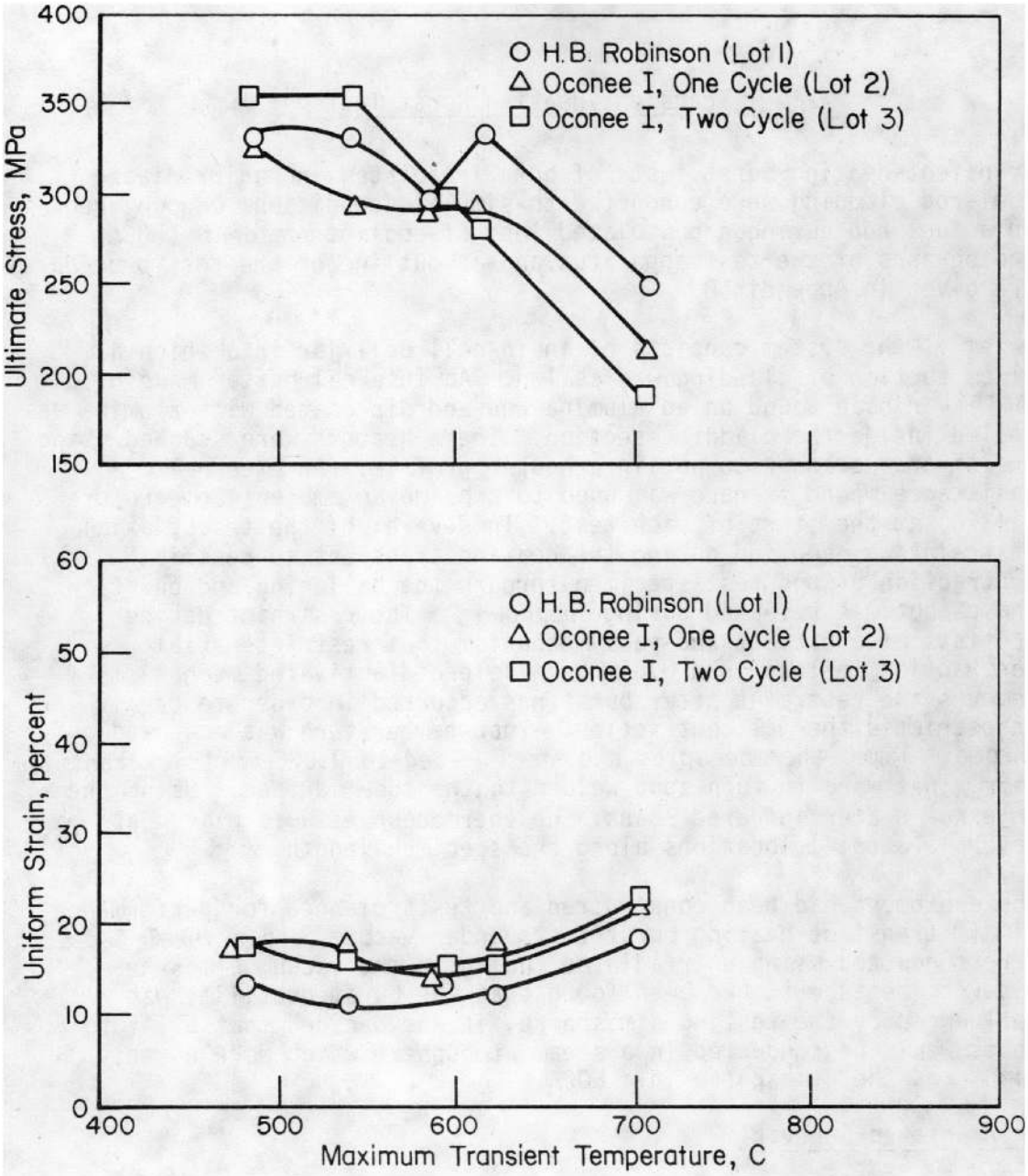

FIGURE 97. EFFECT OF TRANSIENT ANNEALING AT 5.6 C/SEC ON THE STRENGTH AND DUCTILITY OF SPENT-FUEL CLADDING AS MEASURED IN EXPANDING MANDREL TESTS

Test temperature 371 C; strain rate 0.025/min.

Transient-Heating Burst Tests

Transient-heating burst tests of both irradiated and unirradiated fuel-rod cladding were conducted to simulate conditions encountered in a fuel rod during a postulated loss-of-coolant accident (LOCA). Photographs of the test apparatus and an outline of the test procedures are given in Appendix D.

Briefly, the system consists of an in-cell bell jar into which a 51-cm section of cladding was sealed. An internal heater made of Kanthal ribbon wound on an alumina rod and dip coated with alumina was sealed inside the cladding section. These heaters were scanned using an infrared scanner to obtain a heater profile. An external resistance-wound furnace was used to provide an ambient temperature (343 C) at the start of each test. In several of the tests, axial restraint was applied during the heating transient to restrict contraction of the test specimen through the ballooning and burst phases but was released during cooldown. The restraint device consists of a ratchet-and-pawl mechanism that restricts axial contraction to less than 0.8 mm. A solenoid-activated mechanism removes the restraint after burst has occurred in order to permit unrestricted thermal contraction. Tube temperature was measured by Chromel-Alumel thermocouples and spot welded to 0.076-mm-thick tantalum tabs, that were in turn spot welded to the tube surface. Using the internal heater infrared scans, the thermocouples were placed at several (3 to 4) locations along the specimen length.

The equipment had been constructed and tests planned for performance of all transient-heating burst tests under vacuum, and several tests were conducted using unirradiated tubing in the vacuum atmosphere. However, because it had been found that the burst ductility was influenced by the testing atmosphere, it was decided that all future tests would be conducted in a steam atmosphere which more closely simulates the atmosphere in a LOCA.

Unirradiated Sandvik

Six transient-heating burst tests were performed using unirradiated tubing fabricated by Sandvik. The specimens were numbered 1 through 6 and the specimen temperatures were measured at four points over the internal heater length (38 cm) of the specimen. The tests were performed in vacuum and the temperature was measured using Chromel-Alumel thermocouples. In tests of Specimens 1, 2, 3, and 4 the

thermocouples were spot welded directly to the tube surface, and in tests of specimens 5 and 6, the thermocouples were spot welded to 3-mm-square by 0.076-mm-thick tantalum tabs which were in turn spot welded to the tube surface. Using the internal heater infrared profile scans, one of the thermocouples for each test was placed on the specimen at the axial and angular position corresponding to the heater peak-temperature position. Specimen 1 had been used to obtain temperature settings for the ramps and had been heated to about 950 C prior to testing using an initial pressure of 6275 kPa. The heating ramp for Specimen 1 was 28 C/sec and the pressure increased from 6275 to 7750 kPa and then decreased to 7655 kPa before rupture occurred. Rupture occurred about 2.5 cm from one thermocouple and the temperature dropped immediately at the time of failure. The specimen temperature profile as recorded by the four thermocouples at a time 25 seconds into the transient, in general, compared well with the temperature profile of the internal heater as determined by the infrared profile which was performed prior to the test.

In the second test, the pressure increased from 6275 KPa to about 7600 kPa, and then decreased slightly to 7584 kPa at the time of rupture. This specimen burst between the separately welded legs of one of the thermocouples. Because the thermocouple was so close to the burst, the temperature at the thermocouple apparently dropped as the specimen ballooned and pulled away from the internal heater.

The initial pressures for Specimens 3, 4, 5, and 6 along with the test results for all six tests are listed in Table 55. For specimens 3, 4 and 5, the bursts occurred within 2 cm of the anticipated burst axial position and within 50 degrees of the anticipated burst circumferential (angular) position.

Specimen 6 was initially pressurized to 690 kPa and failed at the maximum pressure of 835 kPa and a temperature of 1230 C. Rupture occurred near the center thermocouple and some melting of the cladding occurred in the area around the failure, apparently as a result of reaction with the thermocouple. The thermocouple had been spot welded to a tantalum tab. However, past the tab edge, the bare leads touched the cladding. It should be noted that the area of maximum strain was at the hottest heater position, as determined by an infrared heater scan, but the thermocouple-cladding reaction led to the failure in the specimen. Resistance measurements indicated numerous separations in the heater ribbon, possibly caused either by cracking of the embrittled heater ribbon as it cooled or as a result of melting along the heater length.

TABLE 55. TRANSIENT-HEATING BURST TESTS FOR UNIRRADIATED SANDVIK ZIRCALOY FUEL-ROD TUBING

Heat rate 28 C/sec.

Specimen	Initial Pressure, MPa	Maximum Pressure, MPa	Burst Pressure, MPa	Burst Temperature, C	Failure Stress, MN/m^2	Failure Strain, percent
1[a]	6.28	7.60	7.59	813	65.23	-
2	6.28	7.69	7.66	850	65.83	11.7
3	7.24	8.28	7.60	837	65.36	35.3
4	4.14	4.74	4.71	907	40.47	11.5
5	2.05	2.54	2.53	949	21.72	15.5
6[b]	0.69	0.84	0.84	1230	7.16	-

(a) This specimen had been used for temperature calibration and had been heated to about 950 C prior to testing.

(b) Heater melted and the thermocouple reacted with the cladding where it contacted the cladding.

Photographs of Specimens 2, 3, 4, 5, and 6 after testing are shown in Figure 98. The results of all six tests are plotted in Figures 99 and 100, along with data obtained in the same lot of Sandvik material by ORNL.[1] There was good agreement in the relationship between burst pressure and temperature. Although the BCL and ORNL rupture strains showed the same qualitative dependence on temperature, the variations appeared more severe in the BCL test results, as indicated in Figure 100.

Unirradiated Oconee I Archive

Because very little unirradiated Oconee I archive tubing was available, only two transient-heating burst tests were conducted. The tests were conducted in 100 kPa (1 atm) steam and with no restraint. The initial pressures and the test results are listed in Table 57, Page 231. The burst pressures and temperatures compared very well with the ORNL unirradiated transient-heating burst results.

Irradiated H. B. Robinson Cladding (Lot I)

Transient-heating burst tests were performed using irradiated fuel-rod cladding from the H. B. Robinson reactor. All tests were conducted in 100 kPa (1 atm) steam environment. The test chamber was filled with steam and the steam flow over the specimen occurred by convection. In eight of the tests, axial restraint was applied during the heating transient to restrict contraction through the tube ballooning and burst phases with the restraint released during cool down. The restraint device consists of a ratchet-and-pawl mechanism that restricts axial contraction to less than 0.8 mm. A solenoid-activated mechanism removes the restraint after burst has occurred in order to permit unrestricted thermal contraction.

The tests were conducted using 51 cm long sections of tubing from which the fuel had been removed. The tube was internally heated by means of a Kanthal heater wound on an alumina rod and dip coated with alumina. Internal void volume was minimized and adjusted to values on the order of 15 cm^3. An external resistance-wound furnace was used to provide an ambient temperature of 343 C at the start of each test.

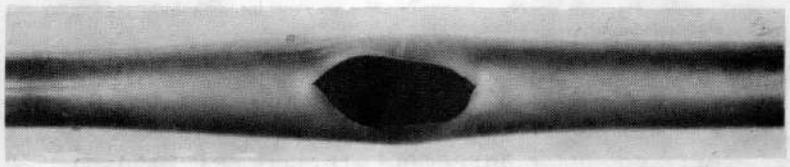

1X Specimen 2 C-3089

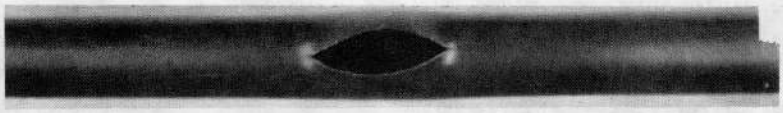

1X Specimen 3 C-3089

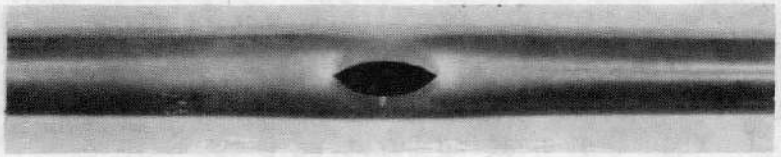

1X Specimen 4 C-3090

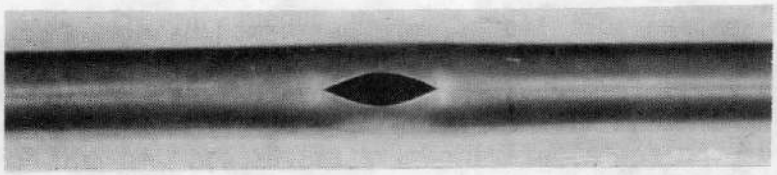

1X Specimen 5 C-3090

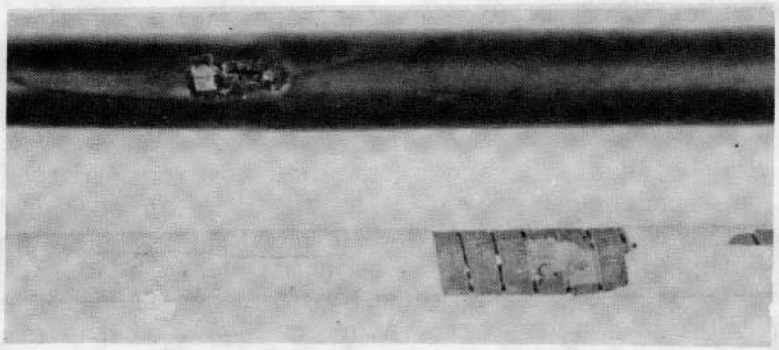

1X Specimen 6 C-3091

FIGURE 98. APPEARANCE OF FAILURE AREAS FOR UNIRRADIATED FUEL-ROD TUBING SPECIMENS AFTER TRANSIENT HEATING BURST TESTS

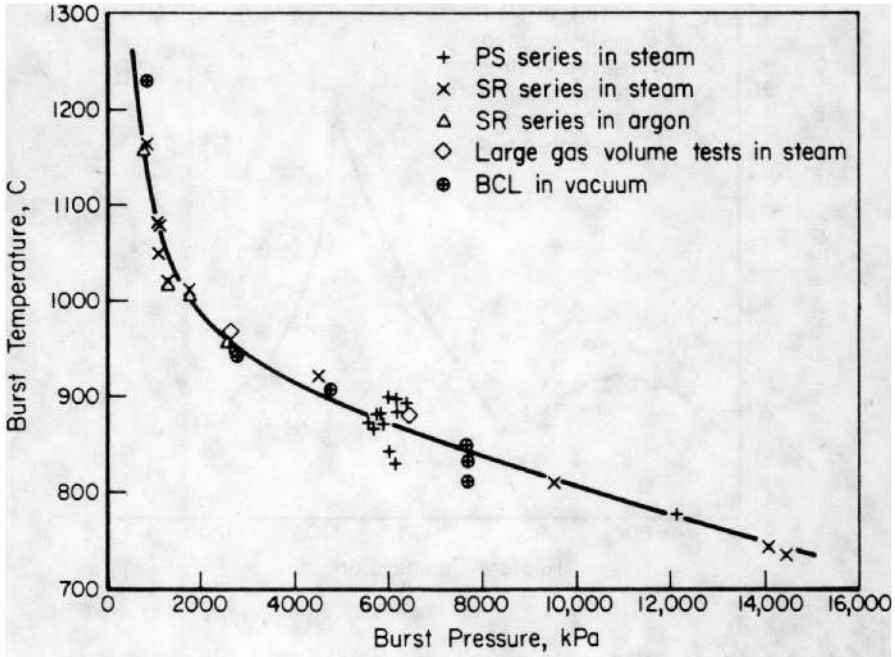

FIGURE 99. BURST TEMPERATURE VERSUS BURST PRESSURE FOR ORNL AND BCL TRANSIENT-HEATING BURST TESTS OF UNIRRADIATED ZIRCALOY TUBING

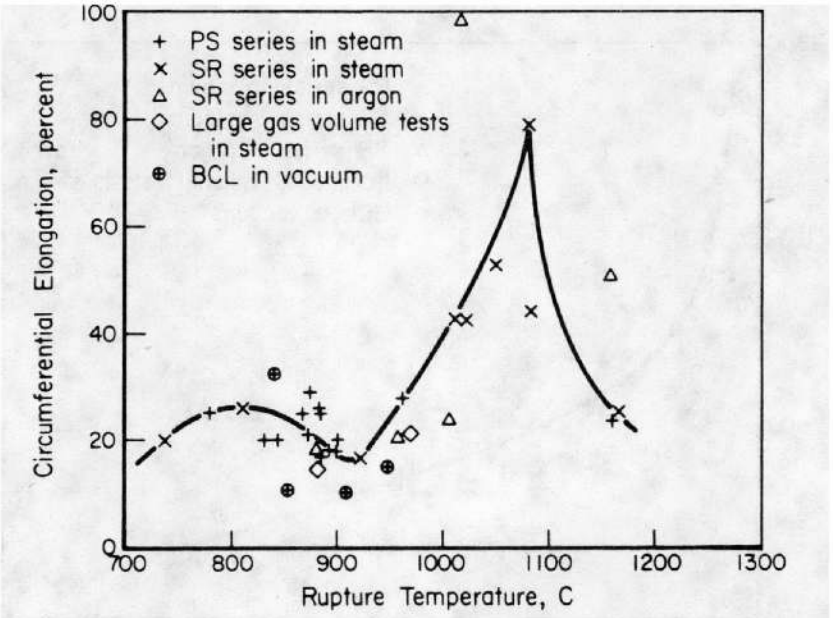

FIGURE 100. AVERAGE RUPTURE STRAIN FOR UNIRRADIATED ORNL AND BCL TRANSIENT-HEATING BURST TEST SPECIMENS

Tube temperatures were measured by Chromel-Alumel thermocouples, spot welded to 0.076-mm-thick tantalum tabs that were in turn spot welded to the tube surface. Thermocouple locations were selected by examination of infrared heater scans, obtained at about 400 C, to select probable failure locations based on maximum heater temperatures. Maximum temperature variations measured at 400 C were typically ± 6 C. Normally, because of restricted access, two thermocouples were attached to the tube when the restraint device was used, while three or four thermocouples were employed for the unrestrained tests.

The test results are tabulated in Table 56 for irradiated H. B. Robinson specimens heated at rates from 6 to 34 C/sec; the results indicate that the application of axial restraint, up to the time of burst in transient-heating burst tests, had no effect on either burst temperature or burst ductility. There was a tendency toward somewhat greater tube-circumferential burst elongations for tests conducted with axial restraint. However, this tendency was the reverse of any expected influence of restraint and therefore was considered to be statistical in nature.

Thermocouple locations with respect to the center of the bursts are also given in Table 56. In 12 tests, the axial burst and thermocouple locations essentially coincide. However, in only four tests did the thermocouple and burst locations coincide with respect to radial position, while in seven tests the burst location was exactly 180 degrees around the dircumference from the thermocouple. In the remaining tests the thermocouple was located between 3.0 and 165 degrees away from the position at which the burst occurred.

Several conclusions were made early in this program and these are discussed more fully in the discussion and conclusion section. However, the basic conclusion that rather severe axial and angular temperature differences (possibly as much as 50 C) exist over the transient-heating burst specimen length and around its circumference during a test appears to be correct. The conclusion that, in general, burst failures will occur at the highest temperature on the tube seems reasonable and acceptable. However, tensile, burst, and expanding mandrel test results of annealed specimens suggest that the strengths of irradiated cladding in the temperatures range above 700 C, which is the range of transient-heating burst tests, are less than those of unirradiated specimens similarly annealed and tested. Therefore, the conclusion that the BCL data for transient-heating burst tests falls below ORNL curve for unirradiated material because of experimental error arising from the inability to locate the thermocouple precisely at the failure location is believed to be incorrect and that the lower values are real.

TABLE 56. TRANSIENT-HEATING BURST TEST[a] RESULTS FOR IRRADIATED H. B. ROBINSON ZIRCALOY FUEL-ROD CLADDING

Specimen	Initial Pressure, MPa	Maximum Pressure, MPa	Burst Pressure, MPa	Burst[h] Temp, C	Failure Stress, MN/m^2	Failure Strain, percent	Thermocouple Distance From Burst Center	
							Linear, cm	Angular, degrees
N8/9-29[c]	0.67	0.97	0.97	1135	7.5	39	0	0
N8/30-50[c]	0.88	0.86	0.86	1071	6.8	25	2.0	0
N8/71-91[c]	1.08	1.37	1.37	1008	10.8	46	0	180
N8/112-132[c,f]	1.43	1.75	1.75	978	13.9	43	0	180
N8/50-70[c]	1.72	2.00	2.00	927	15.9	23	5.5	90
O14/42-62[b]	2.08	2.48	2.48	948	19.7	16	1.2	40
G8/70-89[c,f]	2.97	3.30	3.30	925	26.1	12	0	180
F8/70-90[c,d]	4.20	4.80	4.80	863	38.0	21	0	180
A1/35-55[b,e]	6.30	7.09	6.52	786	51.7	23	4.0	180
A8/42-62[b]	6.23	6.96	6.38	849	50.6	33	0	90
M12/35-55[b]	5.90	6.55	6.47	782(807)	51.3	18	5.0	165
M12/70-90[c]	6.07	6.72	6.58	804	52.1	13	2.5	90
F8/35-55[b]	6.19	6.81	6.58	814(860)	52.1	17	0	180
A1/79-99[b,f]	6.16	6.97	6.61	788	52.4	16	3.0	30
K8/35-55[c]	8.36	9.23	8.72	825	69.1	16	0	0

TABLE 56. (Continued)

Specimen	Initial Pressure, MPa	Maximum Pressure, MPa	Burst Pressure, MPa	Burst[h] Temp, C	Failure Stress, MN/m^2	Failure Strain, percent	Thermocouple Distance From Burst Center	
							Linear, cm	Angular, degrees
K8/14-34[b]	10.21	11.03	10.26	741	81.3	22	4.5	0
K8/70-90[a]	10.24	11.81	10.69	792	84.7	30	6.5	75
N8/91-111[c]	12.58	13.45	12.51	746	99.1	17	3.7	90
K10/105-125[c,g]	8.45	8.93	8.02	746	63.5	34	0	0
K10/71-91[c,g]	1.35	1.59	1.50	897	11.9	16	0	90
K10/35-55[c,d]	0.86	1.02	0.96	999	7.6	16	1.3	90
K10/14-34[c,e]	0.90	1.07	1.04	931	8.2	17	0	0
G8/35-55	10.52	11.43	10.85	763	86.0	17	0.5	180

(a) Heating rate ~28 C/sec unless otherwise indicated.
(b) Restraint applied during test.
(c) No restraint.
(d) Heating rate 15 C/sec.
(e) Heating rate 18 C/sec.
(f) Heating rate 34 C/sec.
(g) Heating rate 6 C/sec.
(h) The highest temperature recorded is listed in parenthesis ( ).

Irradiated Oconee I Cladding

Transient-heating burst tests were performed using irradiated fuel-rod cladding from the Oconee I reactor. The cladding had been irradiated for one, two and three cycles. All tests were conducted in 100 kPa (1 atm) steam atmosphere and no restraint of axial elongation was used. All tests were conducted at a heating rate of 28 C/sec except for a Lot 2 specimen (47111-6) which was conducted at a heating rate of 5.6 C/sec.

Oconee I, One Cycle (Lot 2). The results of the Lot 2 transient-heating burst tests are tabulated in Table 57. These results were consistent with the H. B. Robinson transient-heating burst rates results and all fell below the ORNL burst temperature versus burst stress curve for unirradiated cladding.[1]

Oconee I, Two Cycle (Lot 3). The results of the Lot 3 transient-heating burst tests are tabulated in Table 58. All the test burst temperatures were below the ORNL burst temperature for failures at specific hoop stresses except Specimen 31983A-15 which was initially pressurized to 7.17 MPa, and then increased to 7.92 MPa; this specimen finally burst after the pressure fell to 7.37 MPa. The failure hoop stress for this specimen was 55.8 MPa at a burst temperature of 857 C and was almost on the ORNL burst temperature versus burst hoop stress curve.

Oconee I, Three Cycle (Lot 4). A total of five transient-heating burst tests were conducted using Lot 4 irradiated fuel rod cladding. The pertinent test conditions and test results are summarized in Table 59. The results for the Lot 4 tests appeared to be consistent with the irradiated specimens data obtained throughout this program. The data from the Lot 4 tests also fell below the ORNL curve, as compared to the unirradiated specimen test results.

TABLE 57. TRANSIENT-HEATING BURST TEST RESULTS FOR IRRADIATED OCONEE I (ONE CYCLE) ZIRCALOY FUEL ROD CLADDING
Heating rate 28 C/sec.

Specimen	Initial Pressure, MPa	Maximum Pressure, MPa	Burst Pressure, MPa	Burst[d] Temp, C	Failure Stress, MN/m^2	Total Strain, percent	Thermocouple Distance From Burst	
							Linear, cm	Angular, degrees
47103-4	0.75	1.03	0.99	1066(1085)	7.5	37.6	0	0
47118-12	1.02	1.28	1.24	967(980)	9.4	35.6	0.6	180
47104-3	1.40	1.71	1.67	934(982)	12.7	29.9	0	90
47010-17	2.09	2.35	2.35	924(953)	17.8	37.8	0.6	180
47110-4	4.12	4.48	4.48	854	33.9	15.9	3.8	120
47110-7	6.36	6.84	6.84	831	51.7	31.4	0	150
47110-14	8.41	8.83	7.59	799	57.4	58.9	2.5	150
47111-12	8.40	9.00	8.74	745	66.2	36.7	3.8	30
47110-20	10.34	11.00	10.09	762(788)	76.4	25.3[b]	0.6	150
47111-6[a]	6.16	6.60	5.74	778	43.5	26.4	0	30
47101-16	8.33	8.93	8.27	788(796)	62.6	17.1	0.3	0
47101-11	8.24	8.83	8.53	783	64.6	18.3	0	60
47101-6	4.23	4.69	4.47	803	33.9	10.8	2.3	0
47101-3	3.10	2.52	3.45	892(910)	26.1	9.9	2.5	90
Archive 1[c]	4.12	4.88	4.85	936	36.7	18.2	3.8	90
Archive 2[c]	8.41	9.21	8.62	830	65.2	22.9	5.1	90

(a) Heating rate 5.6/sec.
(b) Burst did not occur at point of maximum ballooning.
(c) Unirradiated specimens.
(d) The highest temperature recorded is listed in parentheses( ).

TABLE 58. TRANSIENT-HEATING BURST TEST RESULTS FOR OCONEE I (TWO CYCLE) ZIRCALOY FUEL ROD CLADDING

Specimen Number	Initial Pressure, MPa	Maximum Pressure, MPa	Burst Pressure, MPa	Failure Stress, MPa	Failure Strain Percent	Temperature[a] C Burst	Thermocouple Distance from Burst	
							Linear, cm	Angular, degrees
31778A-8	0.65	0.86	0.86	6.5	4.7	1,093[b]	3.8	
32211A-13	1.03	1.27	1.24	9.4	12.3	1,043	1.3	290
32211A-20	1.46	1.76	1.71	12.9	19.1	877(943)	1.3	220
31778A-13	2.60	2.91	2.89	21.9	17.8	860(877)	0.5	180
31917A-16	4.27	4.74	4.65	34.2	11.9	850	0.0	0[c]
31965A-12	6.20	6.79	6.33	48.0	31.0	827	0.0	0[c]
31983A-15	7.17	7.92	7.37	55.8	19.1	857(841)	0.0	180
31785A-5	8.59	9.28	8.78	66.5	20.2	782	2.5	90
31785A-9	10.45	11.35	10.85	82.2	12.7	777	0.0	0[c]

(a) Nominal heating rate 28 C/sec. Highest temperature recorded is listed in parenthesis( ).

(b) Temperature went off scale on the recorder on all thermocouples.

(c) Thermocouple located adjacent to the tube rupture.

TABLE 59. TRANSIENT-HEATING BURST TEST RESULTS FOR IRRADIATED OCONEE I (THREE CYCLE) ZIRCALOY FUEL-ROD CLADDING

Heating rate 28 C/sec.

Specimen	Initial Pressure, MPa	Maximum Pressure, MPa	Burst Pressure, MPa	Burst[a] Temp, C	Failure Stress, MN/m^2	Total Strain, percent
47082-12	2.07	2.55	2.55	921	19.9	12.5
47080-3	4.14	4.76	4.14	866	32.2	31.1
47080-13	6.20	6.83	6.83	788	53.2	20.0
47097-3	8.27	9.17	9.17	782(804)	72.0	14.4
47097-7	12.41	13.17	13.17	716	102.6	7.4

(a) The burst temperature is the recorded temperature closest to the failure region, however, if it is not the highest temperature recorded along the rod, the highest temperature is listed in parentheses ( ).

Comparison of Transient-Heating Burst Test Data

Because the unirradiated Sandvik material transient-heating tests were performed in vacuum, the results are not included in this comparison. The Oconee I archive tests were performed in steam and the results are plotted in Figure 101. The Oconee I archive test data are from Table 57. The results of the irradiated H. B. Robinson cladding (Lot 1) and irradiated Oconee I, one-, two-, and three-cycle (Lots 2, 3 and 4) cladding are from Tables 56, 57, 58, and 59, respectively. The burst temperature versus burst hoop stress is plotted in Figure 101 for Lots 1, 2, 3, and 4 material. For the purpose of comparison, the curve which was developed from the ORNL unirradiated Zircaloy-4 transient-heating burst test data [1] is also included in Figure 101.

The results of the irradiated transient-heating burst tests were consistantly lower than the ORNL test results, as can be seen in Figure 101, and the ORNL curve appears to be an upper bound for the BCL test data. Little difference in results could be found between H. B. Robinson and Oconee I test results although it appeared, as expected, that the lower heating rates generally resulted in lower burst temperatures at a specific burst hoop stress level.

Also, the data generated for Lots 2, 3 and 4 (Oconee I, one, two and three cycle) material indicated that little effect on the transient-heating burst hoop stress was caused by increasing the neutron exposure from 10,000 to 30,000 MWD/MTU. This was in agreement with results from tensile, tube-burst, and expanding mandrel tests using annealed specimens, which indicated that removal of irradiation damage was essentially complete above annealing temperatures of approximately 700 C. All the results for irradiated cladding fell below the curve generated from data for the unirradiated cladding burst tests performed at ORNL. There were several possible reasons for this observed behavior. The irradiated cladding may exhibit a lower burst hoop stress when compared to unirradiated cladding may exhibit a lower burst hoop stress when compared to unirradiated material because of differences in test equipment or procedures; because of differences in calculating burst temperatures and burst hoop stresses; or because of an irradiation-induced effects.

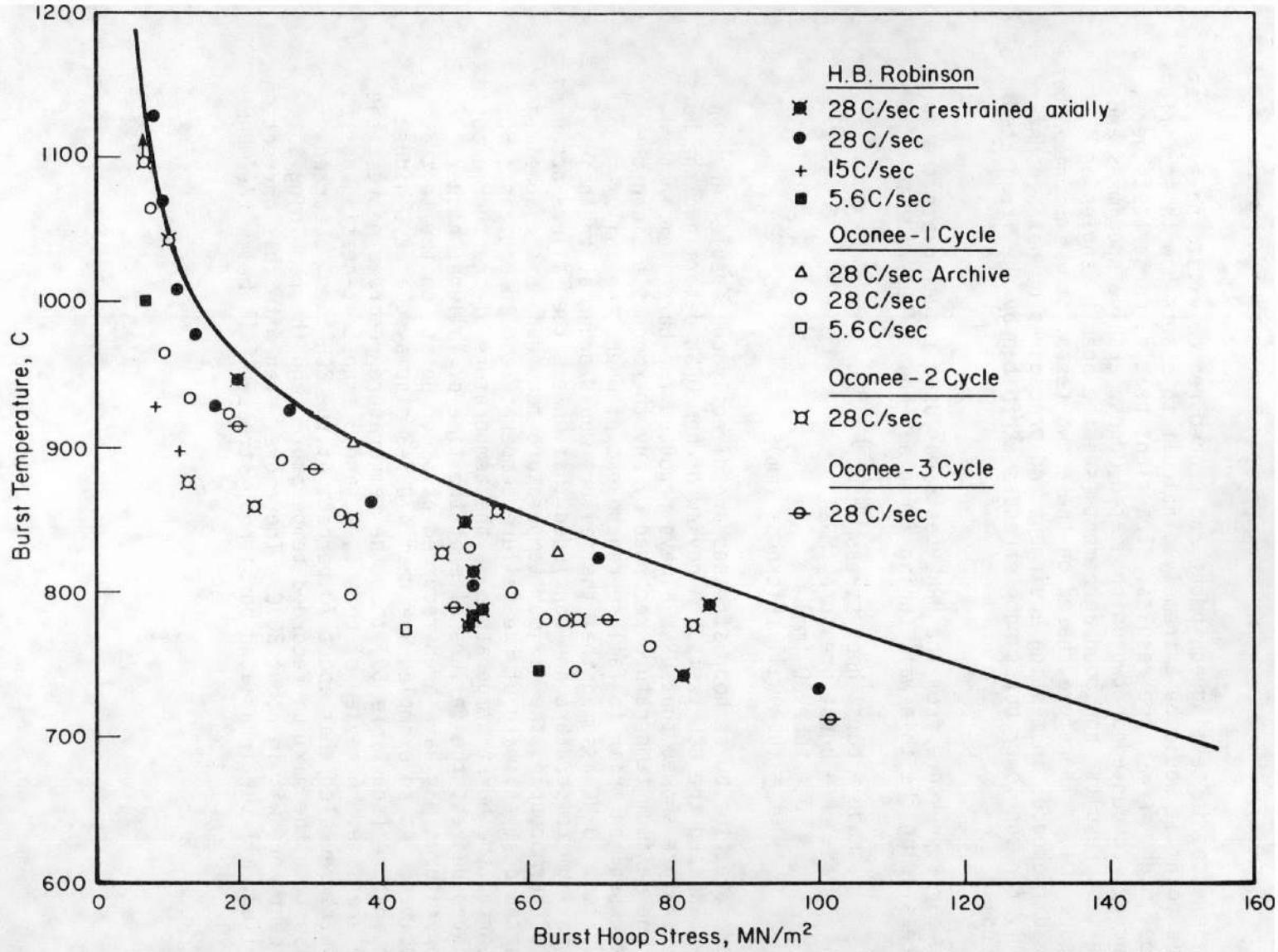

FIGURE 101. TRANSIENT BURST TEST DATA FOR ARCHIVE AND LOTS 1, 2, 3, AND 4 SPENT FUEL CLADDING INCLUDING ORNL CURVE OF UNIRRADIATED TUBING AT 28 C/SEC

Differences in testing equipment and procedures do exist; however, at this point it would be extremely difficult to assess how these differences might affect the results. Transient-heating burst tests were, however, conducted on two unirradiated Oconee archive specimens and the test results show good agreement (see the open triangles on Figure 101). Therefore, based on these two tests, it was assumed that the differences in testing equipment and procedures do not account fully for the lower burst hoop stresses exhibited by the irradiated cladding.

The burst pressure from the ORNL tests was used to calculate the burst stress using the thin wall tubing formula, $\varepsilon_{hoop} = PD/2t$, where

ε_{hoop} = burst hoop stress (MN/m^2)
P = burst pressure (MPa)
D = tube OD (mm)
t = tube wall thickness (mm).

Therefore, the burst hoop stresses are directly comparable for both the ORNL and the BCL tests. A review of how ORNL determined the burst temperature showed that ORNL always reported the burst temperature as the maximum temperature recorded by any thermocouple along the test specimen prior to failure, regardless of where the failure occurred. ORNL assumed that the failure would occur at the point of maximum temperature and concluded that unless the failure occurred on a thermocouple, the maximum temperature recorded on the specimen was the best estimate of the failure temperature. In contrast, BCL reported the burst temperature as the temperature of the thermocouple located nearest the failure site at the time of failure; higher temperatures may have been recorded at other points on the test specimen. As an example, Specimen 47097-3 displayed a 22 C higher temperature (see Table 59) than the temperature recorded nearest the failure site. A review of Lots 1, 2, and 3 transient-heating burst results revealed that about 70 percent of the BCL burst occurred closest to the maximum recorded temperature, and the remaining 30 percent were within about 30 C. Therefore, even with this correction applied, all the irradiated burst hoop stresses fell below the ORNL curve.

It is well known that during irradiation, fuel pellets and cladding interact (PCI) and it is possible that this interaction was the reason for the differences in test results observed between the unirradiated and irradiated test specimens. PCI may also account for the observed scatter in the transient-heating burst stresses when plotted versus burst temperature. A second irradiation-induced effect may be related to the higher stored energy in the highly concentrated dislocation structure of this irradiated Zircaloy. Although residual stresses and point defects were probably annealed out at about 700 C, enough dislocations may have been present and available (if the strain rate was high enough) to be nucleation sites for recrystallization and subsequent grain growth at a lower temperature in this irradiated cladding as compared with unirradiated cladding.

Therefore, at any given pressure, an irradiated cladding specimen with advanced grain growth would be expected to fail at a lower temperature than an unirradiated cladding specimen with a comparatively retarded grain growth. At burst temperatures above 900 C an alpha-plus-beta phase occurred and a very high plasticity was observed. Therefore, the dislocation structure was expected to have little effect on the mechanical properties at very high temperatures. Indeed, from Figure 101 it appears that above 1000 C the burst hoop stress for irradiated and unirradiated cladding were the same. Metallography performed on isothermally annealed H.B. Robinson irradiated cladding (see Metallographic Examination section of this report) showed that recrystallization of the irradiated specimen mirostructure was observed at temperatures as low as 620 C. Recrystallization and grain growth would be expected to result in a lowering of the mechanical strength of the cladding. Since recrystallization of unirradiated Zircaloy cladding would not be expected until higher temperatures were reached, the strength of the unirradiated cladding would be greater than that of the irradiated cladding at temperatures greater than 620 C. Indeed, the results of tensile tests on transient annealed Oconee archive material and the identically annealed irradiated Oconee I cladding test results tended to support this conclusion. Metallography on these unirradiated archive specimens was performed and verified the hypothesis that recrystallization had not occurred until well above the 620 C annealing temperature. Therefore, it appeared that not only was the irradiation induced strengthening recovered by annealing above 620 C, but the strength (stress) fell below that of the similarly annealed unirradiated cladding strength. And only as the temperature approached the alpha-to-beta transition temperature of about 920 C did the strengths of unirradiated and irradiated materials converge. This conclusion is supported by the data presented in Figure 101 and by annealed specimen test results for tensile, burst, and expanding mandrel tests.

DISCUSSION AND CONCLUSION

Analytical and empirical correlations have been or are being developed that are combined into mathematical codes to describe the thermal and mechanical response of fuel rods subjected to postulated off-normal, transient, and accident conditions. A major requirement for use of these codes is a reliable data base. This requirement includes a variety of thermal, physical, chemical, and mechanical properties that influence the Zircaloy cladding behavior under the postulated reactor conditions.

The objective of the proposed program is to provide a mechanical-property data base that can be used to predict the performance of Zircaloy cladding under various off-normal, transient, and accident conditions in a power reactor. The data were developed for both low-temperature off-normal and transient conditions, where the source of cladding loads includes thermal stresses, internal fuel-rod gas pressure, fuel-cladding interaction, and spacer restraint, and for high-temperature accident conditions, where the principal loak is produced by the internal gas pressure. Data were sought for strain-to-failure correlations when burnup is high and a failure is probably due to mechanical interaction at relatively low temperature.

Aside from limited tensile and burst test data, which indicate a general increase in strength and a decrease in ductility, the effects of irradiation on the mechanical properties of Zircaloy are incompletely know. Furthermore, there are several complicating factors in predicting the response of irradiated Zircaloy cladding. The first concerns the effect of increased neutron exposure on property changes and is not well defined. Then, there is the question of annealing of irradiation damage. While recovery of a considerable portion of the irratiation damage can be expected as the temperature is increased, the time-temperature relationship of annealing can profoundly influence response behavior under transient heating conditions. Furthermore, a fuel rod is subject to a unique stress-strain, corrosion, and temperature history over its life that can influence its end-of-life properties, and data illustrating the importance of typical irradiated fuel rod variables are needed. A further source of differences in properties and response of irradiated Zircaloy cladding is the differences in fabrication processes used by the various cladding vendors.

As discussed in the previous paragraph, a number of complicated factors exists that must be considered in interpreting the mechanical properties of irradiated Zircaloy. These include the irradiation exposure level, annealing response, and in-pile and fabrication history. Consequently, material variables that will be evaluated will include mechanical-properties differences, as introduced by various cladding fabricators and fuel-rod burnup or neutron exposure. The annealing response as a function of time and temperature during isothermal annealing, and as a function of heating rate and temperature during transient heating, has also been defined. In addition, individual fuel rods used for test purposes were well characterized as to dimensions, corrosion attack, and possible in-pile distortion or deformation. The purpose of this effort was to establish a basis for choosing a series of test specimens from particular fuel rods or fuel-rod sections and to permit interpretation of scatter in the mechanical-property data that were generated.

Mechanical-property tests are generally intended to simulate the loading and stress conditions encountered by the cladding under postulated off-normal transient and accident conditions. A variety of tests were performed at temperatures up to 700 C. In addition, experiments were conducted to evaluate the annealing of irradiation damage in Zircaloy using hardness, tensile, burst, bend, and expanding mandrel tests in the evaluation. Specimens were annealed under both isothermal and transient heating conditions and tested to determine the time-temperature characteristics of annealing under both types of conditions. Changes in failure strain and in failure pattern and behavior as annealing proceeded were examined. Limited studies were also performed to characterize the annealing behavior of unirradiated Zircaloy cladding.

The mechanical properties of irradiated Zircaloy were determined under uniaxial and biaxial stress conditions encountered by cladding under postulated off-normal, transient, and accident conditions. Claddings of various textures were obtained for the tests from spend commercial fuel rods irradiated to various burnup levels.

The cladding was subjected to detailed examination in order to establish pretest characteristics. As-irradiated strength and ductility characteristics from room temperature to 480 C and at strain rates in the range 0.001 to 2/min were evaluated by tests that included tensile, tube-burst and expanding mandrel. The annealing of irradiation damage was evaluated under both transient and isothermal heating conditions to temperatures of 800 C. Transient-heating burst tests were conducted at temperatures to 1250 C to evaluate cladding behavior under simulated LOCA conditions.

The objective of this program was to provide data concerning the mechanical properties and annealing and burst behavior of irradiated Zircaloy fuel-rod performance under LOCA conditions and during off-normal and transient reactor operation. Cladding from three reactors and fabricated by two vendors was evaluated in the program. The program was then divided into tasks. The first involved material selection and nondestructive testing (NDT) for material characterization. The next was the performance of mechanical-properties tests to characterize the as-irradiated properties of the Zircaloy fuel-rod cladding when tested at room temperature to over 400 C and at strain rates of 0.001 to 2/min (test temperature of 371 C). The third task involved annealing studies to evaluate the effect of transient and isothermal anneals on the strength and inductility of irradiated, annealed, and tested (at nominal temperatures and strain rates) Zircaloy fuel-rod cladding. The fourth task involved conducting transient-heating burst tests of irradiated cladding to 1250 C to determine the cladding response under simulated LOCA conditions. Limited studies using unirradiated cladding material were also conducted (as material permitted) to evaluate the mechanical properties under conditions listed in all four tasks described above.

Unirradiated Zircaloy-4 fuel-rod cladding tubing was obtained from two sources. The unirradiated material acquired early in the program (1976) was sent to Battelle from Oak Ridge National Laboratory (ORNL) and was part of the material supplied to ORNL by Sandvik for the multirod burst test.[1] A limited amount of unirradiated material was acquired later in the program (1978) and was supplied by Babcock and Wilcox (B&W) from their archive stock for the Oconee I commercial power reactor. This archive material was also fabricated by Sandvik. To differentiate between the two unirradiated Zircaloy-4 fuel-rod cladding materials, the material acquired in 1976 was designated Sandvik while that acquired in 1978 was designated Archive.

The PWR-irradiated Zircaloy-4 fuel-rod cladding was supplied by three commercial power reactors. Irradiated fuel-rod cladding material for scoping and preliminary mechanical tests was supplied by one spent fuel rod from the Westinghouse Point Beach reactor. The irradiated fuel-rod cladding material designated Lot 1 was supplied by 27 spent fuel rods from the Westinghouse H. B. Robinson reactor. The remainder of the irradiated fuel-rod cladding material (designated Lot 2 for one cycle of irradiation, Lot 3 for two cycles of irradiation, and Lot 4 for three cycles of irradiation) was supplied by 26 spend fuel rods from the Oconee I reactor.

The characterization of the fuel rod cladding involved visual examination, gamma scanning, spiral profilometry, and eddy-current testing.

The characterization provided the means to assess the general condition of the as-received, irradiated fuel rods and provided evidence of mechanical and chemical interactions to which the rods may have been subjected. This assessment was used to determine the suitability of all of part of the rod cladding for mechanical properties testing and to assess possible differences between various fuel rods and sections of these rods.

The visual examination, special profilometry scans, and eddy-current scans revealed areas that were unacceptable as test specimens either because of visually identified marks on the rod surface, excessive ovality, or eddy-current indications. Highly oval sections of the fuel rods could not be used for tests utilizing insects in the specimens such as expanding mandrel and transient-heating burst tests. Areas with defects or indications of anomalies were also avoided when choosing test specimens. Areas of low flux at the fuel rod ends and at grid spacer locations, as indicated by the gamma scans, were not used for test material and thereby eliminated fluence as a variable parameter.

After the nondestructive characterization, selected rods were destructively characterized. The destructive characterization of the fuel-rod cladding included plenum punch and gas collections, burnup analysis, fluence determinations, microhardness testing and metallographic examination. None of the rods chosen for test material were failed and about 60 percent of the material examined was usable for the mechanical properties tests.

To determine the as-irradiated fuel-rod cladding mechanical properties, the rods were cut into sections and defueled; specimens were then prepared and tested in tensile, tube-burst, expanding mandrel, and bend tests. Tests were conducted in the range from room temperature to 427 C and the mechanical properties were determined as a function of test temperature. Tests were also conducted at strain rates in the range 0.001/min to about 2/min and the mechanical properties were determined as a function of strain rate.

The unirradiated specimens tested in tensile, tube-burst and expanding mandrel type tests exhibit similar trends including a rather smooth decrease in strength (engineering stress) with either an increase in test temperature or a decrease in strain rate. The strains are relatively independent of test temperature up to about 400 C and of strain rates from 0.00r to 2/min for the three types of tests. Above 400 C test temperature, the total strains all tend to increase with increased test temperature except for the expanding mandrel tests. It is felt that the independence of strains on either test temperature or strain rate in expanding mandrel tests is because of the high

stress concentrations at the mandrel edges and these concentrated stresses produce the relatively constant strains to failure. However, in the tensile and tube-burst tests, the total strains increase rapidly between 316 and 427 C. The important facts to note here are that for the unirradiated cladding material, yield and ultimate stresses decrease rather smoothly as the test temperature is increased, the total strains begin to increase above 400 C, and the uniform strains are essentially uneffected by either test temperature or strain rate.

A comparison of mechanical properties for irradiated specimens of both H. B. Robinson and Oconee I fuel rod cladding in tensile, tube-burst and expanding mandrel tests showed that irradiation increased the stress values and decreased the strain values at a particular test temperature or strain rate. However, the trends of both the unirradiated and irradiated curves are the same and the rapid increase in the total strains between 300 and 400 C are attributed to recovery, relaxation of residual and irradiation induced stresses, and defect motion and agglomeration. One possible explanation for the observations in the mechanical properties of Zircaloy-4 is dynamic strain aging. Strain aging occurs in zirconium and many of the zirconium alloys. Identical behavior as observed in the Oconee and H. B. Robinson fuel rod cladding tensile properties were observed by Veevers, et al (5), during the hot tensile testing of Zircaloy-2 in the temperature range from about 200 to 500 C. Keeler (6) observed an increase in the flow stress in zirconium at 300 C in interrupted tensile tests. Kallstrom and Svenzon (4) found dynamic strain aging occurred in the range 400 to 500 C during hot tensile testing of Zircaloy-2 and believed the strain aging was caused by dissolved elements interacting with both mobile and immobile dislocations. Also, they found that the strain aging was accompanied by a low strain rate sensitivity. Note that the Oconee and H. B. Robinson cladding also exhibit a relatively low strain rate sensitivity. A variety of mechanisms have been proposed to account for the strain aging. The formation of tin-rich precipitates (7), segregation of hydrogen (8), Cottrell locking of dislocation-interstitial interaction as with oxygen (5) have all been proposed.

In tensile tests at 482 C, it was found that the increase in stress with increased strain rate was more pronounced than tensile tests conducted at 371 C; the strains remained relatively unaffected by strain rate over the range from 0.004 to 2/min.

Bend tests were conducted using irradiated H. B. Robinson and Oconee I (one cycle) material (Lots 1 and 2) and unirradiated Oconee I archive material. Bend test strength measurements show effects similar to those in tube-burst and expanding mandrel tests when the

test temperature was increased. A greated degree of irradiation strengthening for the cladding from the higher burnup H. B. Robinson as compared with Oconee spent fuel rods was also evident from the bend test results. However, little information concerning cladding ductility was produced from the bend tests except for the significant observation that the cladding was highly ductile in bending. Specimens were routinely bent to a 10 cm radius of curvature, and smaller, without producing failure. Therefore, no further bend tests were conducted.

To determine the fuel-rod cladding mechanical properties after transient and isothermal annealing, the rods were cut into sections and defueled; specimens were then prepared for tensile, tube-burst or expanding mandrel testing. Each specimen was either transient annealed or isothermally annealed. The specimens were then tested in tensile, tube-burst or expanding mandrel tests at 371 C and at the appropriate nominal strain rate. A limited study to determine the mechanical properties caused by annealing was conducted using unirradiated Sandvik and Oconne I archive fuel-rod tubing. The tubing was tested in tensile, tube-burst and expanding mandrel tests. The results of these tests and tests using irradiated fuel-rod cladding were then compared. Some differences in absolute stress and strains values for the two types of unirradiated material reflect the differences in fabrication, cold working and stress relieving. However, it was first noted that the unirradiated materials which were transient annealed exhibited no indications of stress peaking or strain minimums which were so prominent in the curves for irradiated and transient annealed fuel-rod cladding. The Oconee I archive material had a general decrease in total strain as the transient temperature was increased but showed a peak at 704 C and a continued decrease at higher annealing temperatures which was not exhibited by the Sandvik tubing. The reason for this peak in total strain appears to be associated with the onset of recrystallization and a similar increase was seen to occur in the irradiated Oconee I material but at a slightly higher transient annealing temperature. The total strain values also remained high for higher annealing temperatures. The irradiated H. B. Robinson material also exhibits a rapid increase in total strain at between 700 and 800 C and also remain high at higher annealing temperatures. Several extremely important facts emerge from the transient annealing and testing data.

(1) The stress values peaked at transient annealing temperatures between 350 and 600 C if the heating rate is greater than or equal to 14 C/sec. This peaking of stress suggests a thermal aging process possibly involving interactions between impurity atoms and irradiation induced defects. Overaging also appeared to occur rapidly as recovery processes associated with defect agglomeration proceeded at transient annealing temperatures below 600 C.

(2) Perhaps of greatest significance is the fact that the recovery of ductility (increase in strain) lagged the decrease in strength (strain) in the irradiated fuel-rod cladding but the recovery of stress and strain appeared to begin at the same transient annealing temperature for unirradiated fuel-rod tubing. The data indicate that for irradiated fuel-rod cladding. Only after recovery, as measured by stress decreases, was essentially completed does the total strain values recover to those characteristic of the as-irradiated specimens This lag suggested that the defect arrays produced during irradiation and possibly defect agglomeration during annealing at temperatures between 400 and 600 C serve as crack nucli to initiate premature failure during plastic straining. Whether this was the mechanism for decreased ductility is uncertain, but such an explanation would be consistant with the fact that ductility recovery significantly lagged the recovery in strength properties.

(3) Another significant observation is the fact that, at least for the transient annealing temperature range chosen for these tensile tests, once recovery occurred, the ultimate and yield stresses dropped below those of unirradiated tubing and the uniform and total strain increased above those of the unirriadiated tubing values at the same transient annealing temperature. This suggested that because of increased nucleation sites at irradiation-induced defects, the grain structure of the irradiated and annealed material was finer and, therefore, the material had somewhat lower strength and higher ductility after annealing, as compared with unirradiated material.

(4) The data from tensile and tube-burst tests of annealed specimens from Lots 2, 3, and 4, irradiated for one-, two-, and three-cycle in the Oconee I reactor, indicate that the strengths peaked or saturated at between 20,000 and 30,000 MWD/MTU.

(5) For Lot 1 fuel-rod cladding annealed and tensile tested, an apparent change in anisotropy accompanied annealing. The tube-wall and tube-diameter reduction measurements indicated that the wall reduction exceeded the diametral reduction in the as-irradiated fuel-rod cladding and was reversed after annealing. Thus, irradiation appeared to produce a more isotropic acting material, and annealing caused a return to the anisotropic behavior characteristic of unirradiated cladding.

(6) The effects of isothermal annealing on the mechanical properties in tensile, tube-burst and expanding mandrel tests were similar and the mechanical property versus annealing time curves exhibited similar trends. The changes in properties were caused primarily by recovery, recrystallization, and grain growth. However, the exact manner in which the material properties change was related to a complicated interaction of residual stresses, number of defects, defect structure, microstructure,

temperature, and time. In general, however, at annealing temperatures above 700 C, irradiated Zircaloy-4 fuel-rod cladding is fully annealed and exhibits little or no changes for annealing times up to 60 minutes. Between annealing temperatures of 600 and 700 C, the irradiated cladding is fully annealed after an annealing time of about 1 minute. Between annealing temperatures of 400 and 600 C, it appears that if the annealing time is sufficiently long, the irradiated fuel-rod cladding would be fully annealed and all effects of irradiation would be annealed out. Below about 400 C, little or no change occurs for annealing times as long as 60 minutes.

(7) A final correlation became apparent when the mechanical properties results from the tensile, tube-burst, and expanding mandrel tests were compared. All the tests results exhibited the same trends after being transient or isothermally annealed and tested at 371C and at nominal strain rates. Figures 102 and 103 are comparisons of the data for H. B. Robinson tests of specimens transient annealed at 28 C/sec and 5.6 C/sec. Figure 104 is a comparison of the data for Oconee I (one cycle) tests of specimens transient annealed at 28 C/sec. Figures 105, 106 and 107 are comparisons of the data for H. B. Robinson tests of specimens annealed at three different temperatures, 538, 593 and 704 C for annealing times to 30 minutes. These figures show that essentially the same type of data and trends were obtained from all three tests. Because of this, annealing of tensile and expanding mandrel specimens was dropped and emphasis was placed on the tube-burst annealing test data. Selected annealing tests were conducted, however, to obtain absolute values for tensile and expanding mandrel stresses and strains for specimens transient and isothermally annealed.

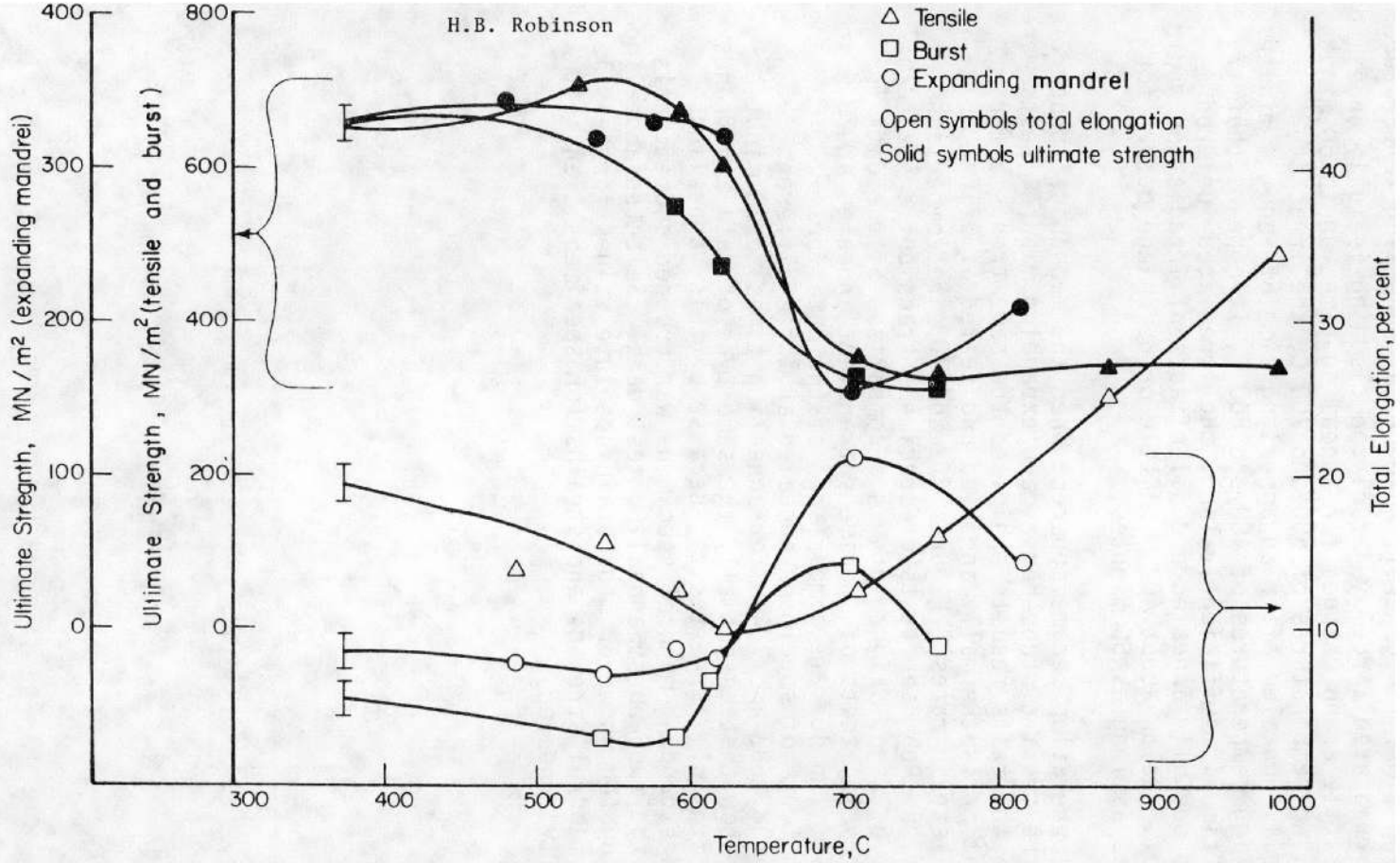

FIGURE 102. DEPENDENCE OF ULTIMATE STRENGTH AND TOTAL ELONGATION AS MEASURED IN IN TENSILE, TUBE-BURST AND EXPANDING MANDREL TESTS ON MAXIMUM TEMPERATURE ACHIEVED UNDER TRANSIENT ANNEALING CONDITIONS

Test temperature 371 C, heating rate 28C/sec.

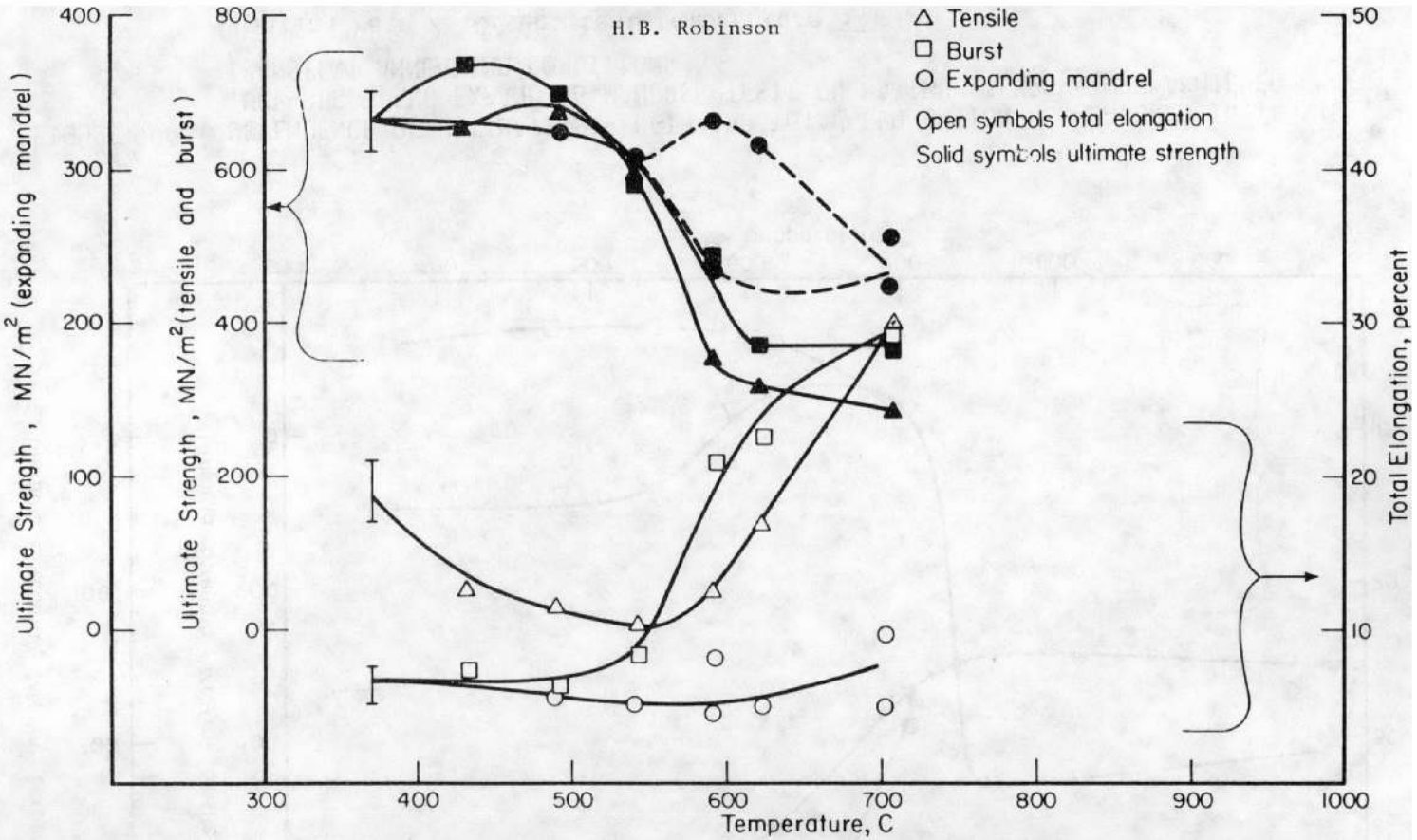

FIGURE 103. DEPENDENCE OF ULTIMATE STRENGTH AND TOTAL ELONGATION AS MEASURED IN TENSILE, TUBE-BURST AND EXPANDING-MANDREL TESTS ON MAXIMUM TEMPERATURE ACHIEVED UNDER TRANSIENT ANNEALING CONDITIONS

Heating rate 5.6 C/sec; test temperature 371 C.

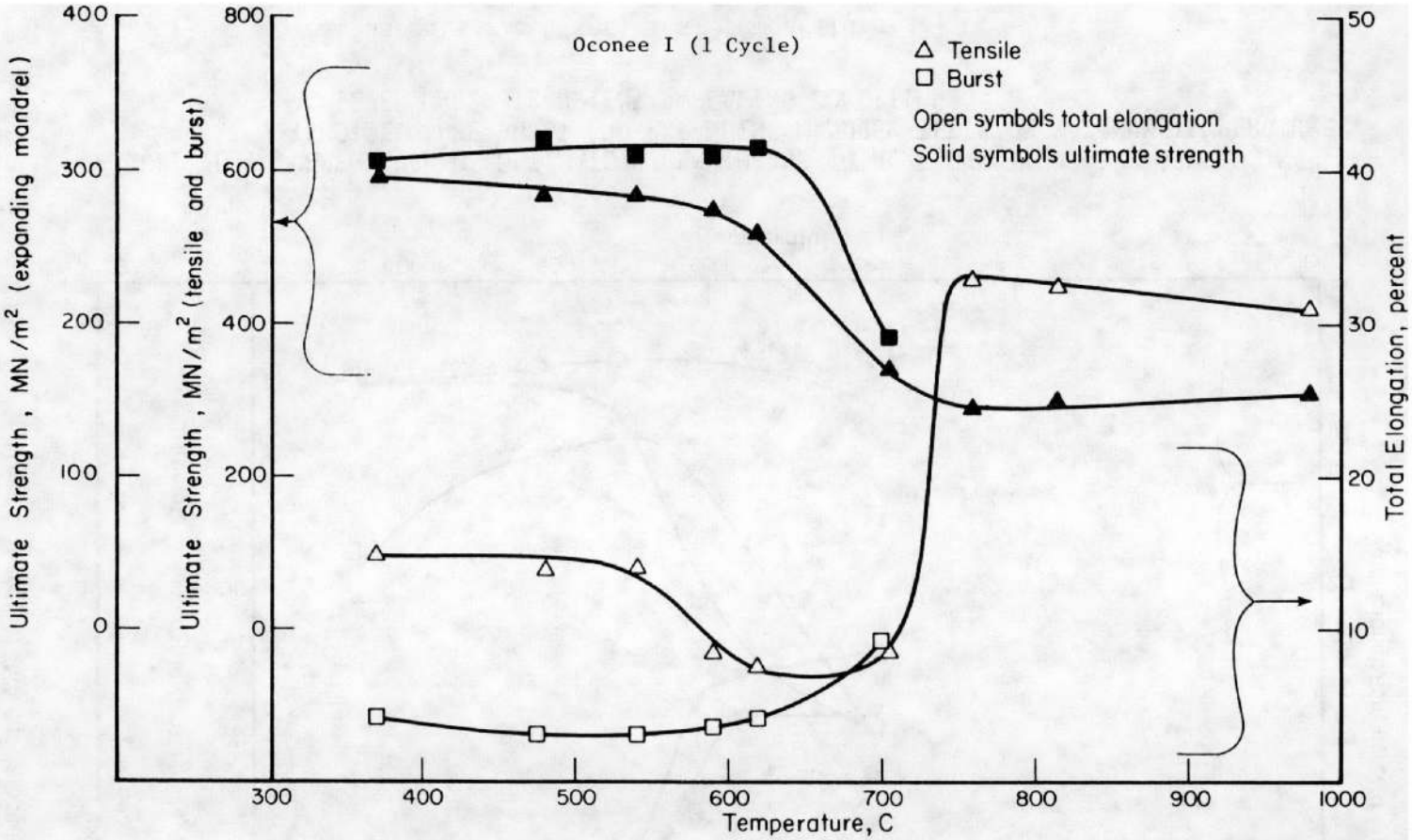

FIGURE 104. DEPENDENCE OF ULTIMATE STRENGTH AND TOTAL ELONGATION AS MEASURED IN TENSILE, TUBE-BURST AND EXPANDING-MANDREL TESTS ON MAXIMUM TEMPERATURE ACHIEVED UNDER TRANSIENT ANNEALING CONDITIONS

Heating rate 28 C/sec; test temperature 371 C.

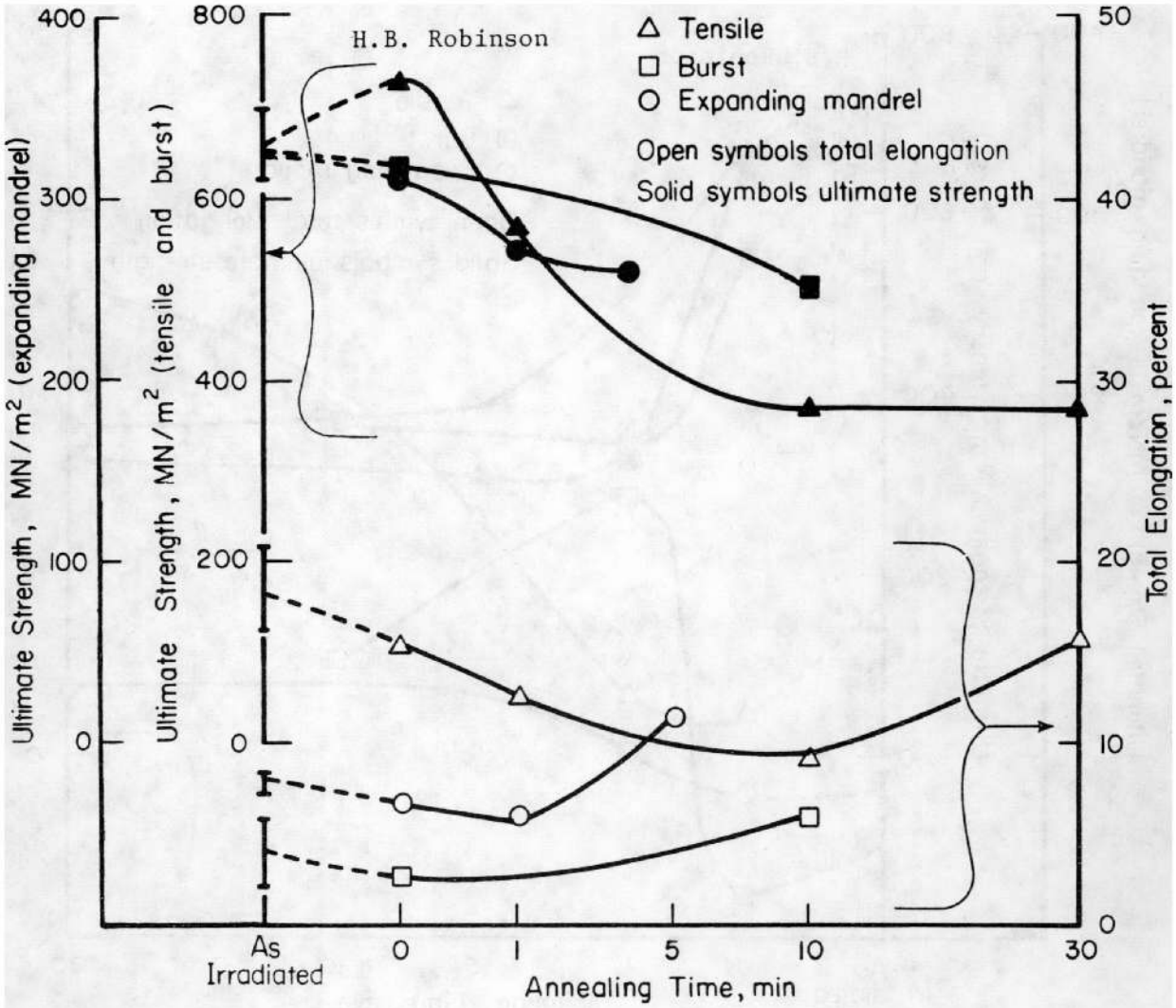

FIGURE 105. DEPENDENCE OF ULTIMATE STRENGTH AND TOTAL ELONGATION AS MEASURED IN TENSILE, TUBE-BURST AND EXPANDING MANDREL TESTS AT TEMPERATURE UNDER ISOTHERMAL ANNEALING CONDITIONS

Heating rate 28 C/sec; annealing temperature 538 C; test temperature 371 C.

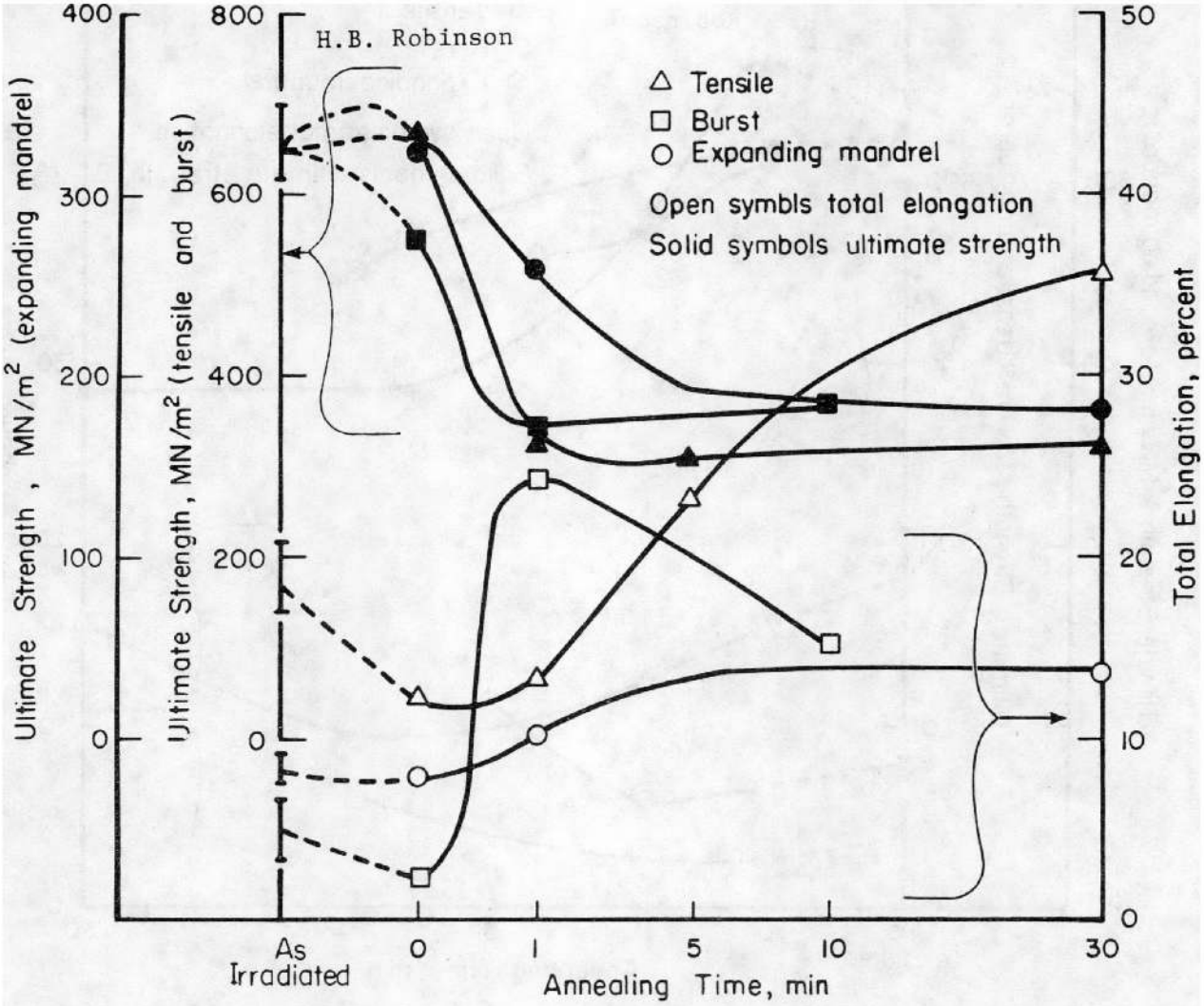

FIGURE 106. DEPENDENCE OF ULTIMATE STRENGTH AND TOTAL ELONGATION AS MEASURED IN TENSILE, TUBE-BURST AND EXPANDING MANDREL TESTS ON TIME AT TEMPERATURE UNDER ISOTHERMAL ANNEALING CONDITIONS

Heating rate 28 C/sec; annealing temperature 593 C; test temperature 593 C.

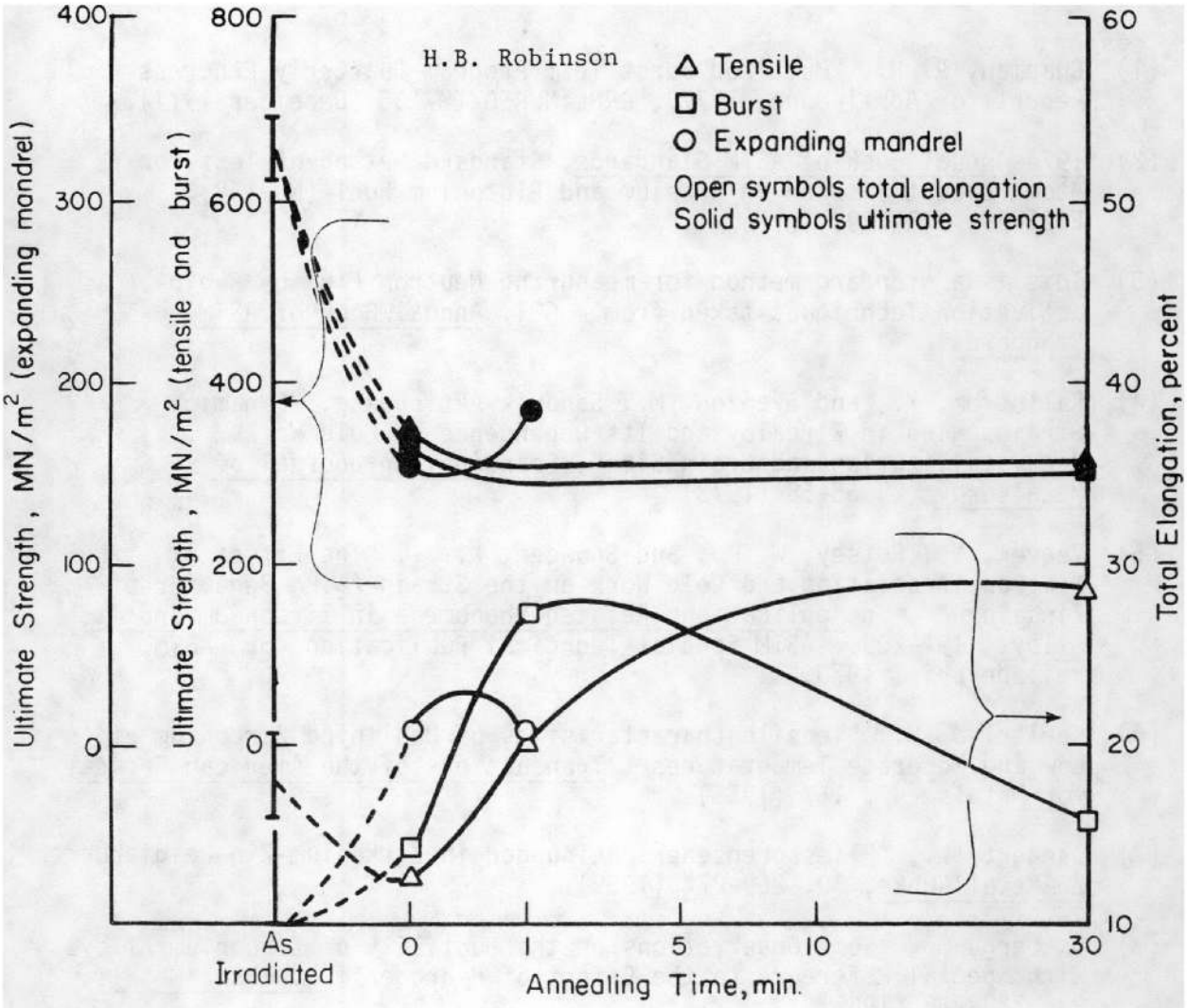

FIGURE 107. DEPENDENCE OF ULTIMATE STRENGTH AND TOTAL ELONGATION AS MEASURED IN TENSILE, TUBE-BURST AND EXPANDING MANDREL TESTS ON TIME AT TEMPERATURE UNDER ISOTHERMAL ANNEALING CONDITIONS

Heating rate 28 C/sec; annealing temperature 704 C; test temperature 371 C.

REFERENCES

(1) Chapman, R. H., "Multirod Burst Test Program Quarterly Progress Report for April-June, 1977", ORNL/NUREG/TM-135 (December 1977).

(2) 1974 Annual Book of ASTM Standards, Standard Method of Test for Atom Percent Fission in Uranium and Plutonium Fuel (Nd-148), E321-69, 721-729.

(3) This is a standard method for measuring Neutron Flux by Radio-activation Techniques taken from # 621, Annual Book of ASTM Standards.

(4) Kallstrom, K., and Svenzon, M., Sandvik Aktiebolag, "Dynamic Strain Aging in Zircaloy and Its Dependence on Cold Work, Recrystallization and Grain Size", Scandinavian Journal of Metallurgy, 2, 55-58 (1973).

(5) Veever, K., Rotsey, W. B., and Snowden, K. J., "The Effect of Neutron Irradiation and Cold Work on the Strain-Aging Behavior of Zircaloy-2", in Applications-Related Phenomena in Zirconium and Its Alloys, 194-209. ASTM Special Technical Publication 458, ASTM, Philadelphia, 1970.

(6) Keeler, J. H., "Tensile Characteristics of Unalloyed Zirconium at Low and Moderate Temperatures", Transactions of the American Society for Metals, 47, 157 (1955).

(7) Bangert, L., "Fliessgrenzenerscheinungen in Zirkonium-Zin-Leigierungen", Z. Metallkunke, 50, 269-274 (1959).

(8) Ostberg, G., "Some Observations on the Ductility of Zirconium Alloys With Special Reference to the Effect of Hydrogen", J. Inst. Metals, 93, 223-228 (1965).

APPENDIX A

A FULL DESCRIPTION OF EQUIPMENT AND PROCEDURES FOR GAMMA SCANNING, SPIRAL PROFILOMETRY, AND EDDY-CURRENT TESTING

Gamma Scanning

The primary objective of gamma scanning is to measure gross gamma activity (> 0.5 MeV) along the length of a fuel rod and to determine fuel column length. The level of activity is related to the cladding thermal neutron exposure and to fuel burnup and can be used to provide comparative burnup data. Secondarily, fuel-column gaps or areas of unusual gamma activity can be distinguished.

Equipment

The scanner utilizes two 5.5-m precision ball screws. Over the scanning length of 5 m, the bias is +3.33 mm; the manufacturer's tolerance is ± 0.0178 mm per thread and each thread has a 6.4-mm pitch. A crosshead spans the ball screws and moves the rod holder past a slit collimator. The screws are driven by a dc motor, continuously variable from 0 to 1750 rpm, that has a 1 percent accuracy (± 5 rpm at 500 rpm and ± 17.5 rpm at 1750 rpm).

The rod guides hold the rod at a fixed distance of 16.5 ± 0.076 mm from the face of the slit collimator. The collimator is a lead plug with a Mallory 1000 insert that forms a slit 1.9 cm wide and 20 cm long with a variable height of 0 to 3.2 mm.

Lead collimating rings are positioned between the slit collimator and the 7.6 cm NaI (Ta) counting crystal. The distance between the slit collimator and the crystal is variable from 0 to about 1.5 m and is dictated by the rod-activity intensity.

Procedures

The signal from the NaI crystal is fed to amplifiers and to an analyzer that can be used as a single-channel analyzer or as an analyzer that records all counts above a specified level. The single-channel analyzer records all counts in an energy window. For the measurements made, the analyzer operates with a low-level discriminating circuit that enables all counts of energy greater than a specified energy to be recorded, e.g., energies $\geq$ 0.5 MeV.

A count-rate signal is fed to one pen of a dual-pen, quick-response, variable-speed recorder. A chart tick marker activates the second pen and indicates rod-scanning intervals of 1.6 mm. Therefore, axial rod location can be determined to within ± 0.8 mm.

Prior to scanning a fuel rod, the gamma-energy low-level discriminator is set using calibration sources. The most active rod is then loaded into the rod holder, the counting crystal is positioned and the collimator slit width adjusted to obtain a reasonable count rate. Each rod is scanned in turn from top to bottom in a single pass at a rate of 50 ± 0.8 mm/min. Figure A-1 is a typical (Rod D-4) gamma scan.

Spiral Profilometry

Spiral profilometry is performed for fuel rod diametral measurements and for detection and characterization of local cladding anomalies such as blisters, depressions, and ovality.

Equipment

The profilometer consists of in-cell support apparatus and sensing heads and out-of-cell recording equipment. The in-cell portion of the profilometer is a precision device for holding and rotating the rod while the sensing heads transverse the length of the fuel rod section. The rods are held vertically and axially stationary in the rotating chuck for scanning. For each revolution of the rod, the transducer sensing heads move 3.2 mm axially yielding a spiral trace of the rod. The travel of the sensing heads is approximately 1.1 m, so the rods are scanned in overlapping segments and axially repositioned after each segment. Overlap reference scribe marks are made at 0.9, 1.8, 2.7, and 3.6 m along the fuel rod length. All but the top 13 to 15 cm of rod can be scanned in this manner. The sensing devices are two opposed linear variable differential transducers (LVDT). Each LVDT is mechanically driven by a sensing-head assembly which floats in an air-bearing chamber. The sensing heads which ride directly on the rod are 3.2 mm diameter sapphire rods.

The transducer outputs are fed into the out-of-cell electronics which consist of a Type 72 Two Channel Differential Transformer Input Module and a strip-chart recorder. The output of a Model 300 D Transducer Amplifier-Indicator is fed into one side of a Honeywell Two-Pen, Two-Inch-Chart, 30 mv Single Span Recorder to give a permanent trace of the LVDT signals. The other side of the recorder is used to place a "tick" mark on the chart. Each tick mark represents 2.5 mm of travel along the profiled rod segment. The sensitivity of the Differential Transformer Input Module is adjusted so that a mechanical displacement of

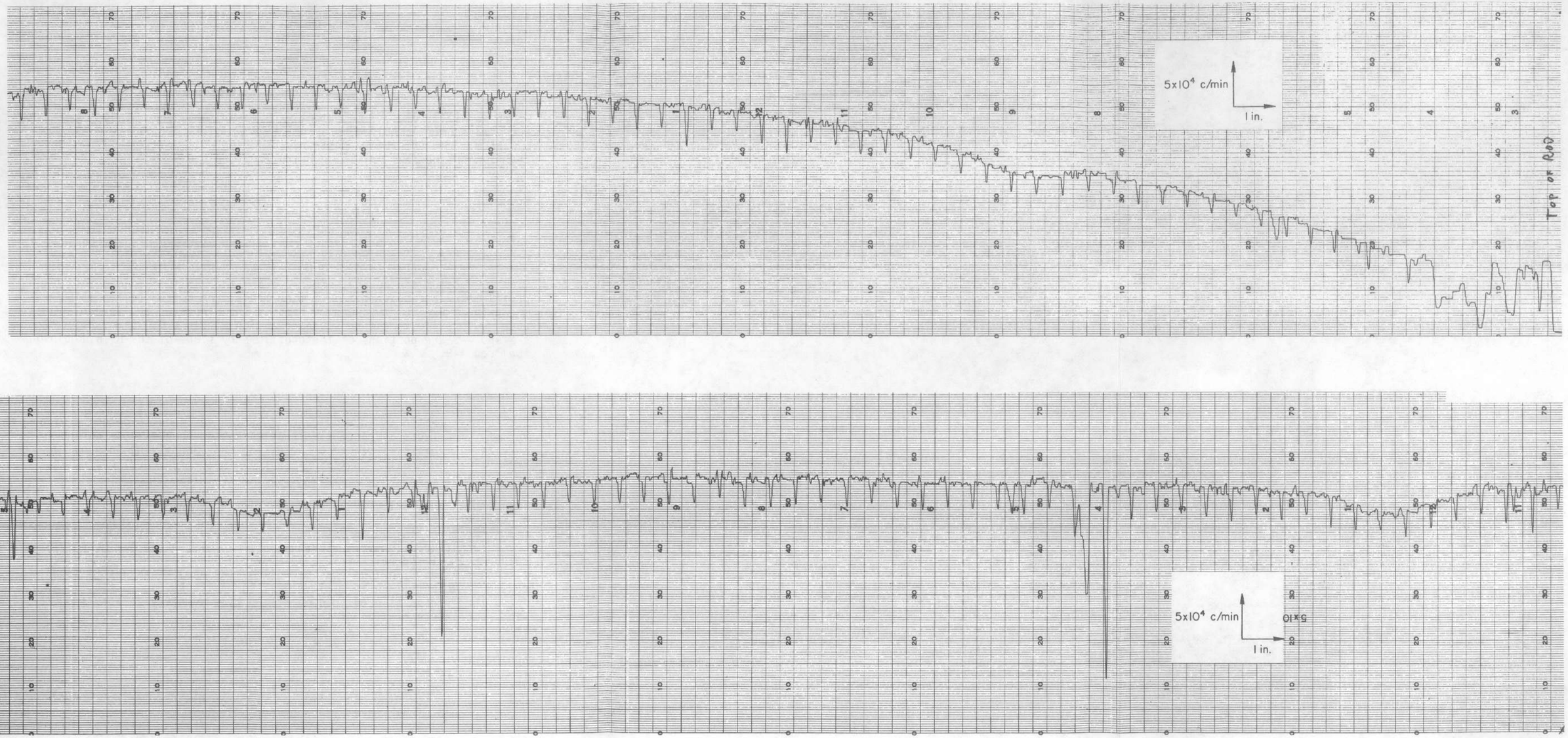

FIGURE A-1. TYPICAL PORTIONS FROM GAMMA SCAN OF H. B. ROBINSON ROD D-4

0.025 mm will yield 2.5 mV output from each transducer. Thus, when each transducer is nulled on a rod of known diameter, variation of ± 0.25 mm from this known reference diameter will be displayed on the chart, with one chart division being equal to 0.005 mm.

Procedures

Each rod is cleaned with an acetone-soaked paper wipe to remove loose materials. Prior to profiling a rod, a step standard of diameters above and below the fuel rod nominal diameter is run for calibration. Each rod is scribe marked at 0.9, 1.8, 2.7, and 3.6 m positions as measured from the bottom of the rod. The rods are then in turn loaded into the profilometer and scanned in 0.9-m segments from bottom to top at 50 mm/min axial travel of the sensing heads. The step standard is run after each rod profile to assure standardization within ± 0.005 mm. Figures A-2 and A-3 are portions of the profilometry scans of the H. B. Robinson fuel rod A-8.

Eddy-Current Testing

Rods are inspected in an eddy-current system designed to detect a wide variety of defects and anomalies that can occur in fuel rods during service. Emphasis is placed on detecting and identifying internal defects given the basic constraints of the single-frequency, encircling-coil type of eddy-current system.

The defects and fuel rod conditions of interest cover a variety of types and geometrical configurations. The eddy-current system provides a means for detecting these defects by using both in-phase and quadrature phase-sensitive detectors. These signal outputs, often called absolute readouts, indicate relatively gradual variations in electrical properties associated with fuel rods as well as the abrupt changes in signals caused by defects such as small holes, short cracks, and pitted areas. These three readouts used in combination help identify defects and provide some interpretation of the signal indications.

Equipment

The eddy-current system consists of three basic parts: (1) the test coil, (2) the scanning mechanism, and (3) the electronic instrumentation. Each of these parts is described below.

(1) The test coil is the type that encircles the fuel rod. It is wound on a Lucite bobbin having a 11.7-mm-diam center hole that

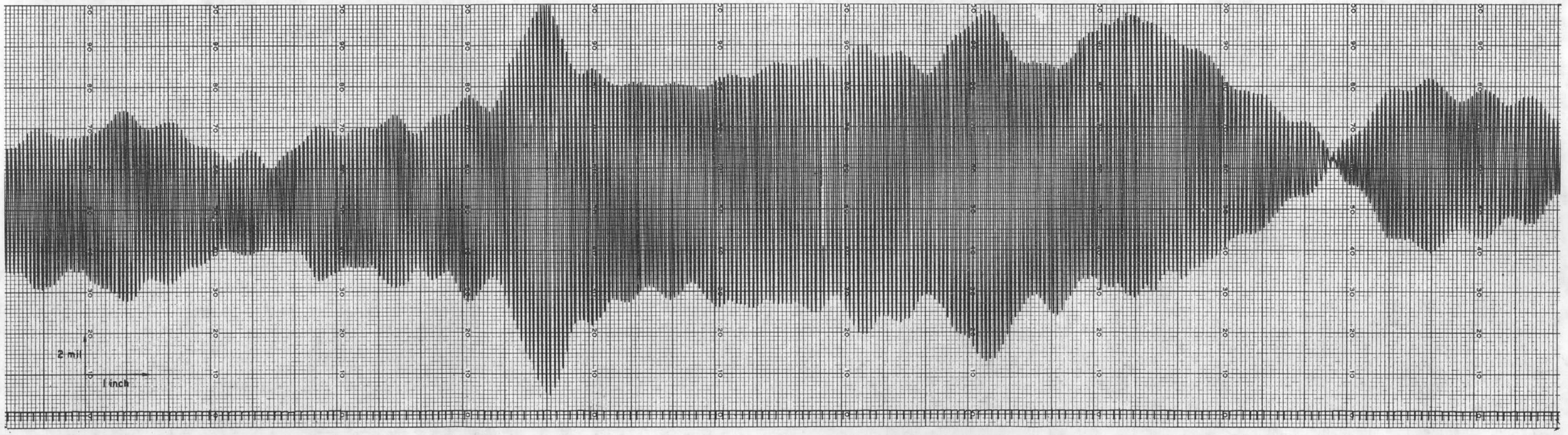

FIGURE A-2. PORTION OF H. B. ROBINSON ROD A-8 PROFILOMETRY CHART SHOWING EXTREME OVALITY

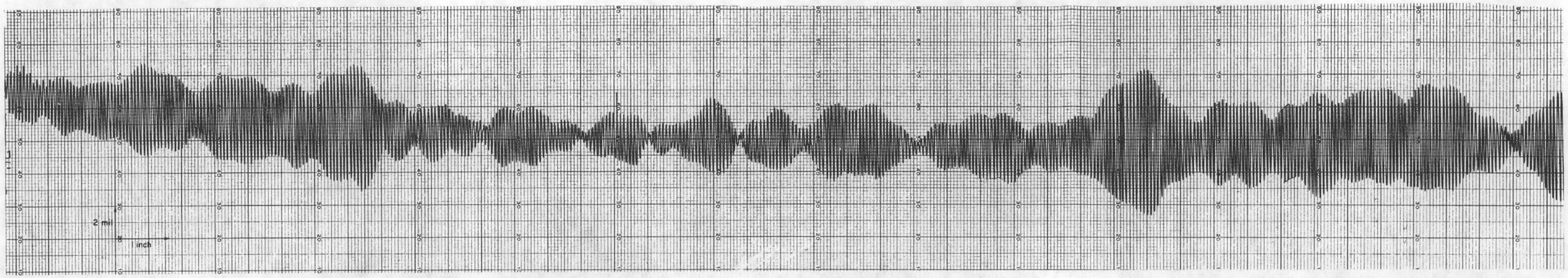

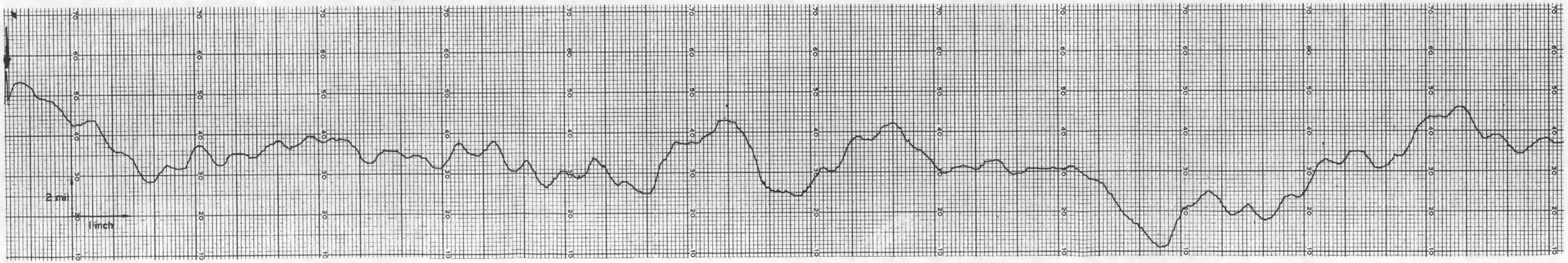

FIGURE A-3. ILLUSTRATIONS OF SPIRAL AND STRAIGHT PROFILOMETRY SCANS OVER SAME REGION FOR H. B. ROBINSON ROD A-8

encircles the rod. The bobbin contains a groove that is 0.51 mm wide and machined to within 0.25 mm of the center hole. The coil consists of 31 turns of Number 40-gage insulated copper wire. This design provides good sensitivity and resolution but with enough clearance to scan rods that have heavy crud and appreciable ovality.

(2) Scanning of the fuel rod is facilitated by sliding it through two open-ended chucks, with the test coil located between the chucks. The test coil is moved in the X direction (right to left), while the fuel rod is held fixed by the chucks. The bobbin is attached to a pivot mechanism that allows the coil to move in the y (horizontal) and z (vertical) directions. This compensates for curvature in the rod and eccentric crud buildup. The scanning mechanism is driven by turning a long, threaded shaft at a constant rate. The test-coil pivot is attached to a threaded plate that is also supported by two guide shafts. The test coil moves at an approximate linear speed of 51 cm/min. A limit switch is shorted by a cam for each revolution of the threaded rod. This provides a tick mark on the chart recording for every 1.6 mm of test-coil travel of the fuel rod.

(3) Figure A-4 is a block diagram of the essential parts of the eddy-current instrumentation. The heart of the system is the NDT-6 eddy-current instrument that can be operated with either single or dual encircling and probe type test coils. The NDT-6 provides sinusoidal test-coil energization at frequencies ranging from 1 to 2,000 kHz and phase-sensitive detection for in-phase and quadrature readout for any of these frequencies. The in-phase component is selectable over a range of 360 degrees.

Each fuel rod is scanned using the following instrument settings:

Test-coil excitation frequency	400 kHz
Phase rotation	263.5 (arbitrary)
Signal amplifier gain	200 (high scale)
Scanning speed	51 cm/min

Procedures

The rods are inspected in 0.9-m portions by the scanning mechanism. Circumferential marks are scribed in the cladding every 0.9 m to provide reference indications on the chart recording. Defective areas on the fuel rod corresponding to signal indications on the chart can be located with an accuracy of ± 1.6 mm.

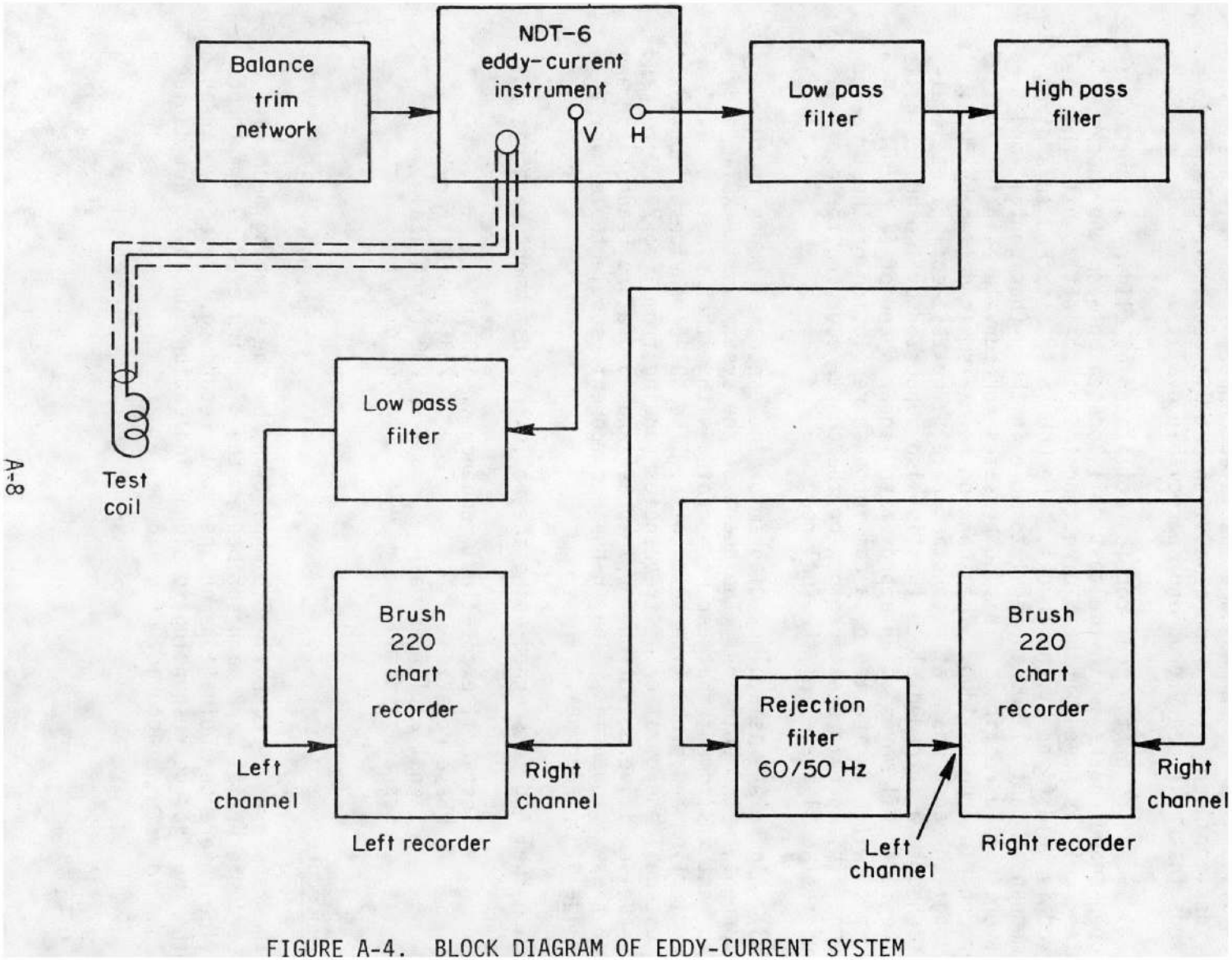

FIGURE A-4. BLOCK DIAGRAM OF EDDY-CURRENT SYSTEM

APPENDIX B

A FULL DESCRIPTION OF EQUIPMENT AND PROCEDURES FOR PLENUM PUNCH AND GAS COLLECTION, BURNUP ANALYSIS, FLUENCE DETERMINATION, MICROHARDNESS TESTING, METALLOGRAPHIC EXAMINATION, AND ANNEALING OF CLAD

Plenum Punch and Gas Collection

The purpose of plenum punch and gas collection is to determine the rod void volume and to collect the rod's internal gases for isotopic analysis.

Equipment

Gases are collected from the fuel rod using an in-cell puncturing device and an out-of-cell collection system. Following puncturing and measurement of the stabilized system pressure, the gases are collected into metal bulbs using a Teopler pump. The fuel rod's internal gas pressure is calculated using the measured volume of the collected gas and the internal rod volume.

Procedures

The procedure involves the following steps. A fuel rod is inserted through a gastight punch chamber that is sealed with Teflon seals and brass nuts at each end of the chamber. The entire system--punch chamber, expansion system, pressure gages, and collection system--is evacuated to a few microns pressure (generally < 5). After leak rates are established for both the in-cell and out-of-cell portions of the system, the system is again evacuated, the punch-system pressure is recorded along with in-cell punch-chamber temperature and collection-vial temperature, and the rod is punctured. Pressure readings are recorded at the time of puncture and at 2- and 5-min intervals thereafter until the system equilibrates. The rod gas is expanded into a calibrated volume and a second pressure reading is recorded. From these data and the rod void volume measured in a subsequent operation, the amount of gas contained in the rod can be calculated.

To calculate the internal void volume, the punch chamber and evacuated rod are pressurized with 552 kPa helium which is subsequently expanded into a calibrated volume. A series of ten measurements are performed to obtain maximum accuracy and precision. Similar measurement of the puncture chamber volume is performed before puncturing the rod. The

difference between the rod plus punch-chamber volume and the punch-chamber volume only is the rod internal void volume.

Burnup Analysis

Burnup analysis is performed by the mass-spectrometric neodymium-148 method. The samples are dissolved in 12 N HNO_3-1.0 N HF and diluted appropriately. Burnup calculations are performed according to ASTM method E321-69, where the total percent fission of heavy element atoms is:

$$F_T = \frac{F^1 \times 100}{U^1 + P^1 + F^1} \quad ,$$

where

F^1 = the number of fissions per atom of U-238
U^1 = the total uranium atoms per atom of U-238
P^1 = the total plutonium atoms per atom of U-238.

A U-235 thermal fission yield for Nd-148 of 1.68 percent is used in the calculations. The percent fission heavy-element atoms, F_T, is accurate to ± 2 percent. Converting to burnup in megawatt days per metric ton introduces additional error in that MWD/MTU = $F_T \times 9.6 \pm 0.3 \times 10^3$.

Fluence Determination

Cladding samples in the form of rings are sectioned from the irradiated fuel rods to analyze and to determine the fast-neutron flux and fluence. Prior to analysis, the cladding samples are mechanically defueled, then cleaned in nitric acid to remove any adhering fuel. They are further cleaned in boiling hydrochloric acid for corrosion-product removal. The samples are chemically analyzed for iron content and radiochemically analyzed for Mn-54 activity. The fast neutron flux is then calculated from the Fe-54 (n,p) Mn-54 reaction using the following equation:

$$A = N_0 \sigma^f \phi^f (1-e^{-\lambda t_i})(e^{-\lambda t_w}) \, ,$$

where

A = disintegrations of ^{54}Mn per sec

N_o = atoms of ^{54}Fe in original sample

σ^f = mean fission-spectrum cross section for the reaction, cm^2

ϕ^f = total neutrons/cm^2-sec in the fission spectrum

λ = ^{54}Mn decay constant = 0.693/314 day half-life

t_i = time of irradiation, days

t_w = time between reactor shutdown and counting time, days.

The Fe-54 (n,p) Mn-54 activation cross section (averaged over the fission spectrum) is reported as 75 millibarns (mb) (ASTM E261). Since 69.2 percent of the fission spectrum lies above 1 MeV, the activation cross section that was used to calculate the flux above 1 MeV corresponding to the above fission-averaged cross section is:

$$\sigma^f\ (E > 1\ \text{MeV}) = \frac{\int_0^\infty \sigma(E)\ f\ (E)\ dE}{\int_{1\ \text{MeV}}^\infty f\ (E)\ dE} = \frac{75\ \text{mb}}{0.692} = 108\ \text{mb}$$

The flux above 1 MeV is then calculated from the activity using

$$\phi\ (E > 1\ \text{MeV}) = \frac{A}{N_o(0.108 \times 10^{-24})(1 - e^{-\lambda t_i})\ e^{-\lambda t_w}}\ .$$

This flux is then reported "in terms of the Fe-54 (n,p) Mn-54 fission-spectrum averaged cross section of 75 mb". The flux, computed from a given measured activity, is thus seen to be dependent upon the cross-sectional value used. In particular, the use of the fission-spectrum averaged cross section will introduce errors into the measurement of fluences whose spectra differ markedly from that of the fission spectrum. It is assumed that the fission spectrum distribution is representative.

Microhardness Tests

The purpose of microhardness measurements is to determine average hardness or hardness gradients of irradiated materials.

Equipment

A Tukon Microhardness Tester manufactured by Wilson Mechanical Instruments Co. Inc., with a Microton Stage and tunable stage vise is used at the BCL Hot Lab. The hardness tester has been modified for remote operation. The sample stage, weights, microscope objectives and accessory equipment are located in the cell behind shielding walls. The microscopic viewing optics and operational controls are located outside the cell for direct operation.

Two types of indenter can be used for microhardness measurements, Knoop and 136 degree Diamond Pyramid (Vickers). The Knoop indenter point consists of a diamond accurately ground to produce indenting surfaces consisting of four planes; the diamond is securely embedded in a suitable mount. The 136-degree Diamond Pyramid indenter is commonly referred to as the Vickers Indenter and is an accurately ground diamond in the form of a pyramid which has an included angle of 136 degrees on its diagonals. It is also suitably mounted for attaching the indenter beam.

Specimens are ground and polished in preparation for hardness testing using a Buehler grinder with an Automet attachment. The appropriate sequence of grinding and polishing paper or compounds is used to prepare the specimen surface.

Procedure

A specimen of cladding is first mounted as a transverse or longitudinal metallographic specimen in a bakelite mount and held in the mount with epoxy.

The surface of the specimen is lapped and polished and must be free of scratches so that the outline of the impression can be clearly observed and the length of the impression can be measured accurately. An impression is made on the sample surface using either a Knoop or diamond pyramid (Vickers) indentor under a predetermined load (25 g to 50 kg). A filar eyepiece on the microscope enables measuring the indent diagonals. Indents are made away from the specimen edges and at some distance from each other so the readings will be representative of the material hardness.

Indents are also made parallel and at right angles to the tubing axis to evaluate any texture effects of microhardness of the irradiated Zircaloy cladding material.

Calculation and Standardization

After the length of an impression has been measured and converted from filar units to millimeters, the Knoop Hardness Number (KHN) is read directly from the provided Table KV-45. The Knoop Hardness Number is based on the unrecovered projected area; therefore, the long diagonal of the indentation is measured. By measuring the horizontal diagonal of the impression, the recovered indentation hardness number may be calculated from the equation:

$$I_r = 2L/lw$$

where I_r = Knoop Number based on the recovered projected area

L = Applied load in kilograms

l = Measured length of long diagonal in millimeters

w = Measured length of short diagonal in millimeters.

The operation of the loading and indentation system is checked by hardness measurements of a certified hardness standard. The standard is of the same approximate hardness as the object to be measured.

Metallographic Examination

The purpose of metallographic examination is to characterize the optically resolvable microstructural features of fuel and cladding. This includes but is not limited to:

- Clad corrosion products
- Crud deposits
- Clad hydride formation and orientation
- Fuel-clad interaction
- Grain size
- Porosity size and distribution

Equipment

A Leitz metallograph is used for examination and photomicrography. The metallograph stage, located within the cell, has X-Y and rotary motion. All controls and camera accessories are located and operated from outside the cell. The metallograph is capable of photography magnification over the range 7X to 750X. The magnification is adjusted through use of various objective eyepiece lenses in combination with a changeable bellows length. A xenon light source is used for illumination. Bright field, polarized light, and sensitive tint

are available. A filar eyepiece is available for making optical measurements.

Grinding and polishing operations use Buehler low-speed wheels with an Automet attachment for holding the samples and controlling grinding/polishing pressure. Although generally not needed, vibratory polishers are available.

Reagents

Commonly used materials and reagents used in the metallographic preparation are listed below:

- Mounting Epoxy - Araldite Type - Hardener Type 951
- Grinding Paper - Silicon Carbide - resin bonded to adhesive back, 120, 240, 400, and 600 grit
- Polishing Cloths - Texmet - Adhesive backed chemotextile material, no nap
  - Microcloth - Synthetic rayon cloth fibers bonded to cotton twill backing, low nap
- Polishing Media - Linde A - 0.3 micron alumina hexagonal alpha
  - Linde B - 0.05 micron alumina cubic gamma
- Grinding and Polishing Lubricant - Water
- Fuel Etchants (Most Common) - 85 parts hydrogen peroxide AR Grade, 30 percent, stabilized
  15 parts sulfuric acid AR Grade 36N
- Clad Etchant (Most Common) - 50 parts hydrogen peroxide AR Grade, 30 percent stabilized
  45 parts nitric acid AR Grade, 16N
  5 parts hydrofluoric acid AR Grade, 28N.

Procedures

A 1.9-cm sample of fuel rod is sectioned from an area of interest. The fuel may then be removed and the specimen epoxy fixed in a

Bakelite mount.

A mount for a transverse specimen consists of a Bakelite cylinder 3.2 cm diam, 3.2 cm high with a 1.3 to 1.6-cm-diam center hole. A zero-degree marker pin is located in this hole. The specimen is placed first in a stainless steel sleeve with an ID about 0.1 mm larger than the maximum sample clad OD. Note that if the clad is not to be examined and edge rounding at the clad OD is of no consequence, the stainless steel sleeve is not necessary. The specimen is then placed in the cavity in the bakelite mount. The epoxy is allowed to cure for 12 hours.

The mount for a longitudinal specimen is a 3.2-cm-diam by 2.5-cm-high bakelite cylinder. A 1.3-cm-deep by 2.9-cm-diam flat bottomed cavity is machined out of the top of the mount. A 1.6-mm-diam hole is drilled into the mount. A pin in the hole serves as a marker to indicate the top end of the specimen.

If the clad edge preservation is desired, a tight fitting stainless steel sleeve is placed around the specimen or a silica-epoxy coating is applied on the clad surface before sectioning. In either case, the sleeve must be machined or the silicon-epoxy coating ground down so that the clad surface lies flat on the bottom of the mount cavity. The specimen is placed in the mount and the epoxy mounting and impregnation procedures are identical to those used for transverse mounting.

Grinding is accomplished using an Automet attachment on a low-speed grinding wheel. The automet holder can accommodate up to five specimens at a time. If five specimens are not being processed, the extra holes are filled with blanks. The specimens are ground using 120, 400, and 600 grit SiC paper, in that order. If grinding depth is important, the specimens are ground to the point where the specimen surface is just exposed. A micrometer is used to measure the mount height. This serves as a starting reference point for micrometer measurements of mount height after subsequent grinding. For longitudinal mounts with depth marking pins, the pins serve as depth markers.

Polishing is by low speed polishing wheel using Texmet cloth with Linde A and water. A final polish, if necessary, is performed on a vibratory polisher with microcloth and a Linde B water slurry.

Specimen surfaces are etched to bring out desired microstructural features using the appropriate etchant. Etching is accomplished by swabbing the surface with a cotton ball soaked in the etchant. Immediately after etching, the specimen surface is washed with water.

Then, the surface is dried by blowing air over it.

The microscopic examination is performed on a Leitz metallograph. Photographs are taken at specified locations and magnifications. Note that the fuel and clad are first examined and photographed in the as-polished condition. Then the fuel is etched, examined, and photographed. Finally, the clad is etched, examined, and photographed. Photographs are generally taken using Polaroid P/N film. Provisions for the use of sheet film are available. A written record contains the mount number, specimen identity rod number, specimen surface preparation (as-polished or etched) and photograph identification number.

Calibration and Standardization

The magnification obtained with the metallograph is a function of the objective lens, the eyepiece lens, and the camera bellows length. The system is calibrated for magnification against a stage micrometer with spacings of known dimensions. These spacings are measured on a photograph and the measurements are compared to known spacing to obtain the magnification obtained with that specific lens combination and bellows length. With everything staying the same, this magnification does not change. However, objective lenses are subject to degradation (browning) as a result of radiation damage and must be replaced periodically. When a lens replacement is made, the system is recalibrated.

Annealing of Cladding

Unirradiated and irradiated cladding specimens are annealed and subsequently tested in tensile, burst, or expanding-mandrel tests to determine the effect of both transient and isothermal annealing on the cladding mechanical properties.

Equipment

The annealing equipment consists of a quartz tube surrounded by a water-cooled induction coil of copper tubing. The system also has a solenoid operated valve for the gas quench at the inlet (top) of the furnace and a vacuum pump to evacuate the furnace at the outlet (bottom) of the furnace. The power is supplied by a controlled, variable LEPEL induction heater power supply. The furnace and power supply are shown in Figure B-1.

The specimen temperature is recorded using Chromel-Alumel thermocouples attached to the specimen. The temperature and heating ranges are controlled using a Data Trak, temperature controllers, and controlled power supplies. (See Figure B-1). The equipment can be used to anneal specimens from 1.3-cm half rings to 17.8-cm tube-burst specimens.

Procedures

With unirradiated specimens, the power supply setting, temperature controller setting, and Data Trak curves are determined for isothermal and transient annealing of hardness, tensile burst, expanding mandrel, and bend specimens.

After the irradiated specimen has been cleaned, a Chromel-Alumel thermocouple is spot welded to the specimen and the specimen is mounted in the furnace. The furnace is evacuated to $\leq$ 10 microns pressure and the controller, power supply and Data Trak are programmed for the required heating rate, maximum temperature, time at temperature, and quench sequence. The specimen is annealed, removed from the furnace and the thermocouple removed. The specimen is then transferred into the mechanical testing cell for the appropriate mechanical property test. The operating console is also shown in Figure B-1. Typical heating curves are shown in Figures B-2 and B-3.

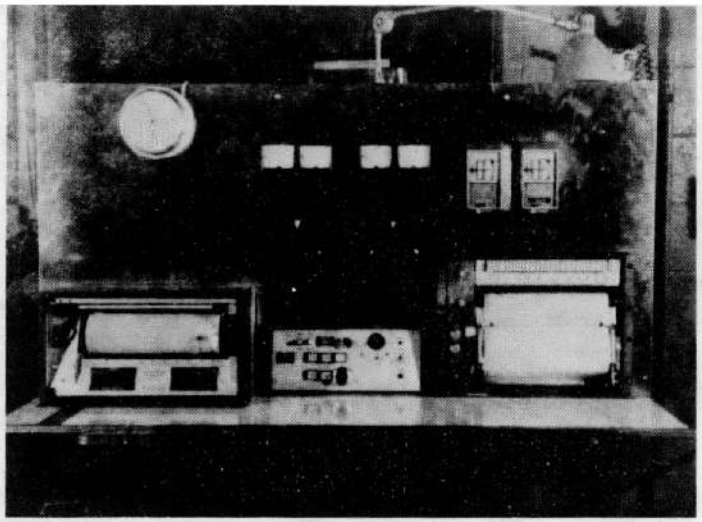

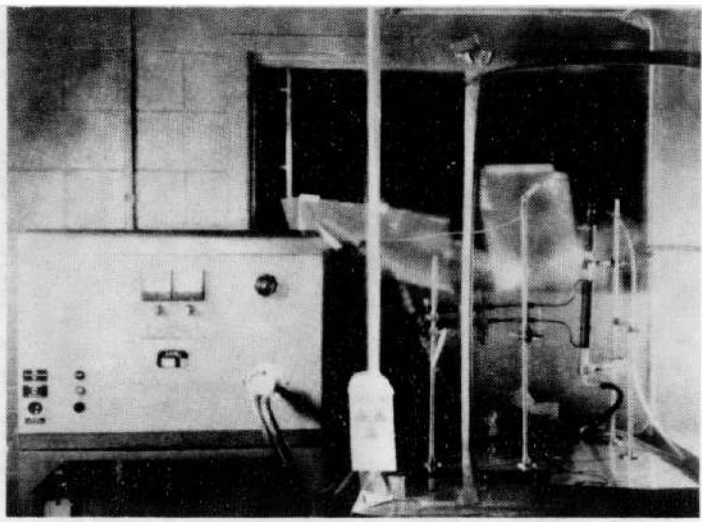

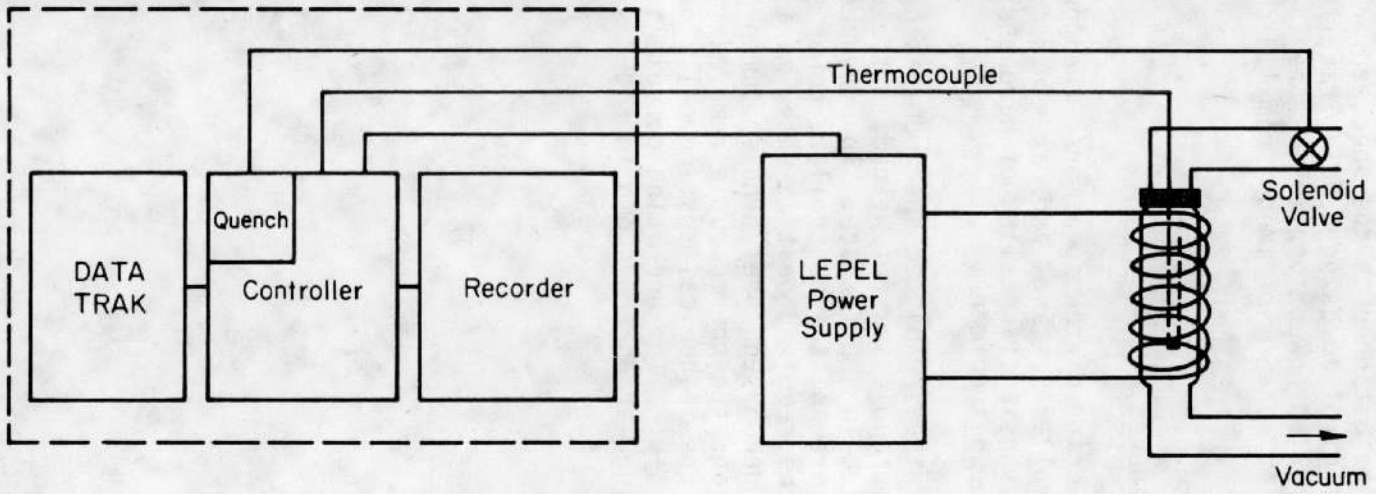

FIGURE B-1. ANNEALING FURNACE AND OPERATING CONSOLE WITH SCHEMATIC OF THE SYSTEM

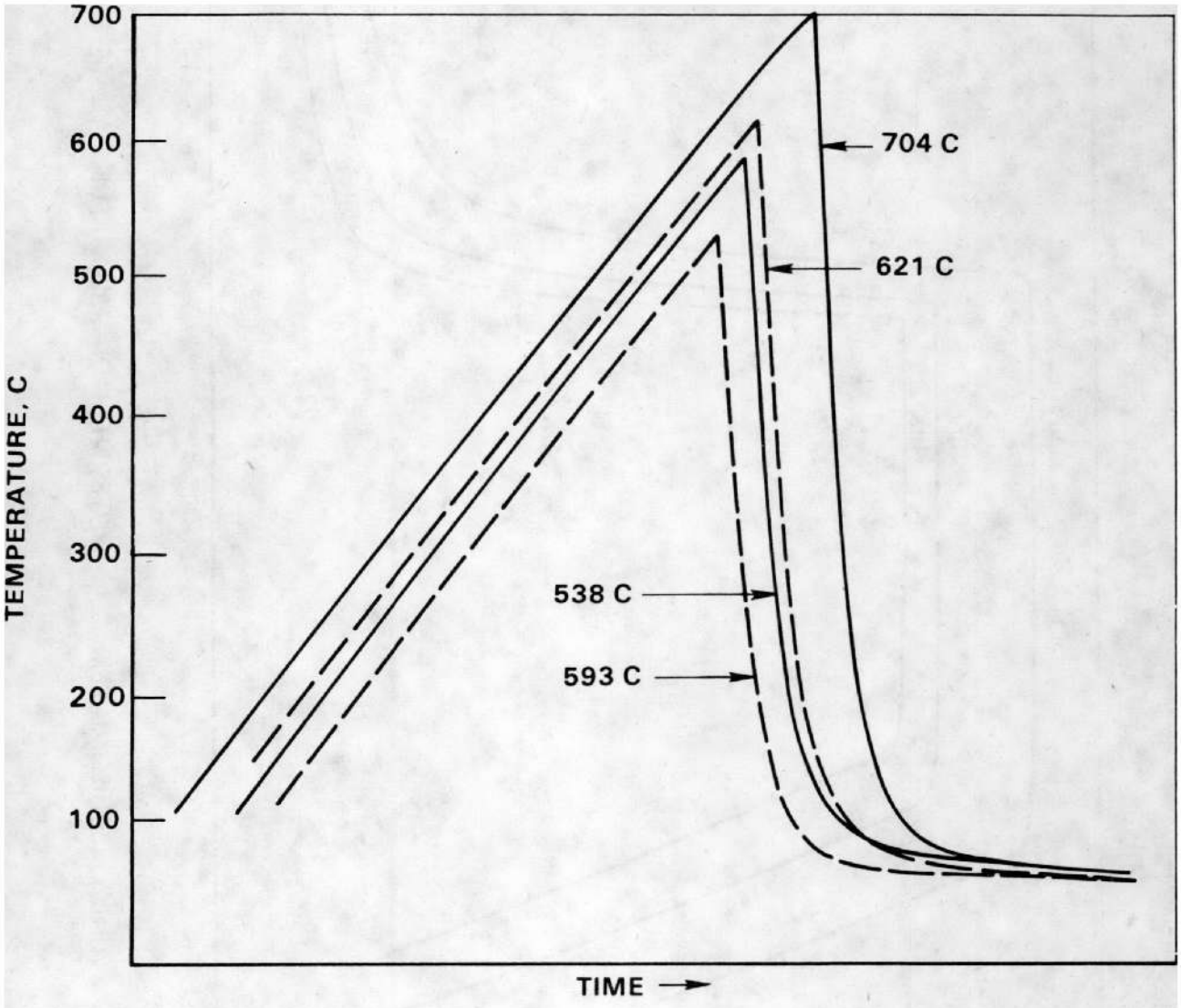

FIGURE B-2. TYPICAL TRANSIENT ANNEALING CURVES

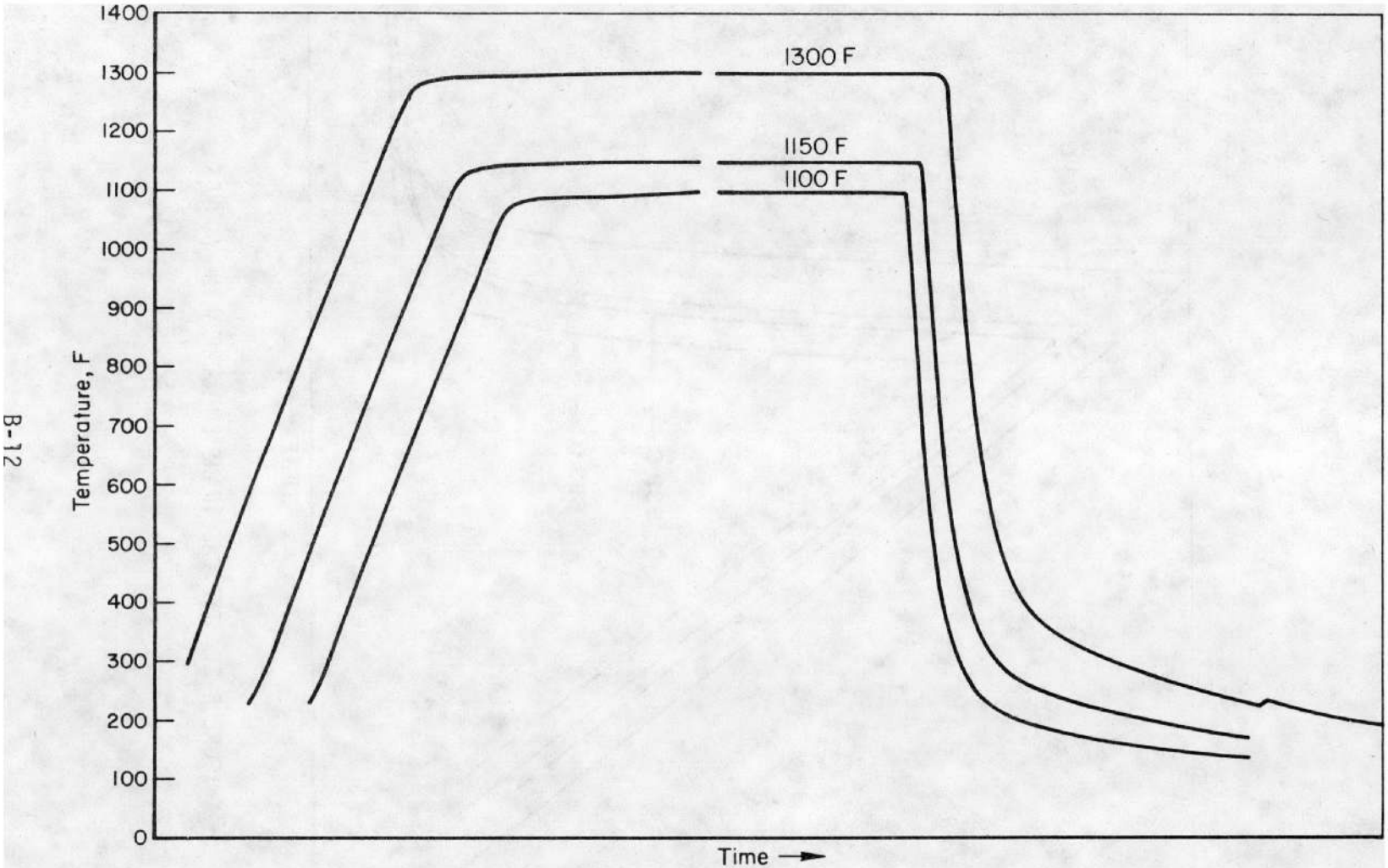

FIGURE B-3. TYPICAL ISOTHERMAL ANNEALING CURVES WITH INITIAL HEATING RATE OF 50F/SEC

APPENDIX C

A FULL DESCRIPTION OF EQUIPMENT AND PROCEDURES FOR TENSILE, TUBE-BURST, EXPANDING MANDREL, AND BEND TESTS

Tensile Tests

Tensile tests are performed on 12.7-cm specimens from which the fuel has been removed. The tests are conducted at room temperature to 482 C and at strain rates from 0.0025 to 2.5/min. Facilities are available for testing irradiated or unirradiated tubing specimens.

Equipment

The tensile machine is a 9100-kg load Instron that utilizes a frame located in the Hot Cell and a control console located outside the cell. The temperature is measured by a calibrated, sheathed thermocouple and is recorded on a calibrated temperature recorder with the appropriate temperature range. A Satec extensometer, fitted with an Instron clip-on type strain gage, is used to measure the specimen elongation.

Procedures

An unirradiated dummy tube specimen with three spot-welded thermocouples along its length is placed in the Instron load frame. This specimen is fitted with a knife edge extensometer. The heater furnace is placed around the specimen. A sheathed thermocouple, placed through the access hole in the furnace, rests directly on the specimen center gage section and near the center spot-welded thermocouple. Power-supply settings are then determined to yield a thermal gradient of ± 3 C over the specimen gage length and the central spot-welded thermocouple and sheath thermocouple readings are compared. The sheathed thermocouple is then used during testing of irradiated specimens to indicate the gage-length temperature. This specimen is then removed from the testing machine.

An irradiated specimen is measured and fitted with end plugs and marked as required. The specimen is then loaded into the tensile grips and the knife-edge extensometer attached. This assemblage is placed in the Instron load frame and the upper pin inserted. The heater furnace is placed around the specimen and the sheathed thermocouple placed in contact with the specimen gage section.

The specimen is heated to the required temperature, then pulled in tension to fracture. The strain gage extensometer indicates specimen elongation from initiation of the test until maximum strength is reached and the elongation thereafter is calculated using the time to failure and load frame crosshead speed. The Instron load cell indicates the load during the test. The Instron chart yields a load elongation curve for each test.

After fracture, the furnace is removed and the specimen examined, measured, and photographed as required.

Equations

The stress is calculated using the equation:

$$\sigma = \frac{L}{A} \quad ,$$

where

σ = stress in pascals

L = load in neutons (nt = lb/4.45)

A = original cross-sectional area in m^2.

The strain is calculated using the equations:

$$\text{uniform strain } \varepsilon_1 = \frac{l_1 - l_o}{l_o} \quad , \quad \text{nonuniform strain } \varepsilon_2 = \frac{rt}{l_3} \quad ,$$

where

l_o = specimen original extensometer gage length in cm

l_1 = specimen gage length at the maximum load in cm

l_3 = specimen original length between tensile grips in cm

r = Instron crosshead speed in cm/min

t = time from maximum load to failure in minutes.

The total strain is calculated as:

$$\text{total strain} = \text{uniform strain} + \text{nonuniform strain } (\varepsilon_T = \varepsilon_1 + \varepsilon_2).$$

The method of calculating strain rate and total elongation from tensile test data was revised to accord with procedures used in ASTM E8-69 in order to permit comparison with other published results. The physical arrangement for the tensile tests is shown in Figure C-1.

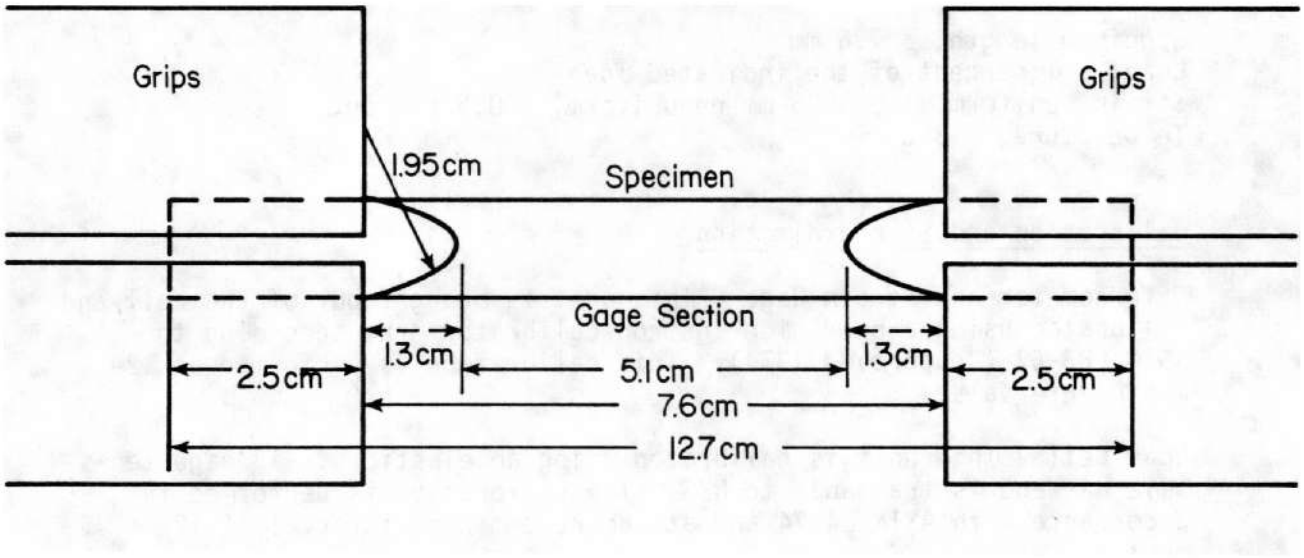

FIGURE C-1. SPECIMEN ARRANGEMENT FOR TENSILE TESTS

The arrangement is modified from that described in ASTM E8-69 in that the grip is located at the shoulder of the internal bullet. This arrangement is used in order to minimize specimen length and conserve material. No influence of grip location, either at or behind the bullet shoulder, was observed in tests performed to evaluate possible effects on data generated in the tests.

Specimen strain from zero to approximately maximum load is being measured in this program by a 5.1-cm Satec knife-edge extensometer. Because of slippage when specimen necking occurs, the extensometer is removed at or slightly before maximum load and subsequent strain is determined from crosshead movement.

ASTM E8-69 defines the gage length as the distance between bullet ends (5.1 cm in the current arrangement). Consequently, since this convention is used by other experimeters, the 5.1-cm gage length was used to calculate strain rates and strains beyond maximum load, i.e., total strain. Up to the maximum load, extensometer readings and a 7.0-cm gage length in conjunction with crosshead motion were used in calculating uniform strain.

Precision and Accuracy

Specimen length, ± 1.6 mm
Load, ± 1 percent of the indicated load
Strain, uniform, ± 0.0025 mm nonuniform, ± 0.5 percent
Temperature, ± 3 C

Calibration and Standardization

Extensometer and Strain Gage - This unit is brought out of the cell and calibrated using a precision Instron calibrator drum according to ASTM E83-67 (Reapproved 1974). This calibration is performed at 12-month intervals.

Load Cell - This unit is calibrated using an elastic strain gage tensile bar and is traceable to NBS. The calibration is performed in accordance with ASTM E4-74 and at the recommended interval of 12 months.

Sheathed Thermocouple - This unit, which is in contact with the specimen during testing, is calibrated against an NBS standard thermocouple at the BCL instrument laboratory.

Thermocouple Wire - Wires used for these tests are batch calibrated against an NBS standard thermocouple at the BCL instrument laboratory.

Instron Load Frame and Console - These instruments are calibrated, adjusted, and tested by an Instron factory representative at 12-month intervals.

Tube-Burst Tests

The objective of clad tube-burst tests is to determine the mechanical properties of cladding materials under biaxial stress conditions.

Burst tests are performed from 27 C to 425 C and internally pressurized with a silicon oil. The maximum temperature can be increased to about 550 C if a special high-temperature oil is used. The pressurization rate of the burst system is variable from 0.15 to 140 $kg/mm^2/min$ and the maximum pressure the system will produce is 14 kg/mm^2. The burst system is programmable and is automatically controlled through pressure and volume signal feedback circuits. The control parameter for the tests is rate of volume expansion.

Specimens can be tested with the fuel intact or the fuel can be removed and the tube filled with alumina pellets to reduce both the oil volume in the specimen and the stored energy in the system. After a specimen has been either tested to rupture or plastically deformed, a transverse metallographic mount is prepared for measurement of plastic strain.

Equipment

A schematic diagram of the burst-test system is shown in Figure C-2. The system is laboratory built, using commercially available equipment such as a Milton Ray controlled-volume pump, Exact waveform generator, Hewlett Packard X-Y Recorder, Heise pressure gage, Satec LVDT, Baldwin-Lima-Hamilton pressure transducer, Data Track drum programmer, Daytronic amplifier, Digi Tec scaler, autoclave high-pressure valves, and Swagelok stainless steel tubing fittings.

Procedures

The tube-burst system components are checked out and calibrated. An unirradiated tube of the material to be tested is filled with high purity alumina pellets and fitted with Swagelok type pressure fittings to simulate the configuration and geometry of an irradiated test specimen. The simulator tube, with thermocouples spot welded over its length, is mounted on the in-cell pressurization test fixture and a beaded thermocouple is secured at the center of the gage section. A three-zone furnace heats the gage length to a temperature (as indicated by the spot-welded thermocouple) within specified limits, and the furnace power-input adjustment procedure for attaining a uniform gage-length temperature is recorded. The spot-welded thermocouple and bead thermocouples outputs are then compared. The adjustment procedure, along with the beaded thermocouple output, are used to control the irradiated test specimen temperature.

To determine the volume change associated with system expansion as a result of pressurization, a heavy-walled, nondeforming specimen of approximately the same internal void volume as an irradiated test specimen is mounted on the in-cell pressurization test fixture and brought to temperature. System expansion curves (pressure versus volume) are generated for each volume-expansion rate and temperature combination required.

An irradiated cladding burst test specimen is then prepared, fitted with pressure-tight end fittings, and filled with alumina pellets when necessary. The specimen is mounted on the in-cell pressurization

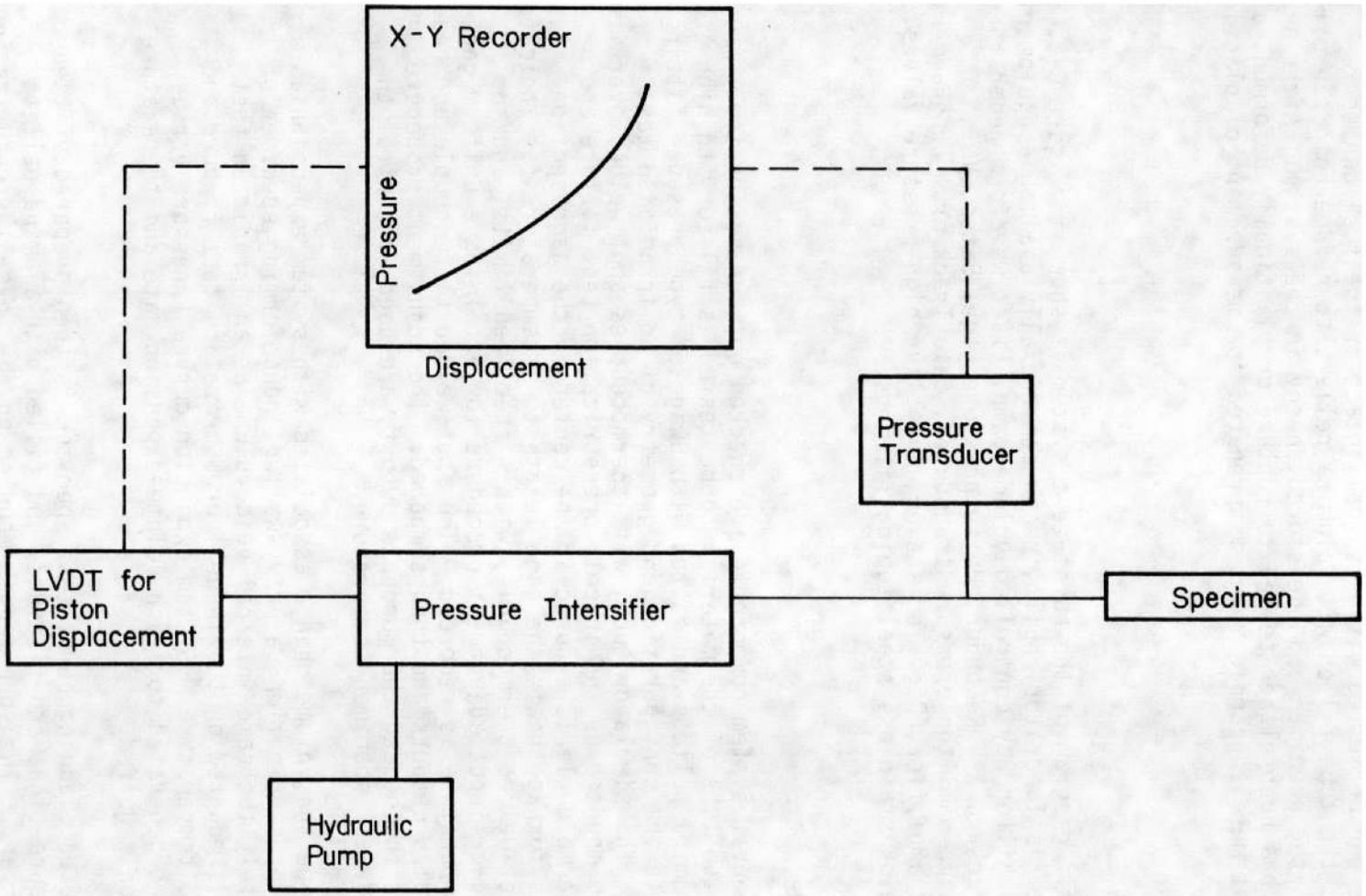

FIGURE C-2. SCHEMATIC DIAGRAM OF BURST TEST EQUIPMENT

test fixture, fitted with the beaded thermocouple at the center of the gage section, and brought to the required temperature. The specimen is tested to failure, removed from the test fixture, and measured to determine the region of maximum strain. The tested specimen is then cut and mounted as a transverse metallographic mount to determine the failure strain.

Pressure and volume data are obtained from the pressure-versus-volume curve for specific volume-expansion rates and temperatures.

Equations

Using the appropriate system expansion curve and the burst test pressure-volume curve, the volume change in the specimen is determined by the difference and is then plotted against pressure. From this curve the 0.2 percent offset-yield pressure and maximum pressure is obtained. The hoop stress is calculated using the thin wall formula

$$\sigma = PD/2t$$

where

σ = hoop stress (MPa)

P = pressure (MPa)

D = tube nominal diameter (mm)

t = tube nominal wall thickness (mm).

In calculating the 0.2 percent offset yield strength, the pressure required to produce a volume change associated with a diametral strain of 0.2 percent is used. For the ultimate strength, the maximum pressure is used. The uniform strain is calculated from the volume change associated with the maximum pressure.

The relation of Δ Volume and of diametral strain (ε) of the specimen is; ΔV specimen = $1.73 D_0^2 \ell_0 \varepsilon$ where D_0 and ℓ_0 are the original specimen diameter and length. The derivation of the equation is given in the Tube-Burst Test Equations section of this appendix.

Precision and Accuracy

Specimen length, ± 1.6 mm
Pressurization rate, ± 5 percent
Volume, ± 2.13 mm^3
Temperature, ± 3C

Calibration and Standardization

The three burst-test parameters requiring calibration are pressure, volume, and time. A zero to 17.6-kg/mm^2 precision Heise pressure gage is sent to BCL instrument laboratory at 12-month intervals for calibration traceable to NBS. The Baldwin Lima Hamilton zero to 21.1 kg/mm^2 pressure transducer is pressurized and directly compared (standardized) with the calibrated Heise gage either prior to testing a series of specimens, if tests are conducted over short-term ($\leq$ 1 week) or at 1-week intervals during long-term testing ($\geq$ 1 week).

The intensifier (piston displacement) volume is measured by measuring the oil displaced from zero to full stroke. The volume is determined by both direct measurement and by weighing the oil and calculating the volume using the temperature-corrected oil density. The volume is considered linear over this range since preoperational tests indicate the intensifier piston Δ volume versus Δ displacement is linear to $\pm$ 1.64 mm^3. The Satec LVDT output is then calibrated to the intensifier piston displacement. This calibration is performed at 12-month intervals.

The Exact waveform generator ramp time is calibrated using a precision stopwatch and the pressurization rate checked as required at 1-week intervals.

Tube-Burst Test Equations

In a tube-burst test the specimen is pressurized using an hydraulic pump and pressure intensifier (differential piston). The volume change of the system (system + specimen) is measured by determining linear piston displacement as a function of the applied pressure. Calibration curves that are obtained (at the relevant test temperature) give a correction for the compressibility of the fluid plus elastic expansion of the system. To account for the compressibility of the liquid in the test specimen, a thick-walled nondeforming dummy specimen containing a volume closely equivalent to that of the specimen is used during the calibration.

Thus, for the calibration run:

$$\Delta V_{Total} = \Delta V_{Sys} + \Delta V_{Dummy} \quad ,$$

where ΔV_{Sys} = compressibility of fluid + elastic expansion of containment.

Experience has shown that the calibration curve is repeatable with a very high degree of reproducibility. It is worth noting that in general the additional volume of liquid in the specimen has very little effect on the calibration curve ($V_{System} >> V_{Spec}$).

From the test curve obtained for a burst specimen (pressure/ΔV_{Total}), a ΔV_{Spec}/Pressure curve is derived. The volume change in the specimen, ΔV, is given by:

$$\Delta V = \frac{\pi}{4} D_f^2 \ell_f - \frac{\pi}{4} D_o^2 \ell_o \quad , \tag{1}$$

where D_f, ℓ_f are the final ID and length, respectively

D_o, ℓ_o are the initial ID and length, respectively

and $D_f = D_o (1 + \varepsilon_D)$, $\ell_f = \ell_o (1 + \varepsilon\ell)$,

where ε_D, $\varepsilon\ell$ are diametral and longitudinal strains, respectively.

For a closed end burst test, $\sigma_h = 2\sigma_\ell$

and $$\varepsilon_D = \frac{\sigma_h}{E} - \frac{\nu\sigma_\ell}{E} = \frac{\sigma_\ell}{E} (2 - \nu)$$

$$\varepsilon_\ell = \frac{\sigma_\ell}{E} - \frac{\nu\sigma_h}{E} = \frac{\sigma_\ell}{E} (1 - 2\nu)$$

where σ_h = hoop stress, σ_ℓ = axial stress, ν = Poissons ratio and

E = elastic modulus.

Thus $$\varepsilon_D = \varepsilon_\ell \left[\frac{2 - \nu}{1 - 2\nu}\right]$$

For $\nu = 0.33$ (Poisson's ratio),

$$\varepsilon_D = 5\ \varepsilon_\ell$$

For elastic strains in the specimen, substituting for ℓ_f, D_f in Equation (1) we obtain:

$$\Delta V_{Spec} = \frac{\pi}{4} \{[D_o(1 + \varepsilon_D)]^2 \ell_o(1 + \frac{\varepsilon_D}{5})\} - \frac{\pi}{4} D_o^2 \ell_o$$

which reduces to

$$\Delta V_{Spec} \simeq 1.73\ D_o^2 \ell_o \varepsilon_D \cdot \text{ (Since } \varepsilon_D^2, \varepsilon_D^3 \text{ terms are small)} \tag{2}$$

For plastic strain (uniform) in the specimen we need only consider the diametral component, since the axial component will be only elastic.

Thus $$\Delta V \simeq \frac{\pi}{4}\{[D_o(1 + \varepsilon_p)]^2 \ell_o\} - \frac{\pi}{4} D_o^2 \ell_o$$

$$= \frac{\pi}{2} D_o^2 \ell_o \varepsilon_p$$

$$\Delta V_{Spec} = 1.57 D_o^2 \ell_o \varepsilon_p \quad (3)$$

Expanding Mandrel Tests

The expanding mandrel test is intended to simulate the interaction of a longitudinally cracked fuel pellet with the restraining Zircaloy cladding.

Equipment

The test apparatus consists of an eight-section mandrel with beveled surfaces, which are driven apart, and into the cladding inside surface under the action of the internal wedges. The essential components involved in the test are shown in Figure C-3. The split-mandrel inserts are 18.75 mm long and the test specimen length is from 6.4 to 7.6 cm long with the intention of achieving plain strain conditions during the test.

The test apparatus is assembled and the tests are conducted in a 9,100-kg Instron compression testing machine. A clam shell resistance furnace with a view window is used to heat specimens that are to be tested at elevated temperatures.

Procedures

A test specimen, with the fuel removed, has a thermocouple spot welded to it. The specimen is lowered over the support post, the split mandrel inserts are positioned inside the specimen, and the wedge is lowered onto the beveled insert surfaces. The clam-shell furnace is closed around the specimen and the temperature, as indicated by the spot weld thermocouple, is raised to the test value.

At temperature, the wedge is driven into the insert level surface forcing the inserts apart. Areas on either side of the expanding mandrel inserts are strained until failure occurs. Transverse

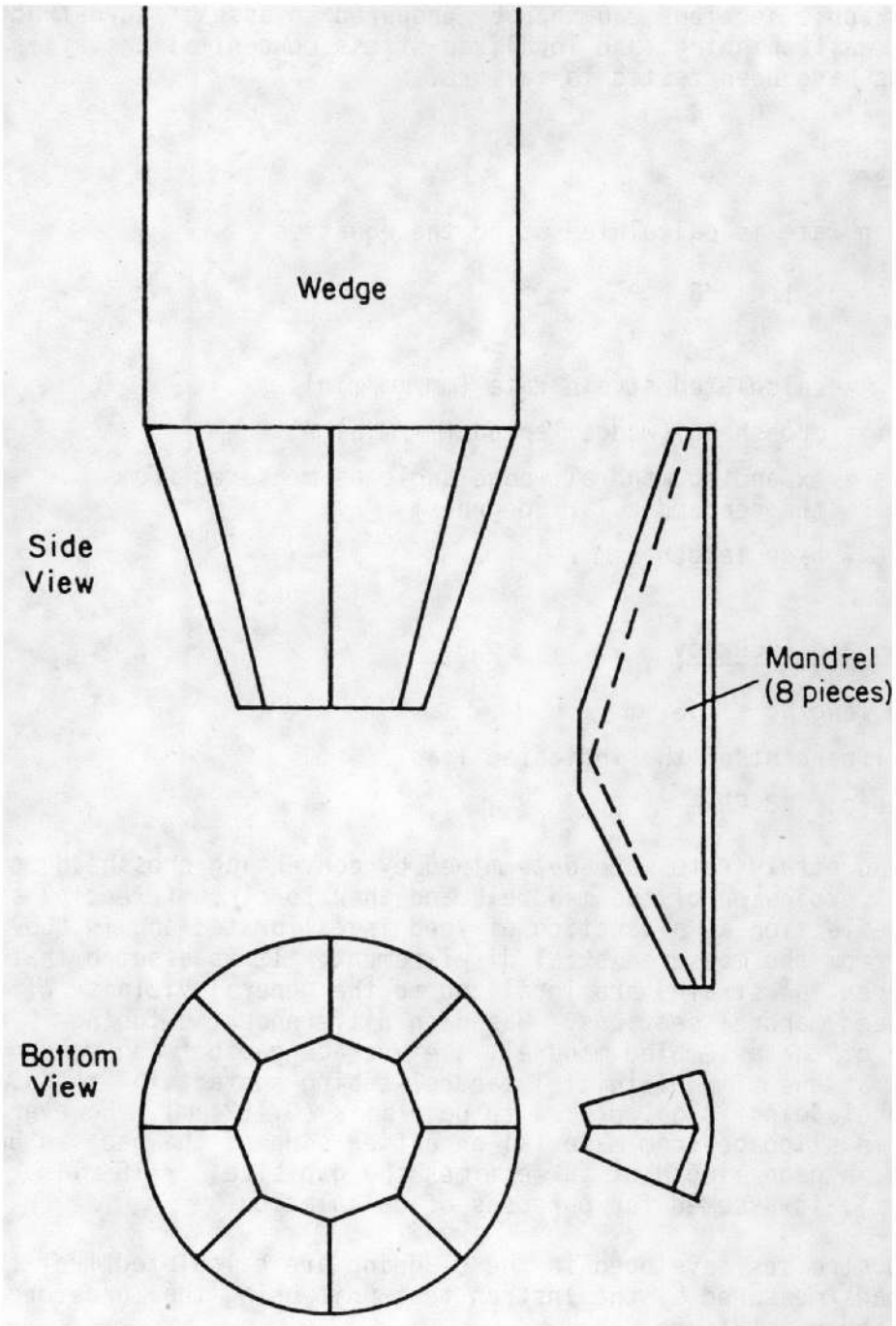

FIGURE C-3. SCHEMATIC OF EXPANDING MANDREL TEST ELEMENTS

metallographic sections can then be prepared to assess microstructure changes, wall thinning, and localized stress concentrations after the specimens have been tested to failure.

Equations

The strain rate is calculated using the equation

$$\dot{\varepsilon} = \dot{Y} \tan \theta / G$$

where

$\dot{\varepsilon}$ = calculated strain rate (mm/mm/min)

$\dot{Y}$ = crosshead (wedge) speed (mm/min)

θ = expanding mandrel wedge angle as measured from the perpendicular (degrees)

G = gage length (mm).

Precision and Accuracy

Specimen length, ± 1.6 mm

Load, ± 1 percent of the indicated load

Temperature, ± 3 C

Strain and strain rates are determined by converting crosshead motion to radial expansion of the mandrels and then to circumferential strain. System deflection as a function of load is calibrated and is subtracted from the measured axial displacement. It is assumed that the circumferential strains are localized to the general vicinity of the gap between mandrel sections. Based on differences in tubing ID and diameter of the assembled mandrel, the average gap between mandrel sections at the time of initial mandrel-tubing contact for the H. B. Robinson cladding is calculated to be 6 mils (0.152 mm). However, since some slippage from material on either side of the gap can be expected, a gage length of three times the gap size, or 18 mils (0.457 mm), is assumed for purposes of calculation.

The hoop stresses developed in the cladding are calculated from the axial loads measured by the Instron test unit using the load-force diagram shown in Figure C-4.

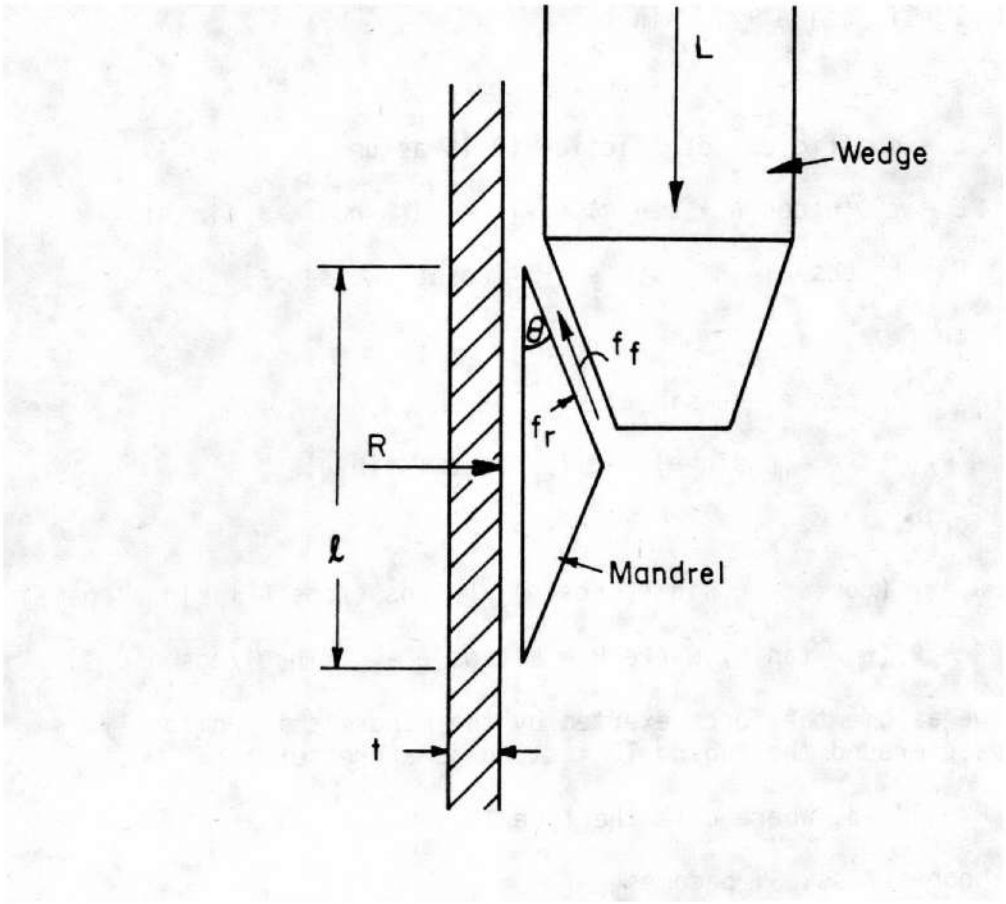

L = axial compressive load
f_r = wedge-mandrel-face normal force
f_f = wedge-mandrel-face frictional force
θ = wedge/mandrel angle (15 degrees)
R = radial reaction force on tube wall
l = mandrel length (0.75 in., 19 mm)
t = tube wall thickness (24.8 mils, 0.63 mm)

FIGURE C-4. LOAD-FORCE DIAGRAM FOR EXPANDING MANDREL TEST

To calculate the stresses it is noted that

$$L = f_f \cos\theta + f_r \sin\theta,$$

where $f_f = \mu f_r$

and μ = coefficient of friction (0.15 assumed),

so that $L = f_r(\mu \cos\theta + \sin\theta)$ or $f_r = L/(\mu \cos\theta + \sin\theta)$.

Also $R = f_r \cos\theta - \mu f_r \sin\theta = f_r(\cos\theta - \mu \sin\theta)$.

Solving for f_r,

$$f_r = R/(\cos\theta - \mu \sin\theta)$$

Therefore $R/(\cos\theta - \mu \sin\theta) = L/(\mu \cos\theta + \sin\theta)$.

Solving for R,

$$R = [L(\cos\theta - \mu \sin\theta)(\cos\theta)]/[\mu \cos\theta/\cos\theta + \sin\theta/\cos\theta]$$

$$R = P/(\mu + \tan\theta) \text{ where } P = L(\cos\theta - \mu \sin\theta)/\cos\theta$$

Now, if we assume the force exerted by the mandrels is uniformly distributed around the tubing ID, acting as a pressure, P,

$$P = R/\pi \ell d, \text{ where d is the tube ID,}$$

and the hoop stress, S, becomes

$$S = pd/2t = R/2\pi \ell t = P/2\pi \ell t\,(\mu + \tan\theta).$$

The ultimate stress and uniform strain are calculated at the point of maximum load. In the majority of the tests, failure occurred at the maximum load. However, in a number of tests, the load decreased from its maximum value and failure occurred at an associated lower stress and higher hoop strain.

It is recognized that the assumptions made in analyzing the expanding mandrel test data do not lead to exact solutions and that there is great uncertainty in both the calculated stresses and strains. The strain values appear to be particularly questionable. However, a number of tests were performed in which the specimens were prepared with axial striations approximately 10 mils apart around the tube circumference. Localized strain measurements were obtained from specimens and compare well with the strains calculated from

cross-head motion. In any event, the analysis provides a basis that can be used to establish relative changes in strength and ductility under various test conditions and following annealing.

Bend Tests

The purpose of the bend test is to simulate the bending of a fuel rod due to thermal and mechanical stresses.

Equipment

The bend test apparatus is shown in Figures C-5 and C-6 with a specimen installed. Figure C-5 shows a closeup of the specimen and flared support tubes which keep the specimen from buckling at the central loading points. The three point deflectometer head is also shown. The Instron testing machine, furnace used for elevated temperture tests, and strain gage deflectometer are shown in Figure C-5.

As seen in the figures, the specimen is supported at a point near each end of its length by the support anvils. Load is applied at two points near the central section of the specimen length by the loading ram. The load is autographically recorded during testing by using the electrical signal from the testing machine load cell.

Deflection of the specimen is measured during testing by a three-point deflectometer that is located directly below the specimen. Center point of the deflectometer is kept in contact with the midlength position of the specimen by an upper spring. The outer two points of the deflectometer are attached to an outer rod which is attached to the second arm of the strain gage. The inner rod runs through the center of the outer rod. As the specimen is deflected, the strain gage produces an electrical signal proportional to the relative motion of the two rods. The electrical signal is fed into the same recorder as the load signal, producing a load-deflection curve as a test is run. The deflection can be equated to a radius of curvature.

Procedures

Bend specimens of Zircaloy cladding with the fuel removed are tested either in the as-irradiated or annealed condition. A specimen is filled with a 320 mesh alumina and phosphoric acid slurry, air dried for one day, and furnace dried at 66 C for 12 hours. After filling and drying, the specimen is fitted with two end support flare tubes as shown in Figure C-5, mounted on the four point bend jig, heated

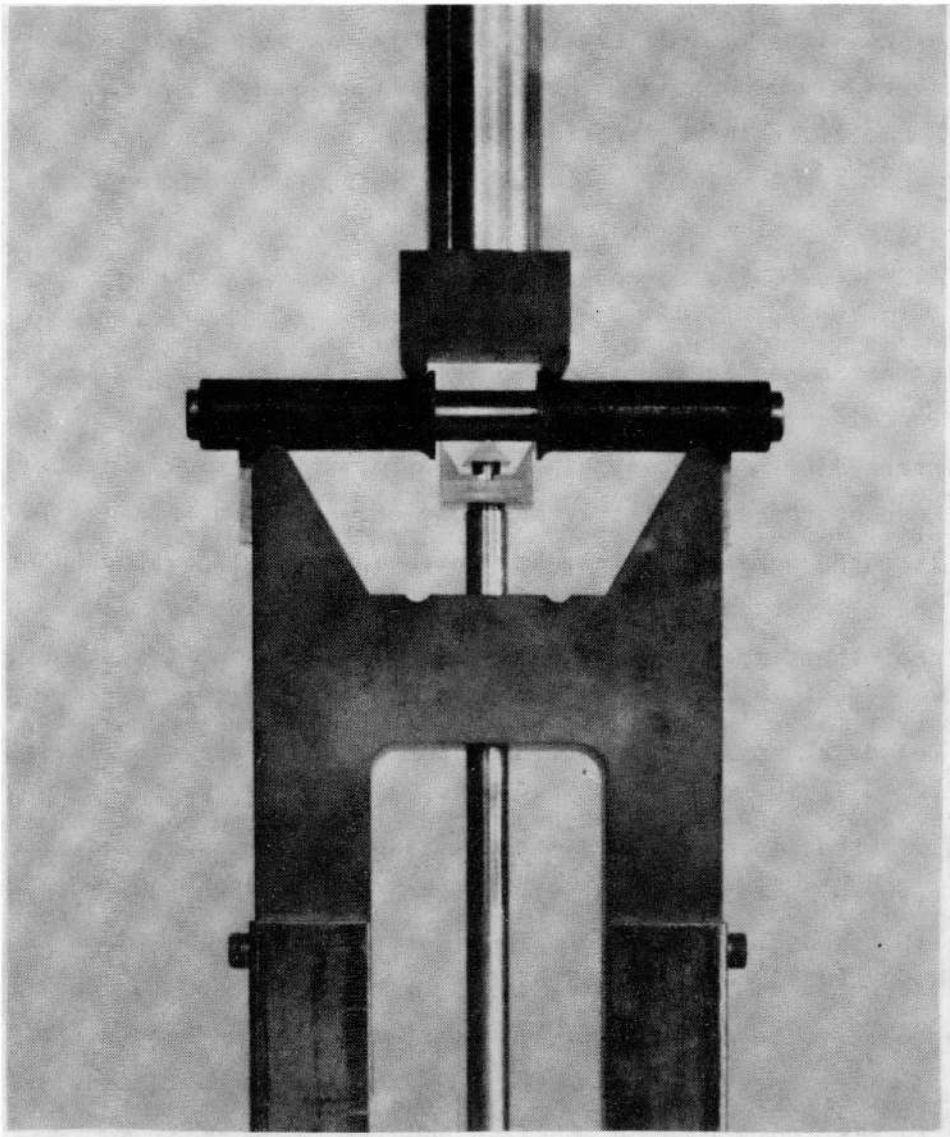

FIGURE C-5. TUBE BEND TEST ARRANGEMENT WITH FLARED SUPPORT TUBES

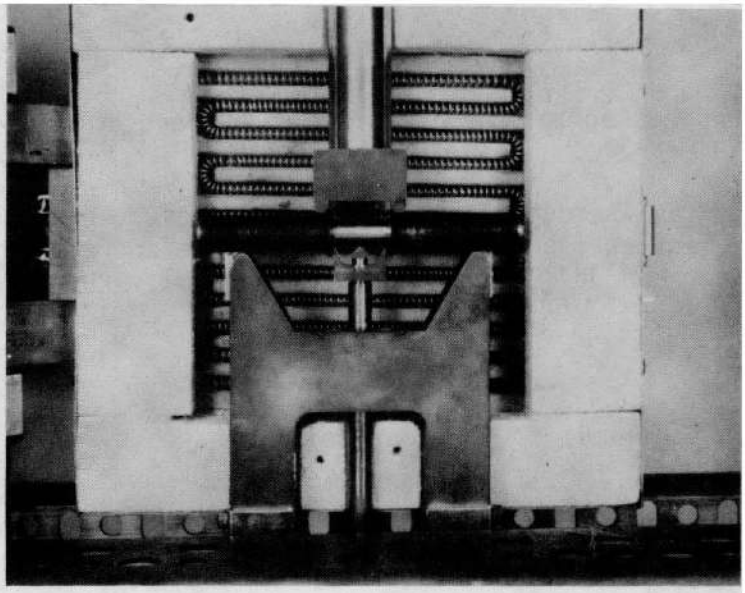

A

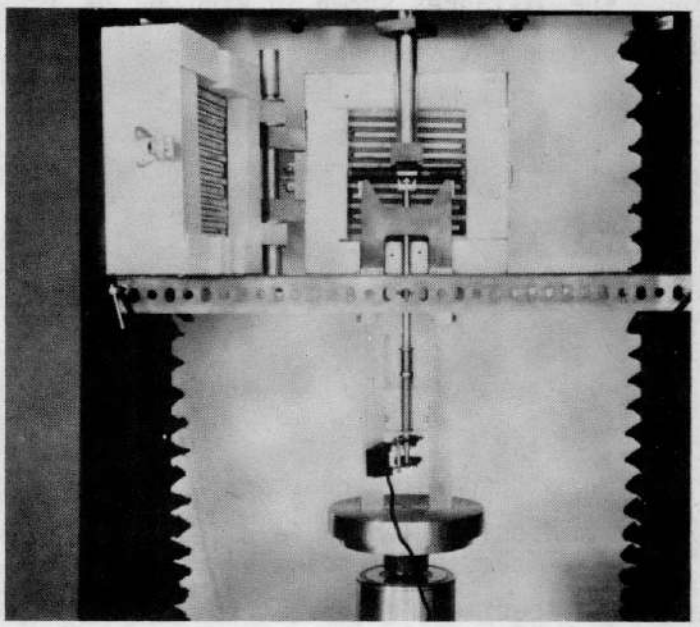

B

FIGURE C-6. BEND TEST EQUIPMENT.

A Shows a closeup of the test specimen, 4-point bend setup upper deflectrometer, and furnace. B is the bend setup in the testing machine and shows the lower deflectometer with a strain gage attached and load cell at the extreme bottom of the photograph.

as required, and tested to failure or to some predetermined radius of curvature.

The specimen is then removed from the test apparatus, examined, and photographed. Test variables include strain rate and temperature. The load and specimen deflection are autographically recorded.

Equations

Figure C-6 is a schematic of the four-point bend test unit.

$$\sigma = my/I$$

where σ = maximum fiber stress

P is the load

Y and L are the distances shown in Figure C-7

I is the second moment of area

$m = PL/2$

$Y = (0.5)(\text{tube OD})$

$I = \pi/64\ (OD^4 - ID^4)$

$\varepsilon = (s-\ell)/\ell$

$\dot{\varepsilon} = [(s-\ell)/\ell][1/t]$,

and

$$s = [\ell^2/4h + h][\tan^{-1}\{(4h\ell)/(\ell^2 - 4h^2)\}]$$

ε = the maximum strain

$\dot{\varepsilon}$ = the maximum strain rate (constant)

s = the maximum specimen length (arc length measured along the bottom of the specimen and across deflectometer)

ℓ = the initial specimen length (across the deflectometer, ℓ = 20.3 mm)

h = the deflection of the specimen (measured by the deflectometer)

t = the time to obtain the strain ε.

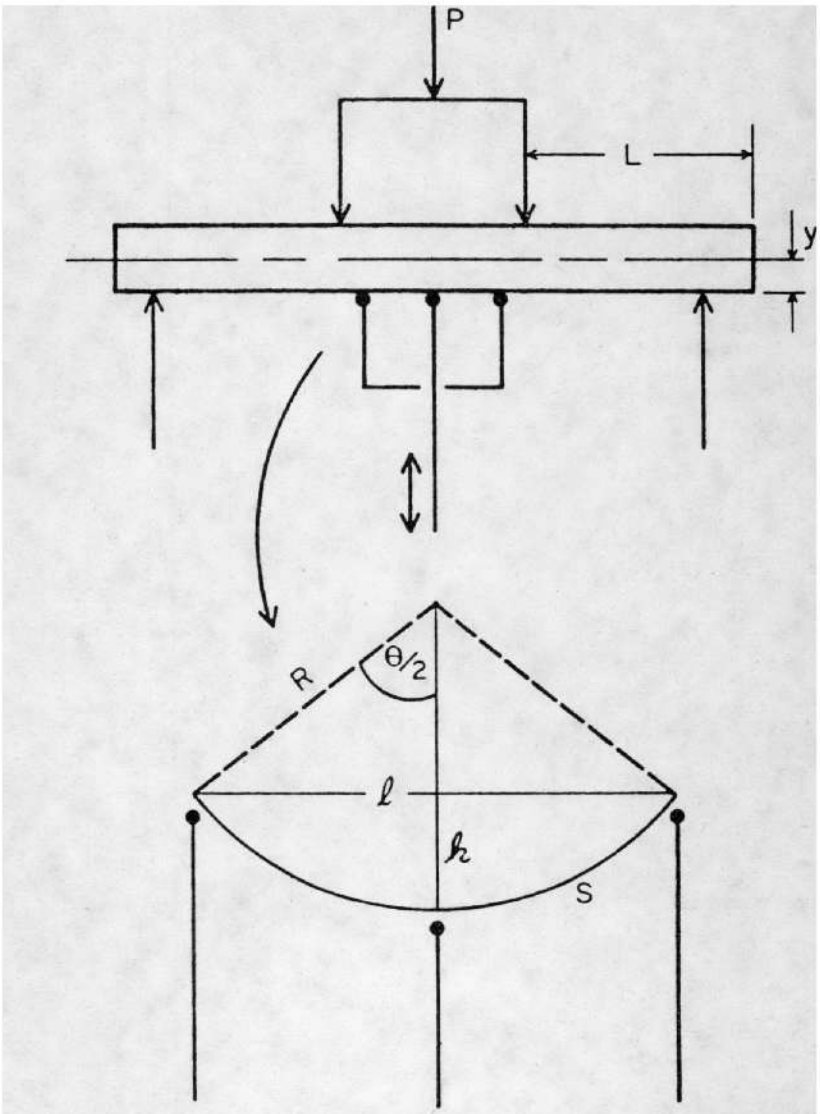

FIGURE C-7. SCHEMATIC OF FOUR-POINT BEND TEST UNIT WITH SPECIMEN DEFLECTION PARAMETERS

Precision and Accuracy

The precision and accuracy of the load is ± 0.5 percent of the full-scale load range. The maximum error of the strain gage deflectometer as defined in the 1974 Annual Book of ASTM Standards (E83-67 reapproved 1974) is 0.005 mm and is classified as a B-1.

APPENDIX D

A FULL DESCRIPTION OF EQUIPMENT AND PROCEDURES FOR TRANSIENT-HEATING BURST TESTS

Transient-Heating Burst Tests

Equipment

The transient-heating burst equipment consists of an internal electrically insulated heater operated inside a 51-cm-long Zircaloy cladding test specimen. An external heater is used for additional heating. The cladding is sealed to withstand 16.5 MPa internal pressure and thermocouples are spot welded to the surface. The two heaters and cladding test specimen are enclosed in a bell housing. (See Figure D-1).

The 13-cm internal heater consists of a Kanthal ribbon wound tightly on a 0.64-cm-diam, high purity alumina mandrel coated with high purity alumina for electrical insulation. The clad specimen is pressure sealed using stainless steel Swagelok fittings and the internal heater leads are electrically insulated using stainless steel Conax fittings with lava seals.

The Chromel-Alumel thermocouples are spot welded to tantalum tabs which are in turn spot welded to the cladding specimen surface. The external heater is a molybdenum-wire-wound furnace. Pressure, heater, and thermocouple connections are made through the stainless steel bottom plate and the entire assembly is enclosed in a stainless steel bell housing.

The specimen is pressurized using helium, the heater power supplies are 110 VAC, and the steam system consists of a commercially available steam generator. The temperatures are read on a multipoint recorder and the pressure readout is supplied by a pressure transducer.

Procedure

Prior to irradiated specimen testing, temperature gradient profiles and control heater voltages are determined using unirradiated specimens.

The apparatus is then put in-cell for irradiated specimen testing. The 51-cm test cladding and internal heater are inserted, the pressure (Swagelok) fittings sealed and the electrical (Conax) connections

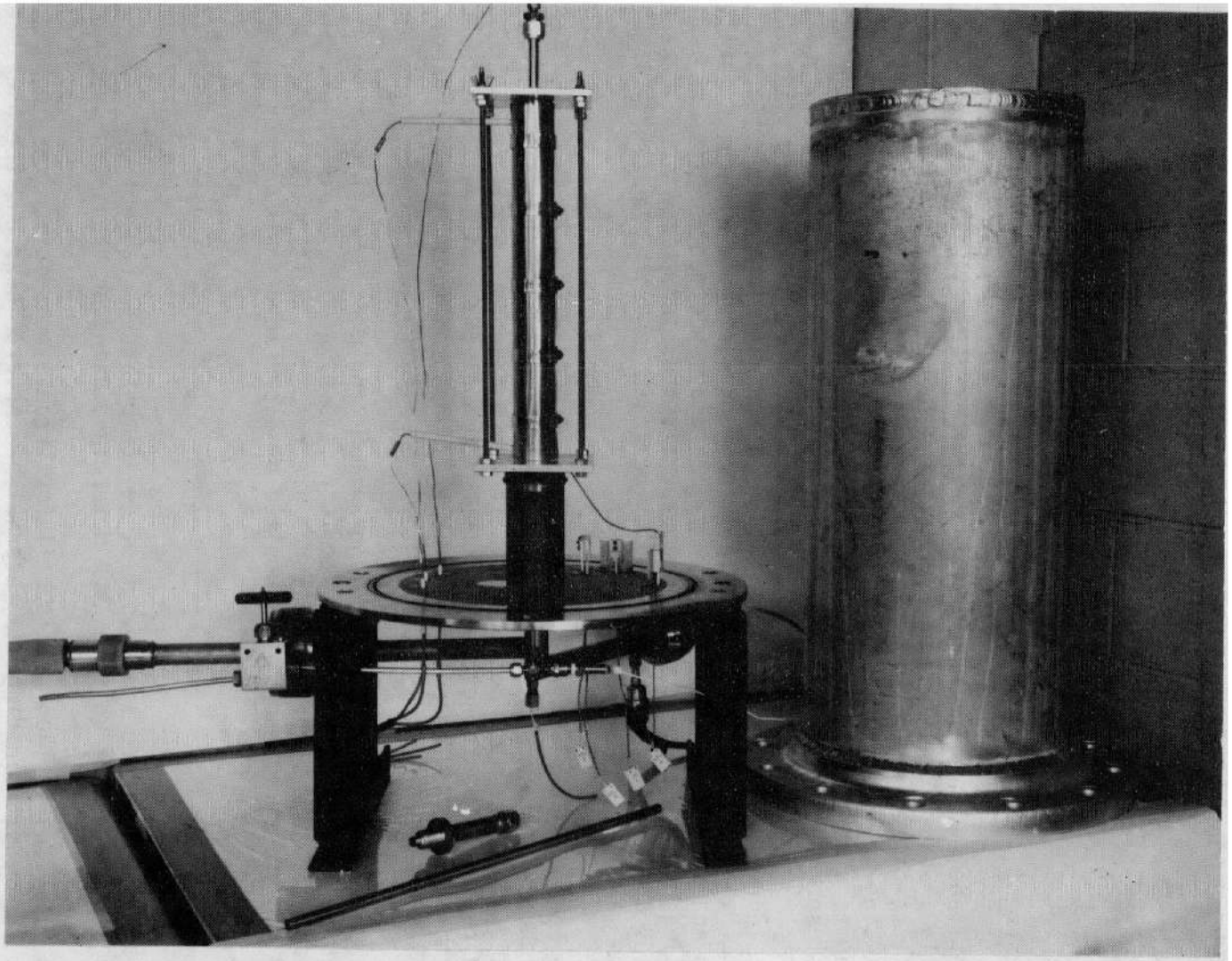

FIGURE D-1. IN-CELL TRANSIENT-HEATING BURST-TEST APPARATUS

sealed. The tantalum tabs with the spot welded thermocouples are then attached using in-cell, remote designed spot welding equipment. The external heater is positioned over the specimen and the entire assembly is sealed in the bell housing.

A pressure from 2.1 to 16.5 MPa is applied to the specimen and isolated. The pressure is then monitored during the test; no control of the pressure is attempted. Steam at atmospheric pressure is admitted to the bell and the specimen temperature is brought to 316 C using the external heater. The internal and external heaters are then ramped to attain specimen heating rates to 28 C/sec. The test is terminated upon either indicated specimen rupture (pressure drop) or attainment of test temperature. The recorded data include specimen temperature and pressure. The specimen failure strain is then determined metallographically or by using the strain measuring device.

The construction, calibration, and testing of a circumferential strain-measuring device were completed. The device uses a linear electrical encoder coupled with a digital readout which makes it ideal for remote strain measurement in the Hot Cells. (See Figures D-2 and D-3). The device was used to measure failure strains on both the transient-heating burst and conventional tube-burst specimens.

The strain-measuring device measures a linear circumferential length around the rod. At a burst point, the measurement is made over the opening and the opening width or cord length is measured using a filar eye piece on an in-cell microscope. An arc length of the measuring wheel over the burst opening is calculated and subtracted from the total circumferential length measurement. The resultant distance is the tube circumference in the burst region. The measured circumference minus the original circumference divided by the original circumference yields the calculated failure strain.

Using this device, several readings, usually 10, are taken around the same point along a rod and averaged to give the circumference at that point. The device permits many readings to be taken in a very short time. The accuracy and precision of the measurements are ± 0.0051 cm on a standard rod of 1.27-cm diam. The accuracy and precision of the measurements on an unirradiated burst rod are ± 0.013 cm. Decreased accuracy and precision on the burst specimens are introduced when the measuring wheel rolls over the burst opening.

A cladding restraining device was built and used during testing of the H.B.Robinson fuel rod cladding and is shown in Figure D-4. This device allowed the specimen to elongate during heatup but held it from contracting upon bursting. This movement simulated a fuel rod being restrained between grid spacers at the time of bursting.

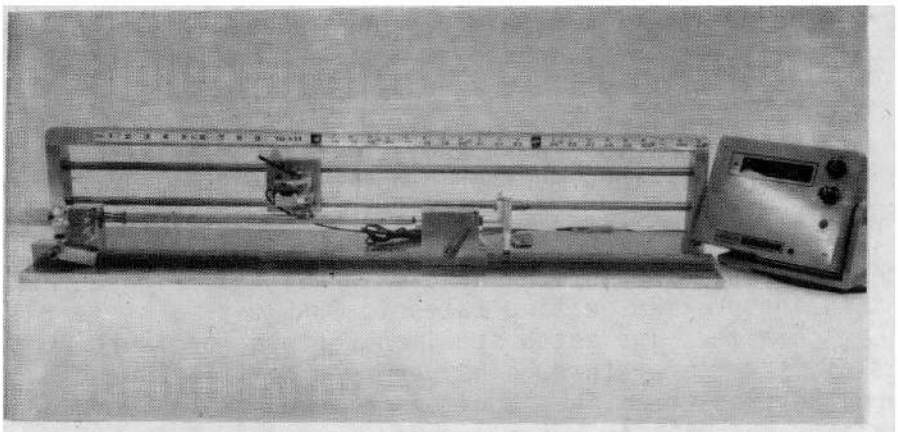

FIGURE D-2. STRAIN-MEASURING DEVICE WITH A STANDARD ROD IN PLACE AND DIGITAL READOUT UNIT

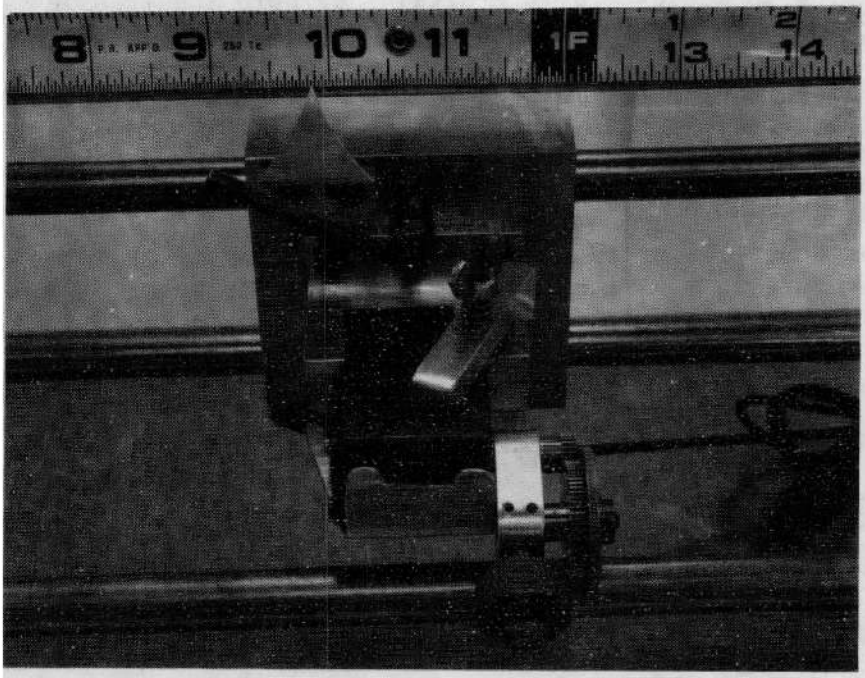

FIGURE D-3. STRAIN-MEASURING DEVICE ENCODER, ENCODER HOLDER, AND TRACING WHEEL ASSEMBLY

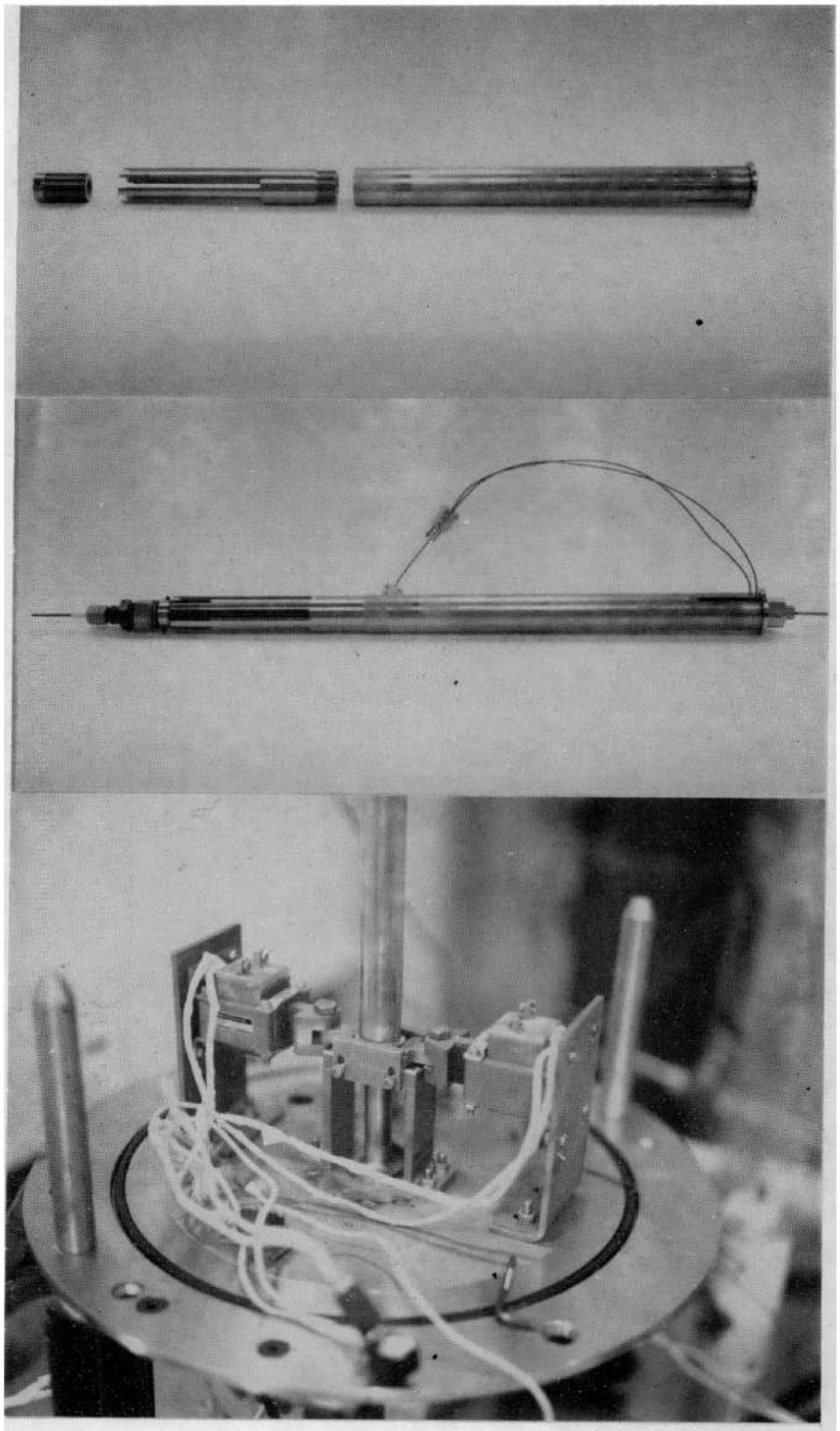

FIGURE D-4. TRANSIENT-HEATING TUBE-BURST RESTRAINT AND RELEASE MECHANISM

DISTRIBUTION LIST

No. of Copies	
320	Distribution under NRC-3
40	Larry M. Lowry
1	Arthur A. Bauer
1	William J. Gallagher
1	Alan J. Markworth
1	Reports Library
	Battelle Columbus Laboratories 505 King Avenue Columbus, Ohio 43201
2	R. A. Watson 336 Fayetteville Street P.O. Box 1551 Raleigh, North Carolina 27602
1	R. B. Adamson, Manager Cladding and Channel Development Vallecitos Nuclear Center General Electric Company Vallecitos Road Pleasanton, California 94566
1	Dr. Michael P. Bohn Aerojet Nuclear Company 550 Second Street, CSC I-9 Idaho Falls, Idaho 83401
1	Manager, Fuel Technology Exxon Nuclear Company, Inc. Research and Technology Center 2101 Horn Rapids Road Richland, Washington 99352
1	Dr. Owen Kruger Exxon Nuclear Company 2101 Horn Rapids Road Richland, Washington 99352

DISTRIBUTION LIST (Continued)

No. of Copies	
1	Dr. J. A. Horak Metals and Ceramics Division Oak Ridge National Laboratory Oak Ridge, Tennessee 37830
1	W. P. Blankenship Westinghouse Advanced Energy Systems P.O. Box 10864 Pittsburgh, Pennsylvania 15236
1	Dr. M. Fischer PNS-Leitung Kernforschung Karlsruhe Postfach 3640 75 Karlsruhe West Germany
1	John T. Mayer Babcock and Wilcox Company Power Generation Group P.O. Box 1260 Lynchburg, Virginia 24505
1	M. A. Rigdon Babcock and Wilcox Company Research and Development Division P.O. Box 1266 Lynchburg, Virginia 24505

NRC FORM 335 (7-77) U.S. NUCLEAR REGULATORY COMMISSION

BIBLIOGRAPHIC DATA SHEET

1. REPORT NUMBER *(Assigned by DDC)*: NUREG/CR-1729, Vol. 1

4. TITLE AND SUBTITLE *(Add Volume No., if appropriate)*: EVALUATING STRENGTH AND DUCTILITY OF IRRADIATED ZIRCALOY TASK 5

2. *(Leave blank)*

3. RECIPIENT'S ACCESSION NO.

7. AUTHOR(S): LM Lowry, AJMarkworth, JSPerrin, MP Landow and LR Kahn

5. DATE REPORT COMPLETED: MONTH February, YEAR 1981

9. PERFORMING ORGANIZATION NAME AND MAILING ADDRESS *(Include Zip Code)*

BATTELLE Columbus Laboratories
505 King Avenue
Columbus, Ohio 43201

DATE REPORT ISSUED: MONTH May, YEAR 1981

6. *(Leave blank)*

8. *(Leave blank)*

12. SPONSORING ORGANIZATION NAME AND MAILING ADDRESS *(Include Zip Code)*

US NUCLEAR REGULATORY COMMISSION
Div of Reactor Safety Research
Office of Nuclear Regulatory Commission
Washington DC

10. PROJECT/TASK/WORK UNIT NO.: Task 5

11. CONTRACT NO.: FIN A4068

13. TYPE OF REPORT: Final Report

PERIOD COVERED *(Inclusive dates)*: 1975 to 1980

15. SUPPLEMENTARY NOTES

14. *(Leave blank)*

16. ABSTRACT *(200 words or less)*

The objective of this program was to provide a mechanical-property data base that could be used to predict the performance of Zircaloy cladding under various off-normal, transient and accident conditions in a power reactor. The mechanical properties of both unirradiated and irradiated Zircaloy were determined under uniaxial and biaxial stress conditions for the purpose of simulating the loading and stress conditions encountered by cladding under these postulated conditions. Claddings for the tests were obtained from spent commercial fuel rods irradiated to various burnup levels. Tensile tests were performed principally to provide a comparison with the results of other uniaxial test data. Burst tests were performed to simulate fuel-rod pressure loading due to internal gases and to evaluate strain capabilities of the cladding under uniform pressure loading. Loads imposed on the cladding from fuel-cladding interaction and from restraint by spacer grids were simulated by expanding mandrel and bend tests. Tests were conducted using specimens in either the as-irradiated condition or the annealed condition.

17. KEY WORDS AND DOCUMENT ANALYSIS

17a. DESCRIPTORS

Zircaloy Fuel-Rod Cladding
Burst, Tensile, Bend and Expanding Mandrel Tests
Transient Burst Tests
Annealing

17b. IDENTIFIERS/OPEN-ENDED TERMS

18. AVAILABILITY STATEMENT: Unlimited

19. SECURITY CLASS *(This report)*: unclassified

21. NO. OF PAGES: 420

20. SECURITY CLASS *(This page)*: unclassified

22. PRICE: $

NRC FORM 335 (7-77)

UNITED STATES
NUCLEAR REGULATORY COMMISSION
WASHINGTON, D. C. 20555